Abstract

ZHAO, GANG. Finite Element Analysis and Design of Welded HSS Connections.
(Under the direction of Emmett Sumner PhD., P.E.)

The design specifications used for the Hollow Structural Sections (HSS) truss connections used in North America has been criticized by many structural engineers. Because of the restrictive limitations on the range of applicability, the preferred HSS chord and branch members often have wall slenderness ratios larger than the limitation of a particular connection design method. In order to find the acceptable limits for the geometric parameters, both HSS chord and HSS web in the gap and overlap connections need to be investigated.

The purpose of this study is to expand the wall slenderness ration limits of applicability used in HSS design. Due to the complicated geometrical factors and special welding and material features of the connections, an analytical method such as the finite element method will be used. Using the finite element method, the stress, strain and deformation response of the connections can be investigated. In addition, the critical failure mechanism within the connection region can be observed.

To get accurate results for the joint behavior, detailed three dimensional finite element models of selected geometries were to simulate real configuration. Different material properties are assigned to the HSS member and the special welding area according to different welding processes.

This study is the first part of an ongoing larger research project that will ultimately develop an experimental test suite on the HSS connection to build an acceptable parameter validity range.

Finite Element Analysis and Design of Welded HSS Connections

By

Gang Zhao

A thesis submitted to the Graduate Faculty of
North Carolina State University
in partial fulfillment of the
requirements for the Degree of
Master of Science

CIVIL ENGINEERING

Raleigh, NC
2006

APPROVED BY:

_____

_____

_____
Chair of Advisory Committee

Dedication

To my wife Ying Su

Biography

Gang Zhao was born in China on November 6th, 1973. While many people are uncertain regarding their ultimate career goals, he decided at an early age to put every effort into becoming an excellent engineer. His interest in becoming an engineer was greatly influenced by his parents who graduated from well-known engineering colleges in China. At Tianjin University, he began his college career in 1992 and received his bachelor's degree in civil engineering in 1996.

Upon graduation, he worked for a top design and consulting firm in China for six years. Although the work was demanding, new discoveries and innovations in the projects greatly enhanced his scope of knowledge in the structural engineering field. Feeling the desire for further academic development, he returned to college for his Master of Science degree at North Carolina State University. His concentration was centered generally on structural analysis and computer aided engineering. He would like to pursue a professional career in structural engineering.

Acknowledgements

First, I would like to express my sincerest gratitude for having the opportunity to complete this thesis. I would like to thank Dr. Emmett A. Sumner for all the patient guidance given over time while I was pursuing my master's degree at North Carolina State University. He served as the chair of my advisory committee and tolerated my unexpected drop-ins at his office and random questioning regarding this thesis and other papers.

Many thanks go to my committee members, Dr. Hassan, Dr. Guddati and Dr. Sumner for serving on my advisory committee and giving me helpful and professional advice.

I would also like to acknowledge with much appreciation, the support from my colleagues in Department of Civil, Construction, and Environmental Engineering and other people who have encouraged me in various ways to ensure that my research succeeded.

Finally, I would like to take this opportunity to express my thanks to my wife for always supporting me.

Table of Contents

List of Tables

List of Figures

Chapter 1 – Introduction

1.1 Background of HSS

1.1.1 Advantage of HSS

The usage of circular and rectangular Hollow Structural Shapes (HSS) for a large number of various kinds of structural applications has increased rapidly in recent years. Along with the pleasing look of this particular kind of section shape, it is also accepted as a strongly effective cross-section against compressive and torsional stresses by the nature of its unique closed, symmetrical geometric character. Although the material cost might be a bit higher compared with other more common shapes for the required grade of steel, the exceptional structural performance of HSS frequently makes up for the extra cost.

HSS offers many other important advantages over other commonly used structural sections: reduced fabrication costs because of high strength-to-weight ratios and reduced coating costs. “It's much easier and faster to coat HSS members than other structural members such as wide flanges, channels or angles, which have more surfaces,” (Steel Tube Institute 2005) according to Perry L. Smith, P.E., a commercial diver and lead engineer for ocean engineering on the project. For example, the surface area requiring protective coating is much smaller because the section is enclosed. The fabrication costs are kept low due to the simple joint weld connection and lack of stiffeners needed. “We prefer HSS because of its high strength-to-weight ratios,” (Steel Tube Institute 2005) says Todd Rose, Supervisor of Outdoor Project Engineering worked for Daktronics “Its superior strength allows us to reduce the size - and thereby the weight”. And finally the HSS has greater structural efficiency, as compared with other shapes. Along with its low drag coefficient, the HSS is regarded by many engineers as an ideal selection among

tremendous structural elements for applications dealing with wind, water, or wave loadings. For these reasons in particular, the HSS is commonly employed in offshore platforms, building and stadium space trusses, as well as some dynamic load carried high way bridge trusses. In addition, the variety of shapes HSS is made in gives designers more flexibility in constructing the trusses. So it's a material that's very easy to design and build with. Overall, HSS offers the best truss design solution for us, economically and from a standpoint of strength and weight. Fig1.1 shows typical HSS truss connection.

Figure 1.1 - Typical Rectangular HSS Truss
T&M Steel Services Inc

1.1.2 Manufacturing Methods of HSS

Steel pipes can be broadly categorized according to different manufacturing methods as seamless pipes made by hot rolling, welded or tip-welded pipes made by bending and welded steel plates. The transformation of a flat strip into a HSS is the result of a series of operations including forming, welding and sizing. Three methods are currently used in North America for the manufacture of HSS. These methods, including two ERW methods and an SAW method, are described in Fig.1.2

(1) (2) (3)

Figure 1.2 - ERW and SAW Manufacturing Methods
Steel Tube Institute of North America

In the AISC HSS Connection Manual (AISC 1997), these three manufacturing methods had been introduced in details as follow.

(1) "Electric Resistance Welding (ERW) Process: In tube mills, a flat steel strip is formed continuously around its longitudinal axis to produce a round tube. The strip edges are heated by either high frequency induction or contact welding and then forged together by weld rolls to create a continuous longitudinal weld without the addition of filler metal. The weld seam is then cooled and processed through a set of sizing/shaping rolls which cold-form it into a round, square or rectangular section."

(2) “Form-Square / Weld-Square (ERW) Process: In weld mills, driven forming dies progressively shape the flat strip by forming the top two corners of the square or rectangular tubes in the initial forming station. Subsequent stations form the bottom two corners of the shape. No cold working of the sides of the shape is performed, and the shape’s seam is welded by high-frequency contacts when the tube is near its final shape and size. The welded tube is cooled and then driven through a series of sizing stations which qualifies the tube’s final dimensions.”

(3) “Submerged Arc Weld (SAW) Process: Two identical pieces of flat strip are placed in a press brake and formed into two identical halves of a finished tube size. A backup bar is tack welded to each leg of one of the half-sections. The two half-sections are fitted together toe-to-toe and welded by the submerged arc process to complete the square or rectangular section.”

HSS-to-HSS truss connections are defined as connections consisting of one or more branch members that are directly welded to a continuous chord passing through the connections (AISC, 2000). Two general means of joining HSS are used by most designers include weld and bolt connections. The bolt method that might be employed for some particular applications depends on the magnitude of the load to be transferred and the thickness of the HSS member. Although the bolt method is widely adopted, the welding is the primary means of joining HSS at connections. Even bolted connections typically use detail material that is welded to HSS. For this reason, there are many related welding design, fabrication, and inspection requirements that are unique to HSS connections (AISC 1997).

1.2 Current Design Guides

The HSS truss design specification generally used before 2005 in the United States includes the Load and Resistance Factor Design Specification for Steel Hollow Structural Sections (AISC 2000) and AISC Hollow Structural Sections Connection Manual (AISC 1997). The former one can also be found in Part 16, Section 2 of AISC LRFD Manual 3rd Edition (AISC 2001). A more detailed description of the HSS connection design procedure is given in the latter one.

The focus of these two manuals is a little different from each other. LRFD Specification for Steel Hollow Structural Sections (AISC 2000) is focus on general properties and design requirements on HSS rather than on other steel sections, yet it uses the similar format for the general LRFD design manual. Tension, compression, torsion and connections are listed in this manual along with other common chapters. The American HSS Manual (AISC 1997) follows the traditional format and fundamental approaches that have been developed by all other AISC design manuals. This manual is intended to cover the common design criteria in routine office practice. It contains the material properties and section dimensions as all other manuals. It is more focus on the connection issues including bolting, welding, and other connection methods as well as different joint categories such as moment connection, simple shear connection, tension, and compassion connection. Design procedures for cap plate, base plate column splices and other supplemental parts are discussed in the manual. Welded truss connections are also detailed in this guide.

While Americans take a very general approach creating design guidelines, Canadian HSS Manual (Packer 1997) is much more focus on the specific design case of

the HSS truss. CISC Hollow Structural Section Connections and Trusses Design Guide (Packer 1997) provides a similar approach solving the HSS design issues as the AISC manual. The topics provided in this Canadian Manual include "material property and cross-sectional geometric definitions with metric units. Other topics included are standard truss design, standard truss welded connections, non-standard truss design, multi-planar welded connections, HSS-to-HSS moment connections, bolted HSS connections, fabrications, welding, and inspection, beam to HSS column connections, trusses and base plates to HSS connections, plate to HSS connections, HSS welded connections subject to fatigue loading, and standard truss examples."

CIDECT - the International Committee for Development and Promotion of Structural Tube is an International Association of Structural Tube Manufacturers founded in 1962. "The necessity to solve the design problems concerning the versatile applications of hollow sections, which are somewhat supplementary to the general structural engineering with plates and open sections and apply particularly to this youngest member in the family of steel sections, led to the foundation of CIDECT in 1962 as an international organization of major hollow section manufacturers" (Dipak Dutta, 1995). CIDECT developed a set of design guides for the construction of Tubular Structures and connection design guides in euro-codes covering "structural stability, joint behavior under predominantly static loading, fire resistance, fabrication, assembly, erection and other aspects." CIDECT's publication "Design Guide for Circular Hollow Section (CHS) Joints under Predominantly Static Loading" (J. Wardenier 1991) is more similar to the current manual on circular HSS connections compared with the American and Canadian Specifications. It contains common chapters including "general design

procedure of tubular structures, fabrication of tubular structures, and joint design under predominantly static loading, bolted connections and worked-out design examples".

In 2005 the American Institute of Steel Construction issued its new 5th edition of "Specification for Structural Steel Buildings" (AISC 2005). The usual specification sections on bolts and welds were included, as well as a new chapter on HSS and box member connections. The specific topics included are "concentrated forces on HSS, HSS-to-HSS truss connections, and HSS-to-HSS moment connections." The latter subject was new to the AISC Specification. The other topics were updated from the 2000 Load and Resistance Factor Design Specification for Steel Hollow Structural Sections. Not like its former editions which only have LRFD format, the 2005 edition has a significant development impact since it includes both LRFD and ASD formats. The growing area shows up in the new book as a whole new chapter describing the design of welded Hollow Structural Section (HSS) connections. Chapter K: "Design of HSS and Box Member Connections" brings the onshore tubular design and construction to the attention of all structural steel designers, who really feel the need to comply with these AISC recommendations. These design rules are based on identified limit states, for a variety of truss-type welded connections, subject to either axial or moment loading. "Design formulas are in general accord with current international recommendations on this topic" (Packer and Henderson, 1997) and they represent a major expansion in HSS connection design scope compared with what are currently available in the U.S. (AWS 2004, AISC 2000).

1.3 Prevailing Analysis and Design Method

Generally, HSS connection design process needs to be manageable by non-specialists in tubular design projects as well as other design procedures. In order to achieve this aim, the new AISC manual has put much emphasis on simplifying the connection capacities to only one limit state or as few as possible limit states. For particular connections and loadings, correspondent modes can be built up. Other failure mode can be excluded by defining certain "limits of validity" controlling acceptable material and geometric parameters. Based on this restriction, connections are generally efficient and are able to carry significant loads. There is often a violation of parameter limit in the wall slenderness of the main chord member. The reason is that generally, structural engineers prefer to choose a large thin chord member and provide increased resistance to overall buckling as a compression chord member while strong tubular connections are actually achieved when thick stocky chord member is used. Actually, it is not a problem for the low connection capacity if the truss members are only lightly loaded.

As an efficient and versatile numerical analysis tool, the Finite Element (FE) method has been used widely in the analyses of different types of model simulations including structural design analysis procedure. In recent years, more attention has been paid to the study on the deformation and fracture behavior of welded tubular joints. Finite Element (FE) method is very versatile and most widely used in the field of structural analysis because by reducing the structural continuums to a finite number of discrete material elements for evaluation, the Finite Element (FE) method permits analysis of

arbitrary structures, even those with irregular shapes, with inhomogeneous material, or other features that exclude the use of classical, analytical methods.

In this project, a series of Finite Element (FE) models for this type of HSS connections will be established to set up the matrix of numerical tests. The features of ASTM A500 square/rectangular HSS will be incorporated (rounded corners, design wall thickness per AISC), welds will be modeled and full solid (brick) and degenerated elements will be used. The material properties will be input as a multi-linear curve with the engineering stress and strain converted to the true stress and strain values. Non-linear material geometric behavior will thus be incorporated. Appropriate material failure criteria will also be incorporated such as monitoring of maximum equivalent plastic strains. Only a half of the connection will be modeled because the connection is symmetric. Symmetrical boundary conditions will be employed along the plane of symmetry. By using different elements to simulate the tubular pipes which are only connected through weld elements, all direct stress transfer between the branches and the connecting chord face will be prohibited in order to force load transfer to occur only via the welds.

1.4 Research Objective and Scope

Structural engineers using design guidance for welded HSS truss connections in North America have complained that the preferred (or even purchased) square/rectangular HSS chord member selected for use in a structure of tension has a wall slenderness (overall width/design wall thickness, or B/t) greater than the limit of validity for a particular connection design method. In these cases, it is important to define or give guidance for HSS connection capacity when operating beyond the current acceptable

limits for geometric parameters. Two types of K connections are generally used in truss design which includes gapped K-connection and overlapped K-connection as show in Fig1.3 and Fig1.4. This research aims only include the investigation of overlap HSS chord to HSS web connections in overlapping K-connection.

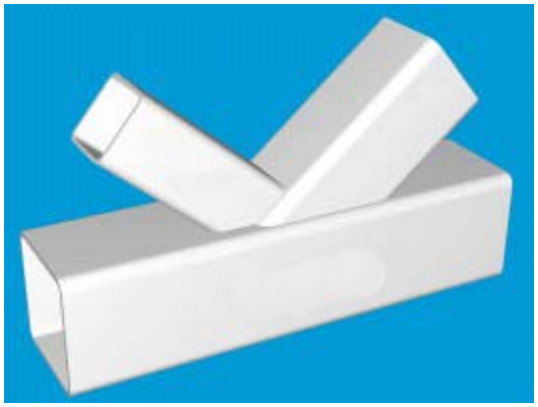

Figure 1.3 - HSS K/N Overlapped Connection

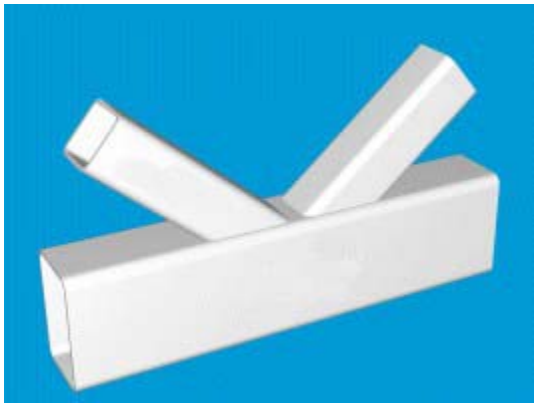

Figure 1.4 - HSS K/N Gapped Connection

This research's scope includes only analytical investigation of the connection and will cover only overlapped K-connections with various levels of compression chord loadings by using ASTM A500 Grade B base metal and selected weld material properties. Various chords and branch wall slenderness values (b/t) and expanded branch-to-chord and branch-to-branch width ratios will be covered in this research. Specifically, the

matrix of '"numerical tests" generated will cover the following range of geometric parameters for overlapped joints:

- 50% overlap described in Fig 1.5

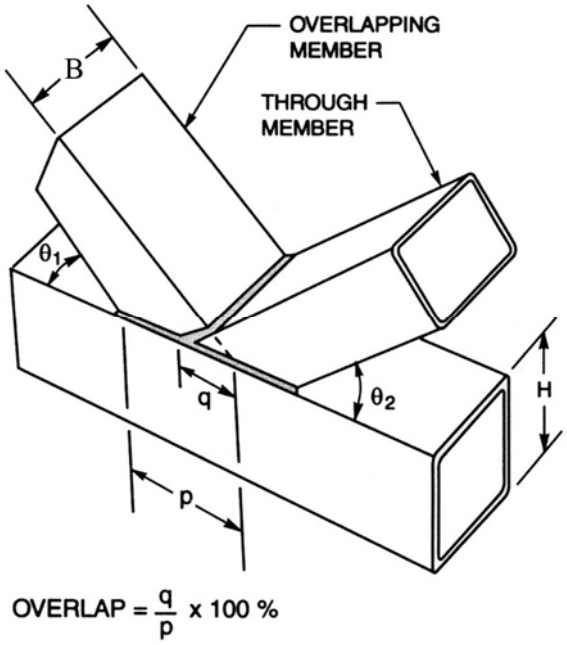

Figure 1.5 - Overlapping K-Connection
(AWS2000 Figure2.20)

- Branch-to-chord width ratio of 0.5 (stepped) and branch-to-branch width ratio of 1.0 (matched) described in Fig 1.6

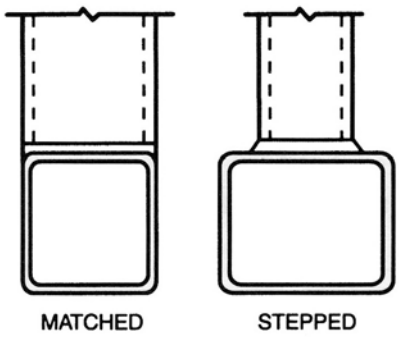

Figure 1.6 - Connection Type for Box Section
(AWS2000 Figure2.14-L)

▪ Wall slenderness (B/t) value of 35 and 46 for chords and for branches. The available HSS sections is listed in Table 1.1 and Table 1.2

Table 1.1 – Available HSS for Wall Slenderness around 35

Rectangular HSS			
B	H	t	Wall slenderness
32	24	5/8	35.4
30	24	5/8	35.4
28	24	5/8	35.4
26	24	5/8	35.4
22	20	1/2	37.0
20	18	1/2	33.0
20	12	5/16	38.2
16	12	5/16	38.2
9	7	3/16	37.2
Square HSS			
B	H	t	Wall slenderness
26	26	5/8	38.6
24	24	5/8	35.4
20	20	1/2	37.0
14	14	3/8	37.1
12	12	5/16	38.2
8	8	1/4	31.3
7	7	3/16	37.2
4½	4½	1/8	35.8

Table 1.2 – Available HSS for Wall Slenderness around 46

Rectangular HSS			
B	H	t	Wall slenderness
32	24	1/2	45.0
30	24	1/2	45.0
28	24	1/2	45.0
26	24	1/2	45.0
20	18	3/8	45.0
12	8	3/16	43.0
10	8	3/16	43.0

Table 1.2 Continued- Available HSS for Wall Slenderness around 46

Square HSS			
B	H	t	Wall slenderness
32	32	5/8	48.2
30	30	5/8	45.0
24	24	1/2	45.0
18	18	3/8	45.0
14	14	5/16	45.1
12	12	1/4	48.5
8	8	3/16	43.0
6	6	1/8	48.7
5½	5½	1/8	44.4

- Chord member load/chord nominal compression strength ratios of -0.8, -0.4, 0

The results obtained from this numerical research will be used to achieve the objectives. The objectives included: 1.Help structural engineers to investigate some of the failure modes common to this type of HSS connection, 2.Investigate expanded chord member and branch member b/t limits of applicability and thus facilitate their design with HSS, 3.Investigate the effect of the chord member load, 4.Investigate the AISC Equations of design strength of overlapped K-connections.

1.5 Thesis Outline

The following is a brief outline of the major topics covered in this thesis:

- Chapter 2 contains an extensive literature review that describes the current state of knowledge on the construction, design and modeling issues of HSS joint of the steel truss bridges and how these problems relate to different geometric parameters of the HSS connections. In addition, a review of the finite element modeling techniques commonly used to model the joints of truss structures is included.

- Chapter 3 outlines in detail the steps involved in selecting the suitable element type, creating the three dimensional finite element models for the connection using ANSYS, applying the correct loads and giving the boundary conditions. A brief summary of the weld form and size is also included.

- Chapter 4 contains a description of the results of the numerical analysis in different load steps. The maximum displacement at different locations was investigated. The load-displacement relationship was also studied.

- Chapter 5 contains a discussion of detailed comparisons of the load-displacement behaviors of different geometric configurations including different branch wall slenderness (b/t ratios) with the same chord b/t ratio and different chord b/t ratios with the same branch b/t ratio. A discussion of the comparison of different chord compression effect on the connections is also included.

- Chapter 6 contains an overview of the conclusions drawn from this research and the recommendations for future research.

- Appendix A contains the first 4 pages of the ANSYS input in the research. Total 70 pages is needed for the whole program input codes which can built up the finite element model in the ANSYS.

- Appendices B-I contain summaries of every model and load case in this research. The load-displacement figures of the studied areas for every case are also listed in this section.

Chapter 2 – Literature Review

2.1 Overview

The present literature review is organized along three distinct lines of focus related to the current research investigation aimed at evaluating the adequacy of existing design practice applied to the K-connection regions design of highway or onshore tubular construction for structural steel designers. The respective several focus areas are: 1) Finite Element Modeling. 2) Welding Behavior. 3) Calculation Methods in Hollow Structural Section (HSS) Truss and Connection Design. 4) Effects and Modeling of Cracks in Tubular Joints. A review of previous and current techniques used in the finite element modeling of these welding connections is included herein.

2.2 Analysis and Simulation of Welding in HSS

2.2.1 General

Welding is defined by the American Welding Society (AWS) as a localized coalescence of metals or nonmetals produced either by heating of the materials to a suitable temperature, with or without the application of pressure, or by the application of pressure alone, with or without the use of filler metal. Because welding is the primary means of jointing HSS at connections and the requirement for the HSS connections is unique, welding design is described in detail in HSS Connection Manual (AISC 1997). "There are numerous welding procedures used in construction industry. In recent years, many of the existing welding processes have been simulated by numerical methods, especially by the finite element methods. The numerical simulation of a welding process is a complicated process containing the interaction of thermal, mechanical, electrical and metallurgical phenomena. It also requires profound knowledge of the welding detail and

master understanding of FEM. The welding at the joint has a special character which translates a nonlinear, local zone within an elastic structure."

Mackerle (1996) in his "Finite Element Analysis and Simulation of Welding" gave a bibliographical review of the finite element methods (FEMs) applied to the analysis and simulation of welding processes. He summarized several topics including modeling of welding processes, influence of geometrical parameters, residual stresses and deformation in welds, fatigue of welded structures and welded tubular joints. In each topic he clearly described the current trends in the application of finite element techniques.

2.2.2 Modeling of Welding Processes

"Many welding processes have been developed. They differ in the manner in which heat is applied and in the equipment used." Mackerle (1996) pointed out in his paper that some of these processes require forging or pressing (plastic welding) to affect the weld while others bring the metal to a fluid state (fusion welding) and require no pressure.

"The finite element simulations usually involve very dense meshes and emphasize resolution within the local weld zone. In contrast to these studies, interactions between the weld zone and the overall elastic welded structure can also be treated. In these cases, complications arise from the elastic coupling between the local weld zone and the overall structure."

2.2.3 Influence of Geometrical Parameters

"Welded structures usually involve complicated geometry and are under severe thermal loads during the process of welding. Geometric parameters significantly affect the properties of welded structures. Their influence can be investigated by parametric

studies." Bleackley M H (1986) in his "Path Dependency of the Rice J -Integral in Weld Geometries" stated that the J -integral method to be examined is the stiffness derivative technique for both two- and three-Dimensional bodies. Apparently, this J –integral is affected by many geometry considerations such as the length, area or volume within the integral path, surface or volume.

The results should be valid for a wide range of other welded structures/components. Some topics include: influence of geometrical parameters on stress concentration factors, on the strength of joints, on the fatigue strength, creep behavior, etc.; effects of weld configurations on stress/strain fields; design concepts.

2.2.4 Residual Stresses and Deformations in Welds

"Because a weld is locally heated by the welding heat source, its temperature distributions are not uniform and change as welding progresses. The strains produced during this process are accompanied by plastic upsetting and, as a result, residual stresses developed after welding is completed. Shrinkage and distortions are also produced. Distortions and residual stresses cause significant problems in the welding of large structures; they can be a major factor for cracking and fracture problems in structures. Preheating of joints is an effective method of reducing the cooling rate of the weld which reduces these distortions and residual stresses. Post-welding heat treatment can also be used. It relieves internal stresses and controls the micro-structure of the weld," Mackerle (1996) also stated in his paper.

Other Residual Stresses topics in Mackerle's (1996) paper include: two- and three-dimensional calculations of residual stresses and deformations in welds, thermo-mechanical analysis of residual stresses, transformation plasticity and residual stresses,

the prediction of residual stresses, effects of residual stresses on significance of defects and weld joint strength, characterization of residual stresses, welding stresses during phase transformation, residual stresses generation and relaxation, residual stresses and their redistribution during annealing, residual stress formation during plastic welding, mechanical stress relief treatment of residual stresses, residual stresses in thick section welds.

2.2.5 Fatigue of Welded Structures

One of the main features of fatigue analysis of welds is the reduction in lifetime caused by notch sensitivity due to stress concentration at the toe of the weld reinforcement. Papers published in scientific journals investigate the effects that welding has on fatigue crack growth, in particular the study of the rate of fatigue crack growth in the base metal, heat-affected zone and weld metal (Mackerle 1996). The practical analysis of the weld-notch effect is of major importance in fatigue and fracture assessments.

Other topics of interest in Mackerle (1996) are: fatigue crack growth of welded joints; influence of residual stresses on the fatigue crack growth; influence of bending stresses on fatigue crack propagation; influence of misalignment on the fatigue strength; effect of weld discontinuities on the fatigue strength; effect of weld geometry on fatigue crack propagation; fatigue crack initiation; influence of cathodes protection on the fatigue resistance; creep fatigue; fatigue predictions of T-joints, cruciform joints, plate joints, fillet welded joints, thin-walled welds, spot-welded joints, corner welded joints, box-section beams, bellows, pressure vessels, pipes, offshore structures, ship structures.

2.3 Calculation Methods for Tubular Joints

2.3.1 Calculation Methods for Tubular K-joints

The majority of HSS truss connections always have one compression web and one tension web member welded or bolted to the chord member. The Warren arrangement is referred to as a K connection and the Pratt as an N connection. The later is a special case of the former; and both can be either gapped or overlapped connections.

The ISO Draft Code for offshore structures has included a formulation for the design of both gap and overlapped tubular K joints under axial loading. Gazzola, F and Lee, M. M. K.(2002) had presented in "Assessment of Strength Equations for Overlapped Tubular K-Joints", also in a series of recent articles, a strength formulation (Swansea formulation) for overlapped K joints, based on a database of joint strength generated by an extensive parametric finite element study. With the view that the Swansea formulation may be adopted to replace that proposed by ISO for design practice, the numerical constants in the Swansea formulation were simplified and a mean bias factor was derived to convert it to the characteristic format.

The ISO formulation (ISO 1999) for calculating the characteristic capacity P_{uj} for K- joints covers both gap (positive g) and overlapped (negative g) joints and is as follows:

$$P_{uj} = \frac{F_y T^2}{\sin\theta} Q_u Q_f$$

Where F_y = minimum specified yield stress of the chord member [or 0.8 of the tensile strength],

Qf: chord load factor

Qu: basic joint strength factor

T: chord wall thickness

θ: brace angle

The accuracy and reliability of the strength equation from ISO for overlapped K-joints, formulated from a database of test joints, has been assessed against that proposed recently by Gazzola, F. and Lee, M. M. K.(2002). They gave the following simplified strength equation, which is formulated from an extensive parametric study using finite elements.

$$P_u = \frac{\sigma_y D^2}{\sin\theta} Q_g Q_m$$

D: chord diameter

Q_m: material factor

Q_g: geometric factor

"These two factors were obtained by further regression analysis, when all other constants were set to the new specified values. Their simplified strength equation was a simple and characteristic format and was proposed to allow it to be adopted for design practice."

In Lee, M. M. K.(1999) paper, he reviewed the ultimate capacity results from an extensive finite-element study of balanced axially loaded K-joints (Lee, M. M. K. 1999). He stated that "overlapping the braces was shown to have a beneficial effect on joint strength for the joints with relatively thick brace walls, where the strength was found to be up to four and a half times that of the corresponding gap joint. The performance of the

available onshore and offshore design guidance for predicting joint capacities was poor, particularly for the overlap joints. A new strength equation developed for the overlap joints has been derived to predict the capacities of the numerical joints studied, as well as those from a test database, with a high degree of accuracy."

$$\frac{P_u \sin\theta}{F_y D^2} = 3.41\gamma^{-1.43}\tau^{0.72}\beta^{0.98} + 0.29\gamma^{-1.13}\tau^{1.77}O_\upsilon{}^{1.57}$$

β, γ, τ are non-dimensional geometric parameters

O_υ = % overlap / 100

2.3.2 Design Equations Derived from Finite Element Method

As most equations in the structural engineering field, the design equations for the tubular joints are based on simplified analytical models that are modified by empirical constants to match test data. Jubran J. and Cofer W.(1995) stated that "a new form for ultimate strength equations for tubular joints is derived using a modified version of the ring model. The new form is capable of modeling the increase in joint strength for joints with large branch to chord diameter ratios." In general, the ultimate strength of a tubular joint can be written as

$$\frac{P}{\sigma_y T^2} = k_1 + k_2\beta + k_3 \ln\frac{1}{1-\beta}$$

β: branch to chord diameter ratio

k_1, k_2, and k_3 are determined by fitting the equation to experimental results.

The current design format for the ultimate strength of tubular joints varies from one code to another. Design equations are derived from test data, either as a lower bound

("Recommended" 1989; "Structural" 1990), from the mean strength ("Rules" 1977; "Offshore" 1984) or from the characteristic strength ("Design" 1985). Typically, design equations are based on simplified analytical models that are modified by empirical constants to match test data.

2.4 Finite Element Modeling of Tubular joints

2.4.1 Calibration and Validation

Traditionally, design equations for tubular joints have been derived from ultimate strength test data. In the past decade, however, there has been increasing recognition of the important role played by using well-validated FE analyses for generating strength data.

Lee, M. M. K. and Dexter, E. M.(2003) have used such a technique extensively to investigate T/Y joints, KK joints, ring stiffened T-joints and gap and overlapped K joints. Their work reported herein is particularly suited for numerical simulation, as even the testing of relatively simple multi-planar joints on a limited scale is difficult and prohibitively expensive. For validation and calibration purposes, rather than selecting individual joint experiments to model explicitly, they decided to revalidate the FE strategy used previously for axially loaded K and KK joints and out-of-plane bending T-joints. By comparing the FE results with the ISO strength equations and the BOMEL test database which is similar to the database used by ISO, they are found correlated sufficiently well to demonstrate the validity of the proposed numerical procedure for both single and multi-brace joints. "Some deviations (particularly residual γ and θ effects) from the data trends predicted by ISO are apparent for all the joint type considered. In addition, the K-joint analyses have revealed that in-plane effects are diminished at much

smaller gap sizes (ξ) than are currently predicted by ISO. These deviations were considered to be due to the scatter of the underlying test database as well as the lack of data within certain parameter ranges and have given some preliminary insight as to some of the inadequacies of the current design equations. The FE modeling techniques established thus form the foundations of the extensive multi-planar joint analysis program undertaken for the Joint Industry Project."

2.4.2 Numerical Results

Jubran J. S. and Cofer, W.(1995) presented in "Finite-Element Modeling of Tubular Joints I Numerical Results" about 12 tubular joint models with varying branch to chord diameter ratios β and branch inclination angles θ, subjected to axial tension, axial compression and in-plane bending moment. "The analyses were performed by using finite-element software that is capable of modeling elastic-plastic material behavior and geometric nonlinearities as well as ductile and brittle fracture. The results showed that the current use of sin (θ) in design equations for inclined branches is reasonable, but somewhat conservative. When compared with the current experimental database, a close correlation of results was obtained for all axial tension cases, and for axial compression and in-plane bending moment cases for low to moderate β values. The results compare well with experimental data for joints with axial tension. For joints with axial compression, the results fall well above the experimental results for large values of β. They pointed out that this property may be attributed to the definition of failure and local buckling for these types of joints and to the possible flexibility of the chord end conditions for the tests. The results for joints subjected to in-plane bending moment fall slightly above those obtained experimentally."

In their analysis, the finite-element modeling was shown to be a promising method to obtain data for the development of design aids for tubular joints. In numerous studies involving specific tests for joint strength with P values up to 0.6, predictions from nonlinear finite-element analyses have consistently compared quite well with those obtained experimentally.

In the stress analysis of the tubular joints, FEM is a verified method as well. Chiew S. et al.(1999) in their "Experimental and Numerical Stress Analysis of Tubular XT-Joint" stated that The SCFs (stress concentration factors) at typical hot spot locations were also calculated by using finite-element (FE) analysis. "The good agreement between the numerical and the experimental SCFs results confirmed the reliability of the numerical modeling of the XT-joint. In addition, the writers' SCFs results were compared with Efthymiou's influence function (IF) method and the ones derived from the corresponding uniplanar T-/X-joints. They built up a typical finite-element model devised for the investigation of the multi-planar XT-joint specimen. Taking advantage of structural symmetry, only one quarter of the multi-planar XT-joint needed to be modeled under the N-brace loadings and the W-/E-brace balanced loadings. The related correct boundary conditions for quarter and half models were needed as well. A convergence study was conducted to find the proper mesh refinement for the SCFs calculation. FE models with increasing element numbers were created under N-brace axial, IPB (in-plane-bending), and OPB (out-of-plane-bending) loadings. The comparison between such FEM SCFs and the Test SCFs at the 10 typical hot spot locations under all the 11 test load cases was summarized." The agreement was reasonably good, and it was clearly stated that the FEM SCFs were conservative at most investigation spots under all

specified test load cases. This confirmed the reliability of the FE modeling of the multi-planar XT-joint specimen.

2.4.3 Gurson Model

Numerical modeling of the fracture effects on the strength of steel circular hollow section joints has not been sufficiently addressed historically. "Crack initiation and propagation is one of the common failure modes for tubular joints subjected to tensile loading. However, simulation using finite elements based on continuum mechanics formulation cannot be used to predict the effect of cracking, which violates the continuity and integrity of material and geometry. Four numerical methods have been used in dealing with crack initiation and propagation: discrete crack model, fracture mechanics, smeared crack model, and continuum damage mechanics." Qian, X. D. et al (2005) offered an alternative approach in modeling the ductile fracture for the strength analysis of tubular joints. "The Gurson model simulates the plastic yield behavior of material very well. Two loading conditions are investigated on tubular bars with the Gurson model."

Their study adopts the void nucleation and growth approach which was established by Gurson (1975). The Gurson model simulates the plastic yield behavior of a porous or void containing material. Under plastic deformation, the material strain hardens, and voids nucleate and grow, and subsequently lead to deformation localization and fracture. It is reported by Thomason (1990) that "all engineering metals and alloys contain inclusions and second-phase particles, to a greater or lesser extent, and this leads to void nucleation and growth…." They concluded at the end of the paper "Simulation of Ductile Fracture of Circular Hollow Section Joints Using the Gurson Model" that finite element analysis using the Gurson model is able to capture fracture failure as reflected in the load

reduction in the load–deformation curve for tubular joints. “The accuracy of the Gurson model depends primarily on the following two factors: 1. Mesh size. 2. Material property. The effect of void growth and nucleation on the tubular joint is also found to be dependent on the load path. Different geometric properties of the joint modify the force flow in the tubular joint, and directly influence the stress distribution, as well as the void growth and nucleation processes.”

2.5 Cracked Tubular Joints

Cracks exist to some extent in nearly all tubular joints, as a result of either manufacturing fabrication defects or localized damage in service. In order to predict the remaining life of a joint with a crack, detailed analysis of the fracture behavior and crack growth behavior of the crack is needed.

2.5.1 Crack Modeling in FE Analysis of Circular Tubular Joints

By mapping circles in two-dimensional planes to three-dimensional intersection curves between tubular members, a complicated three-dimensional mesh generating procedure for tubular joints is changed to a procedure similar to a two-dimensional case. More detailed modeling of welds and cracks can be included to analyze the fracture behavior of cracked tubular joints.

Cao J.J. et al (1998) in their paper “Crack modeling in FE analysis of circular tubular joints” stated that “in order to explore fracture behavior of cracked tubular joints, three-dimensional quadratic solid elements should be used throughout cracked tubular joints with detailed modeling of cracks. In their modeling the mesh generation method proposed for tubular joints simplifies a three-dimensional mesh generation procedure into a procedure similar to a two-dimensional case. By using this method, more detailed

modeling of welds and cracks can be included in tubular joints. For modeling of the cracks without propagation, three or more rings of focused elements should be used, each ring with eight elements and tied nodes being used for a crack tip. For modeling of the cracks with propagation, a multi-tip model with spring's initially connecting successive crack tip positions can be used. The springs can be released successively during an analysis based on material tearing resistance behavior. Hence, crack propagation is simulated while focused elements remain around the crack tip. In order to generate crack tip elements for surface cracks, a coordinate transformation procedure can be used. High quality meshes for cracked tubular joints can be generated by using the procedure proposed in this paper and more accurate crack driving forces (J-integral and Crack Tip Opening Displacement) can be obtained by the analyses using these meshes."

2.5.2 Fatigue Performance of Cracked Tubular Joints

Generally, the static strength of any tubular structures is the primary performance criteria at the design stage. However, most tubular structures are always subjected under severe cyclic loading conditions in practice, and fatigue cracks may develop resulting in fatigue damage. "It has been concluded that fatigue damage is the most frequent single cause of repairs, representing 25% of all repairs to steel platforms in the North Sea (Stacey and Sharp 1997)".

Chiew, S. et al (2004) carried out a group of experimental fatigue tests on three tubular T-joints with the same geometrical parameters subjected to in-plane bending (IPB) only, a combination of IPB and out-of-plane bending (OPB), and a combination of axial loading, IPB and OPB respectively. "Static tests were first carried out to investigate the Hot Spot Stress (HSS) distribution along the intersection of chord and brace, and to

determine the peak HSS and its location when the joints were subjected to these load cases. The peak HSS location was used to determine the placement of the probes. An alternating current potential drop technique was then employed to monitor the crack growth and crack shape development on the joints at a preset number of cycles. The experimental data were recorded, and the fatigue performance of the three T-joints subjected to basic and combined load cases were investigated. The crack growth curves and crack growth rate on each specimen were presented." The results in their paper confirmed that the United Kingdom Department of Energy tubular joint fatigue design T curve derived from a single axis test data is conservative even for combined load cases.

Although the finite element (FE) analysis is still the most widely used method to accurately analyze cracked tubular joints, the FE models must be validated, and their accuracy in terms of fatigue predictions must be quantified by comparing against experimental results (Haswell and Hopkins, 1991).

Chiew, S. et al (2004) also carried out a systematic finite element modeling of tubular Y-joints with any surface crack and located at any position along the brace–chord intersection. "Three-dimensional (3D) solid elements were used to model full-scale cracked tubular joints because they can model the major defects of the joints, and 3D elements models can provide the best results comparing the results from models with different types of elements (Herion et al. 1996). This modeling method is then used to analyze three tubular T-joint specimens which were tested to failure earlier, and they were subjected to IPB only, a combination of IPB and OPB, and a combination of AX, IPB, and OPB, respectively. The numerical results compared favorably with the

experimental results based on the Paris' law, and all of these results demonstrate that the proposed model is consistent and reliable."

2.5.3 Stress Intensity Factors in Cracked Tubular Joints

In the offshore industry, fatigue assessment is often the main concern during the structure's life. Due to the fabrication defects or damage in the service, cracks exit in nearly all tubular joints. The stress intensity factor (SIF) is frequently used as a design parameter to determine the nature of the fracture process and it can be used to determine the residual life of a fatigue damaged structure.

Chiew, S. et al(2001) developed a meshing method on the geometrical model compatible with the American Welding Society (AWS) standard. "This well-graded finite element meshes were generated for a T-joint to obtain the stress intensity factors (SIFs). The numerical analysis indicated that the FE models generated are appropriate to the geometry of the joints since converging values of SIFs were obtained as the meshes used were refined. The accuracy of the Mode I, Mode II and Mode III SIFs demonstrates that the proposed model is reliable".

$$K_I = \frac{G}{2(1-\upsilon)}\sqrt{\frac{2\pi}{r}}v_n$$

$$K_{II} = \frac{G}{2(1-\upsilon)}\sqrt{\frac{2\pi}{r}}u_r$$

$$K_{III} = G\sqrt{\frac{2\pi}{r}}w_t$$

u_r, v_n, w_t denote the local radial normal and tangential displacements of the nodes on the crack surface, G is the shear modulus and v is Poisson's ratio.

2.6 Need for Research

Research has shown that several parameters of HSS connections affect the way the connections behave when certain load is applied on the truss model. Different geometric parameters give different stress and strain pattern as well.

There is a substantial amount of research available that involves the finite element modeling of all types of K, X, N, Y and T tubular connections. Several methods have been reviewed and considered to develop a technique that would be suitable for this research. The methods that were developed and implemented by Lee, C. K. et al (2001) have been identified as the guide for the finite element modeling used in this research.

However, three-dimensional finite element analysis of a complete HSS truss can be complex and time-consuming. Due to the complex nature of the finite element analysis codes, this method has limited application. It can be used in research area but cannot be widely used by structural engineers in their real-world projects. Therefore, there is a need to develop a simplified modeling method that can be implemented by using commonly available commercial software and easily employed.

Chapter 3 – Finite Element Modeling

3.1 Overview

The purpose of this phase was to develop a validated finite element model and obtain the analysis result that can be compared with future experimental data. To achieve this, nonlinear inelastic analyses were conducted for both the weld part and the three HSS members of the joint. Correspondingly, nonlinear material properties were assigned to the weld and the steel. Several failure models including chord wall plastification, punching shear rupture, chord shear yielding and uneven load distribution (weld rupture or local buckling) might be generated after the ultimate yield point (F_u) of the material and the loading condition were defined. Nonlinear analysis can yield accurate results because it employs non-linear, large-deflection, static analysis to predict buckling, rupture and yield loads. This technique employs a nonlinear static analysis with gradually increasing loads (in several load steps) to seek the load level at which the structure becomes unstable. Multi-linear material was used in this analysis.

The commercial finite element software ANSYS was chosen for the implementation of this overlapped K connection model because of the flexibility it provides in defining the connected different parts in FE level and the local material constitutive law.

There was a great deal of detail involved in the creation of the three dimensional models of full scale tubular connection. In an effort to provide an organized overview of the steps involved in the model development, this chapter is separated into five main sections: General Description, Welding Design, Finite Element Model, Load and Boundary Condition and Summary.

3.2 General Description

3.2.1 Geometry of the Connection

In order to accomplish the mission of this research, certain geometric features needed to be specified. Steel pipe with the properties of Cold formed HSS A500 Shaped, Grade B, yield strength F_y =46*ksi*, tensile strength F_u=58*ksi*, was selected. For chord member, square HSS, $14\times14\times{}^{3}\!/_{8}$ or $14\times14\times{}^{5}\!/_{16}$, with wall slenderness ratios of 37.1 or 45.1, was chosen. For two branch members, square HSS, $8\times8\times{}^{1}\!/_{4}$ or $8\times8\times{}^{3}\!/_{16}$, with wall slenderness ratios of 31.3 or 43, was chosen. Therefore, a branch to chord width ratio of 0.57 was set up. In addition, the overlap was set to 50% and both brace angles were set to 45°. As shown in Fig 3.1, the overlap ratio was defined by p/q. The p value was settled when the branch HSS and brace angles were set: $p = 8\times\sin(45^\circ) = 11.3137in$. In order to satisfy the requirement of 50% overlapped connection, the q value was set to 5.6569*in*.

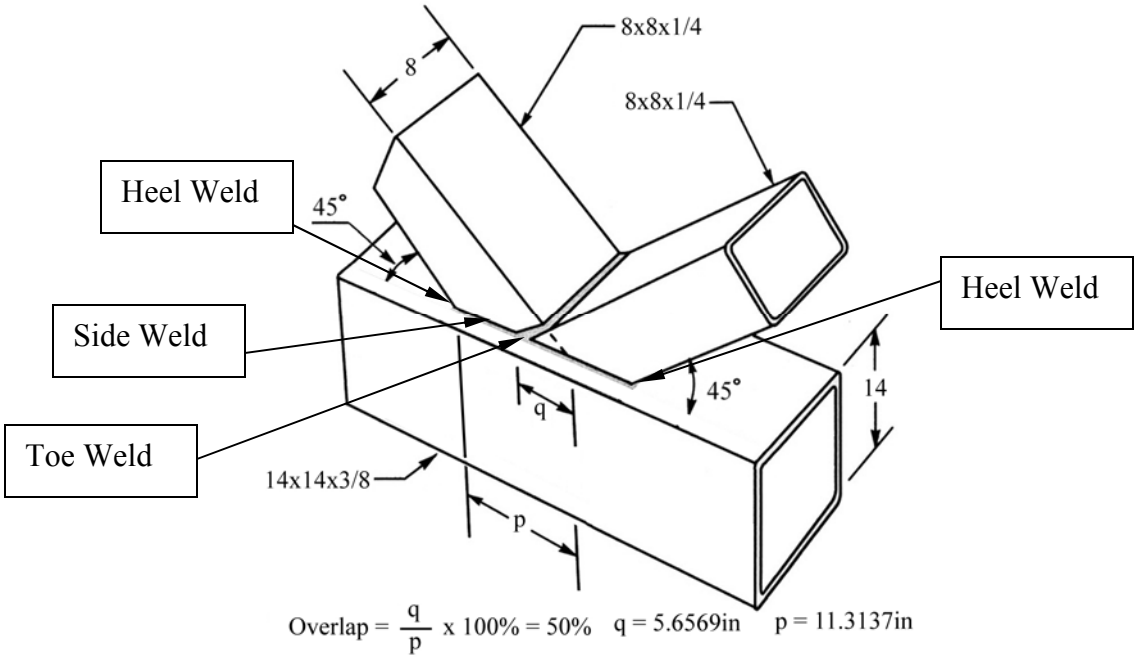

Figure 3.1 - Sample K-Connection for Modeling

The chord member length was set to L = 84.97*in* in order that $\alpha = 2L/H = 12.2$ and thus preclude the end effects caused by the chord member support. The branch member length was set to L=29.9*in* to eliminate the end effects of the branch support. Investigation had been done on the model in which the chord member length was set to 71*in* and the branch member length was set to 25.4*in*. There was no significant change (less than 0.5%) on the load-displacement. Therefore, the length assigned to the chord and the branch was considered acceptable.

In the AISC Manual, Section K23, criteria and limits have been set up for rectangular HSS connections. The HSS connection design is considered acceptable only when the connection configuration is within the following limits:

(1) Joint eccentricity: $-0.55H \leq e \leq 0.25H$, where H is the chord depth and e is positive away from the branches.

$e = (-7 + 4 / \sin(45) / 2) / 14 \times H = -0.29H$ ***PASS***

(2) Branch angle: $\theta \geq 30°$

$\theta = 45°$ ***PASS***

(3) Chord wall slenderness: ratio of overall wall width to thickness less than or equal to 30 for overlapped K-connections. Under investigation in the thesis project.

(4) Tension branch wall slenderness: ratio of overall wall width to thickness less than or equal to 35 Under investigation in the thesis project.

(5) Compression branch wall slenderness: ratio of overall wall width to thickness less than or equal to $1.1(E/F_{yb})^{0.5}$ for overlapped K-connections

R*equirement* $= 1.1 \times (29000 / 46)^{0.5} = 27.62$

Under investigation in the thesis project.

(6) Width ratio: ratio of overall wall width of branch to overall wall width of chord greater than or equal to 0.25 for T-, Y-, cross- and overlapped K-connections

Width ratio = 8/14 = 0.57 ***PASS***

(7) Aspect ratio: $0.5 \leq$ ratio of depth to width ≤ 2.0

Aspect ratio = 14/14 = 8/8 =1 ***PASS***

(8) Overlap: $25\% \leq O_v \leq 100\%$, where $O_v = (p/q) \times 100\%$. p is the projected length of the overlapping branch on the chord; q is the overlap length measured along the connecting face of the chord beneath the two branches. For overlap connections, the larger (or if equal width, the thicker) branch is a "thru member" connected directly to the chord

Overlap = 50% ***PASS***

(9) Branch width ratio for overlap connections: ratio of overall wall width of overlapping branch to overall wall width of overlapped branch greater than or equal to 0.75

Branch width ratio = 8/8 =1 ***PASS***

(10) Branch thickness ratio for overlap connections: thickness of overlapping branch to be less than or equal to the thickness of the overlapped branch

Branch thickness ratio = 1, because same sections were used for the overlapped and overlapping branches. ***PASS***

(11) Strength: $F_y \leq 52ksi$ for chord and branches

$F_y = 46ksi$ ***PASS***

(12) Ductility: $F_y/F_u \leq 0.8$

$F_y/F_u = 46 / 58 = 0.79$ ***PASS***

Different chord member compression loads were also under investigation. Table 3.1 describes the models loads and geometric configurations.

Table 3.1 - Testing Model Configurations

	Geometric Configuration 1	Geometric Configuration 2	Geometric Configuration 3	Geometric Configuration 4
Chord member Branch Member	14 ×14 × 3/8 8 × 8 × 1/4	14 ×14 × 3/8 8 × 8 × 3/16	14 ×14 × 5/16 8 × 8 × 1/4	14 ×14 × 5/16 8 × 8 × 3/16
Chord Step Load Case I	0 *kips*	0 *kips*	0 *kips*	0 *kips*
Chord Step Load Case II	188.845 *kips*	224.23 *kips*	107.37 *kips*	142.76 *kips*
Chord Step Load Case III	377.69 *kips*	448.45 *kips*	214.75 *kips*	285.53 *kips*

3.2.2 Introduction of ANSYS9.0

ANSYS is a three-dimensional finite element analysis commercial tool that can be used for a range of structures. ANSYS Structural provides all the power of ANSYS nonlinear structural capabilities—as well as all linear capabilities—in order to deliver the highest-quality, most-reliable structural simulation results available. A full complement of nonlinear elements, nonlinear and linear material laws and inelastic material models is provided in this software. It not only offers the fanciest intuitive, tree-structured GUI for easy definition of complicated shaped models, but also gives the traditional code input method for some intricate material models.

Through identifying the key-points, lines, areas and volumes, either of the methods can be used to build up a 3-d model by themselves. By using the mapping tools provided by the software, a well defined mesh can be established based on the geometry of the volume. The advantage of the GUI is that it gives users the most direct view of what have been finished according to the user commands. The disadvantage of the GUI is that it is difficult to accurately pick up certain points including nodes and key points. On the contrary, the ANSYS code has the well organized input form and can identify the exact points as many as possible. However, it requires strong 3-d imagination ability to extract the model from the pure text commands. The second method called “direct generation” was selected to build up the HSS joint in order to give the complete control of every node of the model and make the model easy to revise.

3.2.3 Material Properties

Both static and dynamic analyses are included in the ANSYS package. Only static analysis, used to determine displacements, stresses, etc. under static loading conditions, is

adopted in this K-joint analysis procedure. In addition, both linear and nonlinear static analyses are provided. "Nonlinearities can include plasticity, stress stiffening, large deflection, large strain, hyper-elasticity, contact surfaces, and creep" (ANSYS 2004). Nonlinear structural behavior arises from a number of causes, which can be grouped into these principal categories:

- Changing status: Many structural features exhibit nonlinear behavior that is status-dependent
- Geometric nonlinearity: If a structure experiences large deformations, its changing geometric configuration can cause the structure to respond nonlinearly.
- Material nonlinearity: Nonlinear stress-strain relationship is another primary reason of nonlinear structural behavior.

In order to get the correct solution from the model, both geometric and material nonlinearities were included. To investigate the deformation and how strain-stress developed with the load increasing (in ramp load steps), appropriate nonlinear material properties for steel and weld components were required.

In Fig 3.2 a general metal stress-strain curve is illustrated.

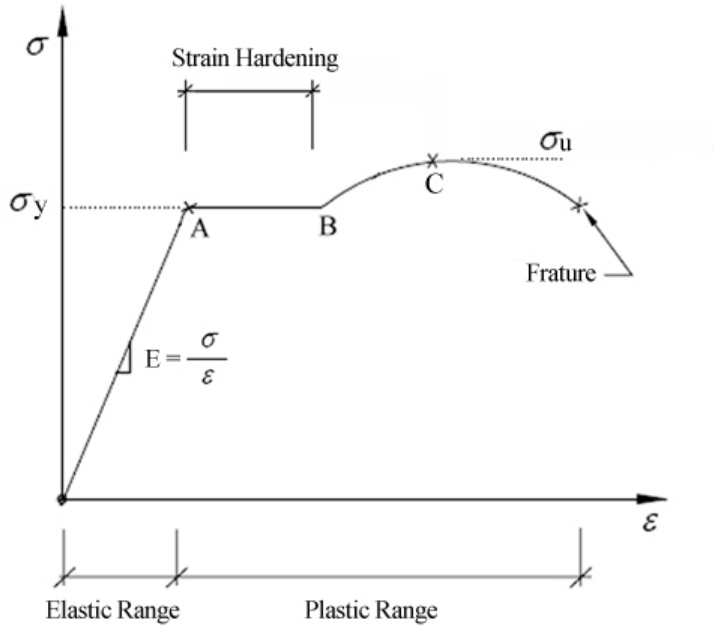

Figure 3.2 - Metal Stress-Strain Curve

In ANSYS, the nonlinear material properties of this model are simplified as multi-linear segments in the stress-strain relationship figure. When ANSYS performs structural analysis, the inelastic material model requires users to input values for elastic material properties (elastic modulus and/or Poisson's ratio) in addition to the inelastic constants that are specific to the model. The elastic material properties must be entered before the inelastic constants are entered otherwise the constants wouldn't be accepted by the program. For the elements representing the structural steel, the elastic modulus used was 29,000 ksi and Poisson's ratio used was 0.3 in the elastic period. All weld parts utilized E70 series electrodes in the connection and same elastic modulus and Poisson's ratio applied as well. According to the data provided by the material test, the stress-strain feature points were input as a part of the material properties. Fig 3.3 and 3.4 show the steel and weld properties used in the ANSYS program. Both material properties were simulated using multi-linear simplification.

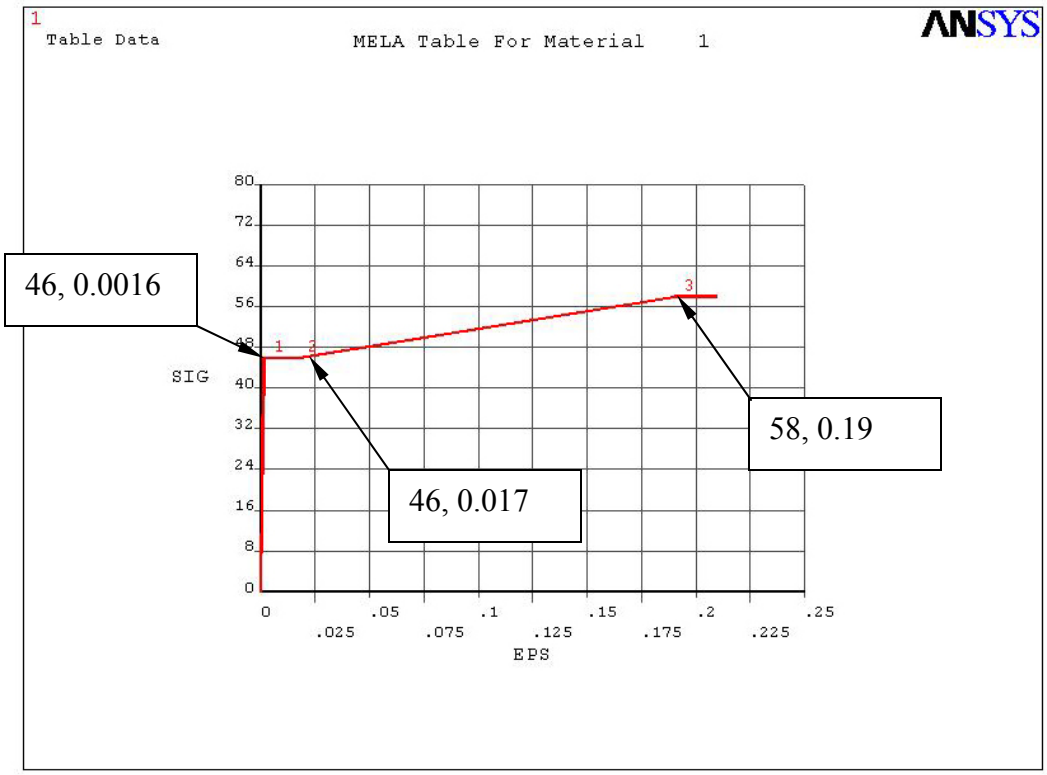

Figure 3.3 - Cold Formed HSS A500 Grade B Stress-Strain Curve in ANSYS

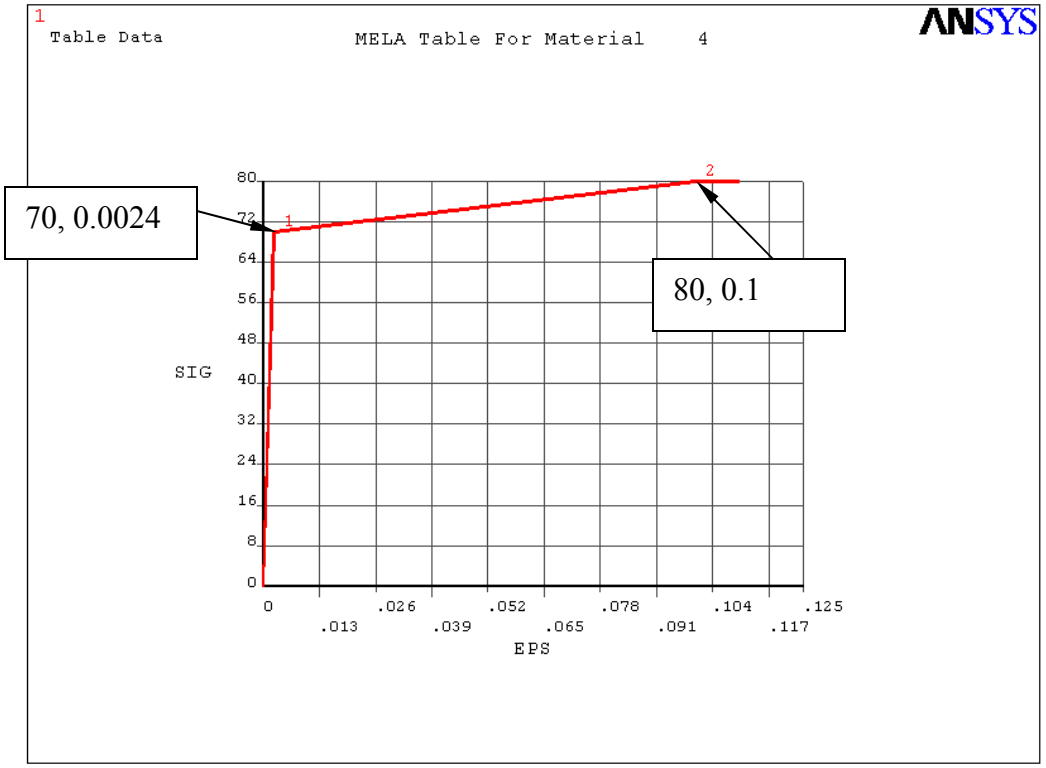

Figure 3.4 - E70 Weld Stress-Strain Curve in ANSYS

3.3 Welding Design for HSS Overlapped K-Connection

3.3.1 General

Welding is the primary means of joining HSS at connection. There are welding design fabrication and inspection requirements that are unique to HSS connections. Additionally, there are some regulations that designers should follow in order to achieve economical structures. In the Hollow Structural Sections Connections Manual (1997), the following provisions are clearly stated to help structural engineers choose the welding forms. "Specify fillet welds rather than groove welds whenever possible, unless the size of fillets becomes such that a groove weld is more economical (generally, when fillet legs are around 5/8 in). When fillets are not feasible, use partial joint penetration (PJP) groove welds where permitted. Avoid complete joint penetration (CJP) groove welds except for butt splices or where required for fatigue or seismic applications."

3.3.2 Welding Details

Weld regions around the branch HSS can be divided into toe zone, side zone, and heel zone according to the angle generated by the two HSS. The general weld pre-qualified details is shown in Fig 3.5.

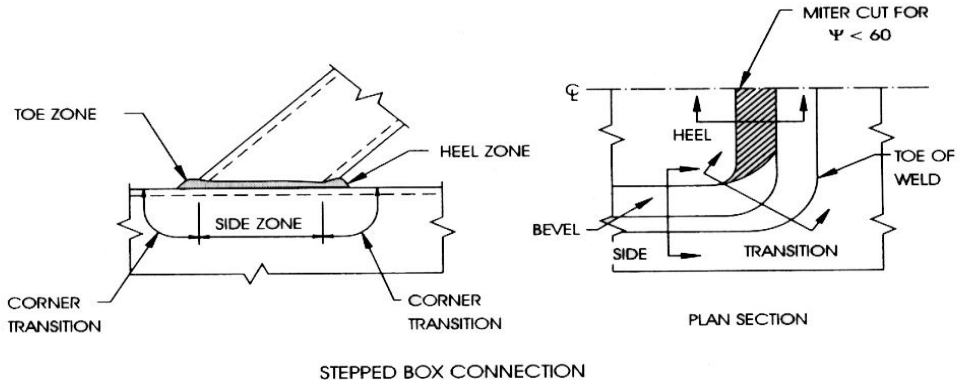

Figure 3.5 - Welding Zones
(AWS 2000 Figure3.5)

The weld connecting the chord HSS and branch through HSS was investigated first. According to the LRFD design manual, Design Strength = $\phi F_w A_w$. Following "Hollow Structural Sections Connections Manual 1997", fillet welds were used rather than groove welds. So fillet welds were tested first. The following procedure is regarding the weld form calculation.

Product: Cold Formed HSS, ASTM A500, Grade B

F_y Minimum Yield Stress (*ksi*): 46

F_u Minimum Tensile Stress (*ksi*): 58

$\phi Rn = 0.75\ (0.6 \times 70)\ (0.707 \times 1/16) = 1.392\ k/in/1/16$

Let D = no. of 1/16*in*

For Fillet Weld Shear on effective area,

Resistance Factor $\phi = 0.75$

Nominal strength = 0.6FEXX

FEXX = 70 *ksi*

$t_{eff} = 0.707\ t$

t = 1/16 *in*

Strength of Welded Joints $\phi Rn = 1.392$ D (per inch)

Strength of Branch Member $0.9F_yA_g$

$1.392D \geq 0.9FyAg$

D: Number of 1/16 weld

Ag for branch pipe $8 \times 8 \times ¼ : 0.233 \times 1 = 0.233 in^2$ (per inch)

$D \geq 0.9 \times 46 \times 0.233 \div 1.392$

$D \geq 6.93$ Let D = 8

Use weld $t = 8 \times 1/16 = 1/2 in = 0.5 in$

Check for maximum requirements for fillet welds:

From "Manual of Steel Construction, LRFD" TABLE 8-1

ASTM Requirements for Properties Affecting Weld ability of Steels

A500 HSS, Grade B, Maximum Thickness = 5/8 *in.* ***PASS***

Check for minimum requirements for fillet welds:

From "Specification for Structural Steel Buildings 2005" TABLE J2.4

Thickness = 3/16 *in* ***PASS***

From "Hollow Structural Sections Connections Manual 1997" Fig 2.7

$0.233 in$ for TOE, SIDE ZONE

Thickness $= 0.233 \times 1.5 = 0.3495 in$ ***PASS***

For both side zone and heel zone, fillet weld is used as well.

The general pre-qualified side and heel weld details are shown in Fig 3.6.

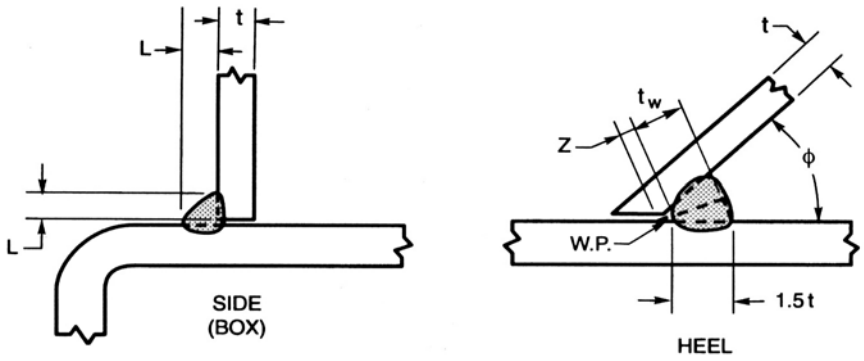

Figure 3.6 - Side and Heel Zone Fillet Weld
(AWS 2000 Figure2.9)

The minimum L requirements are listed in Table 3.2

Note: 1. t = thickness of the thinner part

2. L = minimum size (see table 3.1), E: effective throat

3. $\phi = 15^{o}$ Minimum, not pre-qualified for under 30^{o}

Table 3.2 - Minimum L Requirements
(AWS 2000 Figure 2.9)

	E = 0.7 t	E = t	E = 1.07 t
Heel < 60°	1.5 t	1.5 t	Larger of 1.5 t Or 1.4 t + Z
Side ≤ 100°	t	1.4 t	1.5 t
Side 100°-110°	1.1 t	1.6 t	1.75 t
Side 110°-120°	1.2 t	1.8 t	2.0 t
Toe > 120°	t Bevel	1.4 t Bevel	Full Bevel 60°-90° Groove

For fillet welds, the critical stress in a fillet weld is always considered to be a shear stress. Therefore, tension, compression, and moments acting upon a fillet-welded joint can be resolved into shear in the weld throat.

For both side zone and heel zone, effective throat thickness can be large enough to give the fillet weld required strength for the connection.

The pre-qualified side and heel weld details in this research are shown in Fig 3.7.

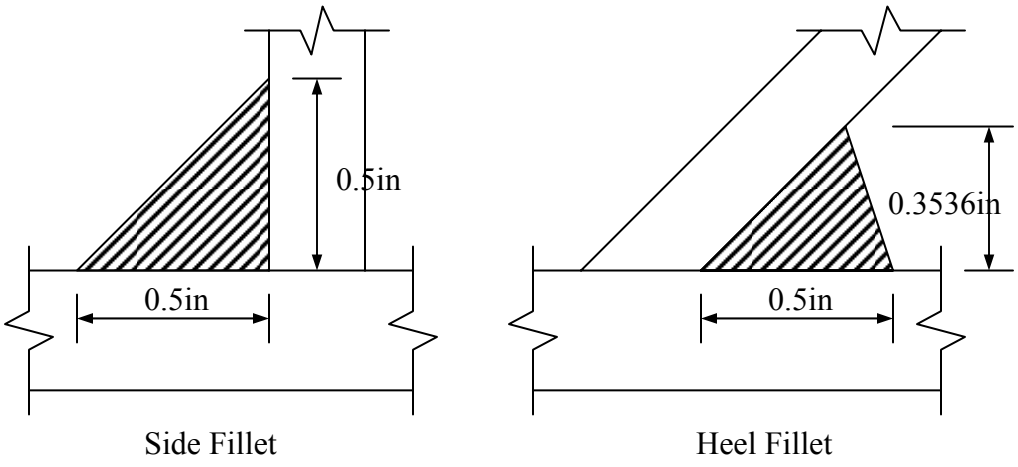

Figure 3.7 - Side and Heel Zone Fillet Weld Detail

For toe zone, effective throat thickness can't be large enough to give the fillet weld required strength for the connection. PJP is the proper welding form for use in this situation.

The general pre-qualified weld toe details are shown in Fig 3.8. The pre-qualified toe weld details in this research are shown in Fig 3.9.

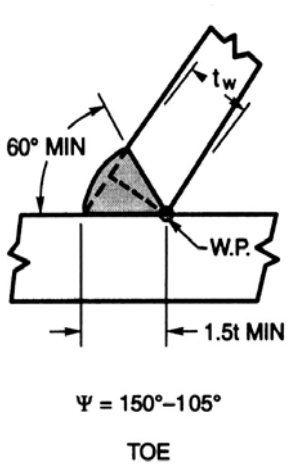

Figure 3.8 - Toe Zone Fillet Weld
(AWS 2000 Figure3.5)

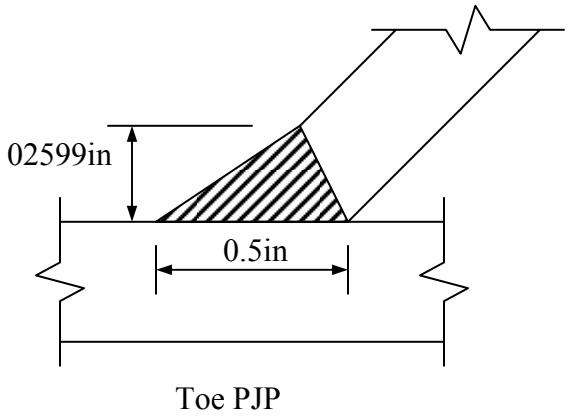

Figure 3.9 - Toe Zone PJP Weld Detail

The weld between the chord HSS and branch overlapping HSS was investigated next. The weld in the heel and side zones was similar to that in the through HSS. Fillet and flare-bevel weld were both used to connect the two branch HSS. According to the geometry of the two HSS, fillet weld was used to connect the flat plates of both branches. Flare-bevel weld was only employed between the outside corner of the through HSS and the bottom of the side plate of the overlapping HSS.

The general pre-qualified flare bevel groove weld details are shown in Fig 3.10. The pre-qualified flare bevel groove weld details in this research are shown in Fig 3.11.

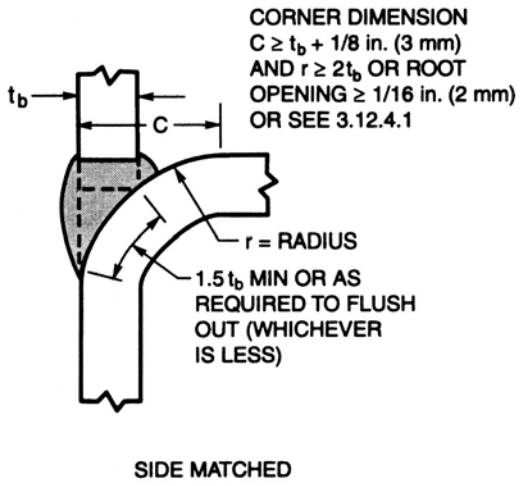

Figure 3.10 - Flare-bevel-groove Butt joint Zone Weld
(AWS 2000 Figure3.5)

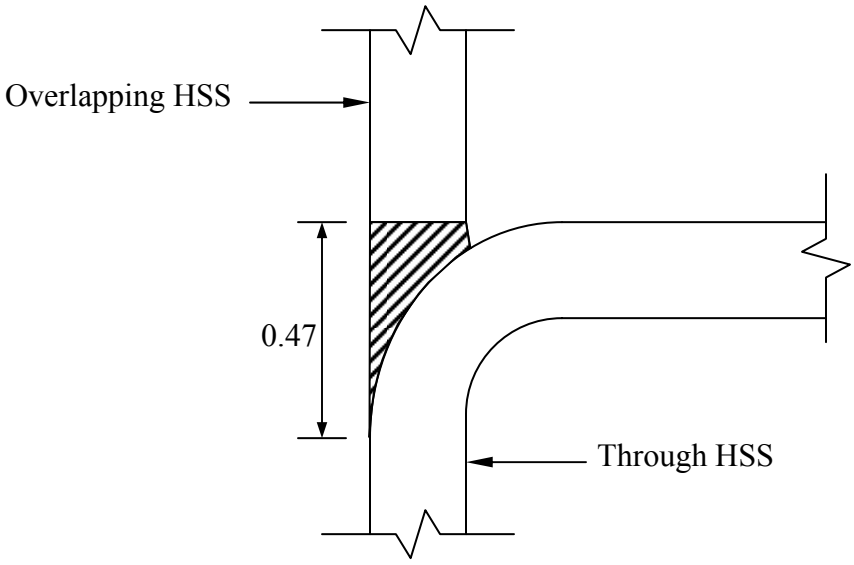

Figure 3.11 - Butt joint Zone Weld Detail

3.4 Finite Element Model

The following paragraphs in this section will outline the modeling techniques used and the development of each component of the finite element models. These components include the chord HSS member, branch through HSS member and branch overlapping HSS member.

3.4.1 Elements Type

"Shell elements have been used widely to model tubular joints, but welds cannot be modeled properly by using shell elements. Solid elements exhibit a high compatibility to model the irregular shape weld connected to the tube. Although a combination of shell elements and solid elements can be used to describe a joint, a comparison of the results from models with different types of elements shows that the best results were provided by models using three-dimensional quadratic solid elements for all tubes and welds" (Cao, J. et al (1998). These 3-D solid elements are available in a number of configurations including certain combinations of the following features: "1. element shapes can be tetrahedrons, pyramids, wedges, or bricks; 2. with or without rotational degrees of freedom; 3. with or without middle-side nodes."(ANSYS 2004)

Only one kind of elements was used in the model with 3-D, 20-node solid element, solid95. Because there are no thermal, magnetic and other non-structural factors affecting the joint, these solid elements belong to the 3-D structural solid element category. Element solid95 is defined by 20 nodes having three degrees of freedom per node: translations in the nodal x, y, and z directions. The element can be degenerated to tetrahedron, pyramid or wedge shape. "Degeneration to the shape of pyramid should be used with caution. The element size, when degenerated, should be small in order to

minimize the stress gradients."(ANSYS 2004) Pyramid element solid95 is best used as filler elements or in meshing transition zones. Tetrahedron element solid95 has a quadratic displacement behavior and is well suited to model irregular meshes. Solid95 is a nonlinear suitable element which can show a geometric nonlinearity in the model. Fig3.12 shows solid95 and its degeneration options.

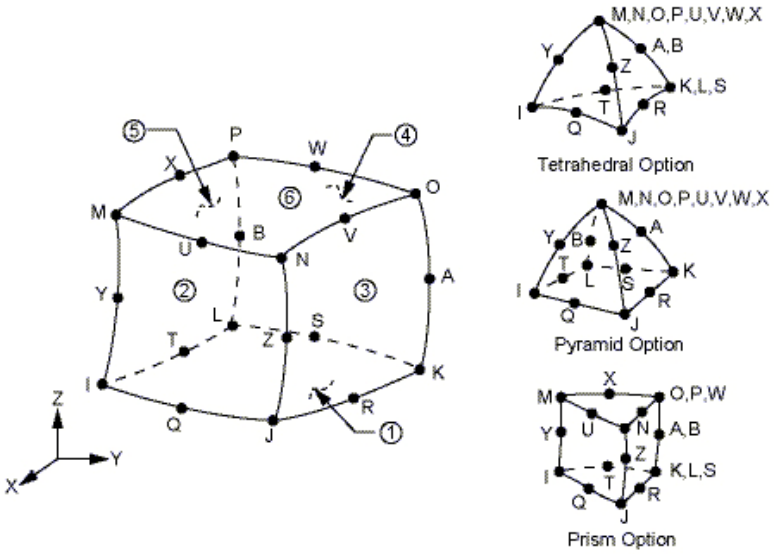

Figure 3.12 - SOLID 95
(ANSYS 9.0 2004)

3.4.2 Meshing Generation

Mesh generation is one of the most important parts in finite element analysis. Defining smooth regular elements and connecting elements by appropriate element types is a common method to build up a good quality mesh model. Errors can be avoided in further calculations when a good quality mesh model is used to assemble element matrix. Various meshing tools are provided by many commercial 3-d modeling programs. Using the tools provided by the software and defining a series of parameters to mesh the 3-d solid volume can automatically establish a good model including a large amount of tetrahedral or brick elements for the model. Refining the mesh on certain area of the

model can make a nice additional contribution to the model. However, such kind of models may not be good enough in many cases because the models need a collection of regular brick elements in some special arrangements to fulfill the unique requirements of the models. The need for different kinds of elements to connect in one region in the model is also a problem for the automatic meshing tools included in the software package.

To generate a suitable model for an overlapping HSS K-connection including three tubular pipes and several welding segments connecting them, neither pure tetrahedral elements nor pure quadrilateral elements meshing is appropriate when using the meshing tools provided by ANSYS. Although quadrilateral elements mesh can generate the regular element arrangement in the model, quadrilateral elements cannot provide sufficient flexibility to simulate the actual shape of the welding part in the connection area of the three pipes and welding segments. On the contrary, using tetrahedral or brick elements to mesh the whole model will generate an irregular mapping on the HSS pipe and a huge number of elements which will increase the time for the program to generate the solution. It is also not practical to refine the mesh on the welding area by using GUI because it is hard to identify the elements in 3-D view and it is even more difficult to pick up elements not on the surface and in irregular environment.

ANSYS provides users with general command code including many common features as other computer program language. A model can be established by using ANSYS code to simulate the welded overlapping K-connection. Node and element positions are established directly in the 3-D space by using the ANSYS code. “DO” loop and “IF” conditionally causes commands are largely used in ANSYS programming. In addition, by writing the code into a file which can be executable in ANSYS, it is more

convenient for users to record and revise the code continuously. Identifying certain nodes or elements is not a mission impossible, but it needs a clear and strong 3-d imagination from the simple command codes.

3.4.3 Chord HSS

Based on the detailed geometric data, chord HSS nodes were generated by giving their 3-D coordinates and assigning node numbers. By using the node numbers, element can be generated by sharing some or all the nodes with other elements. Round corners and flat plates were joined together to build up the chord HSS model. Chord member model is showed in Fig 3.13.

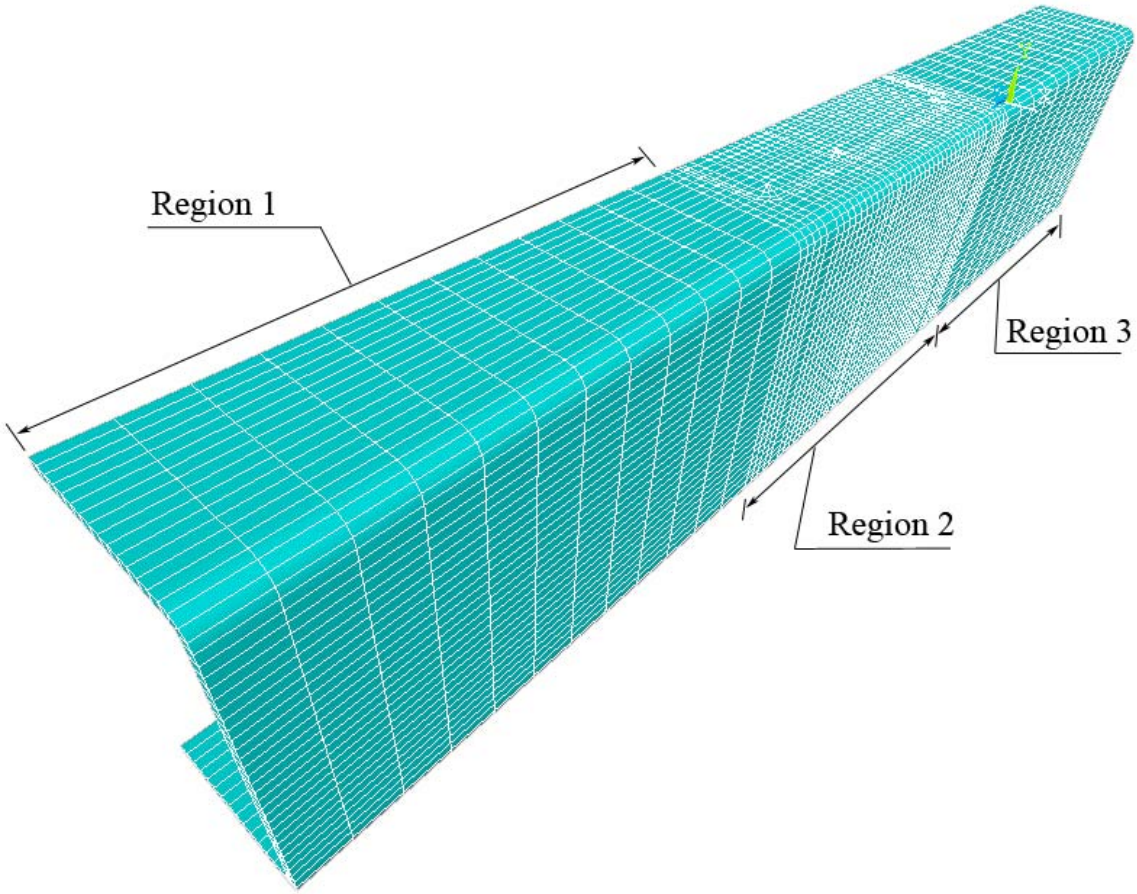

Figure 3.13 - Chord HSS Pipe Model

Coarse elements were used in region 1 and region 3, because they were not connected to the welding area directly. Through them, initial chord compression stress can be distributed evenly along the HSS section and delivered to region 2. Region 2 included a welding area with two branch tubular pipes and additional fine meshed region in order to transfer the branch force into the chord member smoothly. Another reason why the smaller size elements were employed in the region 2 was that a good simulation of plastic and elastic deformation would be generated for the top surface of the chord member after the load delivered from two branch elements increased. Same styles were used to build up the elements to formulate the outside corner and flat plate of the chord HSS.

For the top flat plate of the chord HSS pipe which was not connected with the branch pipe, there was no shape restriction on the formulation of elements regarding the branch pipes. However, certain weld segments, which were some elements in an effort to simulate the welding part in the finite element model, needed to share some nodes and corresponding element face with the top plate of the chord HSS pipe. In this case, welds connecting the outside corner of the branch HSS pipe also had a curve edge on the chord HSS pipe. This curve required the elements of the top plate of the chord HSS member to generate the same curve according to the geometry of the horizontal section of the branch pipe which had a angle of 45^{o} with the chord HSS pipe. Detailed descriptions are shown in the figure below. Because the heel regions of the through and overlapping branch pipe had exactly the same configuration of the weld, only one heel region connecting the overlapping HSS member is showed in the Fig 3.14.

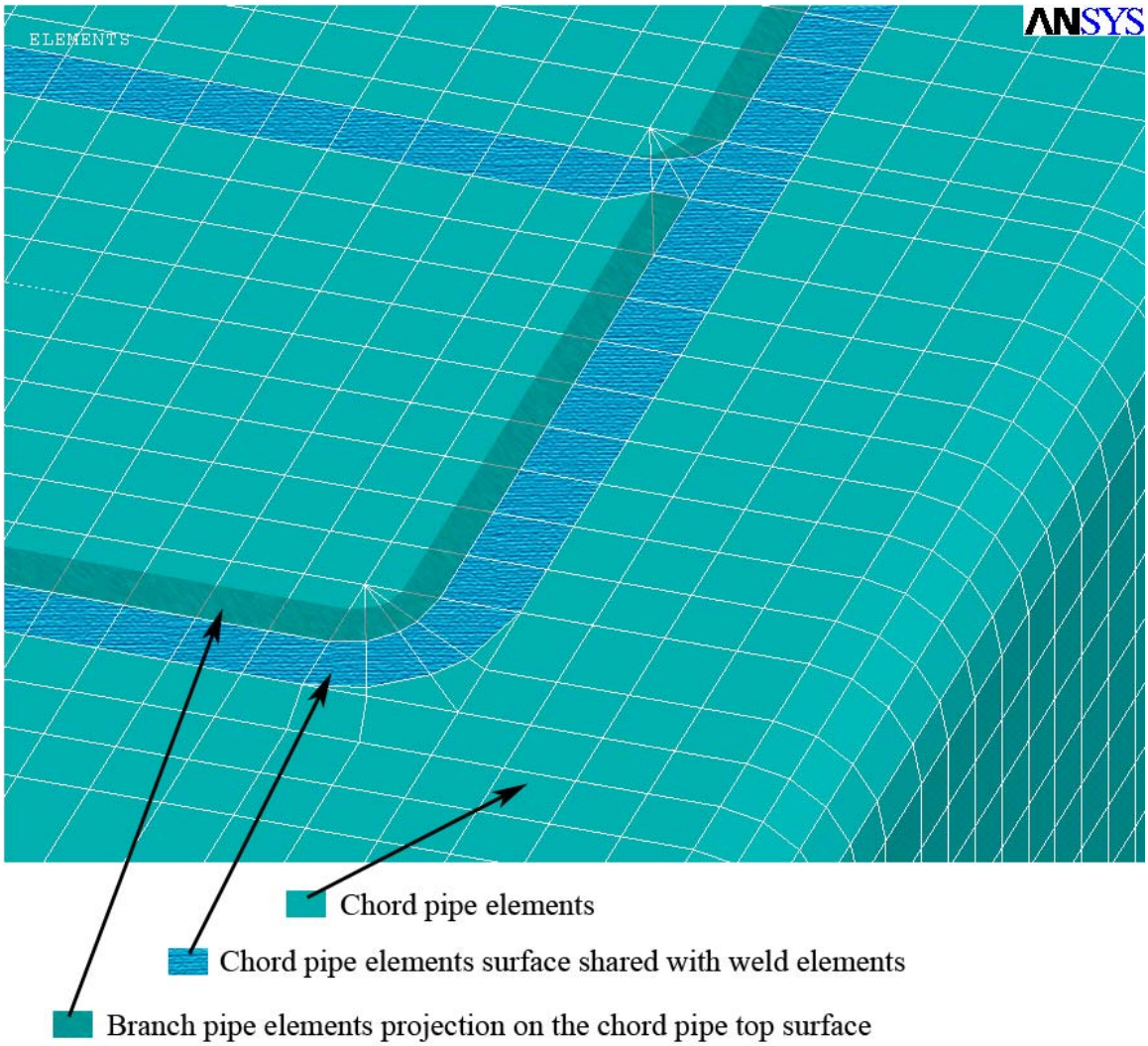

Figure 3.14 - Chord Element Details

3.4.4 Branch HSS

Based on the detailed geometric data and similar technique used for chord pipe, branch pipes were established by solid95 elements and degeneration of element solid95. In order to reduce the number of the nodes and elements yet still maintain enough distance to allow the stress which is transferred from the top of the branch pipe to be evenly distributed, coarse meshed elements were used on the upper portion of the branch pipe. Beginning with the joint of two branch pipes, thinner layer of the elements was used to adapt to the welding part between the two pipes. Wedge shape elements were used for

the overlapping branch HSS pipe edge facing the through pipe. Fig 3.15 shows that the mesh along the branch pipe is even and smooth except the special area connecting the welding on the bottom of the pipe.

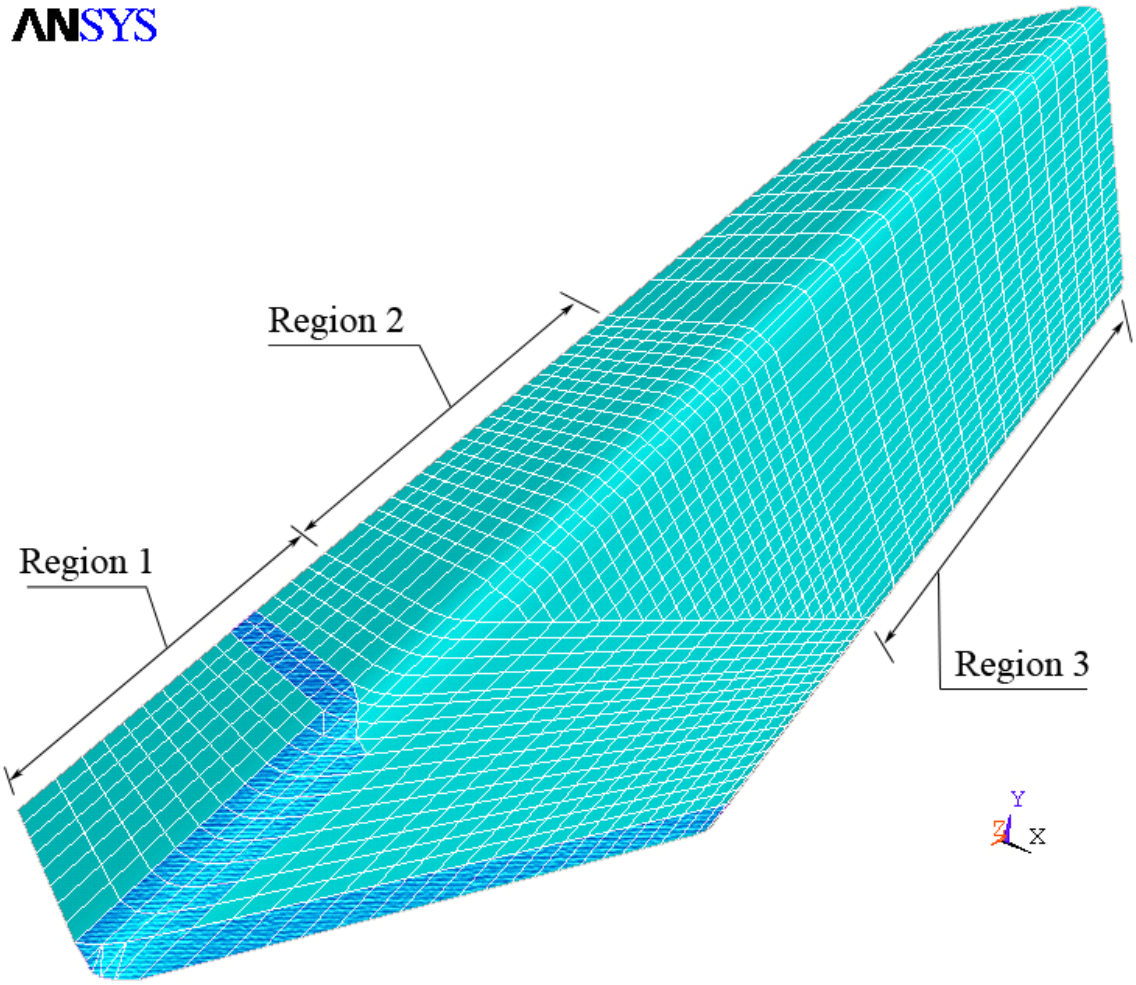

Figure 3.15 - Branch Through HSS Model

Region 1 included thinner element rings where the two branch HSS are connected through the weld. The refined mesh in region 1 provides the possibility that the weld elements between the branches have enough corner nodes to share with the branch elements. To connect the two branch pipes, weld element was needed between the bottom face of the overlapping branch HSS and the outside corner of the through HSS as in a

matched connection case. Some elements of the outside corner of the through HSS were specially refined in order to fit the weld part at the transition area connecting the bevel-groove weld and the toe fillet weld of the overlapping HSS. Region 2 is the transition region which transforms the horizontal branch section to the section with 45 degree slope. Obviously, region 3 included only the coarse meshed elements in order to give the branch enough distance to eliminate the effects coming form the end of the branch. Fig 3.6 shows the detail of through HSS model.

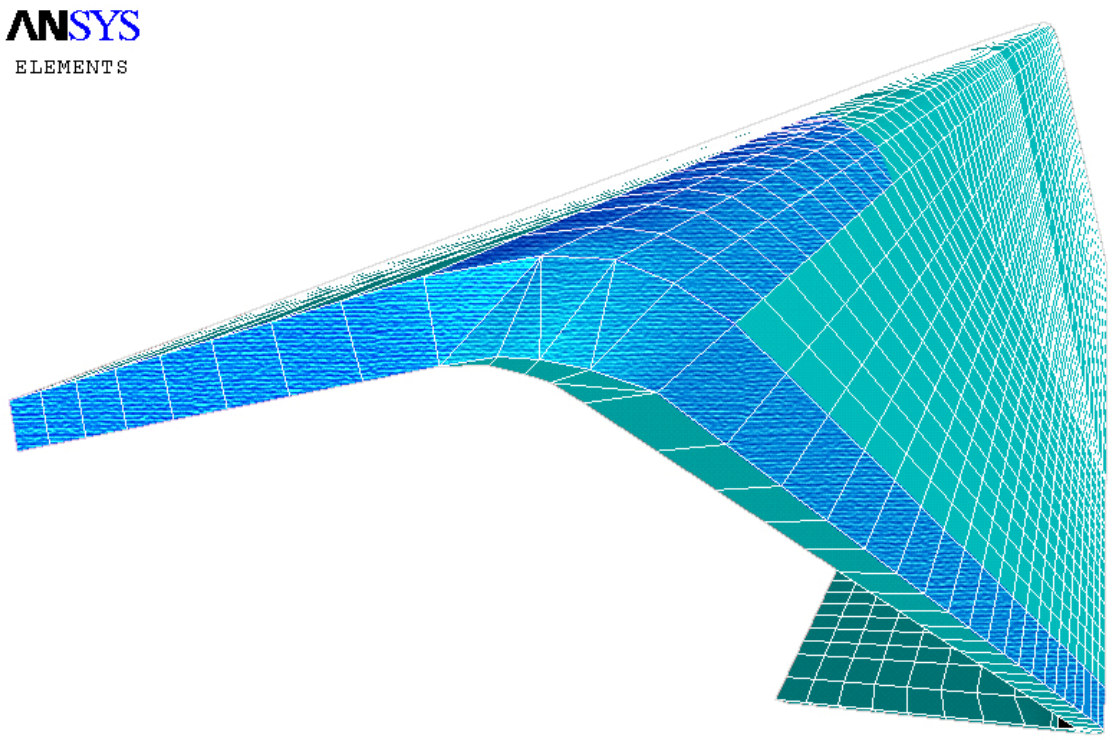

Figure 3.16 - Branch Through HSS Details

In Fig 3.16, the textured area was the element surface of the branch pipe needed to be shared with the weld element which connects the top plate of the chord HSS elements or the other branch HSS elements. Because the toe part of the branch through pipe needed to be designed as a PJP welding form, the corresponding branch pipe elements were built up by using wedge degeneration of the solid95 element. The transformation part of the

corner part of the pipe was also established as gradually transformed from the regular brick element to the wedge element on the toe area of the through pipe. Four main bricks were combined together to formulate the transition region. Each brick was divided into several elements to eliminate unpleasant errors such as warping ratio or matrix Jacobin value exceeding the limit of the program. All four bricks had undivided upper surface in order to connect the following branch pipe elements. Brick 1 has triangle surface to connect the wedge element of the toe region of the branch through pipe. Brick 2 and brick 3 had the same structures. Brick 4 had the intact surface to link the regular brick solid95 element. Fig 3.17 to Fig 3.20 gives the details of how these four bricks were divided into small elements.

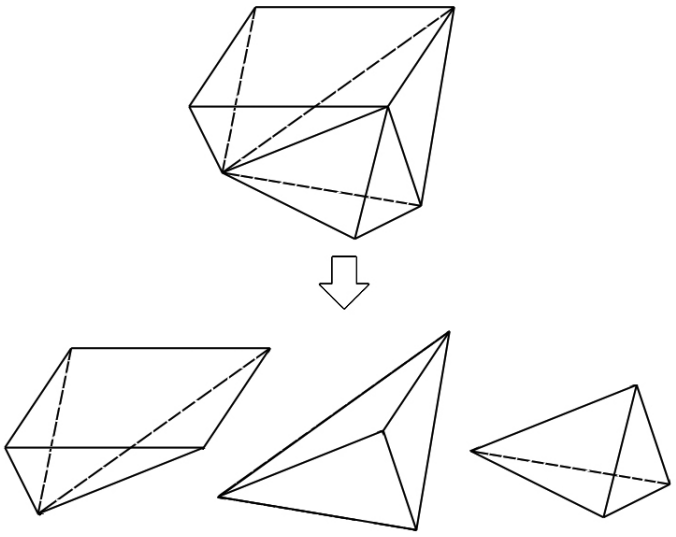

Figure 3.17 - Brick 1 in Transition Region of Through Pipe

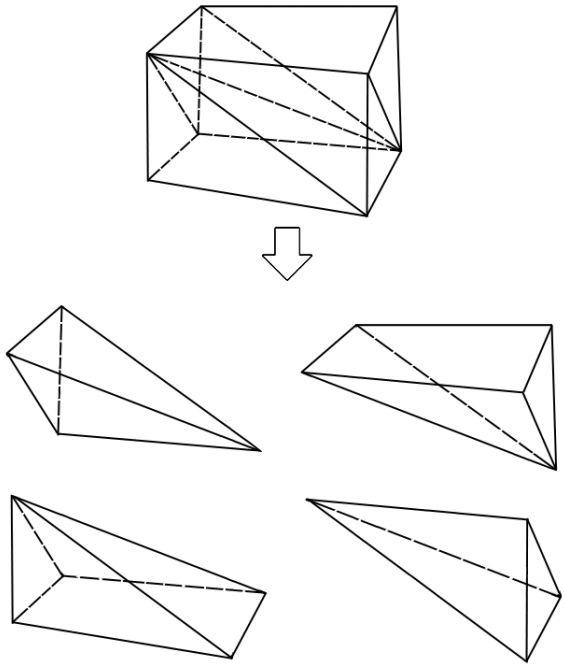

Figure 3.18 - Brick 2, 3 in Transition Region of Through Pipe

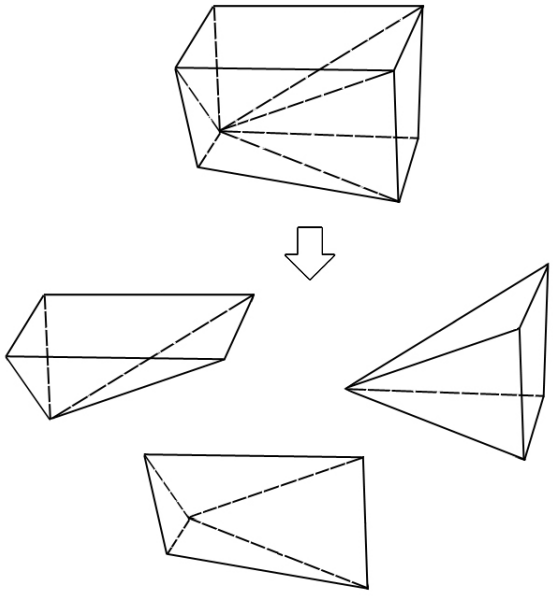

Figure 3.19 - Brick 4 in Transition Region of Through Pipe

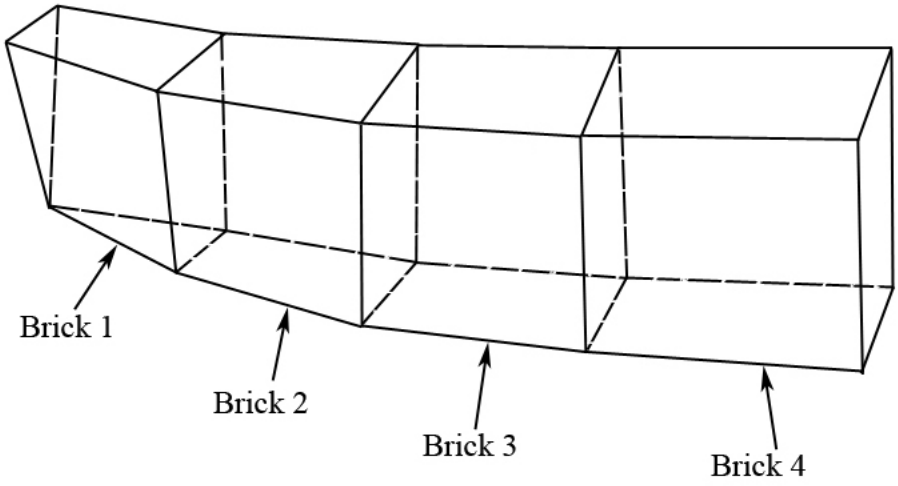

Figure 3.20 - Transition Region of Through Pipe

The same techniques were employed in the overlapping HSS. Three mesh regions were assigned to the different HSS areas as well. There were no difference between the weld connecting the heel region of the overlapping HSS and the through HSS. Wedge elements were used at the side of the overlapping HSS to build up the bottom section which had 45 degree to the horizontal. The elements in the blue area shared face with the weld elements and were refined according to the geometry of the weld. Fig 3.21 shows the mash detail of overlapping HSS branch.

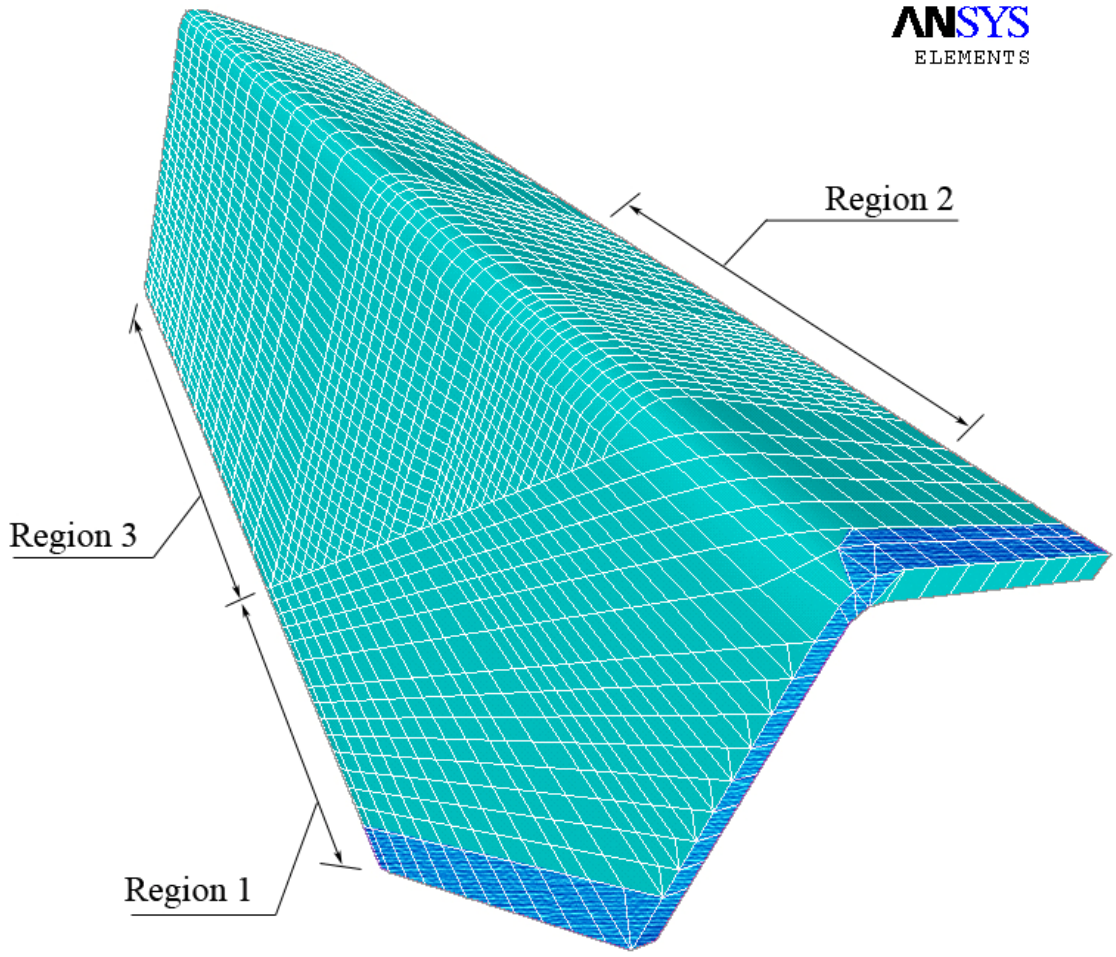

Figure 3.21 - Branch Overlapping HSS Model

3.4.5 Weld Parts in the Connection

It has been clearly explained in many design codes that the weld itself may not be the factor limiting the strength of the joint. The finial purpose of the weld form is to provide a strong enough connection which can guarantee that the joint failure mode excludes the weld failure. Weld forms selected must be adequate to transmit the forces required by the design project. Fillet, PJP and flare-bevel welds were used in this connection and simulated by the program using real sized weld shape and appropriate material property.

Due to the nature of the welds, irregular shaped weld can not be avoided. The degenerated elements such as tetrahedron, pyramid or wedge were used to model the weld part. Through sharing the same nodes with the HSS members of the joint, the weld element could fulfill the function of connecting the three HSS members. So the HSS members were not connected with each other but connected through the weld elements. Fig 3.22 shows the mesh detail of the weld part.

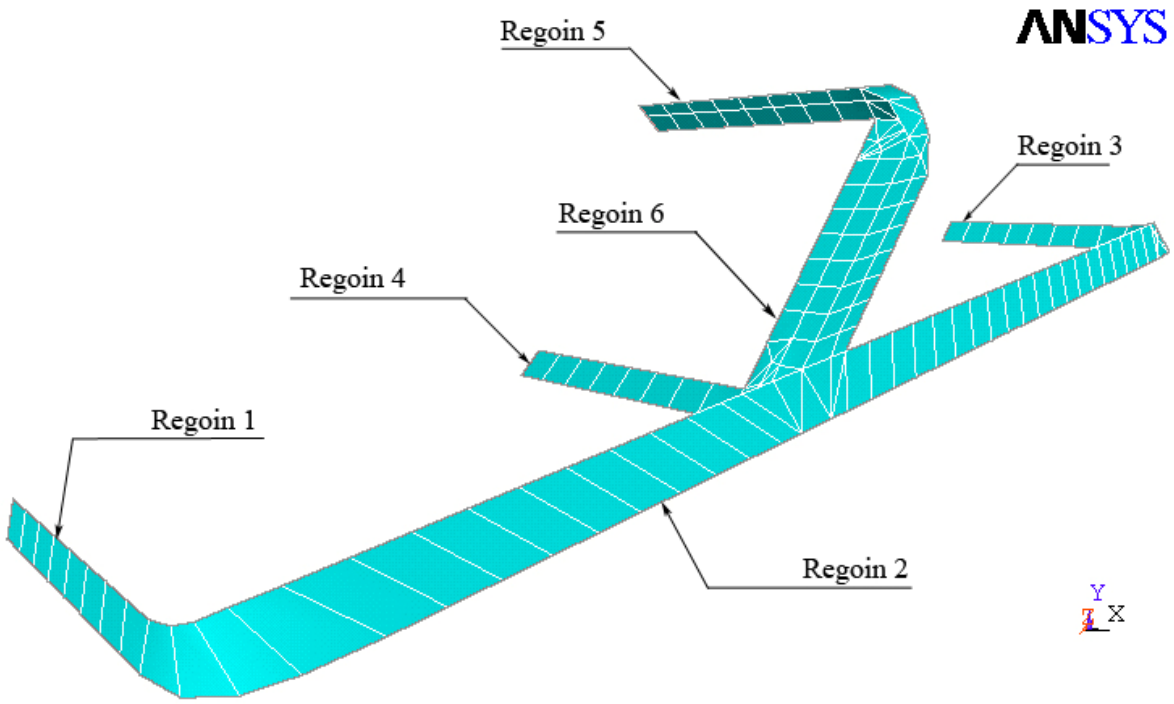

Figure 3.22 - Weld Elements

Region 1: Connecting the heel area of overlapping branch HSS with chord HSS

Region 2: Connecting the side area of two branch HSS with chord HSS

Region 3: Connecting the heel area of through branch HSS with chord HSS

Region 4: Connecting the toe area of through branch HSS with chord HSS

Region 5: Connecting the toe area of overlapping branch HSS with through branch HSS

Region 6: Connecting the overlapping branch HSS with through branch HSS

3.4.6 End Plates

End plates were simulated at both branch and chord ends in order to provide the HSS member ends a stiffer deforming feature in the section compared with the HSS member without any end plates. Since the aim of the model is to simulate the behavior of the HSS truss joint, the end plate had to be built up in the model in corresponding to the real situation. Same elastic modulus was assigned to the end plates but with linear material property which can decrease the running time of the program. Fig 3.23 shows the overview for the connection in this research.

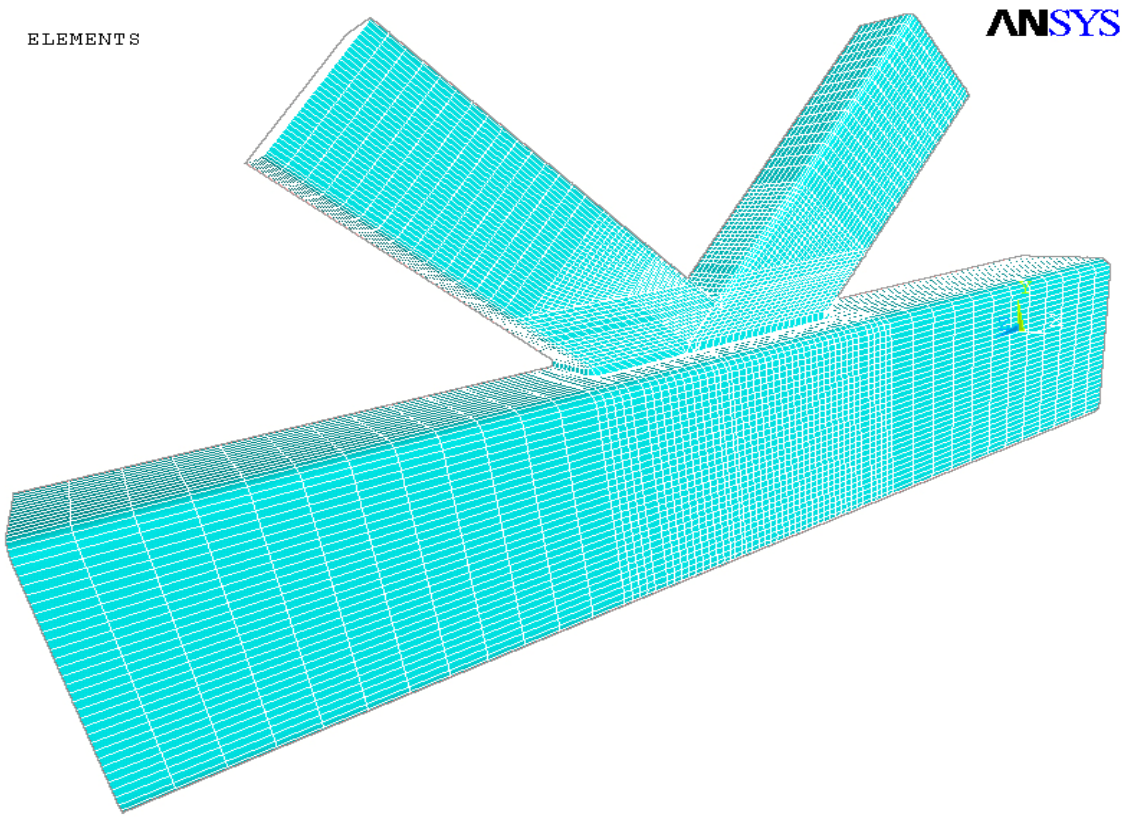

Figure 3.23 - Connection Overview

3.5 Load and Boundary Condition

3.5.1 Boundary Condition

The symmetric feature of the connection geometry and loading can be taken advantage of by investigating only half model. Accordingly, the symmetric boundary condition was also required in the model. Restriction had been put on all the nodes laid on the symmetric plane to prevent the displacement on the x direction which was perpendicular to the symmetric plane. Because there were no rotations on the nodes on the solid95 elements, x-direction movement restriction was enough in the symmetric condition.

Four different types of boundary conditions were considered in the analysis. They were: (a) roller connections at the one end of the chord, fix connection at the other end of the chord member; (b) roller connections at the one end of the chord, fix connection at the other end of the chord member, roller connections at both ends of the branches; (c) roller connection at the one end of the chord member with rotation restriction, fix connection at the other end of the chord member, roller connections at both ends of the branches; (d) roller connection at the one end of the chord member with rotation restriction, fix connection at the other end of the chord member, roller connections at both ends of the branches with rotation restriction. Fig 3.24 shows these four support forms. From the numerical analysis, it was found that the support condition (a) would generate the large displacement and large stress due to the rotation of the connection. The stress distribution of support form (d) was a little different compared with support form (b) and (c) when the branch load was small. However, when the branch load was close to the ultimate connection strength, the displacement, stress and strain results were very

similar for support form (b), (c), (d). The boundary condition (c) was considered to be the most reasonable support form and can best represent the behavior of joints in a HSS truss shows in Fig 3.24.

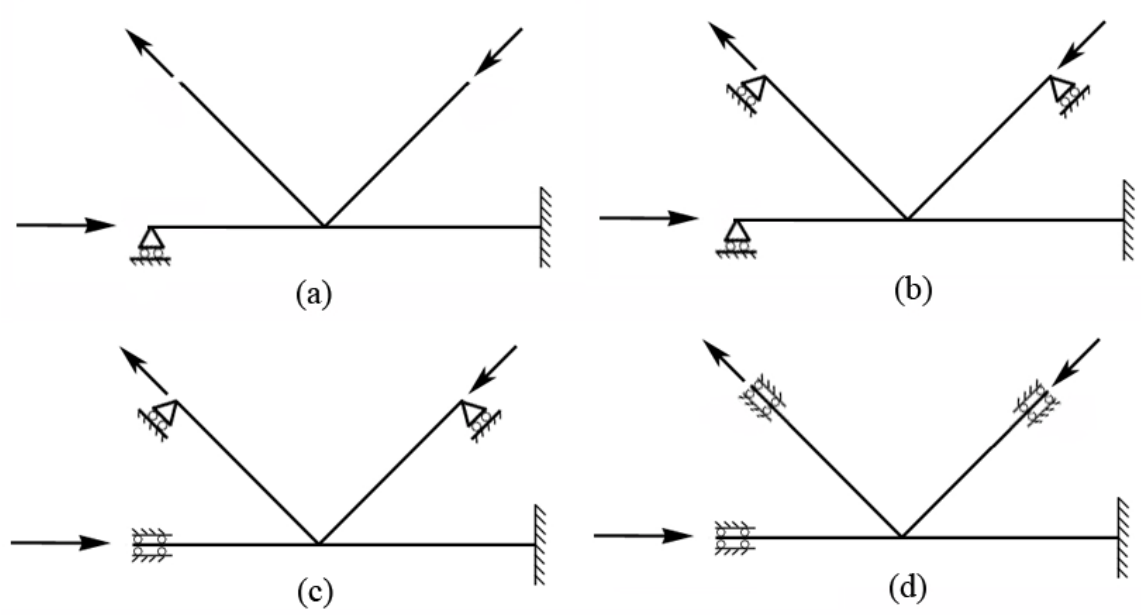

Figure 3.24 - Loading and Boundary Condition

3.5.2 Branch Load

The load directions used are depicted in Fig 3.24. The compression force was executed on the through HSS member while the tension force was given on the overlapping HSS member. It was described in the Lee and Dexter (1999) that "The though-brace-in-compression joints were consistently weaker than the through-brace-in-tension joints. The latter apparently showed fewer tendencies for brace local buckling, though all joints included an element of brace local buckling at or beyond failure." In the summary of this paper, Dexter, E. M. also clearly stated that "The case of a through brace in compression appears to be generally the weaker, limiting joints, though not necessarily so for heavily overlapped joints."

The situation was also verified on the model built up in this thesis by testing a reverse load hierarchy with the tension force on the through HSS member and compression on the overlapping HSS member. The load displacement for the connection with compression force on the through HSS member was higher than the original load hierarchy which meant the former load case offered a larger possibility of reaching the connection failure. Therefore the load hierarchy with tension on the overlapping HSS and compression on the through HSS was proved to be the critical load condition and was used in the following models.

Different from the experimental test which employed the displacement load and recorded the force curve, numerical test of the model only involved several load test steps. To obtain the accurate result, a ramp style load step had to be applied on the model in the analysis. The maximum force for the branch was calculated according to the truss design manual. Starting from zero to the maximum, the load was divided into steps and corresponding analysis results were given out for each step after running the program. Increasing the step number meant more accurate solution for the model. However, due to the geometry complexity of the connection and material nonlinearity, one hour or more was needed for the program to run one load step. Accordingly, 8 ramped branch load steps were selected for every geometry and load configuration.

According to the design manual, for overlapped K-connections, the design strength of the branch, ϕP_n, shall be determined from the limit state of local yielding due to uneven load distribution.

For the overlapping branch, and for overlap $50\% \leq Ov < 80\%$ measured with respect to the overlapping branch,

$P_n = F_{ybi}\, t_{bi} [2H_{bi} - 4t_{bi} + b_{eoi} + b_{eov}]$

b_{eoi} is the effective width of the branch face welded to the chord,

$b_{eoi} = [10/ (B/t)] [(F_y t)/ (F_{ybi}\, t_{bi})]\, B_{bi} \leq B_{bi}$

b_{eov} is the effective width of the branch face welded to the overlapped brace,

$b_{eov} = [10/ (B_{bj} /t_{bj})] [(F_{ybj}\, t_{bj})/ (F_{ybi}\, t_{bi})]\, B_{bi} \leq B_{bi}$

B_{bi} = overall branch width of the overlapping branch, in.

B_{bj} = overall branch width of the overlapped branch, in.

F_{ybi} = specified minimum yield stress of the overlapping branch material, ksi

F_{ybj} = specified minimum yield stress of the overlapped branch material, ksi

For the connections that need to be investigated in this thesis, the ultimate strength of the joints was calculated as follows:

$F_{ybi} = F_{ybj} = F_y = 46 ksi$

$H_{bi} = H_{bj} = 8\ in$

$B_{bi} = B_{bj} = 8\ in$

$B = 14\ in$

Table 3.3 lists the maximum connection strength which was also the maximum load in the numerical test according to the different geometries.

Table 3.3 - Design Strength of the Connection

	Geometric Configuration 1	Geometric Configuration 2	Geometric Configuration 3	Geometric Configuration 4
Chord member Branch Member	14 ×14 × 3/8 8 × 8 × 1/4	14 ×14 × 3/8 8 × 8 × 3/16	14 ×14 × 5/16 8 × 8 × 1/4	14 ×14 × 5/16 8 × 8 × 3/16
	t = 0.349 in t_{bi} = 0.233in t_{bj} = 0.233in	t = 0.349 in t_{bi} = 0.174in t_{bj} = 0.174in	t = 0.291 in t_{bi} = 0.233in t_{bj} = 0.233in	t = 0.291 in t_{bi} = 0.174in t_{bj} = 0.174in
b_{eoi}	2.987	4.000	2.077	2.781
b_{eov}	2.33	1.74	2.33	1.74
P_n *(Branch)* (Maximum Load)	218.48 kips	168.44 kips	208.73 kips	158.68 kips

3.5.3 Chord Load

In HSS truss connection design, chord members are always subject to the force along the chord member direction. Therefore, the effect of the load on the chord member can not be neglected. The analysis of the overlapping K-connection in the thesis also included the chord compression case. In addition to the force that balanced the force transferred from the branch member, three compression force levels were also included in chord member. In order to make the model exhibit the joint behavior under the certain load conditions and avoid the global truss member failure, an applied chord load equal to 80% of the compressive strength was applied on the chord member including the force balancing the branch member load. The ramp load neutralizing the branch force was excluded and other loads were applied in step manner at the beginning of the analysis. In summary, two load manners were included in the chord compression force including the ramp one canceling out the force transferred from branch HSS and the step one designed for the chord member analysis. The chord maximum compression force was calculated as the nominal compressive strength from the steel construction manual.

According to AISC (2005) "The nominal compressive strength, P_n, shall be determined based on the limit states of flexural, torsional and flexural-torsional buckling," using

$$P_n = F_{cr} \times A_g$$

When $\frac{KL}{r} \le 4.71\sqrt{\frac{E}{QF_y}}$

$$F_{cr} = Q \times \left[0.658^{\frac{QFy}{Fe}} \right] \times F_y$$

where

L = laterally unbraced length of the member, in.

r = governing radius of gyration, in.

K = the effective length factor.

Q = Q_a for cross section composed of only stiffened slender elements.

The reduction factor, $Q_a = \frac{A_{eff}}{A}$

where

A = total cross-sectional area of member, in^2.

A_{eff} = summation of the effective areas of the cross section based on the reduced effective width, b_e, in^2.

The reduced effective width,

$$b_e = 1.92t\sqrt{\frac{E}{f}}\left[1 - \frac{0.38}{(b/t)}\sqrt{\frac{E}{f}}\right] \le b$$

where

$f = P_n/A_{eff}$

In lieu of calculating $f = P_n/A_{eff}$, which requires iteration, f may be taken equal to F_y. This will result in a slightly conservative estimate of column capacity.

For doubly symmetric members:

$$F_e = \left[\frac{\pi^2 E C_w}{(K_z L)^2} + GJ\right]\frac{1}{I_x + I_y}$$

Because of the special features of the HSS sections, the warping constant C_w was very small, and the first component of the F_e associated with C_w could be neglected.

The maximum of the step load given to the chord member in this case was limited to: 80% × P_n – branch force × 2 × *sin* (45). 0%, 50% and 100% of the maximum of the step load were given to the modes for different load situations.

Table 3.4 shows the load configurations.

Table 3.4 - Chord and Branch Load for the Connection

	Geometric Configuration 1	Geometric Configuration 2	Geometric Configuration 3	Geometric Configuration 4
Chord member Branch Member	14 ×14 × 3/8 8 × 8 × 1/4	14 ×14 × 3/8 8 × 8 × 3/16	14 ×14 × 5/16 8 × 8 × 1/4	14 ×14 × 5/16 8 × 8 × 3/16
$\frac{KL}{r}$	3.85	3.85	3.83	3.83
b_e	12.315	12.315	11.06	11.06
Q	1	1	0.884	0.884
F_e	8735	8735	8674	8674
F_{cr}	45.9	45.9	40.6	40.6
P_n (Chord)	858.33 kips	858.33 kips	637.42 kips	637.42 kips
Branch ramp Load In 8 load steps	218.48 kips	168.44 kips	208.73 kips	158.68 kips
Chord Step Load 1	0 kips	0 kips	0 kips	0 kips
Chord Step Load 2	188.845kips	224.23 kips	107.37 kips	142.76 kips
Chord Step Load 3	377.69 kips	448.45 kips	214.75 kips	285.53 kips
Chord ramp Load In 8 load steps	308.98 kips	238.21 kips	295.19 kips	224.41 kips

3.6 Summary

The numerical analysis was carried out by ANSYS 9.0. In total, 82880 nodes and 12667 elements constituted the finite element model. 3D brick element solid95 was used. Multi-linear elastic properties of the material of the joint (E = 29000 ksi for elastic steel, $\upsilon = 0.3$) were used. Appropriate support forms were adopted for the model to simulate the truss connection. Combined loads were given to the model in step manner to generate the elements output.

Chapter 4 – Analysis Procedure and Results

4.1 Overview

Finite element analysis as a numerical method provides a way to simulate and analyze actual structures. The nodal result obtained from a FE method is approximated element by element, in a piecewise fashion. Although the structural displacements derived from the nodal results of finite element analysis are not 100% precise, they can provide an accurate solution in the level defined by researchers. "The primary unknowns (nodal degrees of freedom) calculated in a structural analysis are displacements. Other quantities, such as strains, stresses, and reaction forces, are then derived from the nodal displacements as required." (Cook et al 2002). As the displacement results of the structural solution that was provided by ANSYS, structural behaviors of all connection members were derived from the program. The maximum and minimum strain, stress and displacement were observed and areas were presented herein.

4.2 Analysis Procedure

In the solution phase of program analysis, a computer takes over and solves the simultaneous set of equations generated by finite element methods. Because the element solution is usually calculated at element's integration points, different methods have been designed to solve the equations. The solvers can be categorized into two methods with different techniques. One technique is a direct-elimination solver, using equations reordered by alternating diagonal planes. The other technique is an iterative solver, using two-line successive over-relaxation. Both of the solvers can be used to run linear and nonlinear problems. The selection of these two kinds of solvers basically depends on the

complexity and scale of the structural matrix and the computation capacity of the computer.

ANSYS employs the "Newton-Raphson" approach to solve nonlinear problems. In this approach, the load is subdivided into a series of sub-load increments. The load increments can be applied over several load steps. Fig 4.1 illustrates the use of Newton-Raphson equilibrium iterations in a single DOF nonlinear analysis.

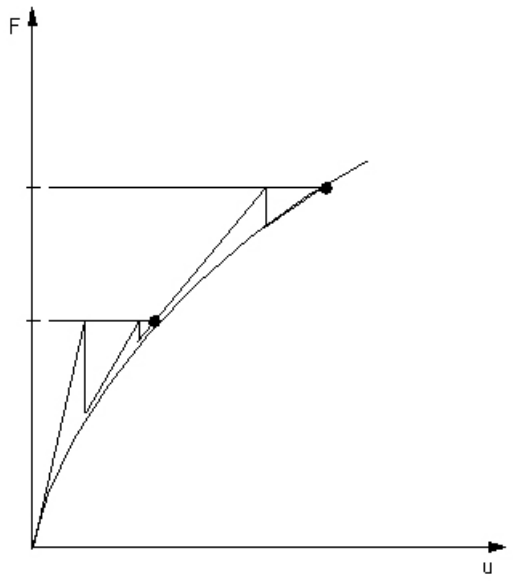

Figure 4.1 - Newton-Raphson in two iterations
(ANSYS 9.0 2004)

Fung et al (2000) clearly stated that "The requirement of the non-positive definite stiffness matrix was suppressed to force a solution in the system so that the geometric instability (buckling in this case) could be studied. Full Newton–Raphson method was used to reassemble the stiffness matrix at each of the iterations." Further behavior of the joint member beyond the member failure or buckling point was investigated in this thesis as well. The same method was applied in the research. Termination criteria were set to "continue after the program non-convergence". After the load reached certain level, the

linear behavior of the branch end displacement gradually developed into a nonlinear curve. This transform was affected by several factors including branch buckling, chord failure, and branch member.

4.3 Non-Linear Analysis Results

4.3.1 General

Because of the material and geometric nonlinearity of the project, nonlinear analysis was used in the program. However, in the first several load steps of the analysis, the nonlinearity wasn't exhibited in the result because both the steel and the weld hadn't reached the yield point. The load displacement curve of the model didn't exhibit a very obvious nonlinear behavior after increasing the load on the branch end. Further study on the stress and strain behavior in this period indicated that maximum stress of some elements had exceeded the yield point. Because nonlinear material property had been assigned to the elements, these elements should have exhibited the nonlinear features. However, because only a small amount of elements had stepped into the nonlinear behavior stage, the total connection still exhibited linear features. The displacement in the period for both chord and branch member did not show big failure or buckling features.

The load displacement curves began to transform into a nonlinear stage beyond a certain load step. The load displacement curves gradually became flat after that. From the tendency of the curve, it can be predicted that the slope of the curve should become 0 at some point beyond the current maximum load which is derived from the design manual.

By investigating these locations of maximum and minimum strain, stress and displacement in the connection, the failure and buckling region can be predicted. The

behavior of the members under increasing branch load can be studied through the observation of the development of the strain, stress and displacement contour.

4.3.2 Displacement in Linear Behavior Range

Before the load displacement exhibited obvious nonlinear features, the connection showed an obvious linear behavior under a certain load limit. Fig 4.2 shows the displacement vector contour of the connection when the connection still exhibited linear behavior. The configuration of the model exhibited in Fig 4.2 to Fig 4.12 is Chord HSS section set to 14 ×14 × 3/8 and Branch HSS section set to 8 × 8 × 3/16

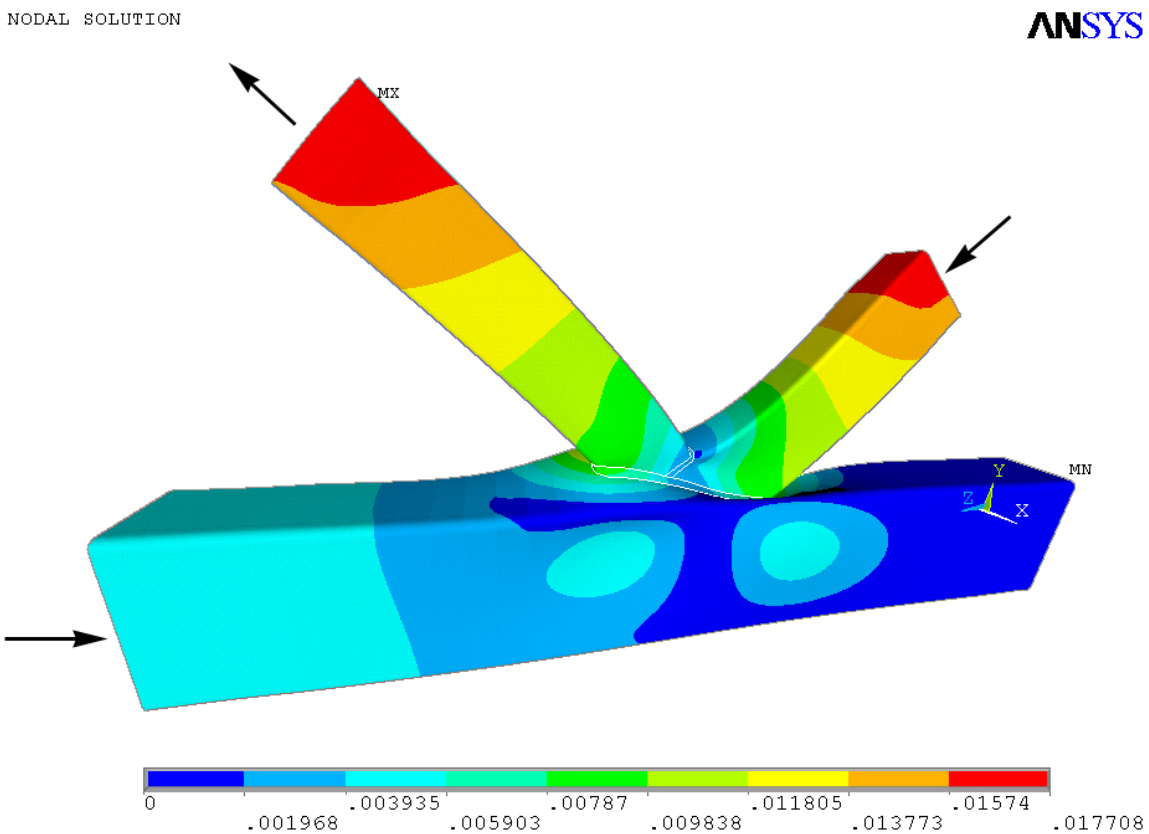

Figure 4.2 – Joint Displacement Vector Contour I (in)

Global coordinate system is also introduced in this figure. Globe Y direction is corresponding to the vertical direction; Global X direction is corresponding to the horizontal direction pointing out of the paper plane. Thus the X-Y plane is the same as

the X-Y plane of the chord section. Global Z direction is pointing out from the fixed end of the chord end to the roller end of the chord member. In this load period, the large displacement vectors displayed in the end of the two branch HSS. The displacement at the tension end was larger than the displacement at the compression end. Because the load given on the branch was limit in the first several load steps, the connection effects dissipated quickly in both branch and chord HSS.

Because the weld connected the chord and the branches, chord member deformation followed the behavior of the branch member. The large displacement for the chord happened on the top surface of the chord member. Fig 4.3 shows that the area connecting to the heel region of the compression branch exhibited a large negative Y direction displacement. Meanwhile, the area connecting the heel part of the tension branch HSS through the weld, exhibited a large positive Y direction displacement.

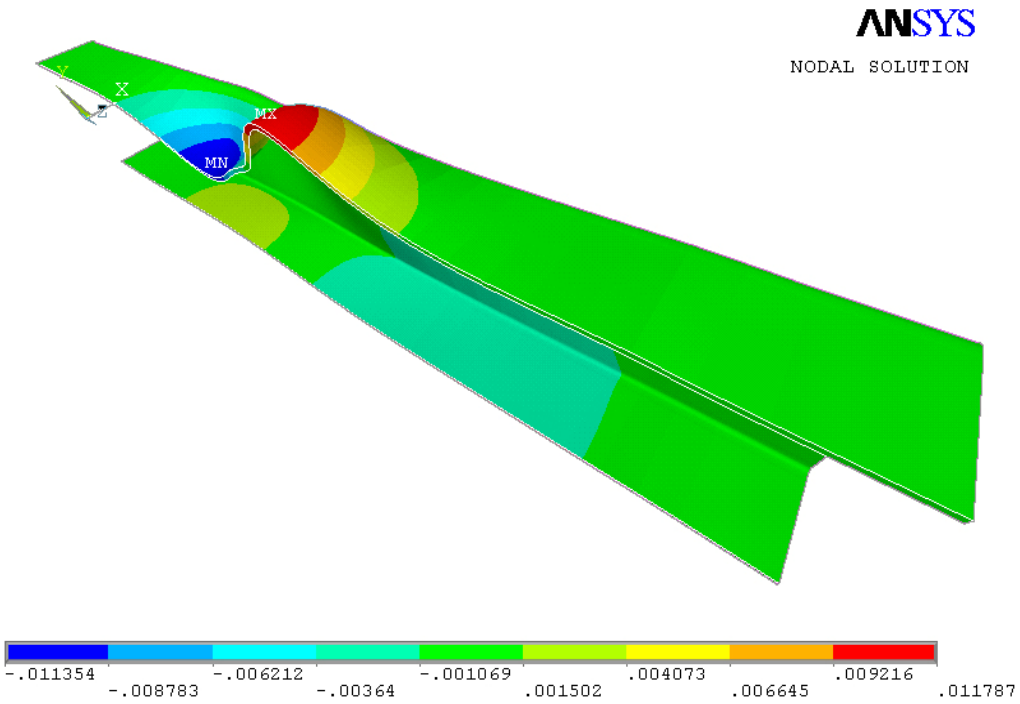

Figure 4.3 – Chord Y Direction Displacement Contour (in)

The deformations on the side face of the chord member in Fig 4.4 also demonstrated the effect of the branch member. The maximum positive X direction displacement occurred at the side plate beneath the area connecting to the compression branch. From the outside of the chord HSS, there is a convex under the branch with a compression load. The maximum negative X direction displacement occurred at the side plate beneath the area connecting to the tension branch. A concave formed under the branch with the tension force.

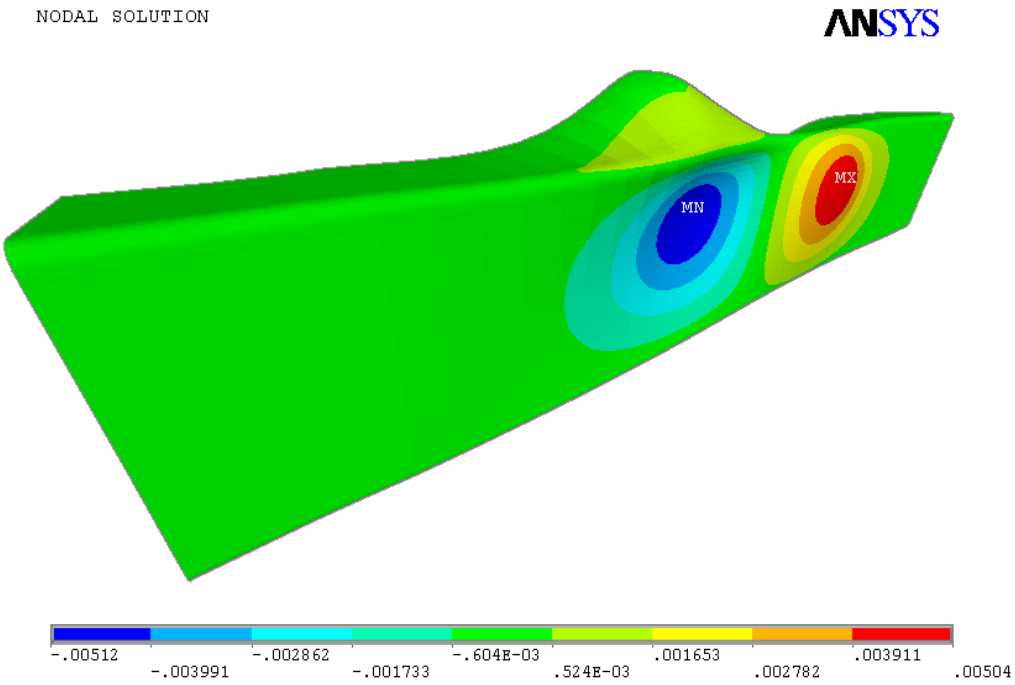

Figure 4.4 – Chord X Direction Displacement Contour (in)

Both of the branches had transferred a positive Z direction force to the chord HSS through the weld on the top surface of the chord member. In order to balance the branch load, the compression was put on the roller end of the chord HSS. In this case, the length of chord HSS on the left of the joint would decrease due to the compression load. The nodal displacements on the right of the connection were close to zero, except the top

surface area close to the connection. Therefore, the maximum negative displacement occurred at the roller end of the chord member.

Fig 4.5 shows the maximum positive Z direction displacement at the middle of the joint. It was because the force transferred from the two branches intersected at that point. The top plate of the chord member gave the resistance of the load transferred form the branch through the weld.

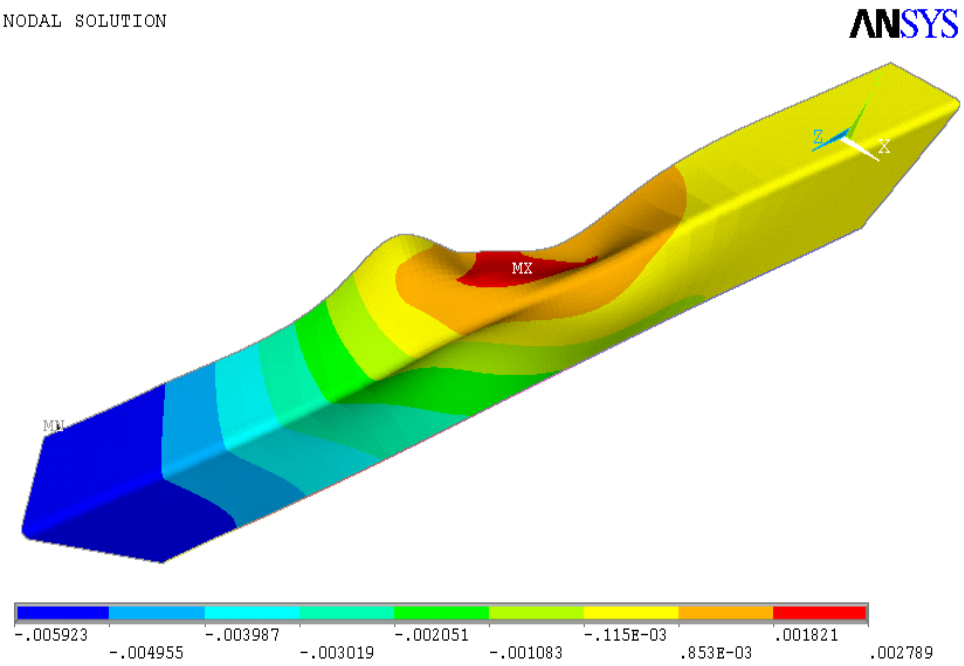

Figure 4.5 – Chord Z Direction Displacement Contour (in)

From Fig 4.6, no large displacement vector occurred at the bottom of the through branch HSS where it connected the chord HSS through the weld. The large displacement only happened at the top end of the branch HSS. Because the part of the overlapping branch HSS was connected to the through branch HSS directly, the area connecting the edge of the overlapping HSS showed very little displacement.

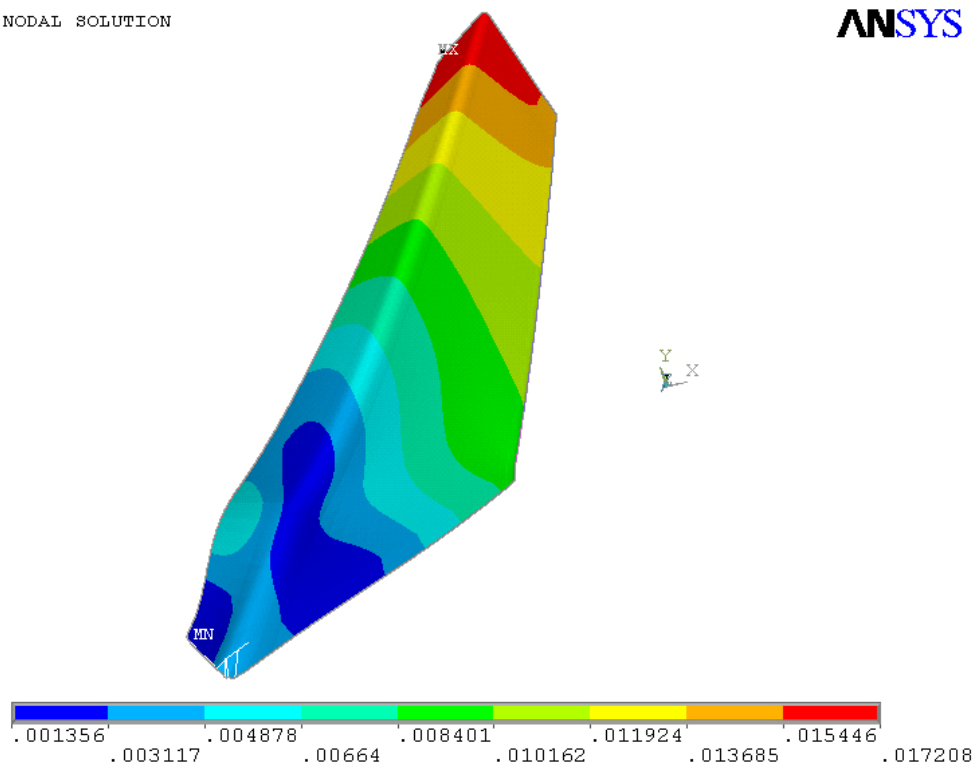

Figure 4.6 – Through Branch HSS Displacement Vector Contour (in)

The overlapping branch HSS exhibited the same displacement vector contour as the through HSS. Large displacement only showed at the end of the branch. The displacement at the bottom edge of the overlapping HSS connecting the other branch or the chord HSS was limited in a very small range. Fig 4.7 shows the detail displacement contour of overlapping branch member.

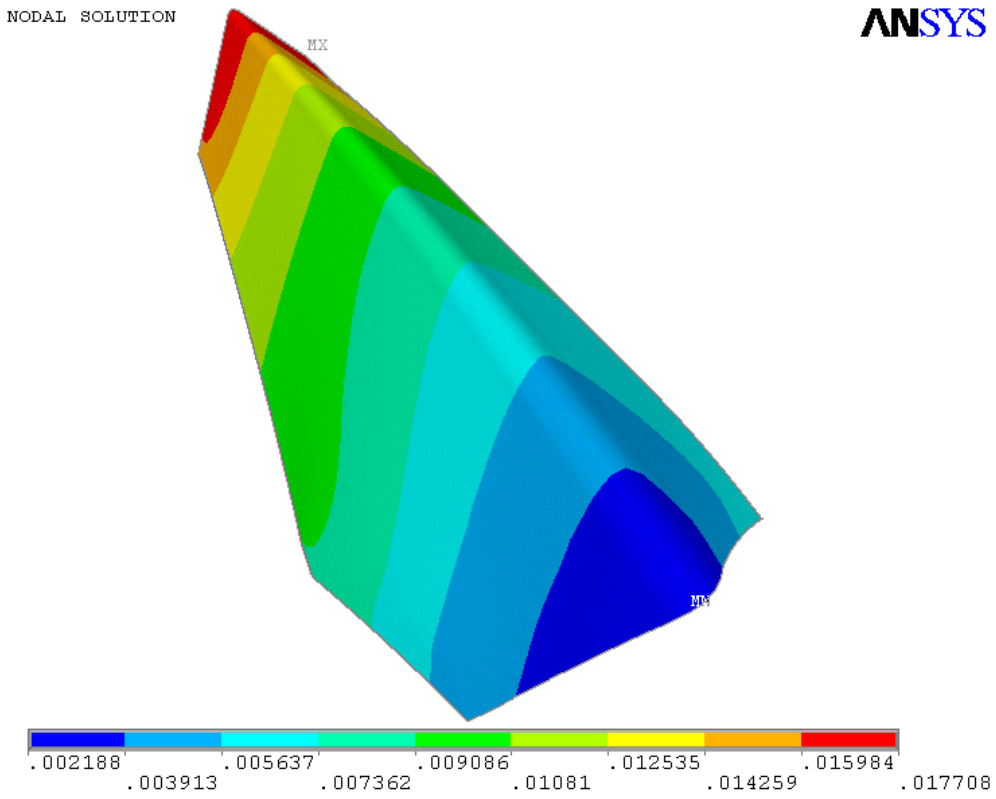

Figure 4.7 – Overlapping Branch HSS Displacement Vector Contour

4.3.3 Displacement in Non-Linear Behavior Range

As the step load increased, the displacement exhibited an obvious nonlinear behavior. The value of the displacement is very large compared with the linear portion of the displacement in the first several load steps. Both the branch and chord member generated large displacement. Fig 4.8 and Fig 4.9 illustrate the general displacement pattern under the load close to the maximum branch strength and where the maximum displacement occurred. In general, the displacement of the joint was a combination of branch compression, branch stretch, chord compression and slight joint rotation.

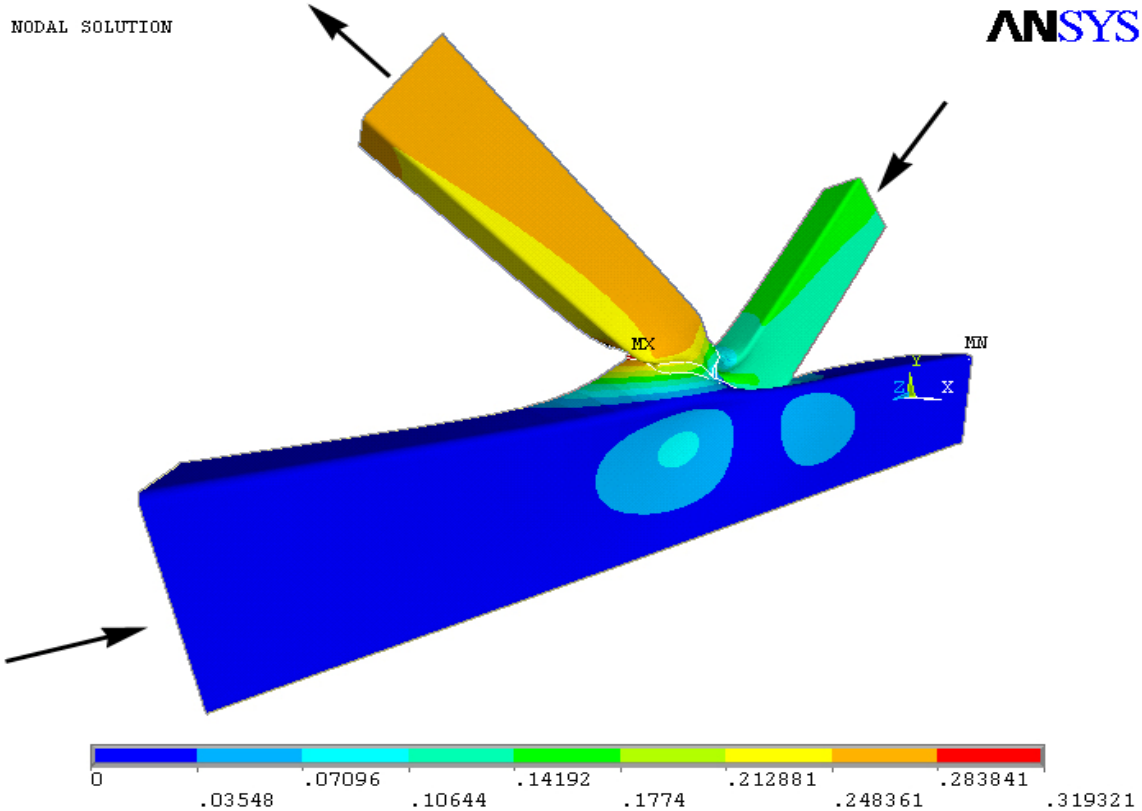

Figure 4.8 – Joint Displacement Vector Contour II (in)

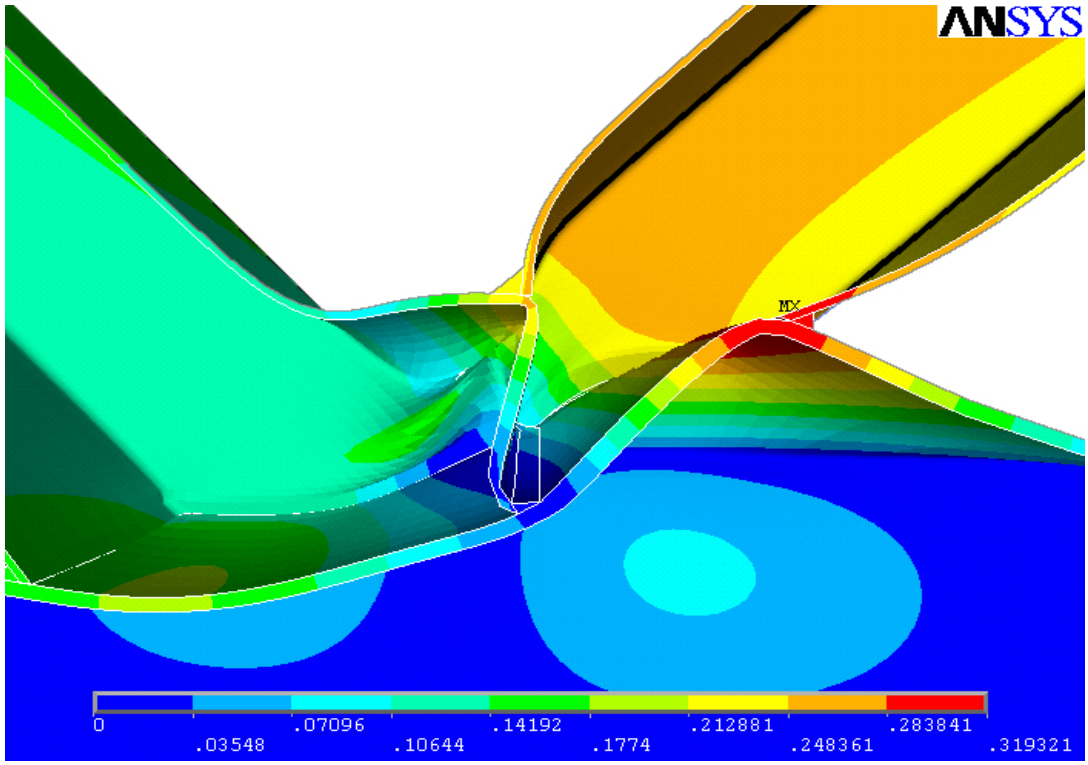

Figure 4.9 – Joint Displacement Vector Contour II Detail (in)

The maximum displacement occurred at weld connection at the heel part of the overlapping HSS and can be observed in the Fig 4.9. Further investigation on the stress strain of this area found that the stress exceeded the yield point and the plastic strain was very large. Due to the large displacement and strain on the top surface of the chord member, the chord made the major contribution to the large branch end displacement which was the symbol of member failure. Therefore, the failure mode was defined as chord member base metal tear-out in this case and chord member local buckling.

The chord member in the nonlinear period had the similar behavior pattern as in the linear period. In X direction, the side plate of the chord didn't show large displacement and plastic strain compared with the chord member top plate large displacement in Y direction. Side plate of the chord wasn't buckled and didn't make the major contribution to the large branch end displacement.

Fig 4.10 illustrates the displacement behavior of the through branch. The plate connecting to the overlapping branch member showed a large displacement and plastic strain. The deformation had a large contribution to the large displacement on the branch. Therefore, the area on the top surface of the through HSS connecting the overlapping HSS would have the tendency to be torn out by the weld. This large deformation was also the main reason of the connection failure. In this case, the failure mode could be defined as branch member base metal tear-out.

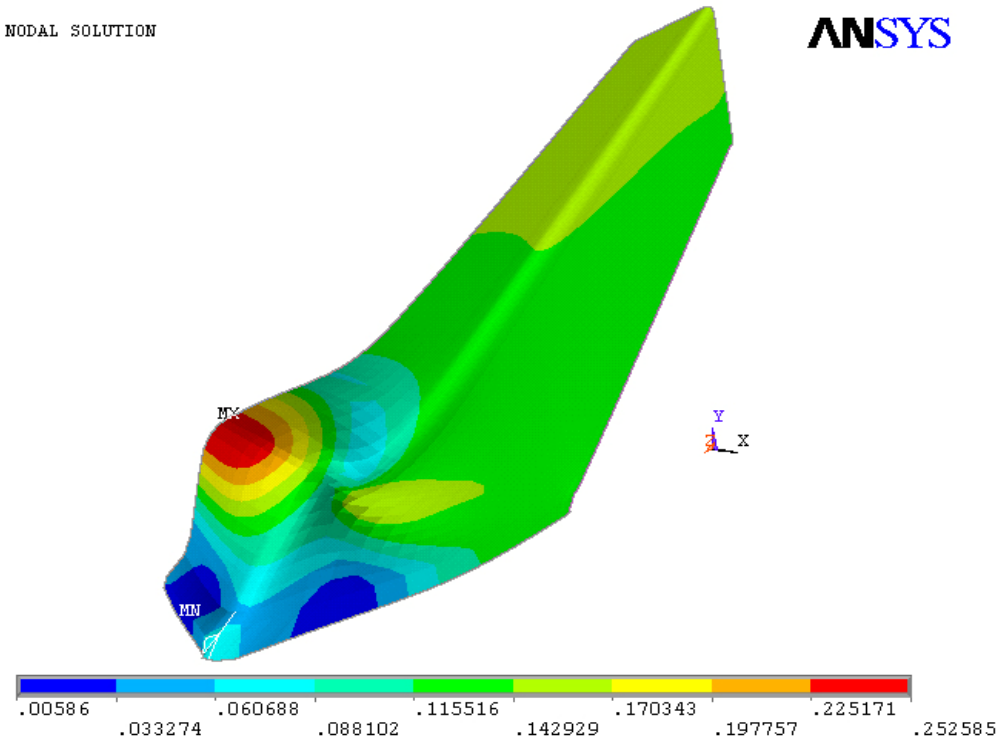

Figure 4.10 – Through HSS Displacement Vector Contour (in)

Further investigation found that the side plate of the through HSS also had the large displacement and large plastic strain during the last several load steps. The X-direction displacement contour displays that the buckling occurred in the area close to the weld connecting two branches. The failure mode of branch member local buckling was defined. The displacement contour is shown in Fig 4.11

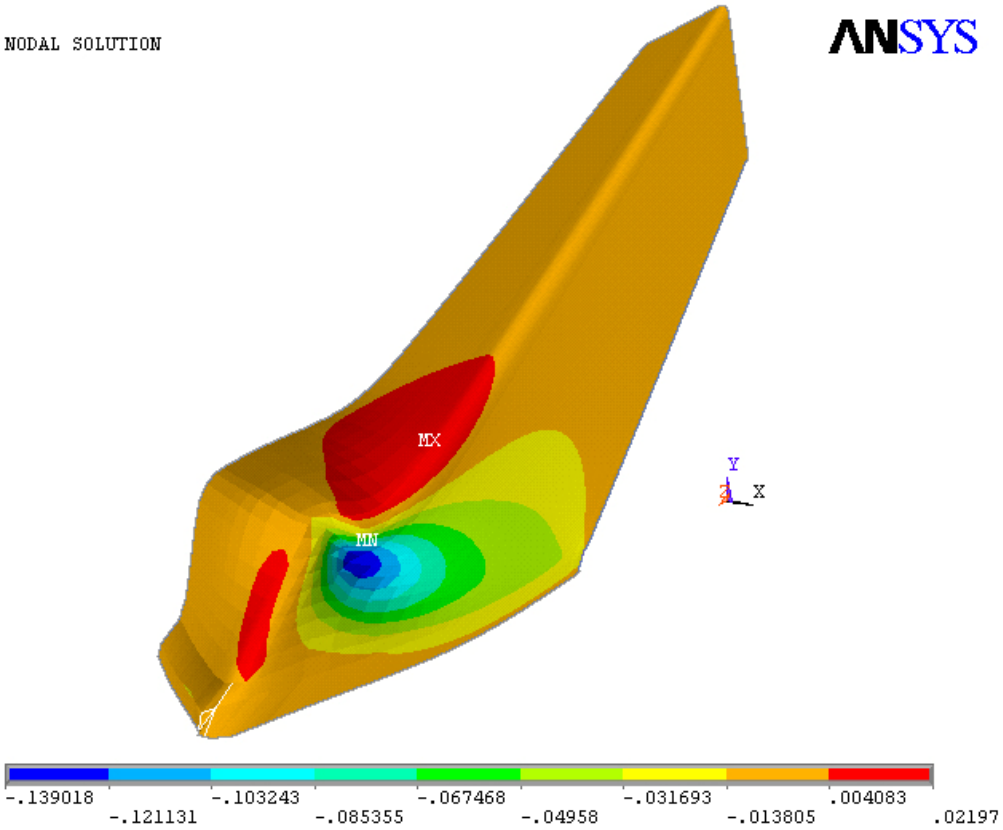

Figure 4.11 – Weld Displacement X Direction Vector Contour

4.3.4 Load Displacement Curve

To clarify the geometry and the load of the connection, table 4.1 had been set up to make the figures clear.

Table 4.1 – Notation Used in Load-Displacement Figures

	Description
KOP50	50% overlapping K connection
C1	Chord HSS section set to 14 ×14 × 3/8
C2	Chord HSS section set to 14 ×14 × 5/16
B1	Branch HSS section set to 8 × 8 × 1/4
B2	Branch HSS section set to 8 × 8 × 3/16
CP0	0% Chord member step load
CP50	50% Chord member step load
CP100	100% Chord member step load

To clarify the location of the hot spot in the connection, those node positions were listed and described in Table 4.2

Table 4.2 –Node Position Description

Tracking Nodes	
Node	General Position Description
1	Through Branch End
2	Overlapping Branch End
3	Overlapping Branch Heel
4	Through Branch Heel
5	Through Branch Toe Connecting the Chord HSS
6	Overlapping Branch Toe Connecting the Through Branch
7	Through Branch Buckling Area
8	Middle of the weld connecting the Through HSS and Overlapping HSS toe
9	Middle of the weld connecting the Chord HSS and Overlapping HSS toe
10	Chord HSS Free displacement End
11	Chord HSS at Tension Branch Heel
12	Chord HSS at Compression Branch Heel

In Fig 4.12 and 4.13 the load-displacement observed nodes were clarified in the maps.

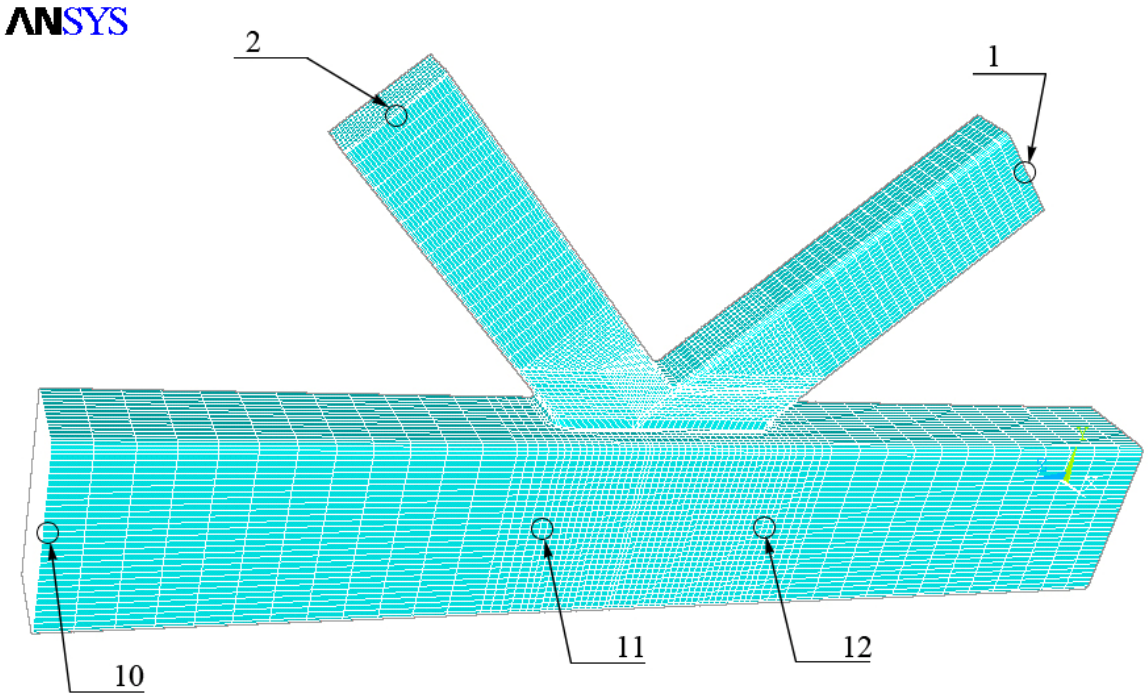

Figure 4.12 – Node Displacement Observation Map I

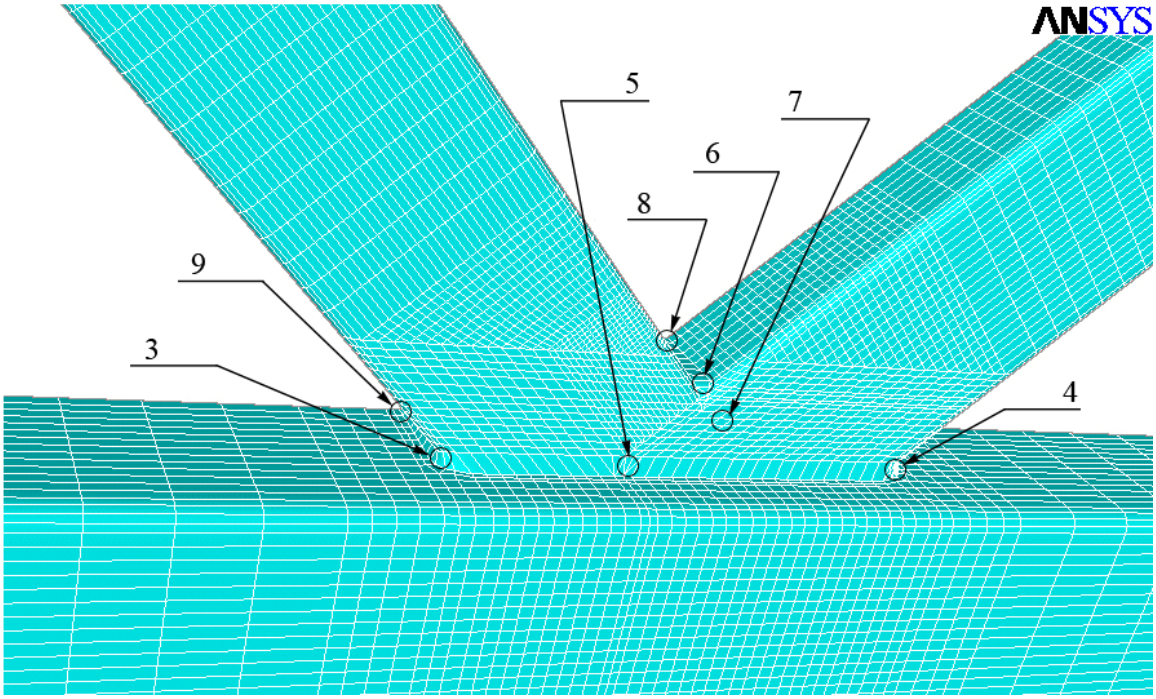

Figure 4.13 – Node Displacement Observation Map II

Feature areas had been selected according to the stress, strain and displacement development. Node 1, 2 gave the general description of the branch end behavior on the

axial direction along the branch HSS. Node 10, 11, 12 gave the general description of the chord member behavior under the chord stepped loads and the effect came from the complex joint behavior. Node 3 to node 9 gave a detailed observation of the feature nodes which reflected the special behavior of the joint.

In Fig 4.14, the branch displacement was defined as the displacement vector starting from the original branch end to the same node's position at the end of the load step in the investigating period. The curve was linear until it reached a load step at which nonlinear features started to dominate. The displacement became infinitely large after the curve exceeded the specified load limit coming from the ultimate connection strength.

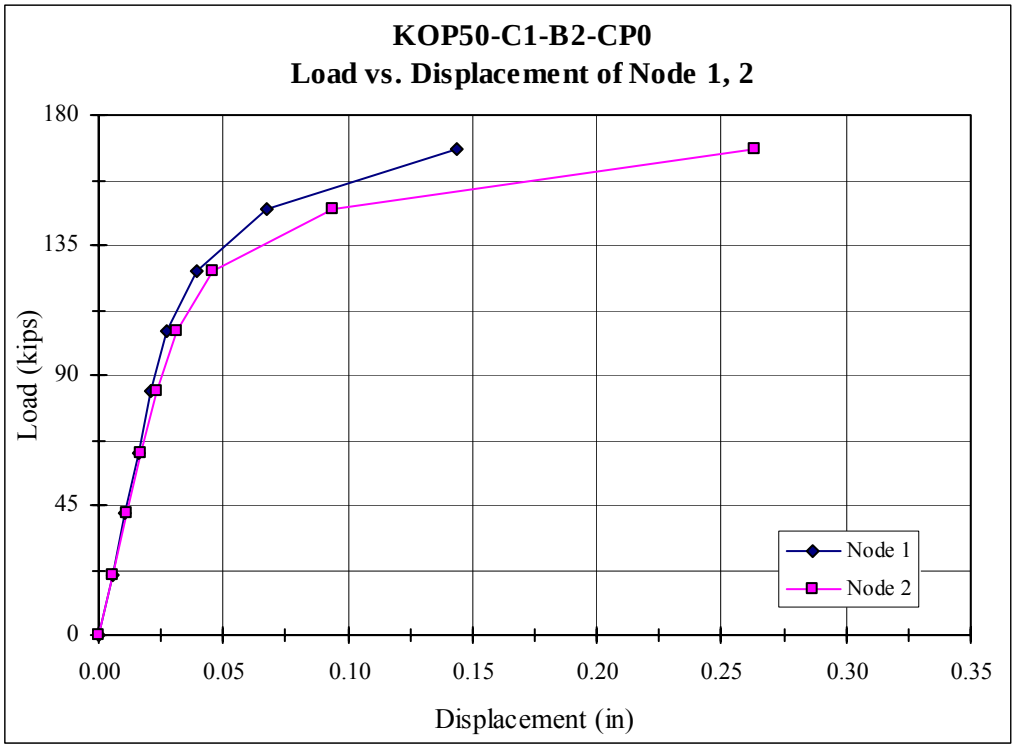

Figure 4.14 - Load-Displacement Relationship 1

Fig 4.15 illustrates that the transition part of the connection also had a large displacement when the connection was close to fail. The displacement of the transition connecting the heel of the overlapping HSS and the side plate of the overlapping part was

smaller than the displacement at the through HSS transition area. It is demonstrated from Figure 4.10 that the largest displacement occurred at the middle of the overlapping heel area. So the difference of the displacement on the same edge of the overlapping HSS was very large. Top surface was buckled in the chord member.

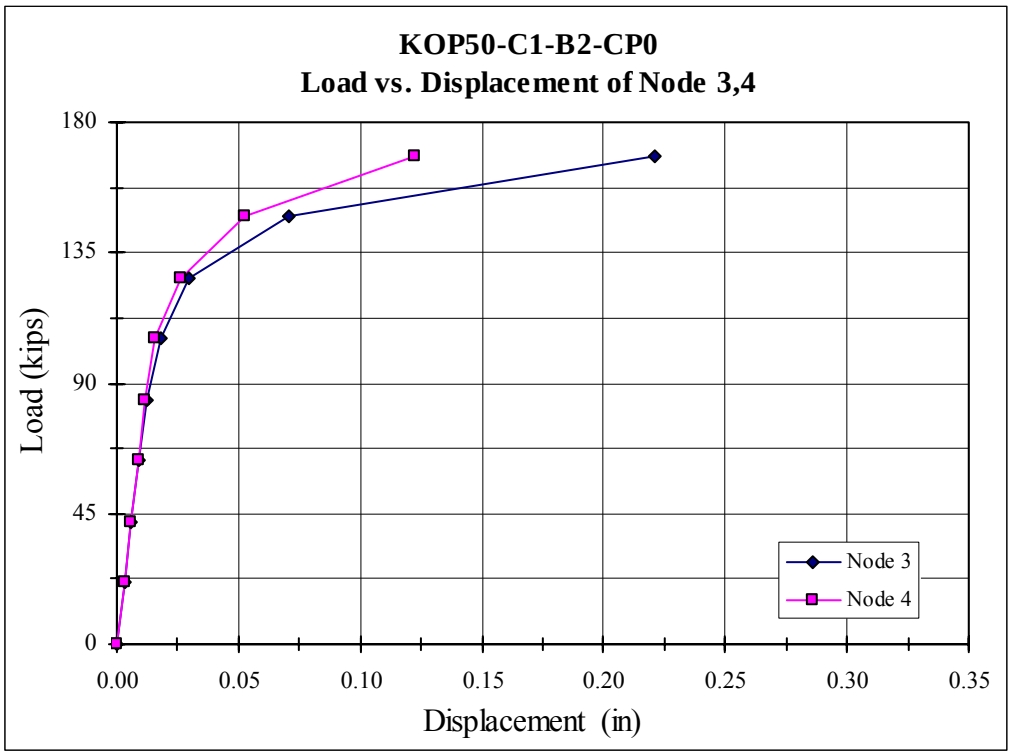

Figure 4.15 – Load-Displacement Relationship 2

The load displacement behaviors for node 5 and node 6 are exhibited in Fig 4.16. It is very obvious that the displacement for node 5 and 6 changed less than for other nodes as the load step increased. The displacement of node 5 was larger than that of node 6 before the load step reached 126.33kips but after that point, the displacement of node 6 became larger and increased faster.

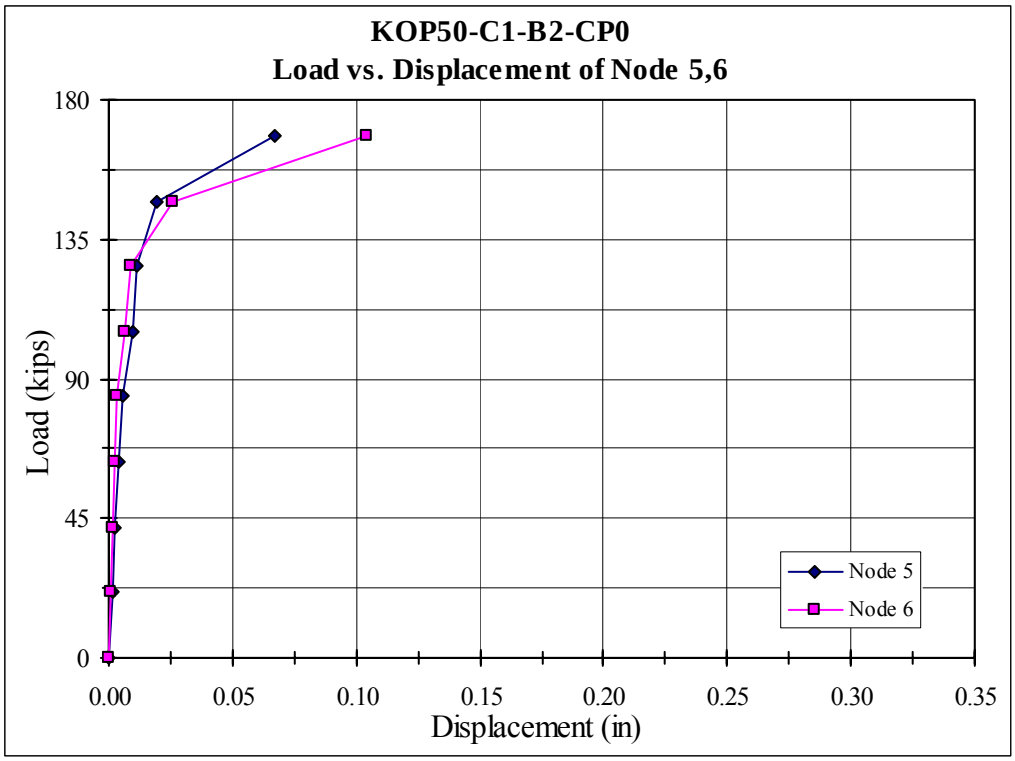

Figure 4.16 – Load-Displacement Relationship 3

The load displacement behaviors for node 7, node 8, and node 9 are exhibited in Fig 4.17. Form Fig 4.17, there are no obvious different in the behavior pattern among node 7, node8 and node9 area.

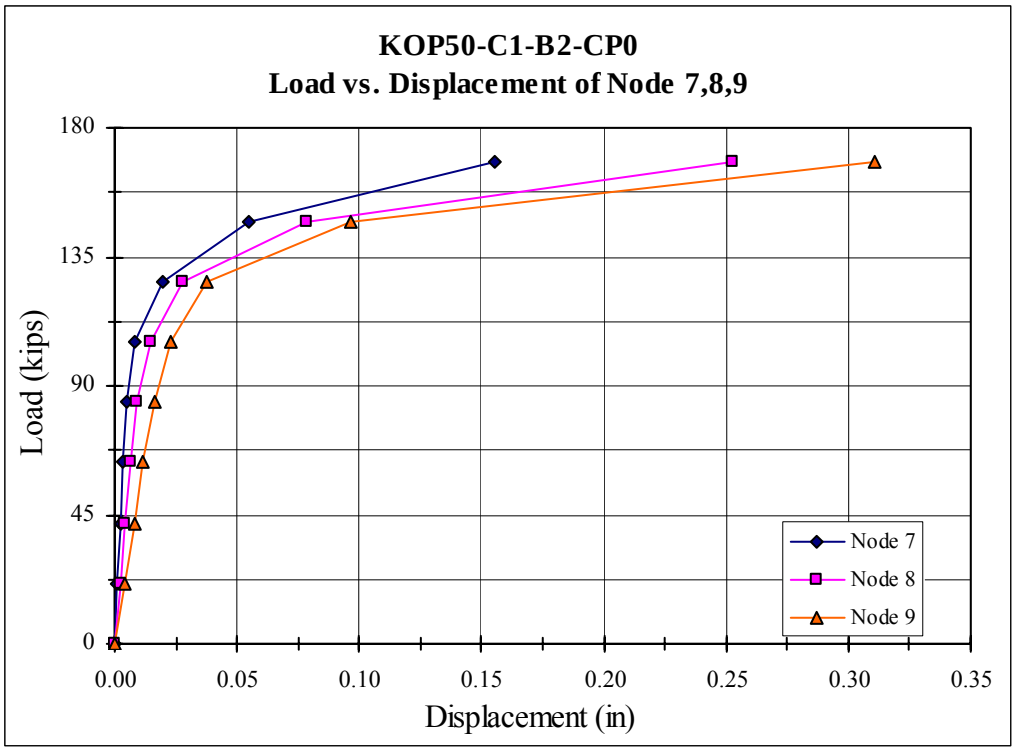

Figure 4.17 – Load-Displacement Relationship 4

The X direction displacement of node 10, 11, 12 showed linear behaviors before the load step reached 126.33 kips in Fig 4.18. The slope of the load-displacement curves for these three nodes were different due to their different locations in the chord HSS. After the load exceeded the 126.33 kips, the three curves exhibited nonlinear features simultaneously.

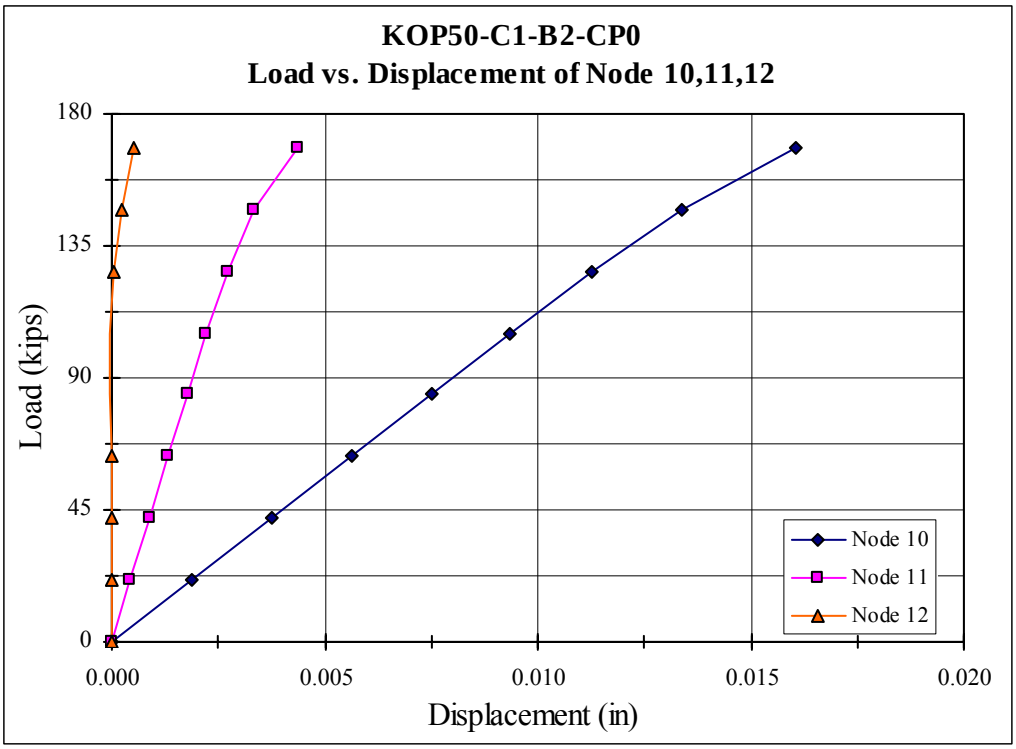

Figure 4.18 – Load-Displacement Relationship 5

4.3.5 Stress Result

In order to find out the correct failure models and locations, stress distribution need to be investigated. The node stress contour delivered a good represent of stress distribution. Von mises stress give out the most meaningful stress map under certain branch load. Von Mises stress, σ_v is used to estimate yield criteria for ductile materials. It is calculated by combining stresses in two or three dimensions, with the result compared to the tensile strength of the material loaded in one dimension. So the finite element stress results are typically presented in Von Mises stress form. The branch load is applied to the model in ramp load style which includes eight load steps. Because the maximum load calculated according the design manual, different maximum branch loads were assigned to different connection geometric configurations. The branch load steps is listed in the Table 4.3

Table 4.3 – Branch Ramp Load and Notation

Notation	Geometric Configuration 1	Geometric Configuration 2	Geometric Configuration 3	Geometric Configuration 4
	14 ×14 × 3/8 8 × 8 × 1/4	14 ×14 × 3/8 8 × 8 × 3/16	14 ×14 × 5/16 8 × 8 × 1/4	14 ×14 × 5/16 8 × 8 × 3/16
	C1-B1	C1-B2	C2-B1	C2-B2
LS1 (kips)	27. 31	21. 055	26. 09	19. 835
LS2 (kips)	54. 62	42. 11	52. 18	39. 67
LS3 (kips)	81. 93	63. 165	78. 27	59.505
LS4 (kips)	109. 24	84. 22	104. 37	79.34
LS5 (kips)	136. 55	105. 275	130. 46	99.175
LS6 (kips)	163. 86	126. 33	156. 55	119.01
LS7 (kips)	191. 17	147. 385	182. 64	138.845
LS8 (kips)	218. 48	168. 44	208. 73	158.68

Fig 4.19 to Fig 4.21 shows how the von mises stress developed when the branch load was increased. From the Load-Von Mises Stress Contours, the development of the stress distribution could be fully investigated. It was found in Fig 4.19 that the maximum stress occurred at location where the corner of the overlapping HSS member connecting the corner of the through HSS branch member. When the branch load increased, the area of the large stress expanded in the weld between the two branches. The branch base metal stress also increased correspondingly in Fig 4.20. Continue increasing the branch load, the large stress was generated at the corner of the heel part of the overlapping HSS member. From Fig. 4.21, most large stress was generated in the weld elements. The HSS branch and chord element were also high stress if element was connected or close to the weld part. The area was also expanded when the branch load is increasing. Additional contours are provided in Appendix B to Appendix E to further describe the development of the stresses within the connection.

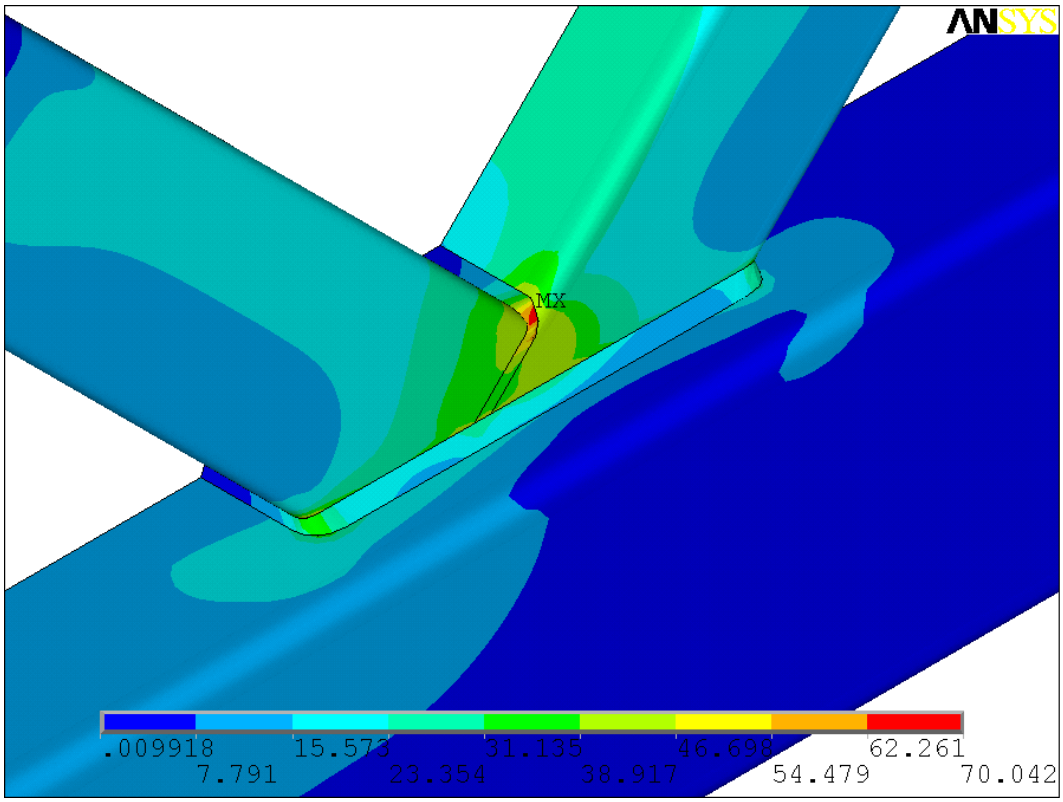

Figure 4.19 –C1-B1-CP0-LS4 Load-Von Mises Stress Contour (ksi)

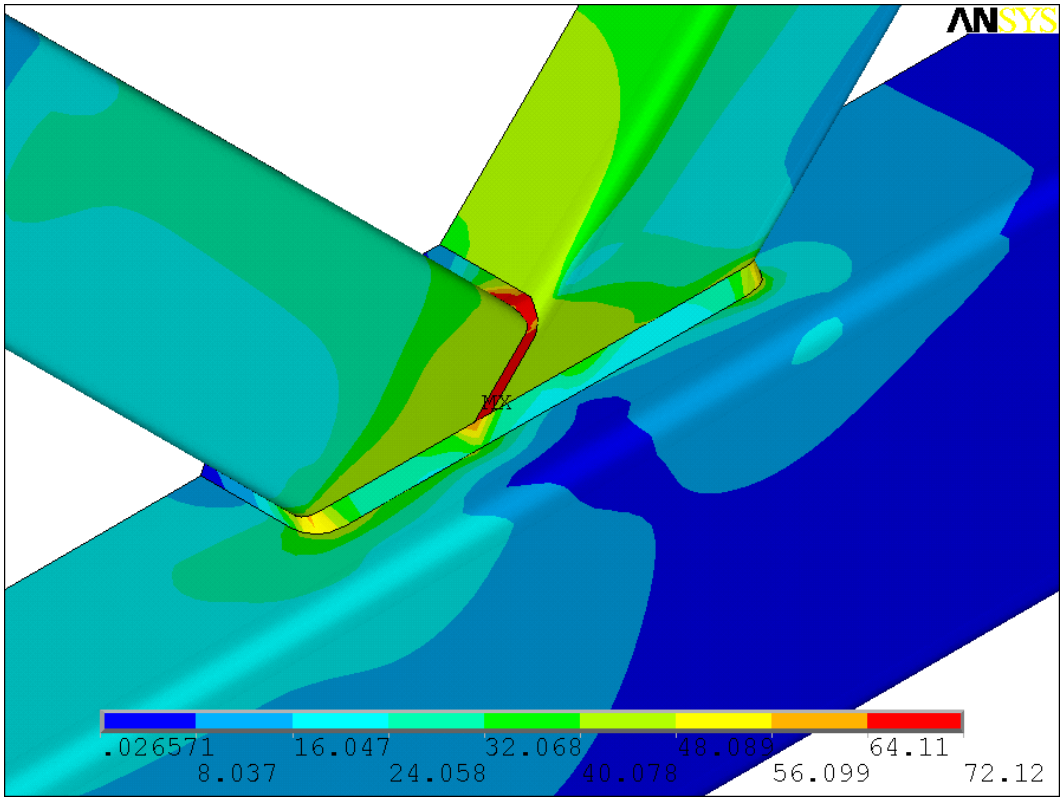

Figure 4.20 – C1-B1-CP0-LS6 Load-Von Mises Stress Contour (ksi)

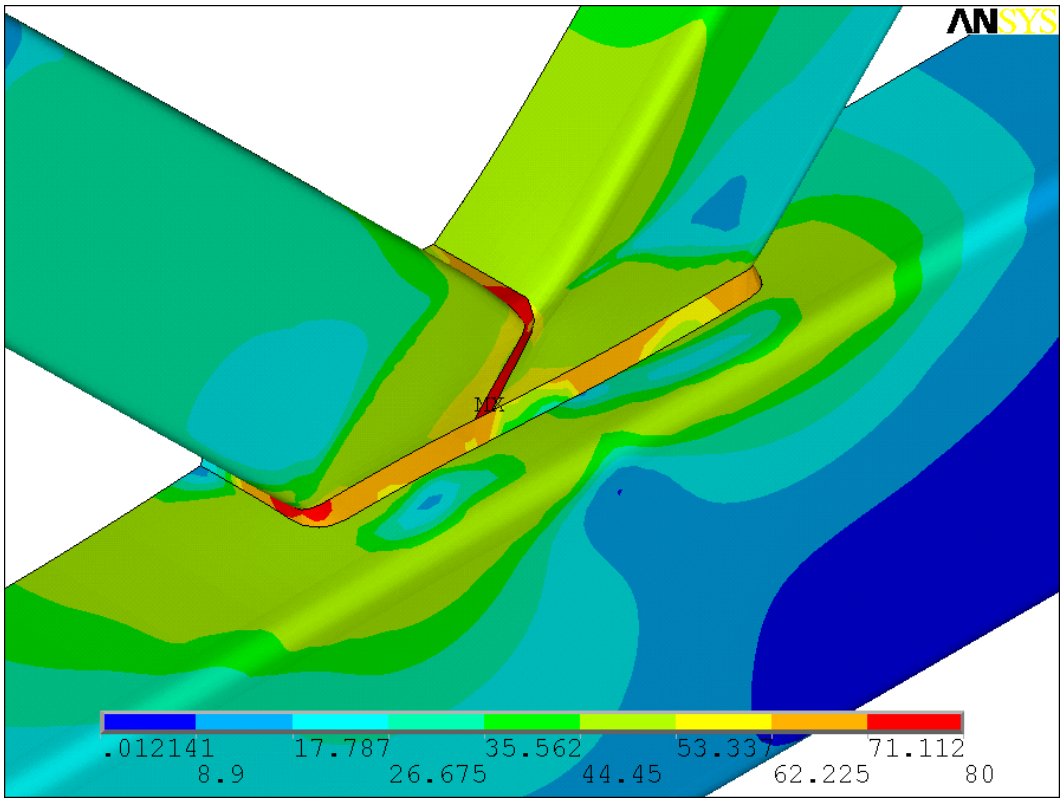

Figure 4.21 – C1-B1-CP0-LS8 Load-Von Mises Stress Contour (ksi)

To further investigate the detail of the stress development pattern for the key area, the load-stress response in the locations specified in Fig. 4.13 need to be evaluated. Observations of the nodal response areas of 1, 2, 10, 11 and 12 as shown in Fig 4.12 shows that the stress response in these areas were linear and the observed stresses were small compared to nodes in areas node 3 to node 9. The Fig 4.22 and Fig 4.23 show the load-stress curve for node areas from node 3 to node 9.

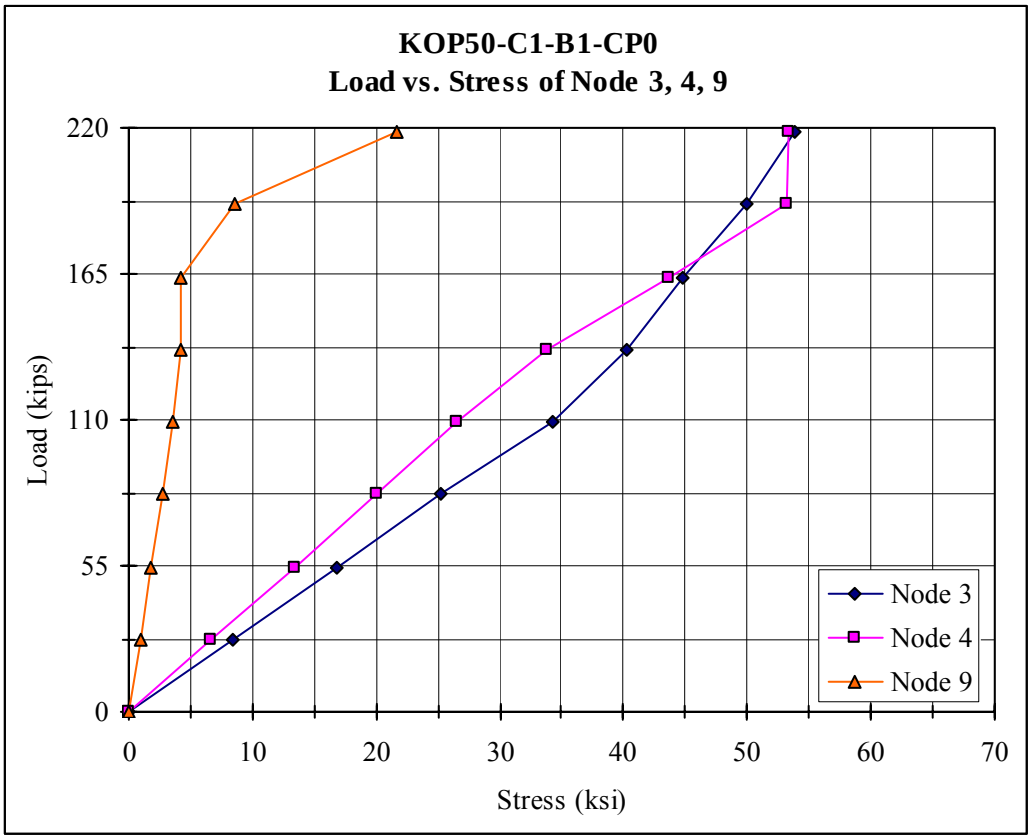

Figure 4.22 – C1-B1-CP0 Node 3, 4, 9 Load-Stress

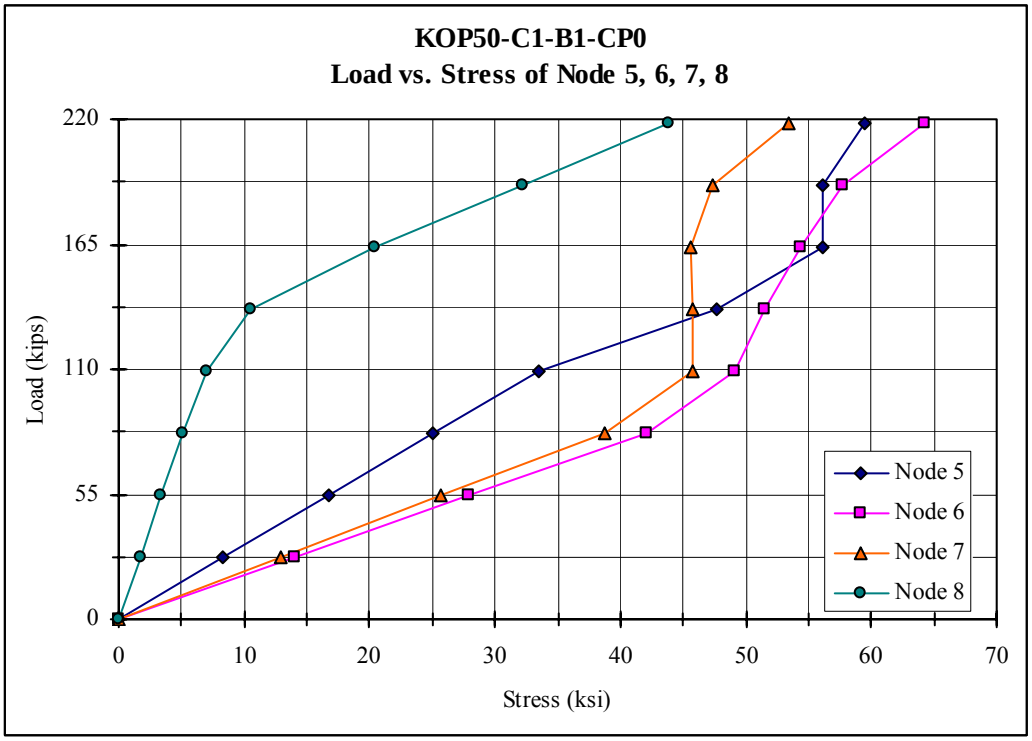

Figure 4.23 – C1-B1-CP0 Node 5, 6, 7, 8 Load-Stress

Node 9 area exhibits linear load-stress behavior in the first 4 load steps. Only slightly change in the slope in load step 5 and 6. The slope is changed dramatically in the last two load step. This behavior is similar as the load-displacement behavior. Node 3 and node 4 area exhibit same behavior as node area 9 in the first 6 load steps. Both load stress curve of node3 and node 4 areas have slope changed in the last two load steps, but not as large as it in node 9 area. The Node 8 load stress curve shape follows the same pattern as node 9 area. The Node 5, 6, 7 load stress curve shape follows the same pattern as node 3 and 4 area. In summary, node 8 and 9 area load stress behavior pattern are similar as the general connection load displacement behavior. This confirms the observed failure mode that developed in the area of node 8 and node 9 can be evaluates using the displacement and stress response.

4.4 Summary

The connection behavior under the gradually increased loads can be categorized into two stages: linear behavior stage and nonlinear behavior stage. Different parts of the joint reached the nonlinear stage almost in the same load situation. The load-displacement for different areas showed a similar curve pattern. Four types of failure models were found in the analyses which include chord member base metal tear-out, branch member base metal tear-out and chord branch member local buckling. Additional load-displacement curve for every load and geometric configuration is listed in appendix B to appendix I. The figures title notations which listed in appendix B to appendix I refer to table 4.1 and table 4.3.

Chapter 5 – Comparison of the Results

5.1 Overview

A large effort put into this research was to build up finite element models simulating the behavior of the HSS truss connection. Different models were established based on the geometric features of the joint. In order to investigate joint behavior under different geometric settings, four HSS with different geometric features had been chosen to build up similar connections but with different b/t ratio of the connection member. As stated in chapter one and chapter three, only two sections with the b/t ratio close to 35 and 46 were assigned to the branch member. The other two sections with similar b/t ratios were assigned to chord member. Four different settings were established by combining and switching the branch and chord sections. Therefore, the comparison between different branch HSS on the same chord HSS and different chord HSS connecting the same branch HSS could be made.

By observing the stress, strain and displacement vector contour, the important area showing the connection's feature behavior could be selected. The investigated areas for the connection were shown in Fig 4.13 and 4.14. Different load-displacement curves were showed in one chart for direct comparison.

The maximum load for the chord member was set to 80% of the maximum compression load derived from the steel design manual (AISC 2005). The calculation procedure was given in chapter 3. From the result of the ANSYS, no global buckling or chord member failure was generated due to the chord compression. Therefore, the modes with different chord compression force were established successfully. Comparison of the

same geometric feature with different step chord load could illustrate the effect of the chord load on the HSS truss connections.

5.2 Failure Mode Determination

As mentioned in chapter 4, three types of failure models were found in the analyses which include chord member base metal tear-out, branch member base metal tear-out and branch and chord member local buckling. The combinations of any two or three failure modes were found in most models under investigation. Several identifying methods had been used to determine the finial failure model. Dexter, E.M. and Lee, M.M.K. (1999) had provided the general solution to the failure mode: "For the overlap joints, failure modes of brace local buckling, or chord member buckling or a combination of both, were identified. The determination of these failure modes was assessed by visually checking the deformed model and the stress and strain plots." Further observation and comparison of the load-displacement curves also could help to study the failure behavior of the connection.

5.3 Same Chord HSS with Different Branch HSS

Because the branch member sections were different, different branch loads were given on the connections. In general, the behavior of two connections with different branch sections and same chord sections was similar. The branch end displacement for the model with thicker wall branch (B1) was larger than with thinner wall branch (B2).

Fig 5.1 shows the comparison for different chord effect on the load displacement curves.

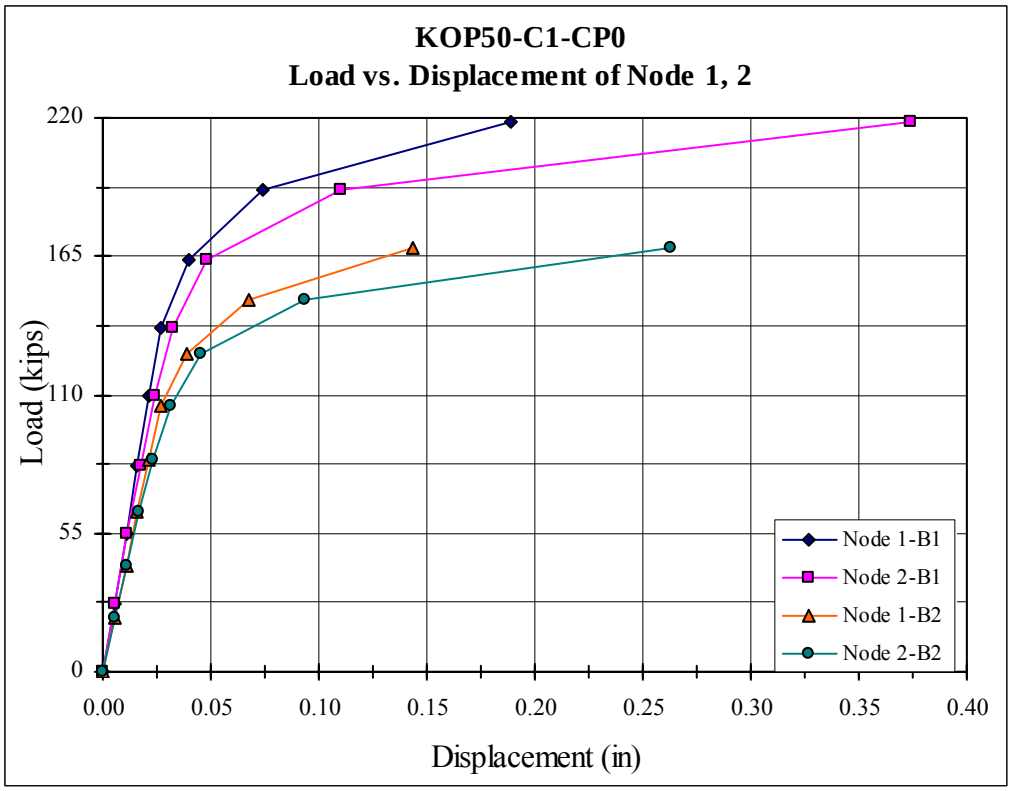

Figure 5.1 – C1-CP0 Node 1, 2 Load-Displacement

From Fig 5.1, the slopes of the two groups of curves representing for different branch wall thickness were slightly different. The maximum branch load for the model with thicker wall was larger than with thinner one. Given the same branch load, the connection with thicker wall showed smaller deformation in both branch ends than the connection with thinner wall. Although the compression end displacement curvature was less than the tension end, two curves evolved into the nonlinear stage at almost the same load step. The model with thicker branch exhibited larger displacement than the model with thinner branch.

From Fig 5.2, the general behavior was similar between the two modes with different branch wall thickness. There was no big difference between the slopes of the two groups of curves representing different branch wall thickness. The maximum branch

load for the model with thicker wall was larger than with thinner one. Given the same branch load, the connection with thicker wall showed almost the same deformation in the linear displacement behavior stage. In the nonlinear behavior stage, the displacement behavior for the two models with different branch wall was in the same pattern. Both slopes of the displacement curves became small at the last load step, but the curve representing the compression branch showed smaller curvature than the curve representing the tension branch. Investigation on the stress at node 3 and node 4 areas found that these areas always had relatively high stress due to the high stiffness in the HSS corner. Meanwhile, the stiffness gave the chord member more constrain preventing the large deformation in this area on the top surface of the chord HSS.

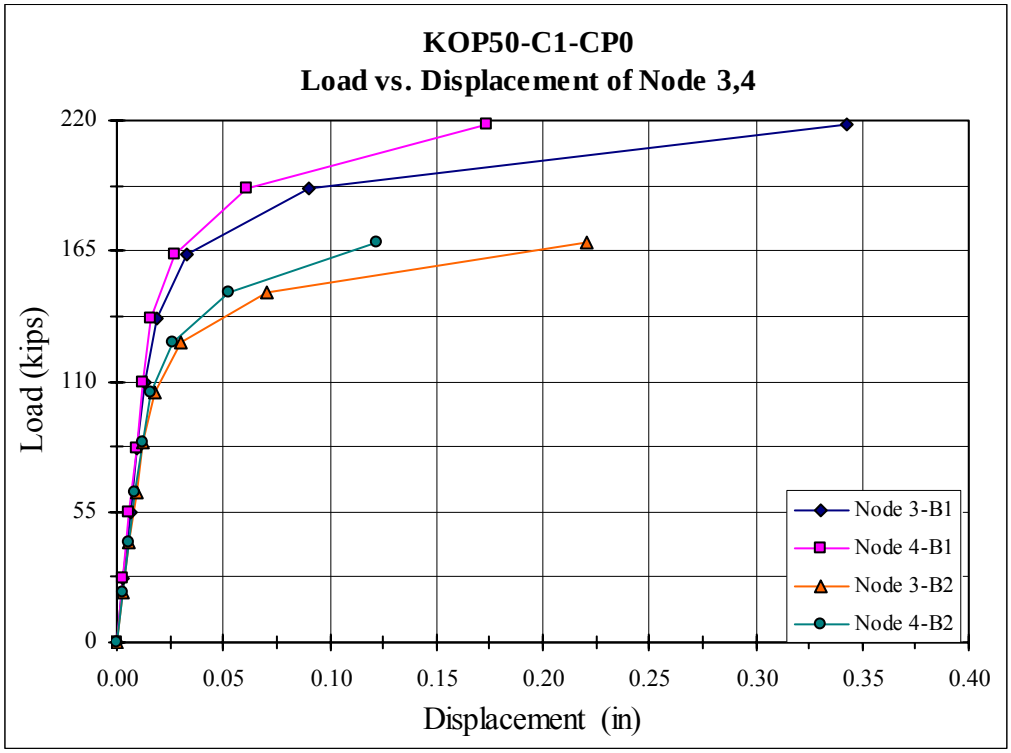

Figure 5.2 – C1-CP0 Node 3, 4 Load-Displacement

In order to exhibit the behavior of the connection, the total displacement range was set to 0.15. The general behavior of node 5, 6 is complex form Fig 5.3. Because these two areas were located at the center of the connection, both the branch side plates and the welds between them provided a strong constraint to these areas. The slight rotation of the joint didn't affect the displacement of these areas much. In the last load step, the model with thicker wall branch exhibited almost the same curve for node 5 and node 6 areas. On the other hand, the displacement for node 5 and node 6 areas for the thinner wall branch exhibited different behaviors. But the total displacement for both node 5 and node 6 were still in the same range as for other areas.

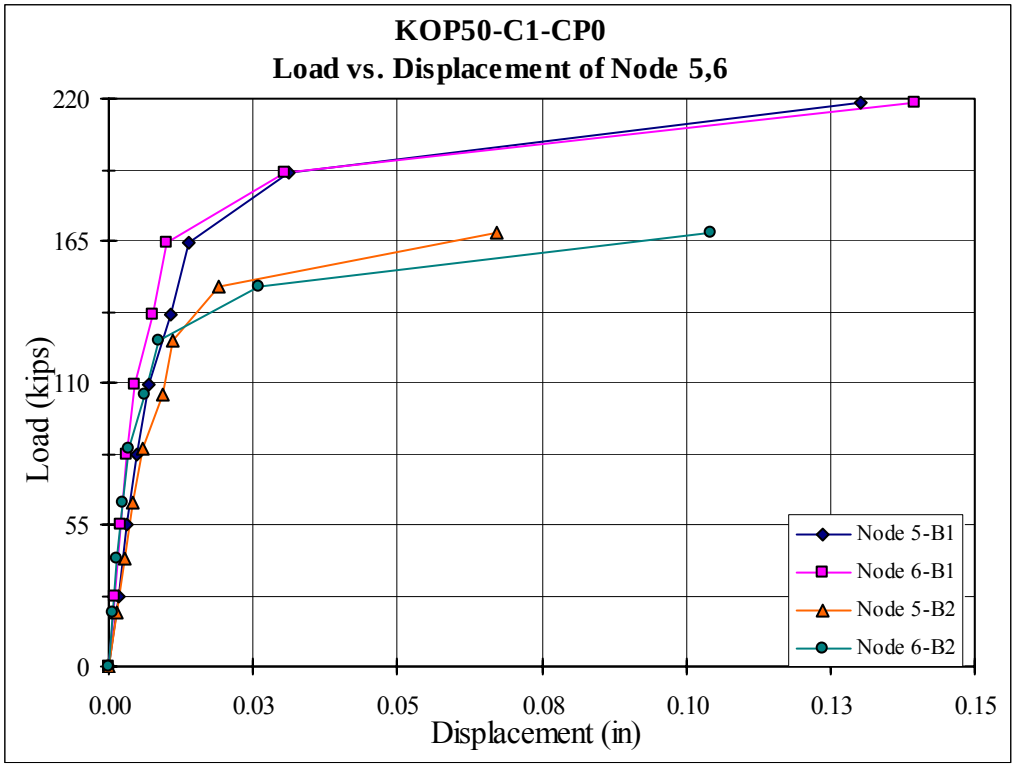

Figure 5.3 – C1-CP0 Node 5, 6 Load-Displacement

Node 7, 8, 9 areas were identified as three different failure mode areas. Further Study on these areas showed that the displacement curves of node 7, 8, 9 showed nonlinear tendency earlier than other curves and in the almost same load step in Fig 5.4 and Fig 5.5. Node 9 also exhibited a smaller slope curve in the last load step than other displacement curves. Comparison had been made between models with thicker wall and models with thinner wall.

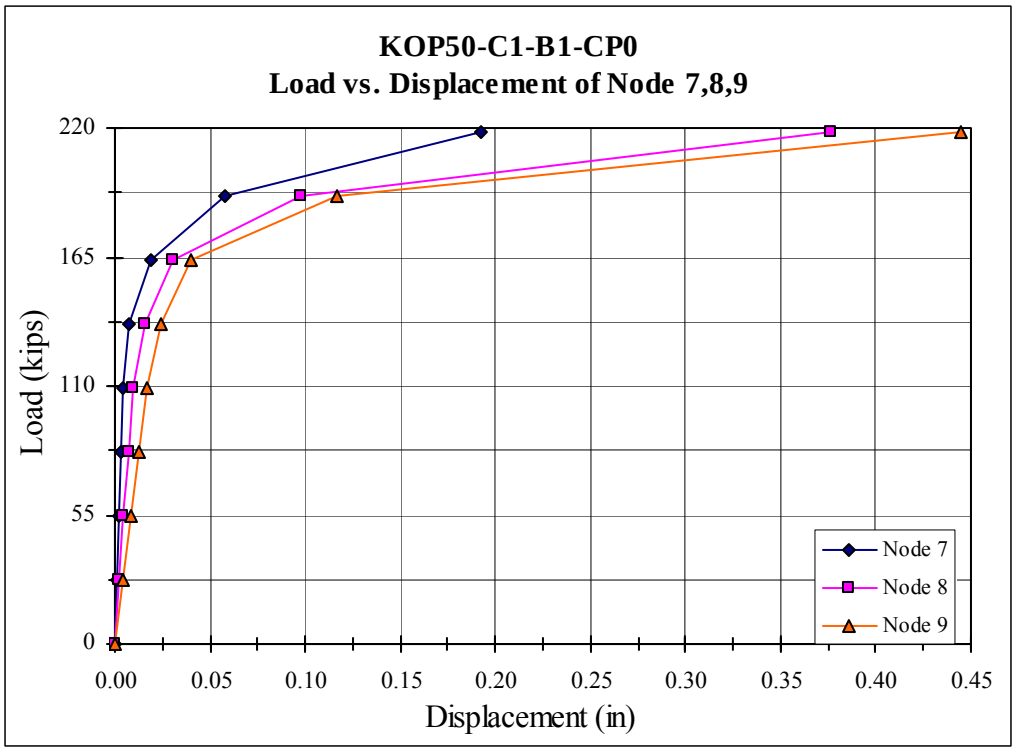

Figure 5.4 – C1- B1-CP0 Node 7, 8, 9 Load-Displacement

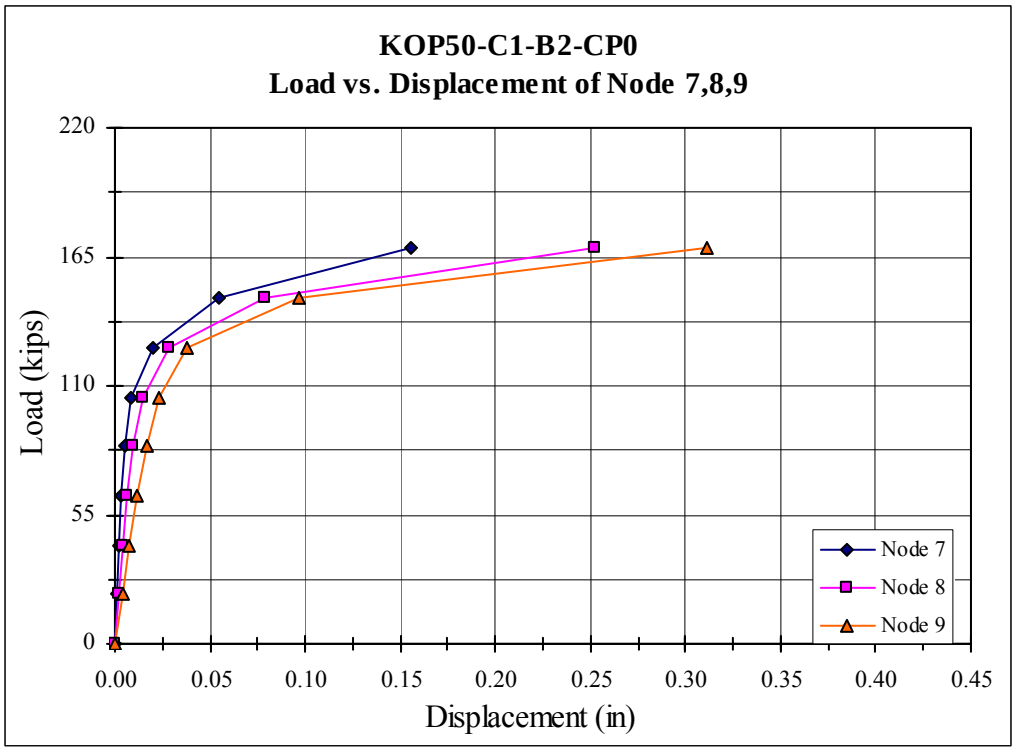

Figure 5.5 – C1- B2- CP0 Node 7, 8, 9 Load-Displacement

Investigation on the chord member longitude stretch was focused on node 10, 11, 12 areas. Fig 5.6 illustrates that the load displacement for the studied areas were kept small linear behavior except in the last two load steps. The two models with different geometric configuration and with different wall thickness exhibited same behavior in the first six load steps.

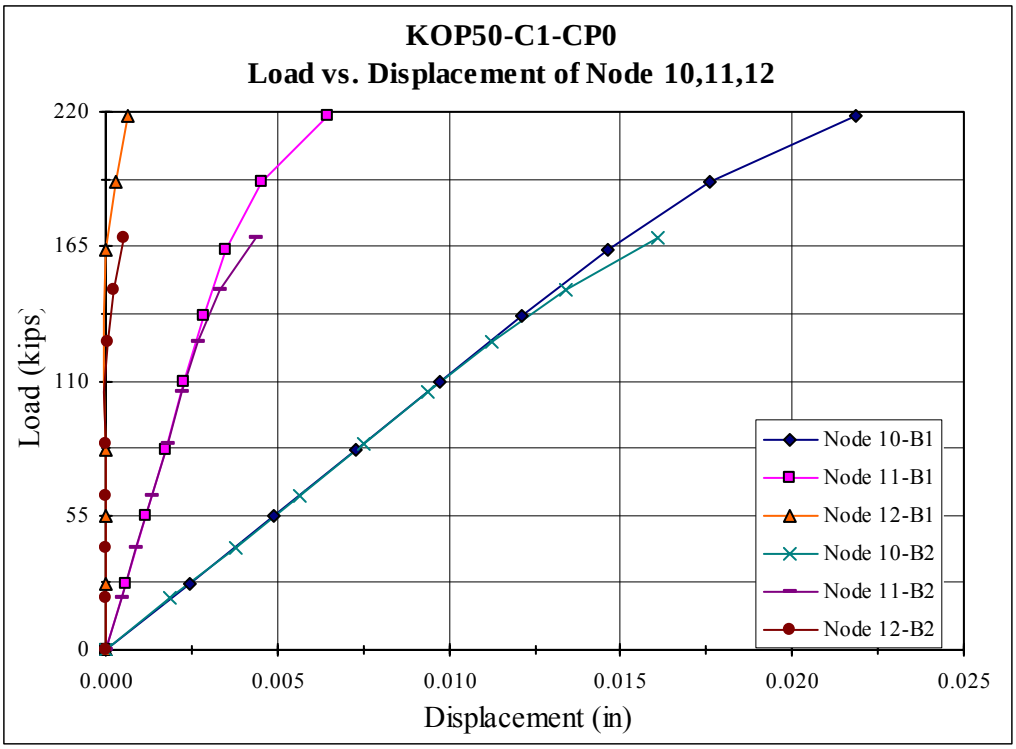

Figure 5.6 – C1-CP0 Node 10, 11, 12 Load-Displacement

Further comparison was made on the models with similar configuration but for chord member with thinner wall. Similar results were derived from the program output.

5.4 Same Branch HSS with Different Chord HSS

Because the branch member sections were same and the chord member section had very limited contribution in calculating the connection ultimate strength, the maximum branch load given on same branch HSS with different chord HSS didn't show large difference as in same chord HSS with different branch HSS. Based upon the calculation, the maximum load, which was also the ultimate strength of the connection, for the thicker chord HSS connection was a little larger than that for thinner chord connection. In general, the behavior of two connections with different chord sections and same branch sections was similar. The branch end displacement for the model with thicker wall chord (C1) was smaller than that for thinner wall chord (C2).

The general behavior of the two models was similar from the Fig 5.7. They reached nonlinear behavior stage in the same load step. The connection with thicker chord exhibited smaller displacement than the connection with thinner chord. Therefore, the thicker chord joint could reach the higher joint strength. In addition, the displacement slope of node1 in the last load step for the thicker chord (C1) was larger than for thinner chord connection (C2). This is represented by the "Node 1-C2" smaller slope in the last load step than "Node 1-C1". This means there was a greater possibility for the thicker chord joint to develop higher connection strength beyond the ultimate strength calculated from the design manual.

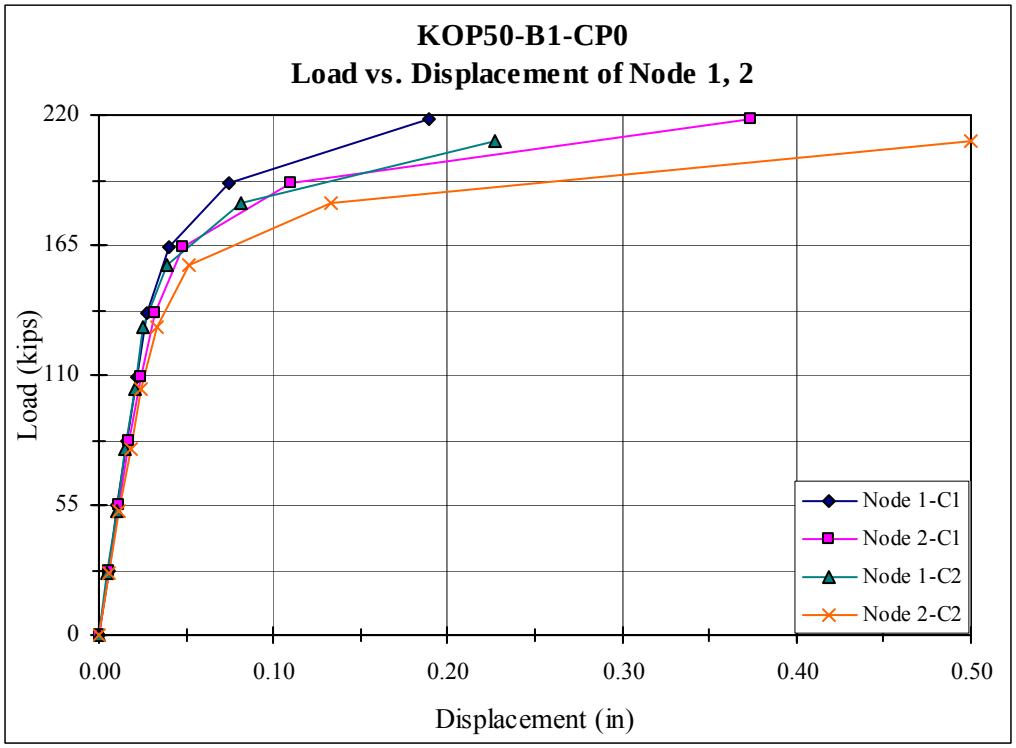

Figure 5.7 – B1-CP0 Node 1, 2 Load-Displacement

The general behavior at node 3 and node 4 areas was similar between the two modes with different chord wall thickness. Investigation on the stress and strain contour at these areas showed that the stress concentration in these areas was dissipated along the

plastic strain development in these areas. Due to the restriction from the branch side plate, there was no large displacement in these areas.

At node 5 and node 7 areas, similar behavior was observed in both thicker and thinner chord connections. The total displacement for node 5 and node 7 areas in both geometric configurations was limited in the same small range.

Comparison was made between chord members with different thicknesses on load-displacements for node 7, 8, 9 areas. Similar load-displacement curves are shown in Fig 5.8 and Fig 5.4. However, the two geometric HSS connections exhibited different displacement behavior in the last load step. The connection with thinner chord wall thickness showed larger displacement. Thus, the connection with thinner chord would fail shortly after the load reached the maximum load. On the contrary, the chord section with thicker wall would develop higher ultimate connection strength.

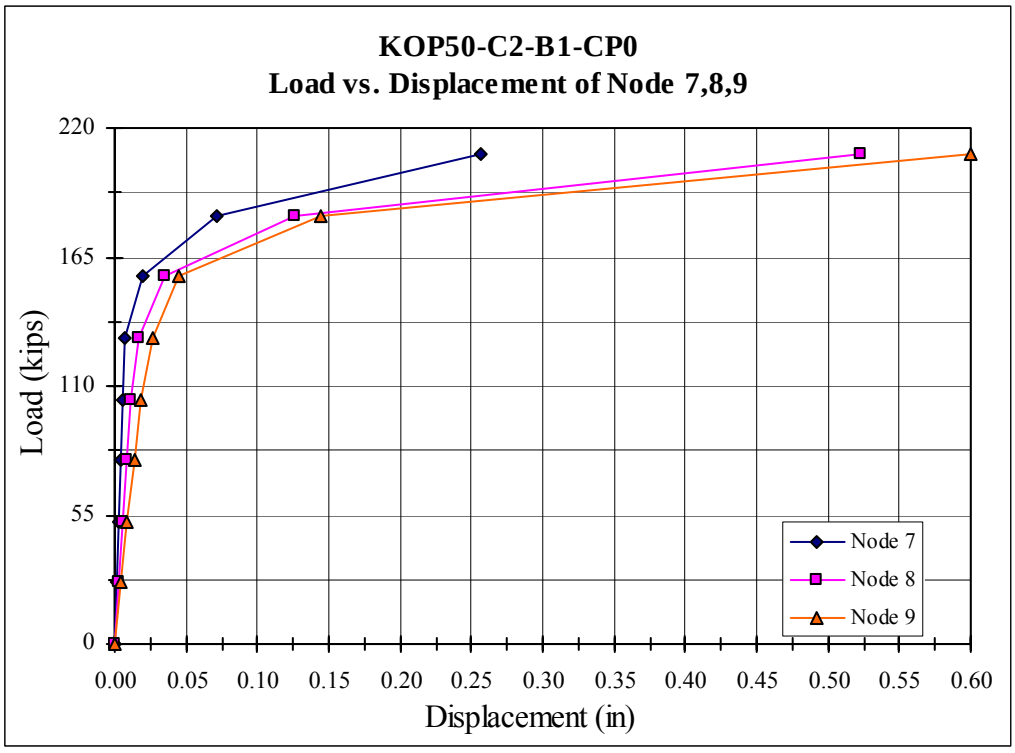

Figure 5.8 – C2-B1-CP0 Node 7, 8, 9 Load-Displacement

The load-displacement curves were different for three investigated areas. Node 10 area showed largest deformation difference between thicker and thinner chord connections among all three investigated areas. Node 11 area showed in Fig 5.9 displacement difference larger than node 12 area, but smaller than node 10 area. Generally, the connection with thicker chord wall showed small deformation in X-direction than the connection with thinner chord wall.

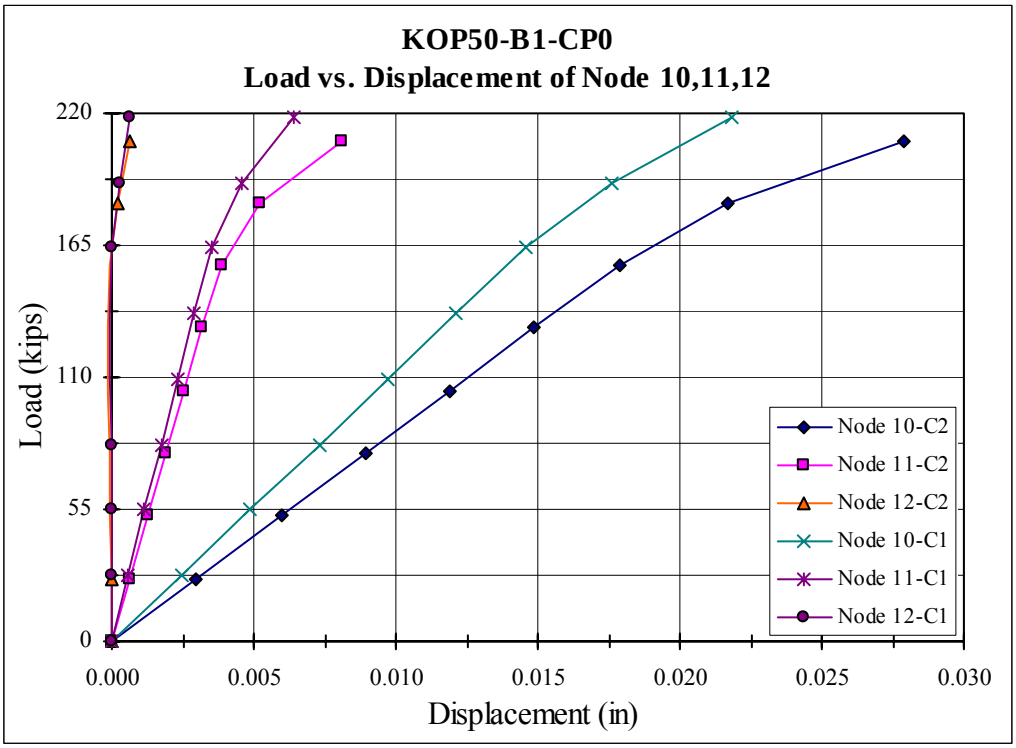

Figure 5.9 – B1-CP0 Node 10, 11, 12 Load-Displacement

Investigation on the models with similar configuration but for branch member with thinner wall was conducted to confirm the research result of the geometric configuration B1-CP0. Similar output was derived from the program and same result was generated.

5.5 Same Geometric Configuration with Different Chord Step Load

In the truss design, there are always some tension and compression load on the chord member. Thus, investigation on the chord member under different chord step loads

is necessary. The procedure of the numerical simulation of the HSS connection behavior under chord compression was to put the required step load at the free end of the chord first, after that, increase the branch load and the corresponding chord load in 8 steps. In this case, the effect of the chord member compression on the truss connection without branch load was generated. Study on the result of this situation showed that the chord member had a slightly positive effect on the connection strength.

Fig 5.10 shows that the initial compression had a positive effect on the load-displacement curve for both tension and compression branch at the first several load steps. But when the branch ramp load reached the last two load steps, the displacement of the branch end with initial chord compression load became larger than that of connection without chord load. This was more clearly exhibited in the tension end than in the compression branch end.

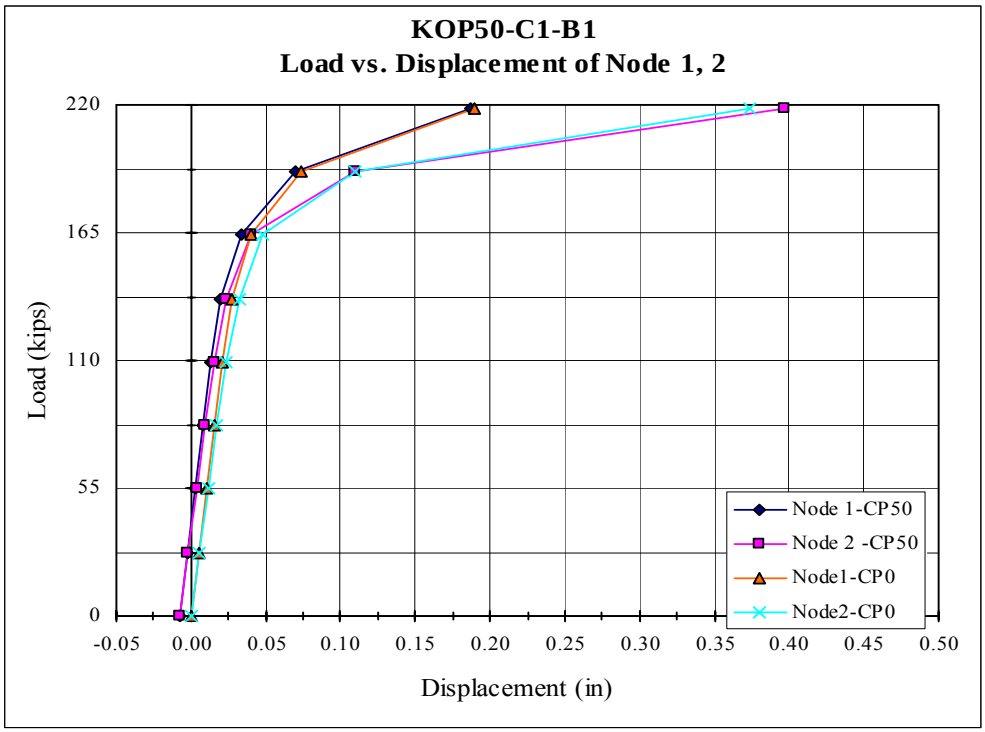

Figure 5.10 – C1-B1 Node 1, 2 Load-Displacement

Fig 5.11 shows that the initial compression had a negative effect on the load-displacement curve for both tension and compression branch at the first several load steps. In addition, when the branch ramp load reached the last two load steps, the displacement of node 3 area with initial chord compression load became larger than that of the connection without chord load. The compression branch of node 4 area exhibited same displacement in the last load step in both chord load CP0 and chord load CP50.

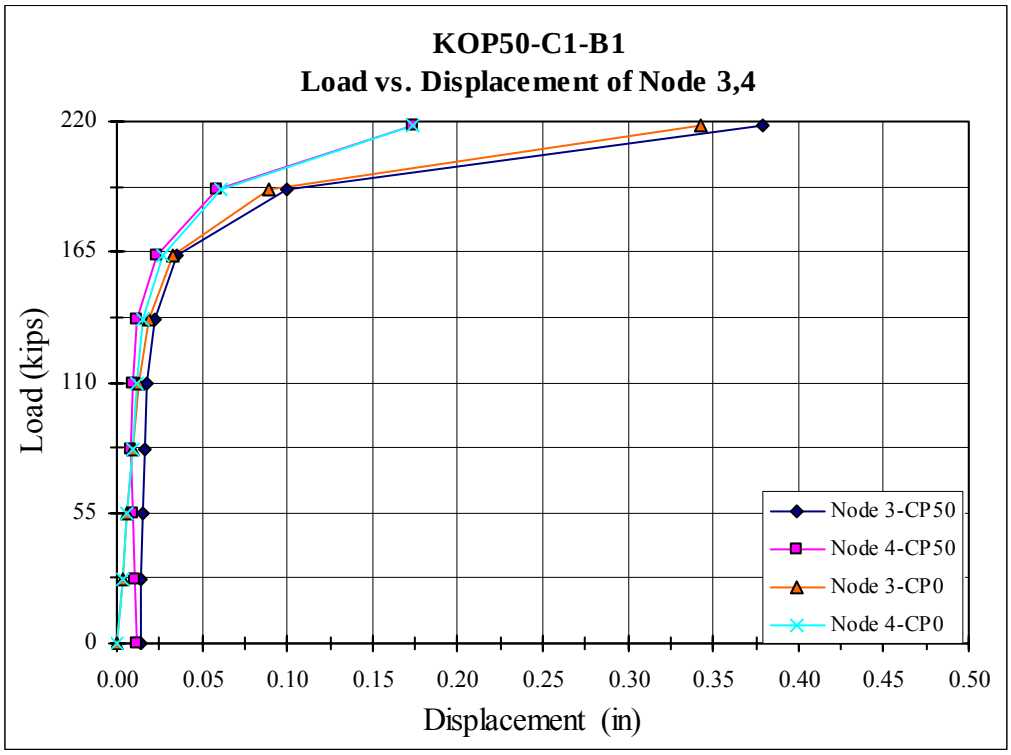

Figure 5.11 – C1-B1 Node 3, 4 Load-Displacement

The displacement for node 5 and node 6 areas was limited to a small range whether or not the chord had initial chord member compression.

Fig 5.12 shows that the initial compression had a little negative effect on the load-displacement curve for all three node areas. With the branch load increasing, the negative effect was getting smaller and the load-displacement became close to the load –

displacement curve without chord member force. Compared with in Fig 5.4, when the branch ramp load reached the last two load steps, the displacement of these three node areas with initial chord compression load became larger than the connection without the chord load. Therefore, the connection without compression load could develop higher connection strength than the connection with initial chord compression load.

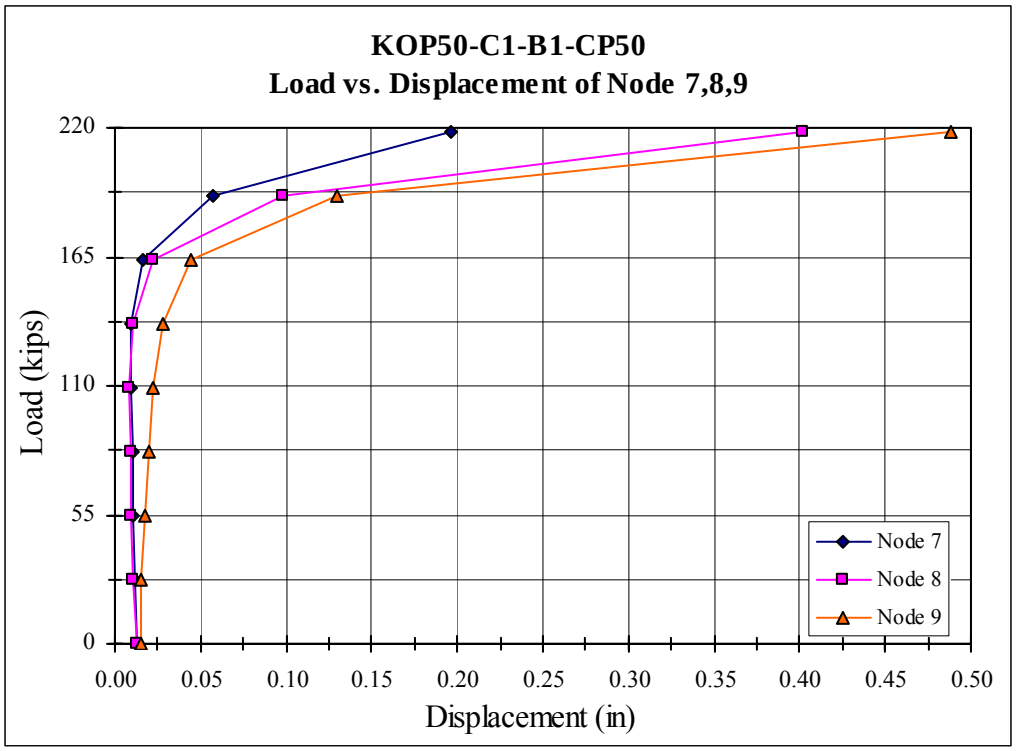

Figure 5.12 – C1-B1-CP50 Node 7, 8, 9 Load-Displacement

5.6 Comparison of the Load Von Mises Stress Behavior

The von mises stress contour exhibit a clear stress distribution and behavior of the weld and base metal in the truss connections. The stress contours with different branch member and same chord member display a similar stress development pattern in the connections. Fig 5.13 to Fig 5.15 shows the stress contour with only different branch member as the Fig 4.20 to Fig 4.22. In Fig 5.13 to 5.15 the branch load is increased from 84.22 kips to 168.44kips. The stress development with different branches exhibited

almost similar pattern. This confirmed the observations on the load-displacement behavior with same chord but different branch member.

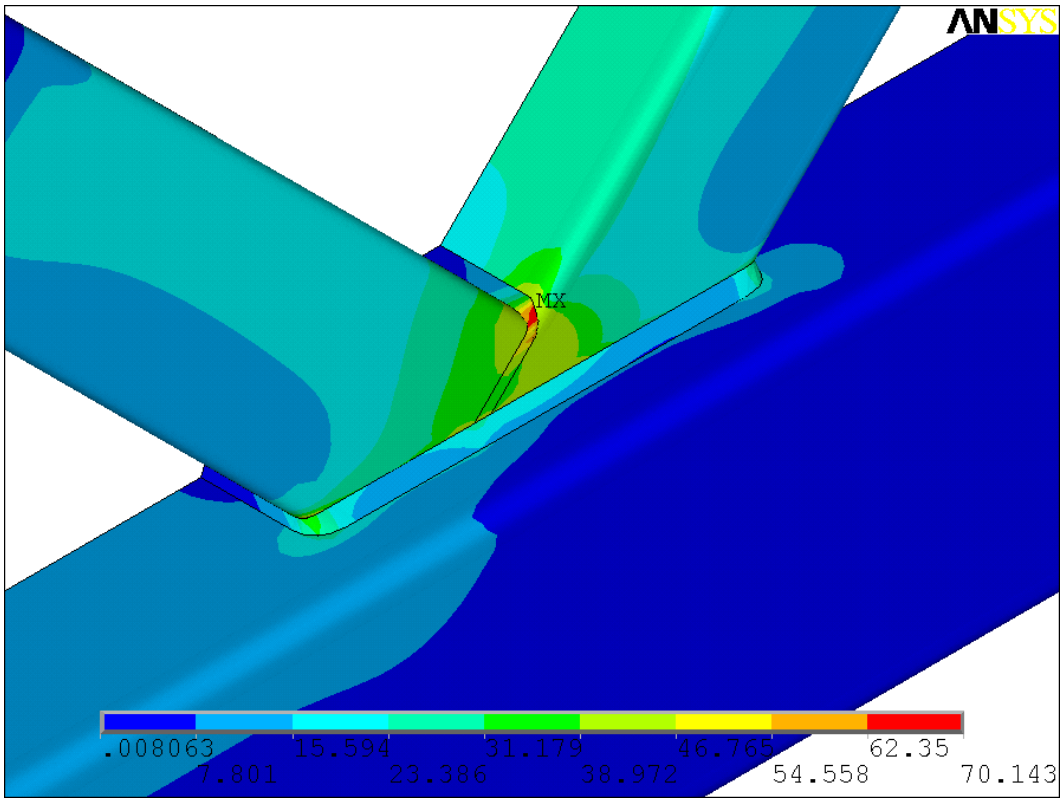

Figure 5.13 – C1-B2-CP0-LS4 Load-Von Mises Stress Contour (ksi)

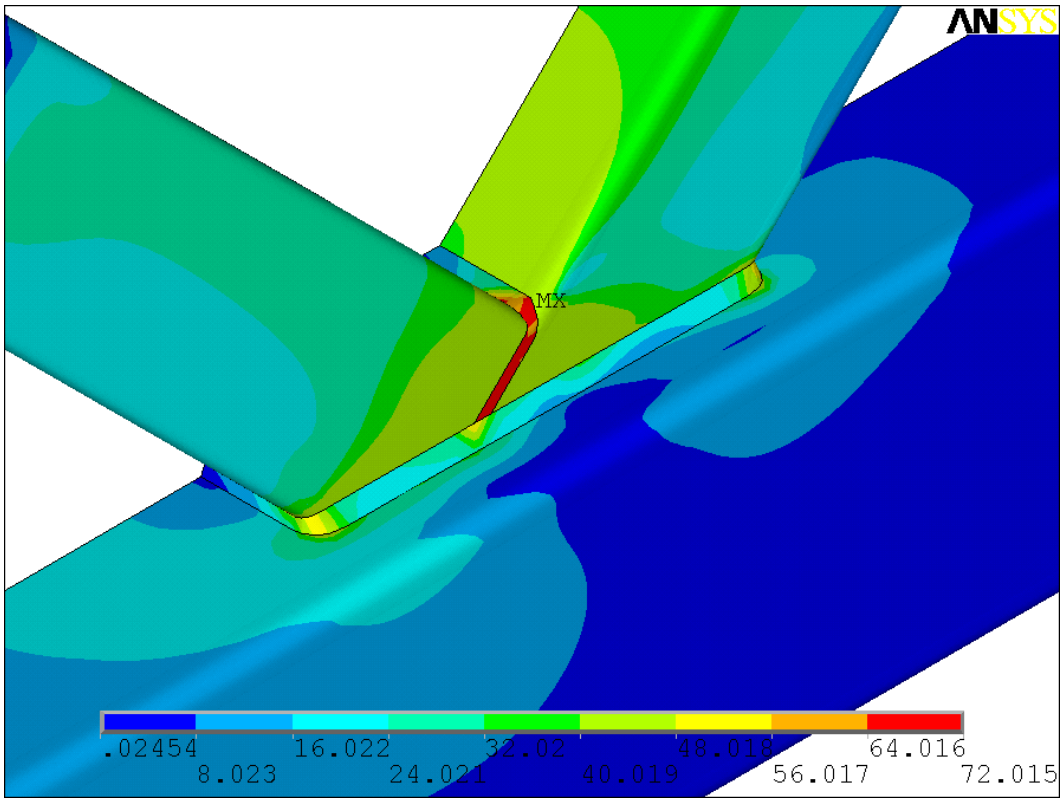

Figure 5.14 – C1-B2-CP0-LS6 Load-Von Mises Stress Contour (ksi)

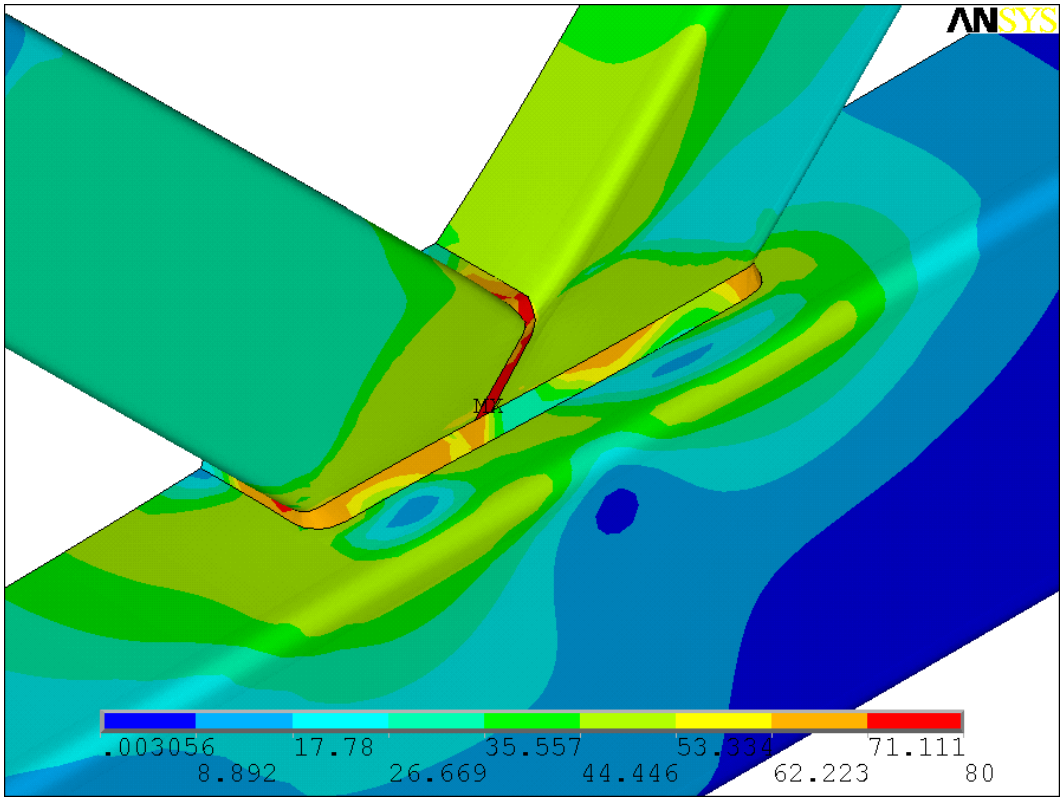

Figure 5.15 – C1-B2-CP0-LS8 Load-Von Mises Stress Contour (ksi)

Investigation on the same branch member but different chord member shows that the connection with thinner thickness chord member exhibit earlier tendency to reach the tensile stress compared to thicker chord member. Fig 5.16 and Fig 5.17 shows two geometric configured connections with different chord members. Although the general behavior is similar, the connection with thinner thickness already reaches the stress limit in load step 7 but the thicker one doesn't. It is also confirmed that the chord member effect on the load displacement behavior. Addition investigation on the load stress curve on the special observation point shows the similar patterns for different branch member and same chord member. Appendixes B to appendix E provide additional load stress curve figures for comparison.

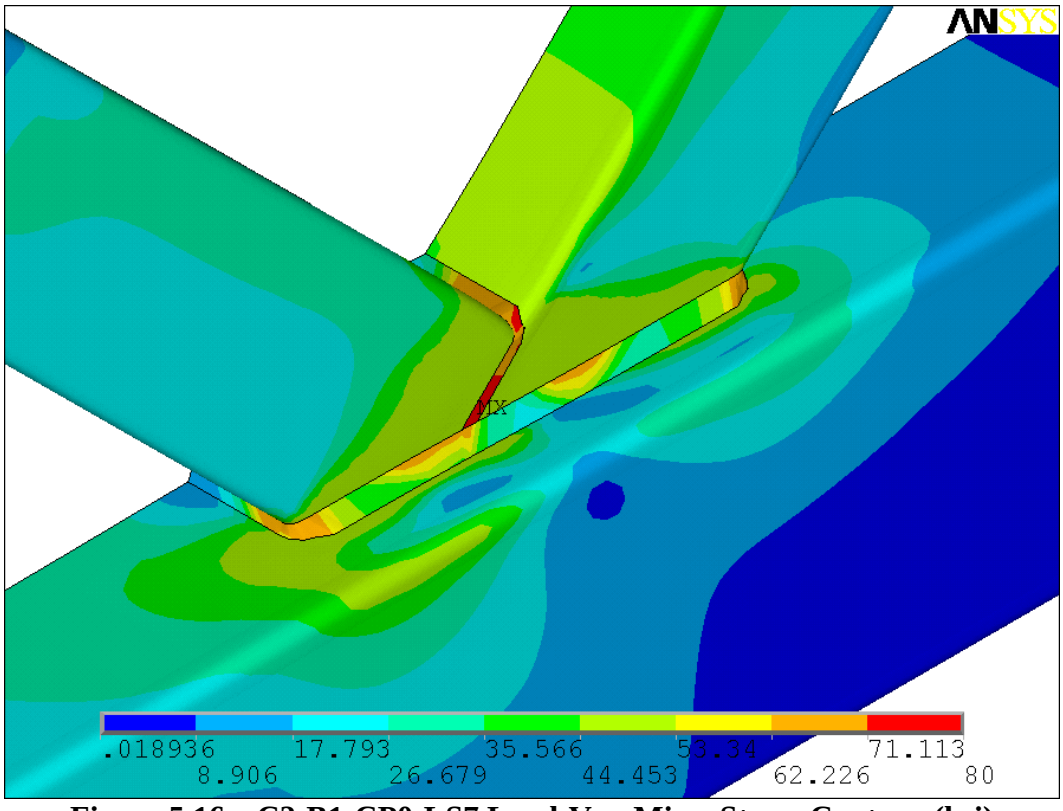

Figure 5.16 – C2-B1-CP0-LS7 Load-Von Mises Stress Contour (ksi)

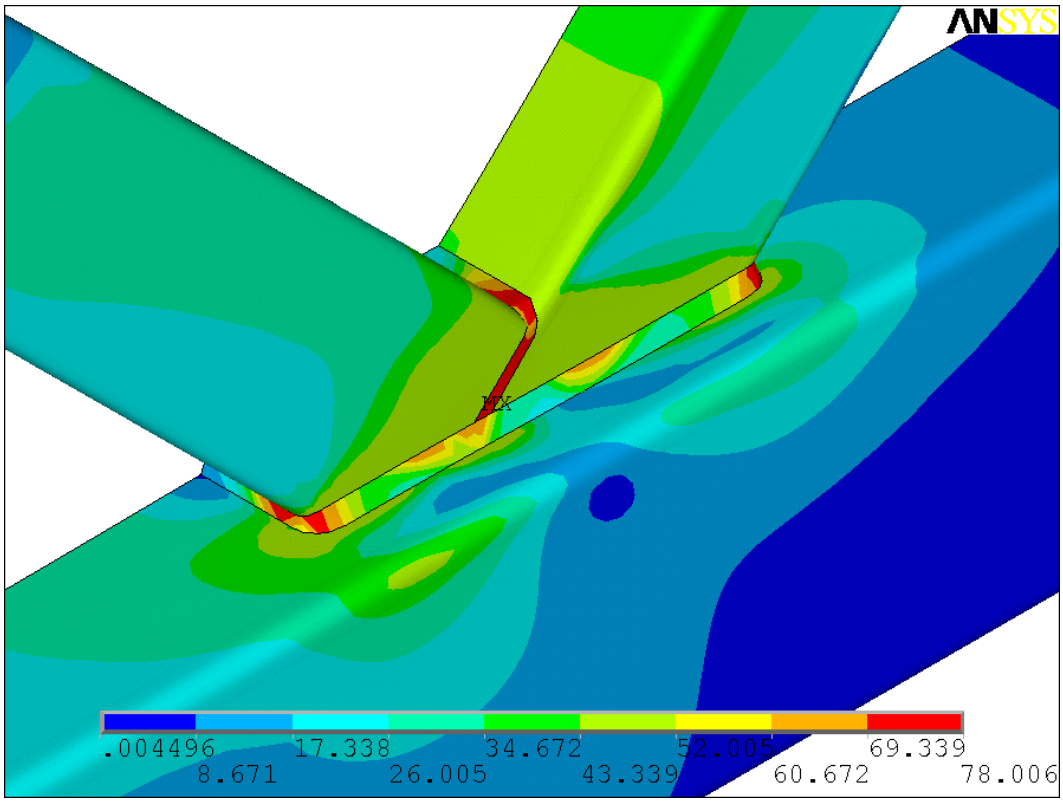

Figure 5.17 – C1-B1-CP0-LS7 Load-Von Mises Stress Contour (ksi)

Chapter 6 –Observations, Recommendations and Conclusions

6.1 General

The observations extracted from the program result of this numerical research are summarized in this chapter. In addition, it contains the recommendations for further refined modeling methods. Also, topics regarding future research and a list of primary conclusions that were made from the result and the comparison of the solutions are described.

6.2 Observations

The 20 node 3-D solid95 elements exhibited a very good behavior in the finite element modeling. Serving as the smallest 3-D components in the model, the element provided a competitive flexibility in assembling the truss joint. The attribute of the element and its degenerations guaranteed a nice simulation of real connections. However, due to the large amount of the elements used in the model, it took a considerably long time to finish the analysis procedure to generate dozens of solutions for different loads and geometric configurations.

The irregular shape of the weld was hard to simulate and poorly shaped elements couldn't always be avoided. Peak strain and stress was always located in the tip point of the sharp angle corner node of the element. After the large load was given to the model, in some areas of the HSS both steel and weld material surpassed the yield point and exhibited inelastic behavior. At this point the stress concentrations were decreased in some areas due to the stress strain redistribution. However, because of the geometric limitation of the weld, especially in the irregular part, the stress concentration was not be eliminated completely.

After the stress or strain in an element of the model first reached the maximum tensile stress of the material limit, the numerical model was not fully converged according to the program convergence criteria. In the real situation, cracks in the base metal would likely form due to the large local deformation in high stress concentration regions. By forcing the program to continue running, obvious nonlinear load-displacement curve was developed. Local buckling of the branch and chord members failure were then observed to be major factors that affect the load-displacement curves.

6.3 Conclusions

The following list summarizes the primary conclusions regarding the behavior of the overlapping K-joint in the finite element model:

1. The 3-D solid element model reasonably predicts the behavior of the HSS truss connection. The finite element models created for this study exhibited the connection strength close to the value calculated following the design manual.

2. Chord member b/t ratio had strong effect on the connection strength compared with branch member b/t ratio when the branch load was close to the ultimate connection strength. Increase the Chord member b/t ratio will decrease the ultimate connection strength.

3. Four types of failure models were found in the analyses which included chord member base metal tear-out, branch member base metal tear-out and branch and chord member local buckling. The combinations of these failure modes were found in all models under investigation. Any one of these failure modes was the trigger of the other two.

4. The AISC equation for the strength of overlapped K-connections is applicable when b/t ratio exceeds the manual limit up to 45.1 for chord and 43 for branch member.

5. The chord member compression didn't have very significant effect on the connection behavior when the branch load was small. When the branch load was close to the ultimate connection strength, increasing the chord member compression load will decrease the ultimate connection strength.

6.4 Recommendations for Future Research

Solid95 elements and degeneration elements are suitable for the analysis of irregular shaped solids. Simple shell elements are recommended for use in low stress gradient areas to reduce the computational time.

To simulate the crack effect in the analysis procedure, special elements or methods are recommended for the model building strategy. If a crack is generated, the element in which the crack develops will have no contribution to the structural matrix. In finite element modeling, the feature of element "birth" or "death" can be employed to study the further behavior of the connection members. A severe reduction factor is multiplied to the element stiffness to make the element have no effect on the global matrix. Special elements with modified middle nodes can be used to simulate the crack tip area. By moving the middle node to the 1/4 of the corner node, quarter point elements can also be used to generate a good simulation of the crack tip area. By properly controlling the features of "birth" or "death" or using quarter point elements, a better simulation of the model could be achieved.

All results generated by FE methods need to be verified by experiments. The experimental tests for the same load and geometric configuration are suggested to provide further verification for the numerical test results.

6.5 Summary

The aim of this study was to investigate the behavior of overlapped K connections with b/t ratios outside the range of applicability specified in the LRFD specification. The investigation was conducted using appropriate modeling methods to predict the behavior of the HSS truss overlapping K-connection. Instead of building up a solid volume and then generating the mesh by the program automatically, elements were directly assembled to control the modeling detail at node level. Descriptions of every geometric configuration, loading condition, constraints and corresponding model results were presented.

It was concluded that the overlapping-K connection is an applicable truss connection form. b/t ratio of connection members and chord member initial pressure has effect on the ultimate connection strength. In addition, the AISC equation for predicting the strength of the overlapped K-connection reasonably predicts the strength for the investigated connection configurations.

References

American Institute of Steel Construction, Inc. (1997). "Hollow Structural Sections Connections Manual" *1997 ISBN 1-56434-045-2*

American Institute of Steel Construction, Inc. (2000). "LRFD Specification for Steel Hollow Structural Sections" *November 10, 2000 Chicago, Illinois*

American Institute of Steel Construction, Inc. (2005) "Steel Construction Manual" *December, 2005 ISBN 1-56424-055-X*

ANSYS 9.0 Documentation (2004), Swanson Analysis System, Inc.

Cao, J.J., Yang, G.J., Packer, J.A., Burdekin, F.M. (1998) "Crack Modeling in FE Analysis of Circular Tubular Joints"
Engineering Fracture Mechanics 61 (1998) 537-553 ©1998 Elsevier Science Ltd. PII: S0013-7944(98)00091-5

Chiew, Sing-Ping, Lie, Seng-Tjhen, Lee, Chi-King and Huang, Zhi-Wei (2004) "Fatigue Performance of Cracked Tubular T Joints under Combined Loads I: Experimental"
Journal of Structural Engineering, Vol. 130, No. 4, April 1, 2004. ©ASCE, ISSN 0733-9445/2004/4-562–571

Chiew, Sing-Ping, Lie, Seng-Tjhen, Lee, Chi-King and Huang, Zhi-Wei (2004) "Fatigue Performance of Cracked Tubular T Joints under Combined Loads II: Numerical"
Journal of Structural Engineering, Vol. 130, No. 4, April 1, 2004. ©ASCE, ISSN 0733-9445/2004/4-572–581

Chiew, Sing-Ping, Lie, Seng-Tjhen, Lee, Chi-King and Huang, Zhi-Wei (2001) "Stress intensity factor for a surface crack in a tubular T-joint"
International Journal of Pressure Vessels and Piping, 78 (2001) 677-685 ©2001 Elsevier Science Ltd. PII S0308-0161(01)00083-7

Chiew, Sing-Ping, Soh, Chee-Kiong and Wu, Nai-Wen (1999) "Experimental and Numerical Stress Analysis of Tubular XT-Joint"
Journal of Structural Engineering, Vol.125, No. 11, November, 1999. ©ASCE, ISSN 0733-9445/99/0011-1239–1248

Cook, Robert D., Malkus, David S., Plesha, Michael E., Witt, Robert J.(2002) "Concepts and Applications of Finite Element Analysis"
2002 ISBN 0-471-35605-0

Fung, T.C., Soh, C.K., Gho, W.M., Qin, F. (2001) "Ultimate capacity of Completely Overlapped tubular joints I, An experimental investigation"
Journal of Constructional Steel Research 57 (2001) 855–880. ©2001 Elsevier Science Ltd.

Gazzola, Fabio and Lee, Marcus M. K. (2002) "Assessment of Strength Equations for Overlapped Tubular K-Joints"
*Journal of Structural Engineering, Vol. 128, No. 1, January 1, 2002. ©ASCE, ISSN 0733-9445/2002/1-119–*124

Gurson, A. L. (1975). "Plastic flow and fracture behavior of ductile materials incorporating void nucleation, growth and interaction."
PhD thesis, Brown Univ., Providence, R.I.

Haswell, J., and Hopkins, P. (1991) "A review of fracture mechanics models of tubular joints" *Fatigue Fract. Eng. Mater. Struct., 14(5),483–497*

Herion, S., Mang, F., and Puthli, R. (1996) "Parametric study on multi-planar K joints with gap made of circle hollow sections by means of the finite element method"
Proc., 6th Int. Offshore and Polar Engineering Conf., Los Angeles, Vol. IV, 68–73.

Jubran, Jihad S. and Cofer, William F. (1995) "Finite-Element Modeling of Tubular Joints I Numerical Results"
Journal of Structural Engineering, Vol. 121, No. 3, March 1995. ©ASCE. ISSN 0733-9445/95/0003-0469-0508

Jubran, Jihad S. and Cofer, William F. (1995) "Finite-Element Modeling of Tubular Joints II Design Equations"
Journal of Structural Engineering, Vol. 121, No. 3, March 1995. ©ASCE. ISSN 0733-9445/95/0003-0509-0516

Lee, C. K., Wong, S. M. and Lie, S.T. (2001) "On increasing the order and density of 3D finite element meshes"
Communications in numerical methods in engineering 2001, 17:55-68 ©2001 John Wiley & Sons, Ltd

Lee, Marcus M. K. and Dexter, Ellen M. (2004) "Finite-Element Modeling of Multi-Planar Offshore Tubular Joints"
OOAE Division for publication in the Journal of Offshore Mechanics and Arctic Engineering, Vol. 126, February 2004 ©ASME

Lee, Marcus M. K. and Dexter, Ellen M. (1999) "Static Strength of Axially Loaded Tubular K-Joints II: Ultimate Capacity"
Journal of Structural Engineering, Vol. 125, No. 2, February, 1999. ©ASCE, ISSN 0733-9445/99/0002-0202–0210

Lee, Marcus M. K. and Dexter, Ellen M. (1999) "Static Strength of Axially Loaded Tubular K-Joints I: Behavior"
Journal of Structural Engineering, Vol. 125, No. 2, February, 1999. ©ASCE, ISSN 0733-9445/99/0002-0194-0201

Mackerle, Jaroslav (1996) “Finite element analysis and simulation of welding: a bibliography”
Modeling Simulation Material Science Eng. 4 (1996) 501–533.

Packer, J.A. and Henderson, J.E. (1997) “Hollow Structural Section Connections and Trusses-A Design Guide” 2nd.Edition *Canadian Institute of Steel Construction, Toronto, ON*

Qian, X. D., Choo, Y. S., Liew, J. Y. R. and Wardenier, J. (2005) “Simulation of Ductile Fracture of Circular Hollow Section Joints Using the Gurson Model”
Journal of Structural Engineering, Vol. 131, No. 5, May 1, 2005. ©ASCE, ISSN 0733-9445/2005/5-768–780

Stacy, A., and Sharp, J. V. (1997). “Fatigue damage in offshore structures—Cause, detection, and repair.” *Proc.*, *8th Int. Conf. on the Behavior of Offshore Structure, Delft University of Technology, Delft, the Netherlands*.

Thomason, P. F. (1990). “Ductile fracture of metals”
Pergamon, Oxford, U.K.

Wardenier, J, Kurobane, Y., Packer, J.A, Dutta, D., Yeomans, N. (1995) “Design guide: For circular hollow section (CHS) joints under predominantly static loading” *CIDECT*

APPENDIX

Appendix A

ANSYS Input (First 4 pages)

```
!~~~~~~~~~~~~~~~~~~~~~~~~~~~~~~~~~~~~~~~~~~~~~~~~~~~~~~~~~~~~~~~~~~~~~~~~~~
!~~~~~~~~~~~~~~~~~~~~~~     ANSYS Version: R9.0-Update-20041104          ~~~~~~~~~~~~~
!~~~~~~~~~~~~~~~~~~~~~~     Code Update:  11:15:12  04/21/2006           ~~~~~~~~~~~~~
!~~~~~~~~~~~~~~~~~~~~~~     Creat By: Gang Zhao                          ~~~~~~~~~~~~~
!~~~~~~~~~~~~~~~~~~~~~~~~~~~~~~~~~~~~~~~~~~~~~~~~~~~~~~~~~~~~~~~~~~~~~~~~~~


!------------------------------------------------------------------------------------------
CTH=2    !-----    Chord Member Thickness# Setting              --------------
BTH=2    !-----    Branch Member Thickness# Setting             -------------
!------------------------------------------------------------------------------------------
!---------------    CTH=1,HSS-14x14x3/8    ;  CTH=2,HSS-14x14x5/16    ----
!---------------    CTH=3,HSS-14x14x1/2    ;                   --------------------
!------------------------------------------------------------------------------------------
!---------------    BTH=1,HSS-8x8x1/4      ;  BTH=2,HSS-8x8x3/16      -------
!---------------    BTH=3,HSS-8x8x5/16     ;                   ---------------------
!------------------------------------------------------------------------------------------


!------------------------------------------------------------------------------------------
!--------------------    General Setting & Constants Process    -------------------
!------------------------------------------------------------------------------------------
/PREP7

!---------- Unit: British Inch Unit
/UNITS,BIN

!---------- Preferences for Number Display
/PNUM,KP,0
/PNUM,LINE,0
/PNUM,AREA,0
/PNUM,VOLU,0
/PNUM,NODE,0
/PNUM,TABN,0
/PNUM,SVAL,0
/NUMBER,0
/PNUM,ELEM,0

!---------- Preferences for GUI Filtering Display: Structural
/NOPR
/PMETH,OFF,0
KEYW,PR_SET,1
KEYW,PR_STRUC,1
```

```
KEYW,PR_THERM,0
KEYW,PR_FLUID,0
KEYW,PR_ELMAG,0
KEYW,MAGNOD,0
KEYW,MAGEDG,0
KEYW,MAGHFE,0
KEYW,MAGELC,0
KEYW,PR_MULTI,0
KEYW,PR_CFD,0
/GO

!---------- Define Element Type
ET,1,SOLID95

!---------- Define Material Properties
MP,PRXY,1,0.3
MP,EX,1,29000
TB,MELAS,1,,3,
TBPT,,0.001586,46
TBPT,,0.01745,46
TBPT,,0.19035,58

MP,PRXY,2,0.3
MP,EX,2,29000
TB,MELAS,2,,3,
TBPT,,0.001586,46
TBPT,,0.01745,46
TBPT,,0.19035,58

MP,PRXY,3,0.3
MP,EX,3,29000
TB,MELAS,3,,3,
TBPT,,0.001586,46
TBPT,,0.01745,46
TBPT,,0.19035,58

MP,PRXY,4,0.3
MP,EX,4,29000
TB,MELAS,4,,2,
TBPT,,0.002414,70
TBPT,,0.1,80

MP,PRXY,5,0.3
MP,EX,5,29000


!---------- Define Program Rang Constants
!---------- Define PI
PI = ACOS(-1)
!---------- Define Layer Variable
NUM_ODD_LAYER = -1
```

```
L_TOTAL = -1
!---------- Define Chord HSS Geometric Constants
B_1 = 14
H_1 = 14
*IF,CTH,EQ,1,THEN
  Wall_1 = 0.349
*ELSEIF,CTH,EQ,2,THEN
  Wall_1 = 0.291
*ELSEIF,CTH,EQ,3,THEN
  Wall_1 = 0.465
*ENDIF
R_corner = Wall_1*2

!---------- Define Branch HSS Geometric Constants
B_2 = 8
H_2 = 8
*IF,BTH,EQ,1,THEN
  Wall_2 = 0.233
  R_corner2 = Wall_2*2
*ELSEIF,BTH,EQ,2,THEN
  Wall_2 = 0.174
  R_corner2 = Wall_2*2
*ELSEIF,BTH,EQ,3,THEN
  Wall_2 = 0.291
  R_corner2 = Wall_2*2
*ENDIF


!---------- Define Chord End Plate Layer #
PPC=2
!---------- Define Branch End Plate Layer #
PPB=3


!-------------------------------------------------------------------------------
!--------------------        Define Chord HSS Pipe         --------------------
!-------------------------------------------------------------------------------
!---------- Define Material #
MAT,1
!---------- Define Section Length
*DIM,CJ,ARRAY,16
CJ(1) = 0
CJ(2) = 30+CJ(1)
CJ(3) = 3+CJ(2)
CJ(4) = 0.5+CJ(3)
CJ(5) = 0.5+CJ(4)
CJ(6) = R_corner2/SIN(PI/4)+CJ(5)
CJ(7) = (H_2-R_corner2*2)/SIN(PI/4)+CJ(6)
CJ(8) = R_corner2/SIN(PI/4)/2+CJ(7)
CJ(9) = R_corner2/SIN(PI/4)+CJ(7)
CJ(10) = (H_2/2-R_corner2)/SIN(PI/4)-4.5+CJ(9)
```

```
CJ(11) = 4.5+CJ(10)
CJ(12) = R_corner2/SIN(PI/4)+CJ(11)
CJ(13) = 0.5+CJ(12)
CJ(14) = 0.5+CJ(13)
CJ(15) = 3+CJ(14)
CJ(16) = 30+CJ(15)
!---------- Define Element Width for Plate
EB_1 = ((B_1/2-R_corner)/B_1)
!---------- Define First Node Layer Pointer
FIRST = 0


!---------- Start Layer Loop
*DO,N,1,15,1

  *IF,N,EQ,1,THEN
    EL = 30/14
    CEND = EL
  *ELSEIF,N,EQ,2,THEN
    EL = 0.75
  *ELSEIF,N,EQ,3,THEN
    EL = CJ(4)-CJ(3)
  *ELSEIF,N,EQ,4,THEN
    EL = CJ(5)-CJ(4)
  *ELSEIF,N,EQ,5,THEN
    EL = CJ(6)-CJ(5)
  *ELSEIF,N,EQ,6,THEN
    EL = (CJ(7)-CJ(6))/20
  *ELSEIF,N,EQ,7,THEN
    EL = CJ(8)-CJ(7)
  *ELSEIF,N,EQ,8,THEN
    EL = CJ(9)-CJ(8)
  *ELSEIF,N,EQ,9,THEN
    EL = CJ(10)-CJ(9)
  *ELSEIF,N,EQ,10,THEN
    EL = (CJ(11)-CJ(10))/9
  *ELSEIF,N,EQ,11,THEN
    EL = CJ(12)-CJ(11)
  *ELSEIF,N,EQ,12,THEN
    EL = CJ(13)-CJ(12)
  *ELSEIF,N,EQ,13,THEN
    EL = CJ(14)-CJ(13)
  *ELSEIF,N,EQ,14,THEN
    EL = 0.75
  *ELSEIF,N,EQ,15,THEN
    EL = 30/14
  *ELSE
  *ENDIF
```

Appendix B

ANSYS Result for KOP50-C1-B1-CP0

Table A.B.1 –Geometric & Load Configuration for KOP50-C1-B1-CP0

	Geometric & Load Configuration
Chord member	14 ×14 × 3/8
Branch Member	8 × 8 × 1/4
Branch ramp Load In 8 load steps	218.48 kips
Chord Step Load	0 kips
Chord ramp Load In 8 load steps	308.98 kips

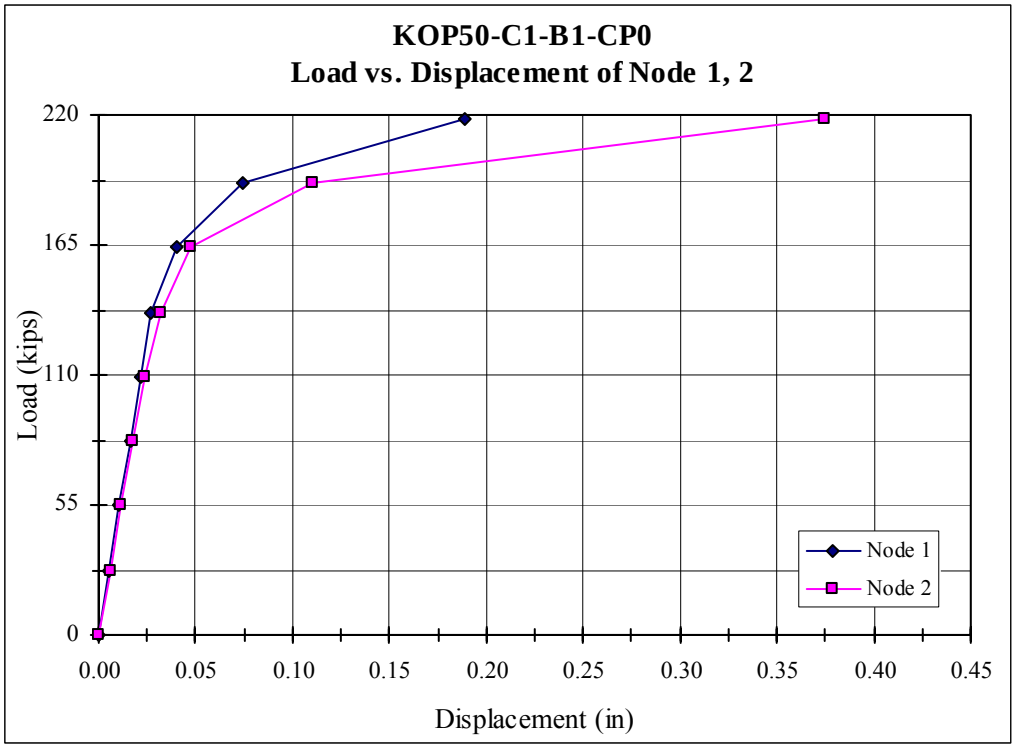

Figure A.B.1 – C1-B1-CP0 Node 1, 2 Load-Displacement

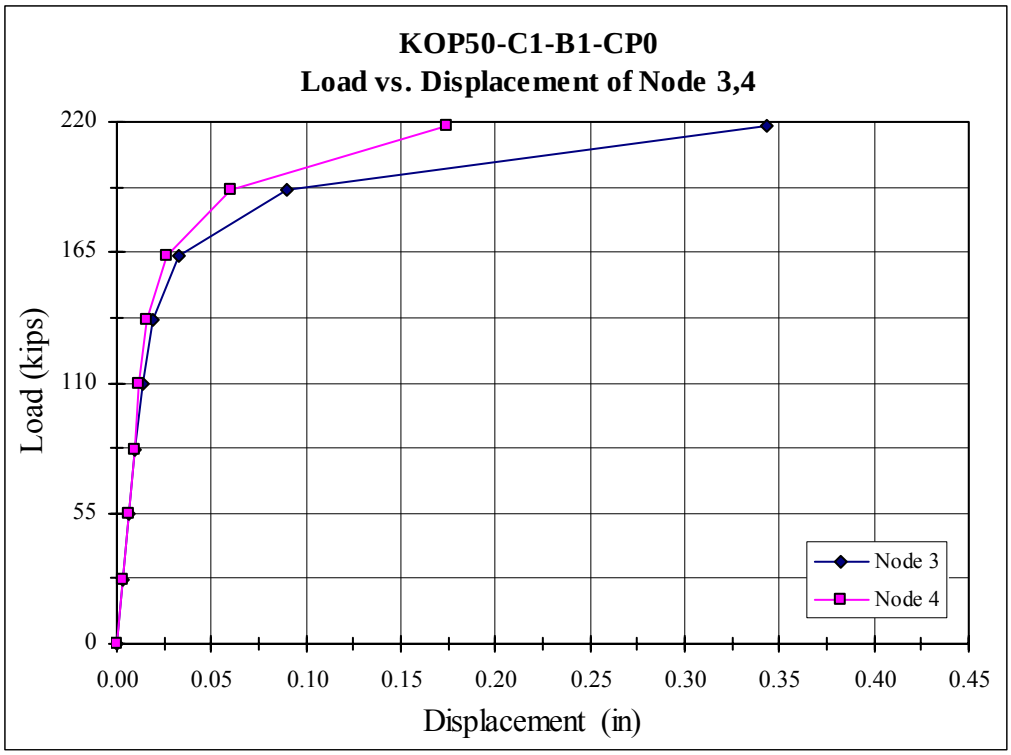

Figure A.B.2 – C1-B1-CP0 Node 3, 4 Load-Displacement

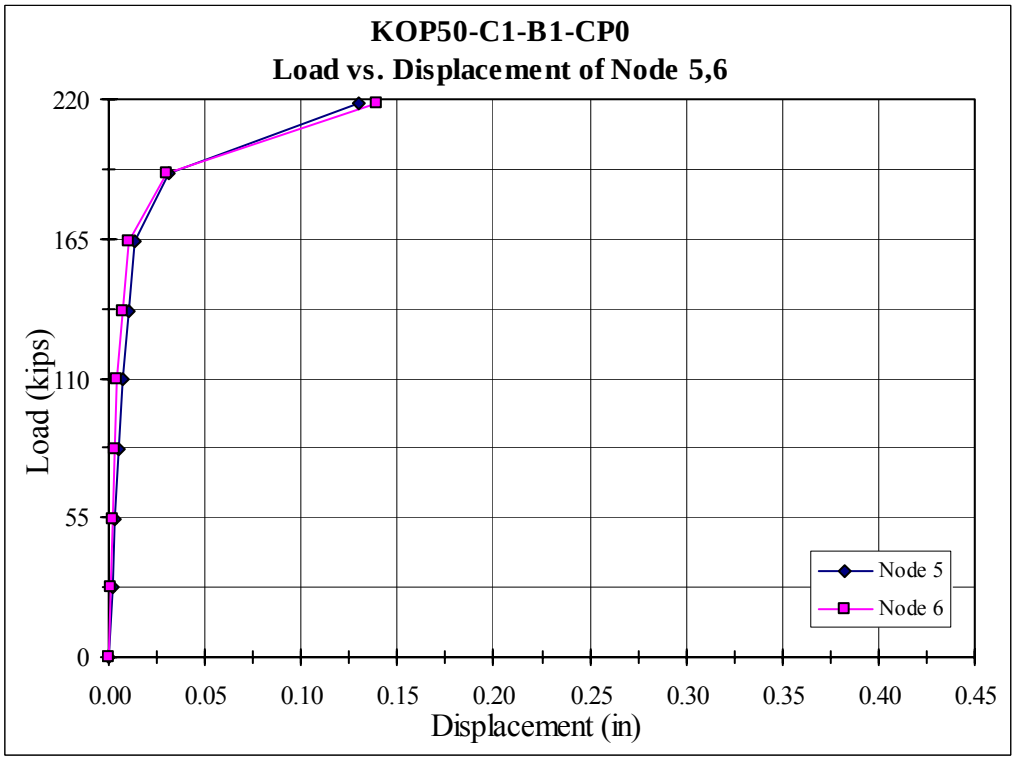

Figure A.B.3 – C1-B1-CP0 Node 5, 6 Load-Displacement

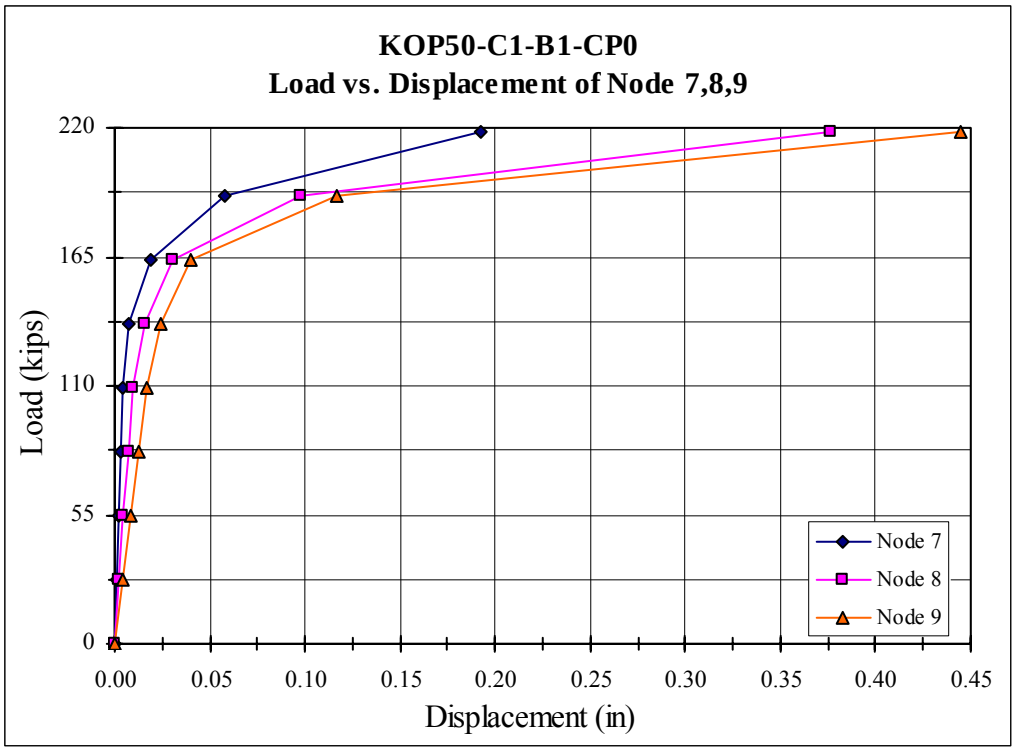

Figure A.B.4 – C1-B1-CP0 Node 7, 8, 9 Load-Displacement

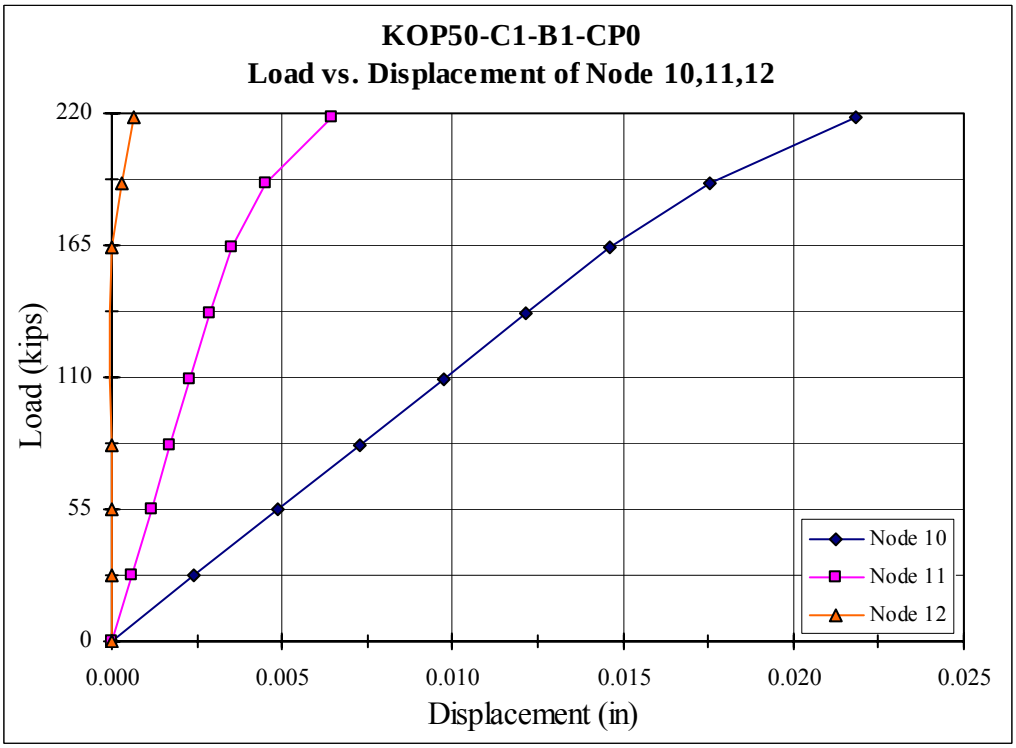

Figure A.B.5 – C1-B1-CP0 Node 10, 11, 12 Load-Displacement

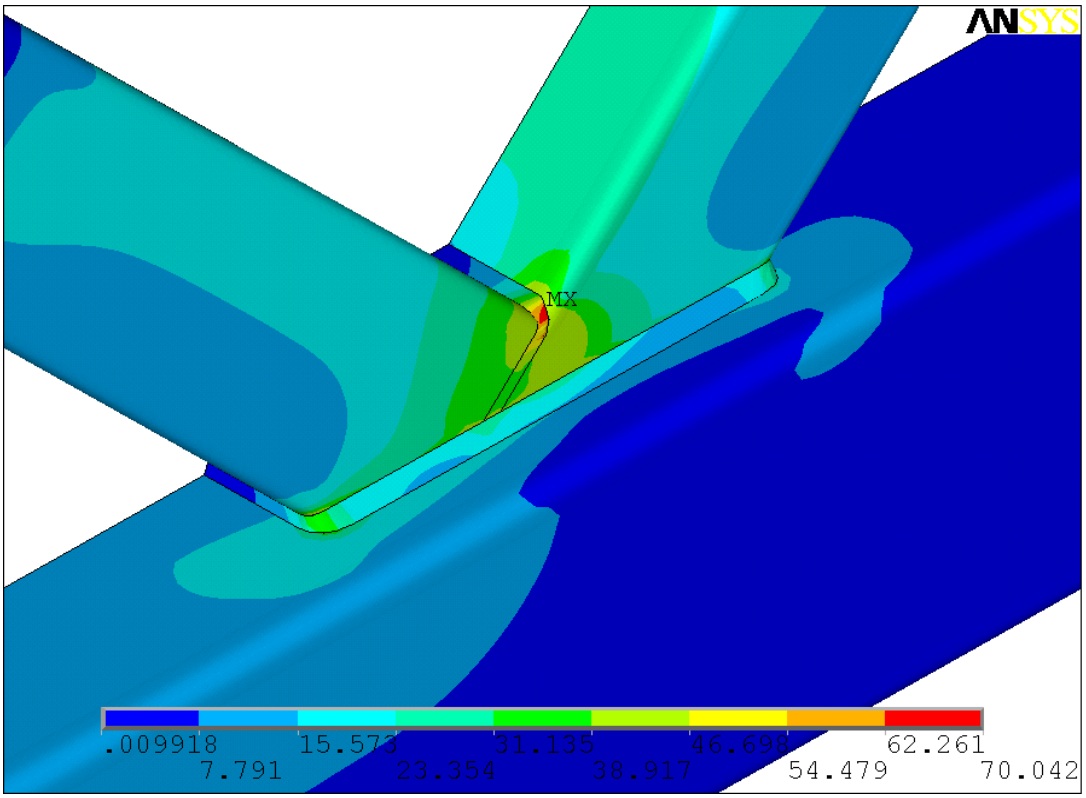

Figure A.B.6 – C1-B1-CP0-LS4 Load-Von Mises Stress Contour (ksi)

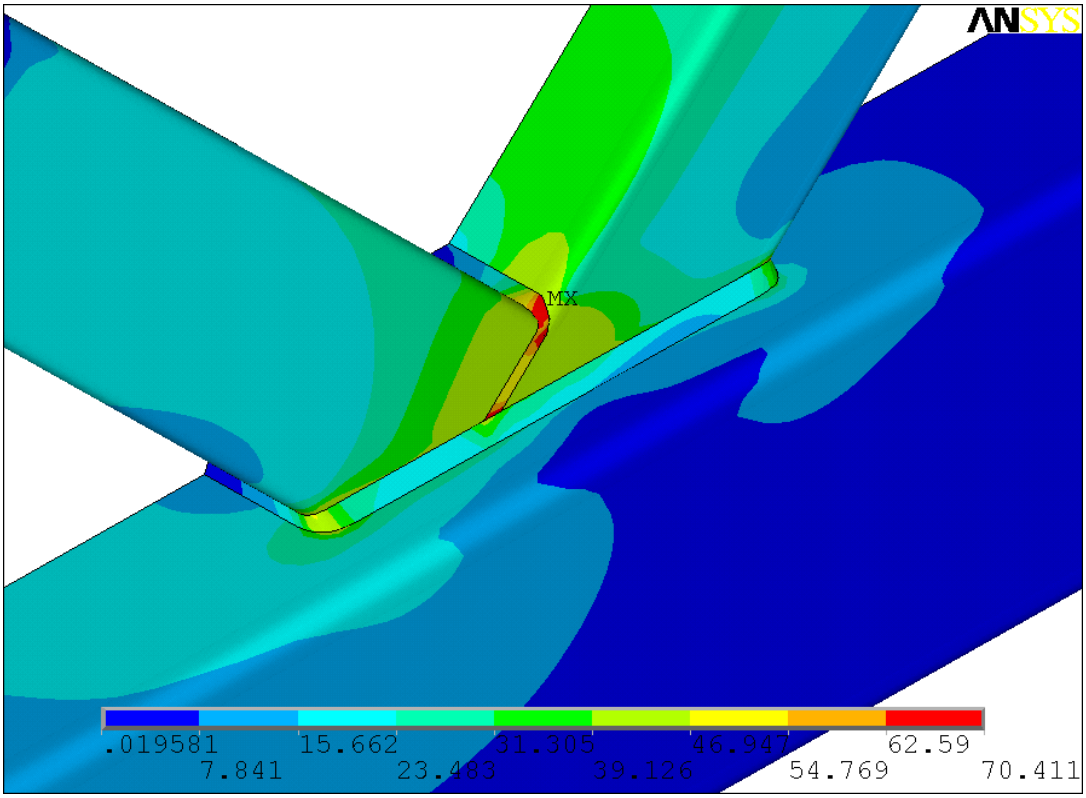

Figure A.B.7 – C1-B1-CP0-LS5 Load-Von Mises Stress Contour (ksi)

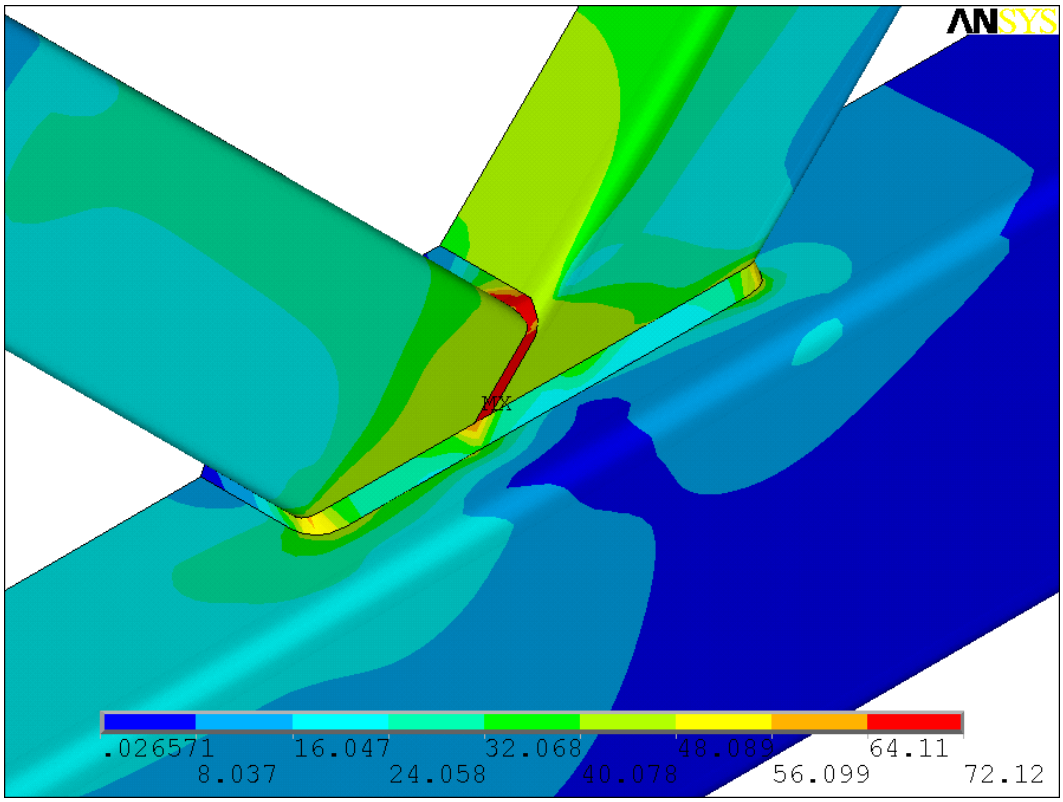

Figure A.B.8 – C1-B1-CP0-LS6 Load-Von Mises Stress Contour (ksi)

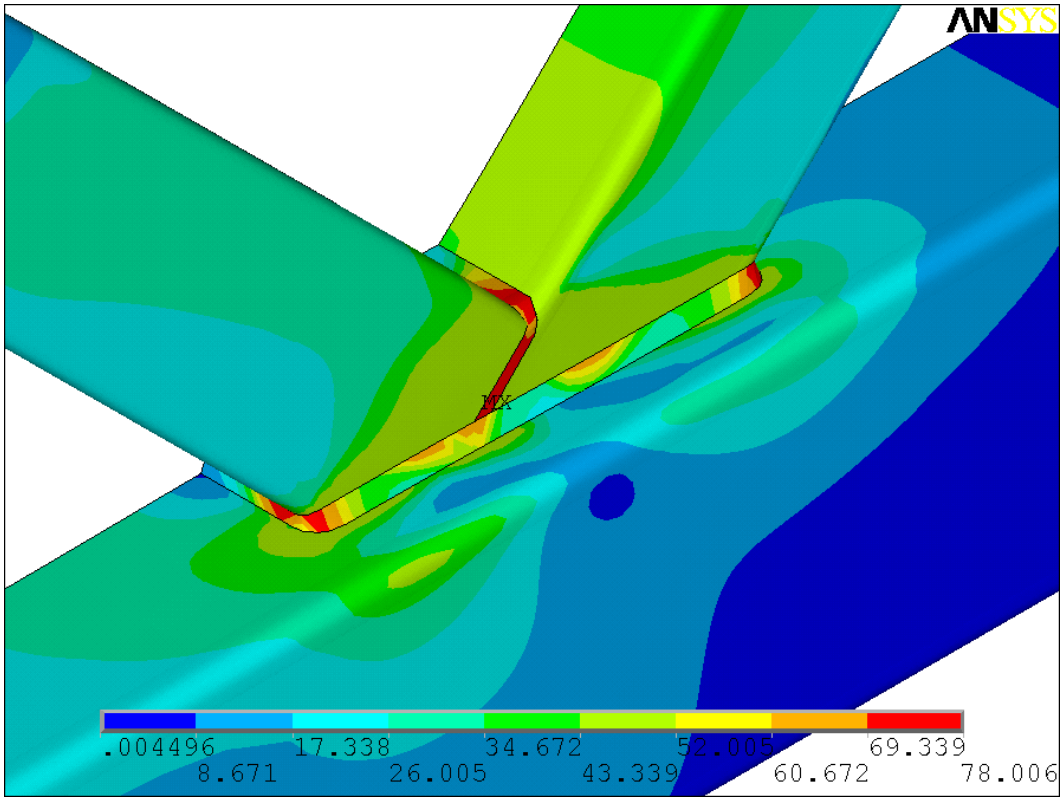

Figure A.B.9 – C1-B1-CP0-LS7 Load-Von Mises Stress Contour (ksi)

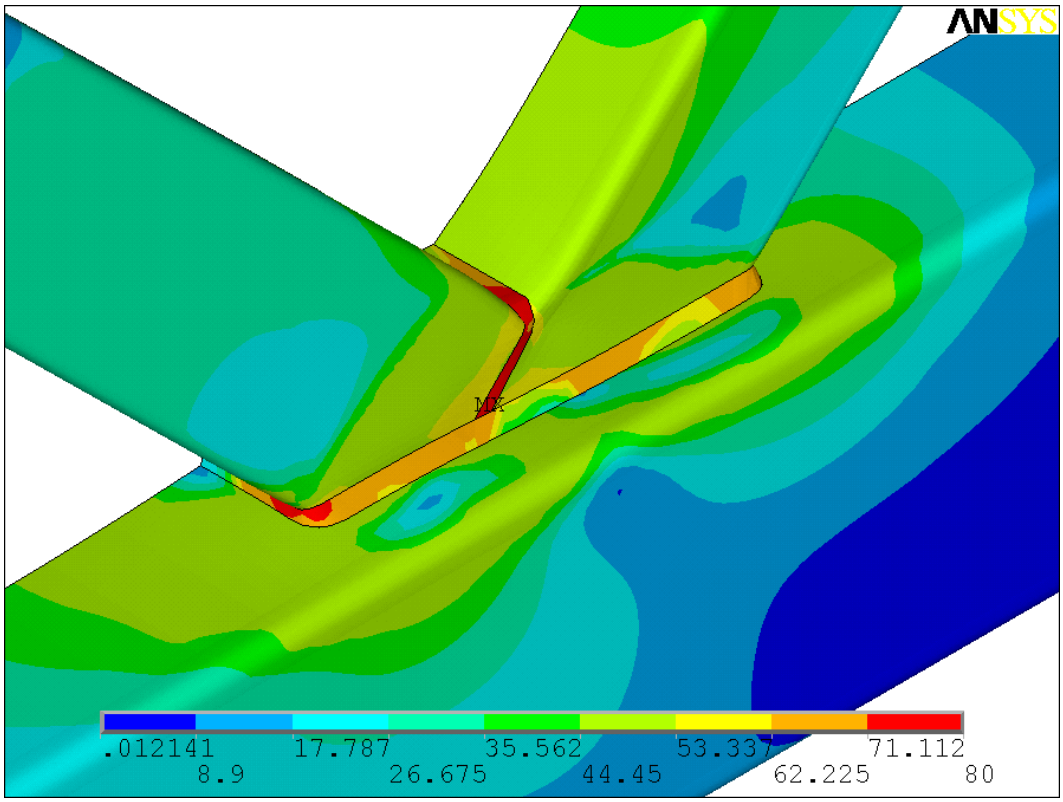

Figure A.B.10 – C1-B1-CP0-LS8 Load-Von Mises Stress Contour (ksi)

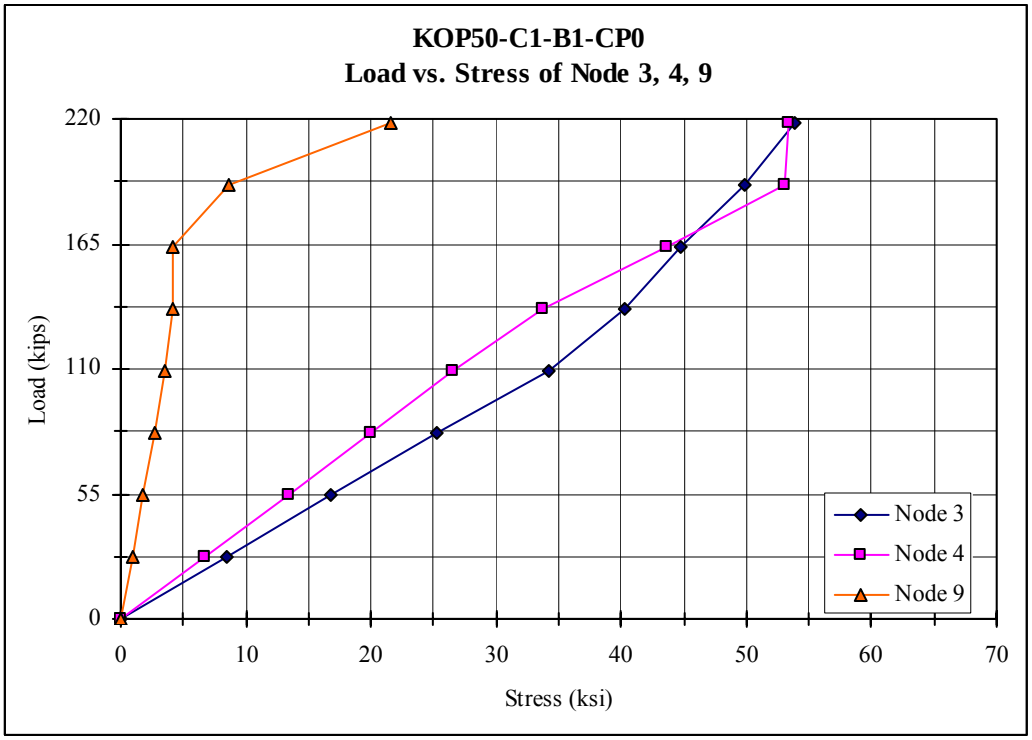

Figure A.B.11 – C1-B1-CP0 Node 3, 4, 9 Load-Stress

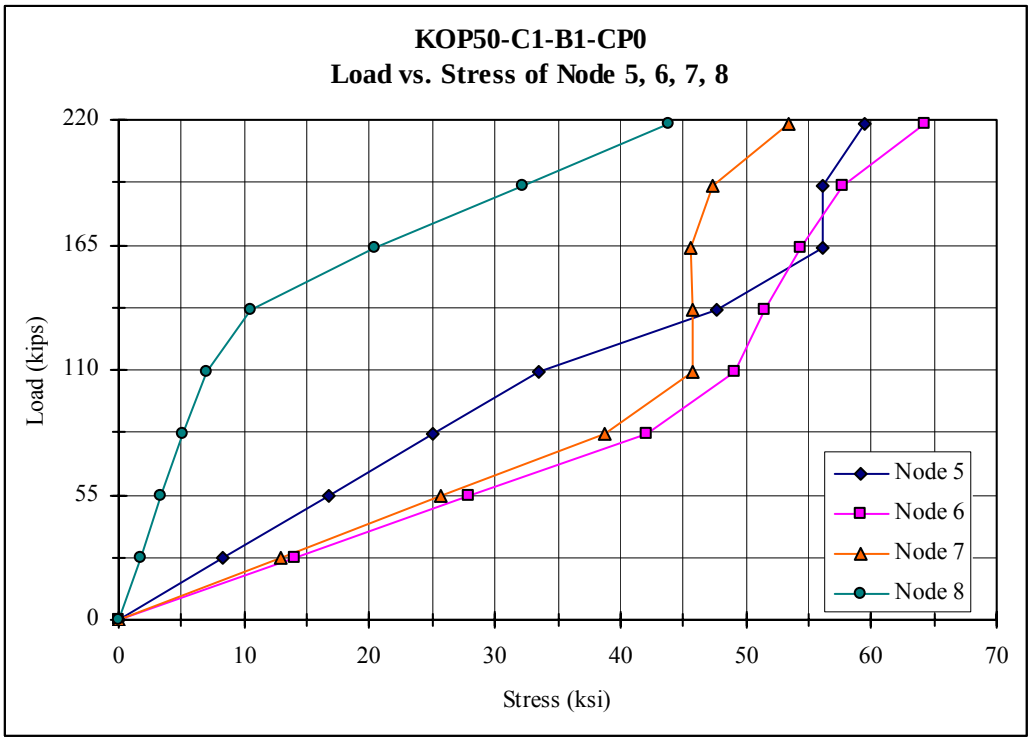

Figure A.B.12 – C1-B1-CP0 Node 5, 6, 7, 8 Load-Stress

Appendix C

ANSYS Result for KOP50-C1-B2-CP0

Table A.C.1 –Geometric & Load Configuration for KOP50-C1-B2-CP0

	Geometric & Load Configuration
Chord member	14 ×14 × 3/8
Branch Member	8 × 8 × 3/16
Branch ramp Load In 8 load steps	168.44 kips
Chord Step Load	0 kips
Chord ramp Load In 8 load steps	238.21 kips

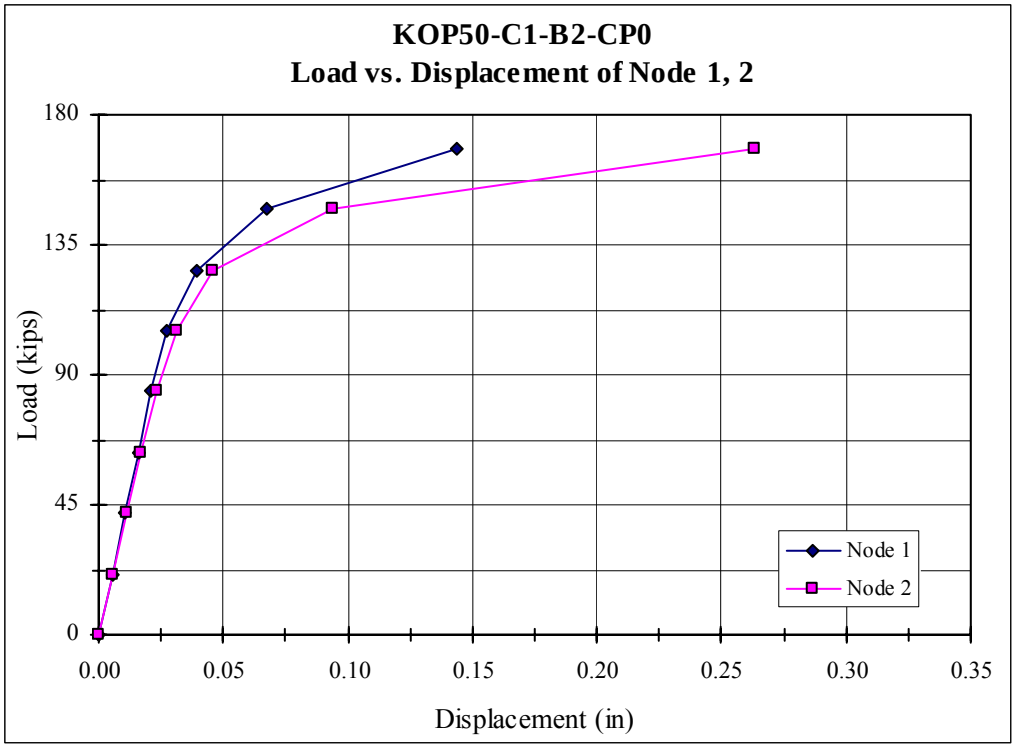

Figure A.C.1 – C1-B2-CP0 Node 1, 2 Load-Displacement

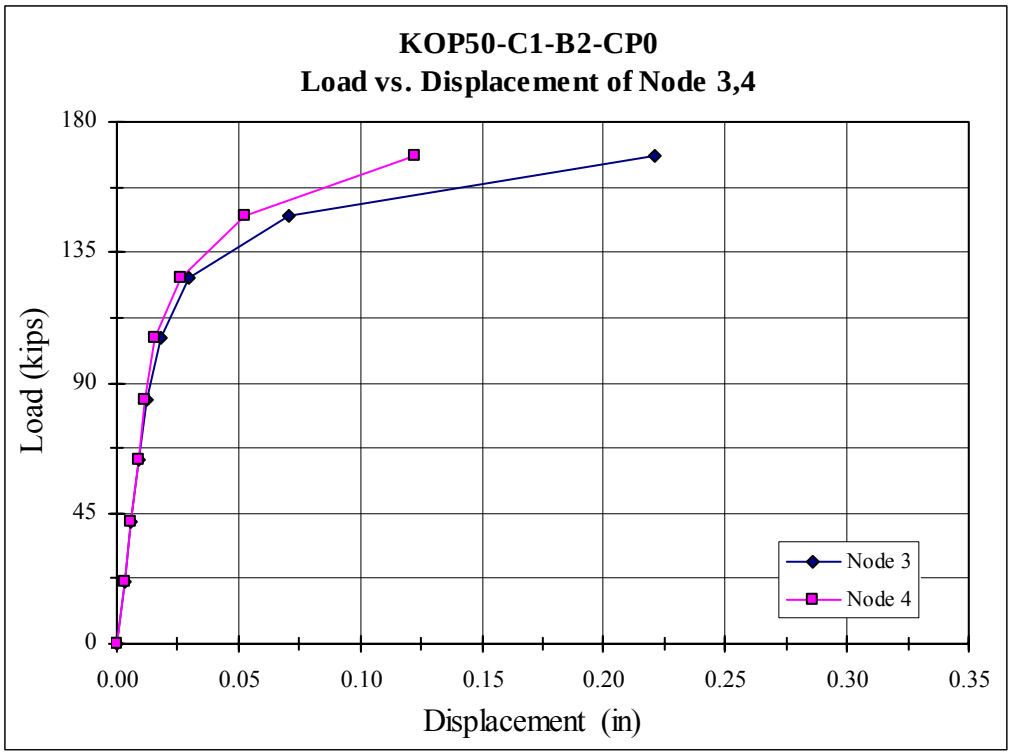

Figure A.C.2 – C1-B2-CP0 Node 3, 4 Load-Displacement

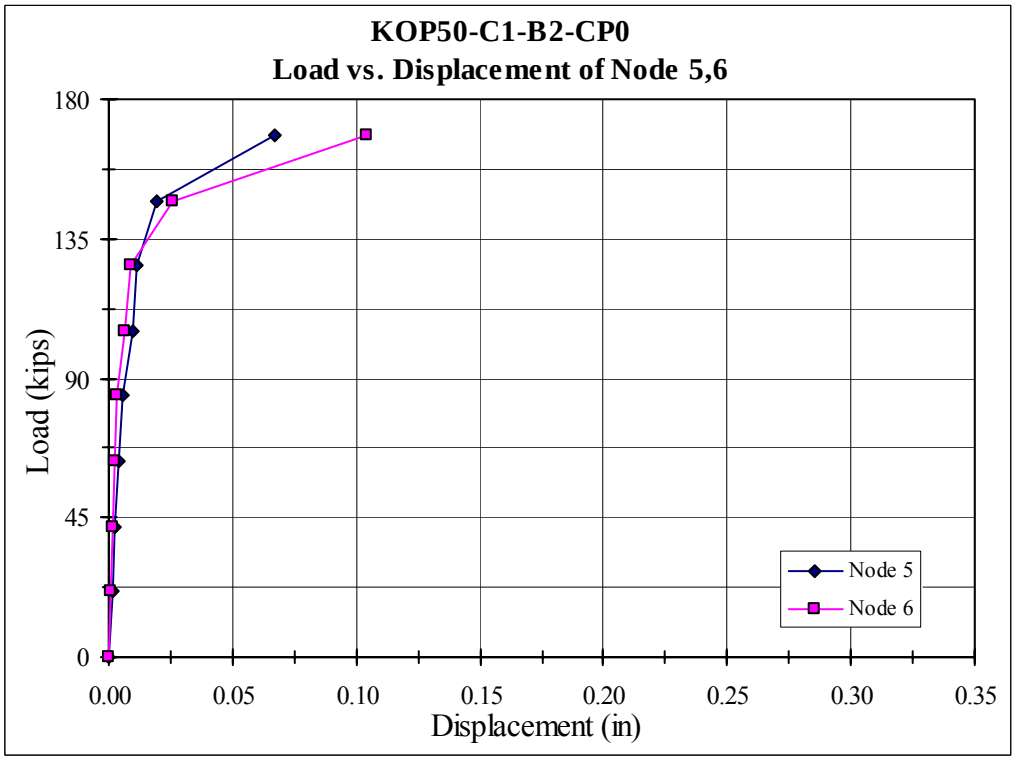

Figure A.C.3 – C1-B2-CP0 Node 5, 6 Load-Displacement

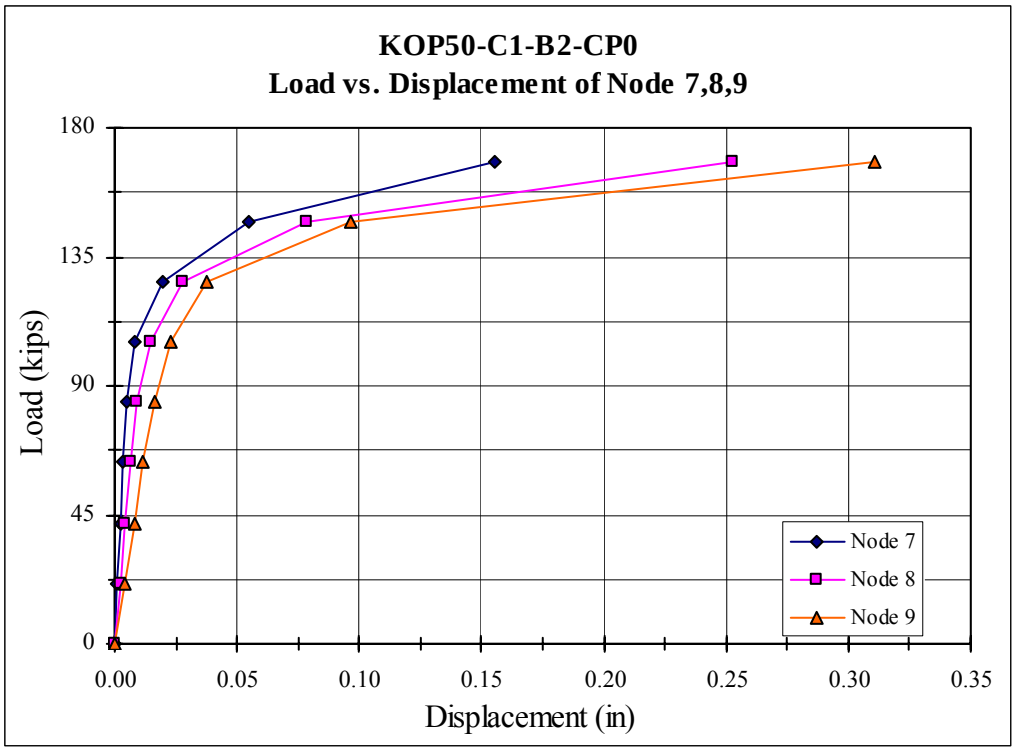

Figure A.C.4 – C1-B2-CP0 Node 7, 8, 9 Load-Displacement

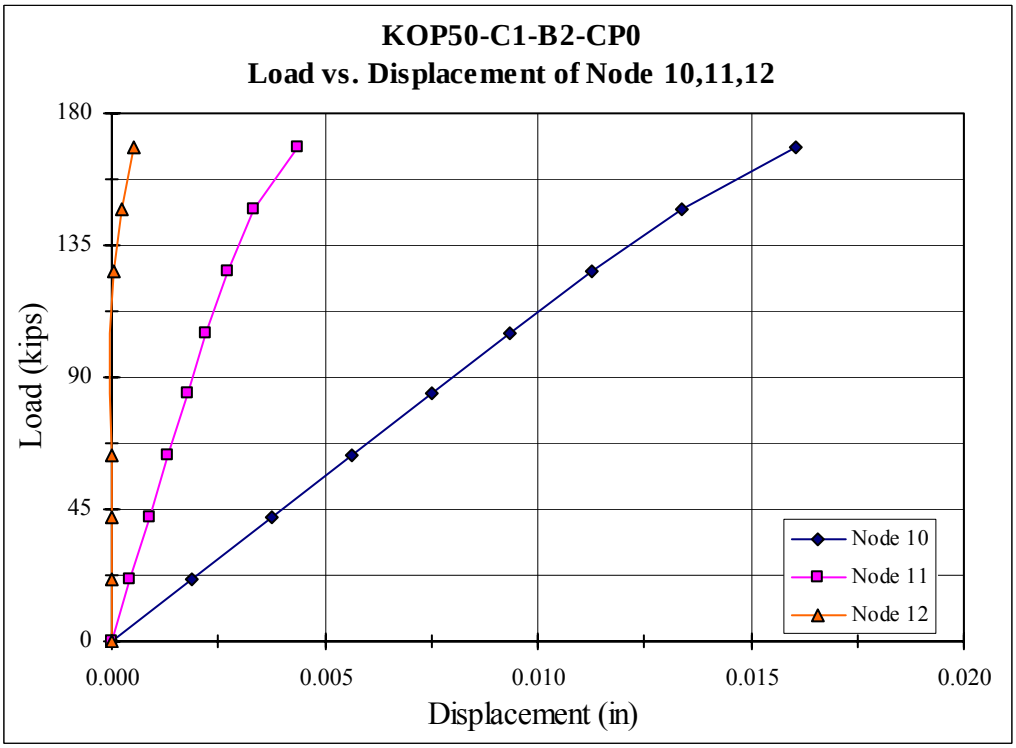

Figure A.C.5 – C1-B2-CP0 Node 10, 11, 12 Load-Displacement

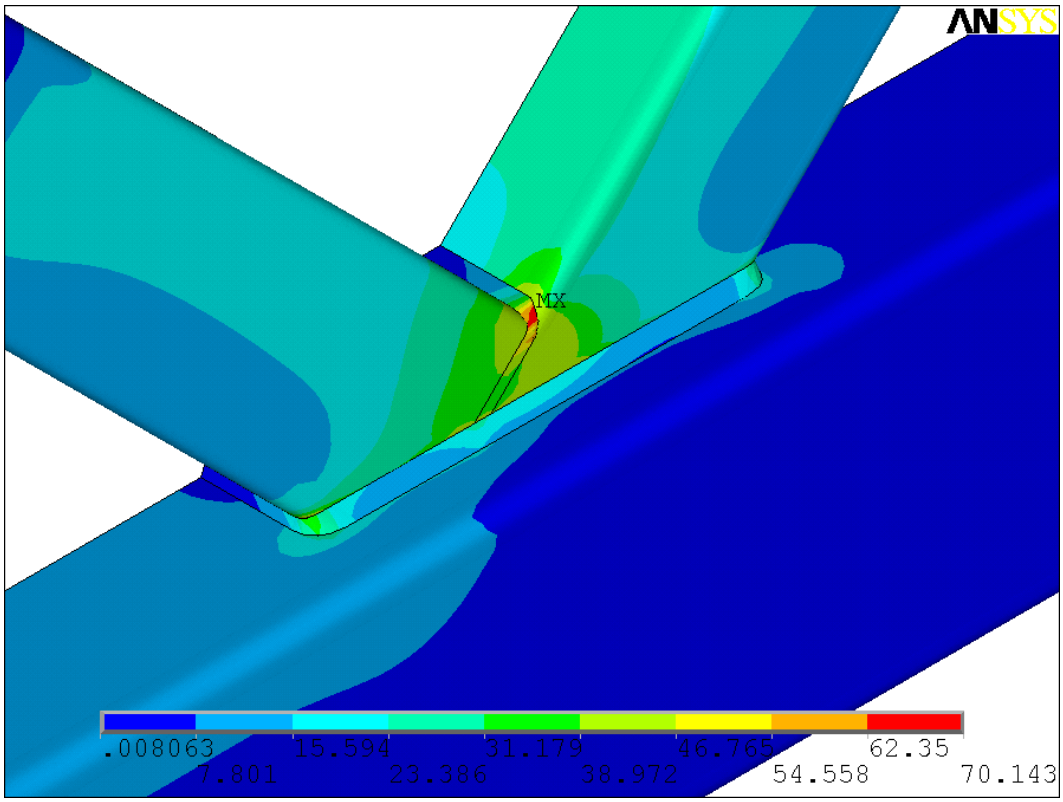

Figure A.C.6 – C1-B2-CP0-LS4 Load-Von Mises Stress Contour (ksi)

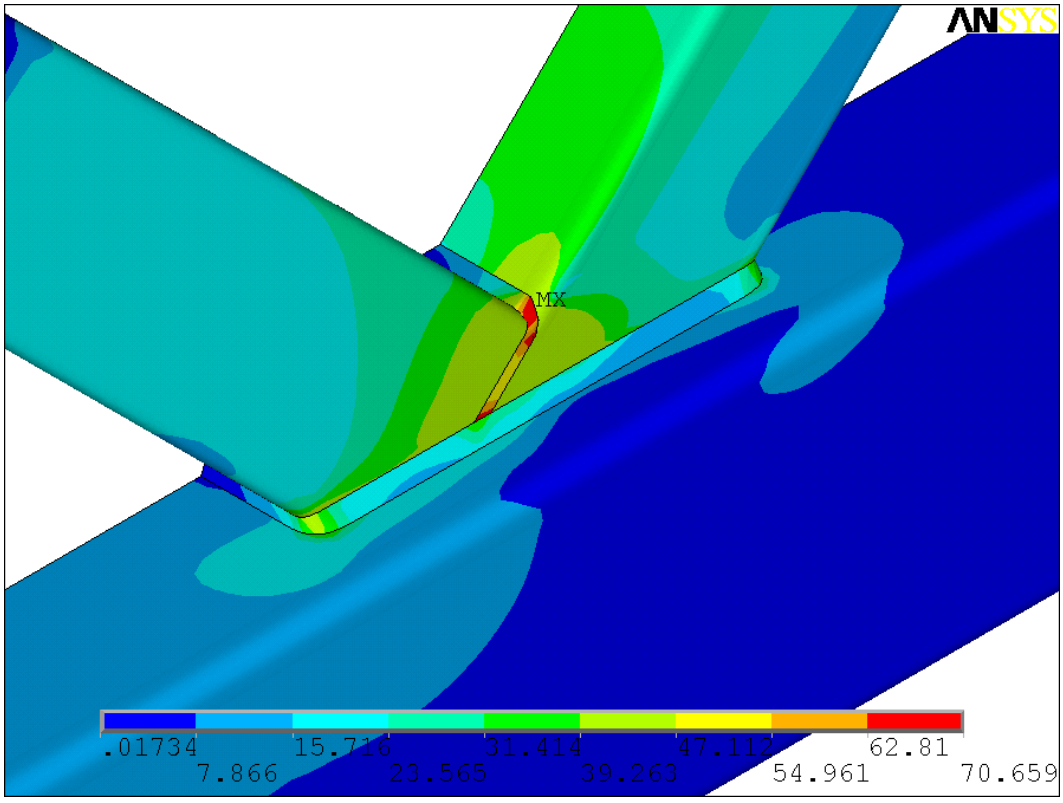

Figure A.C.7 – C1-B2-CP0-LS5 Load-Von Mises Stress Contour (ksi)

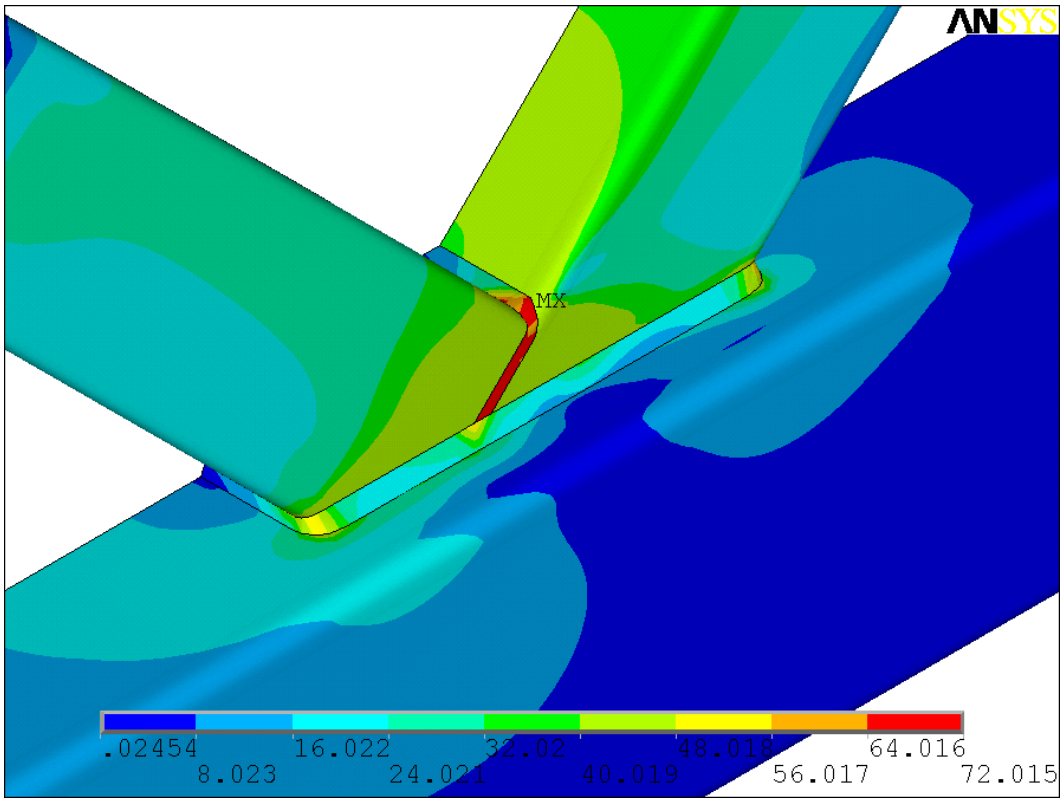

Figure A.C.8 – C1-B2-CP0-LS6 Load-Von Mises Stress Contour (ksi)

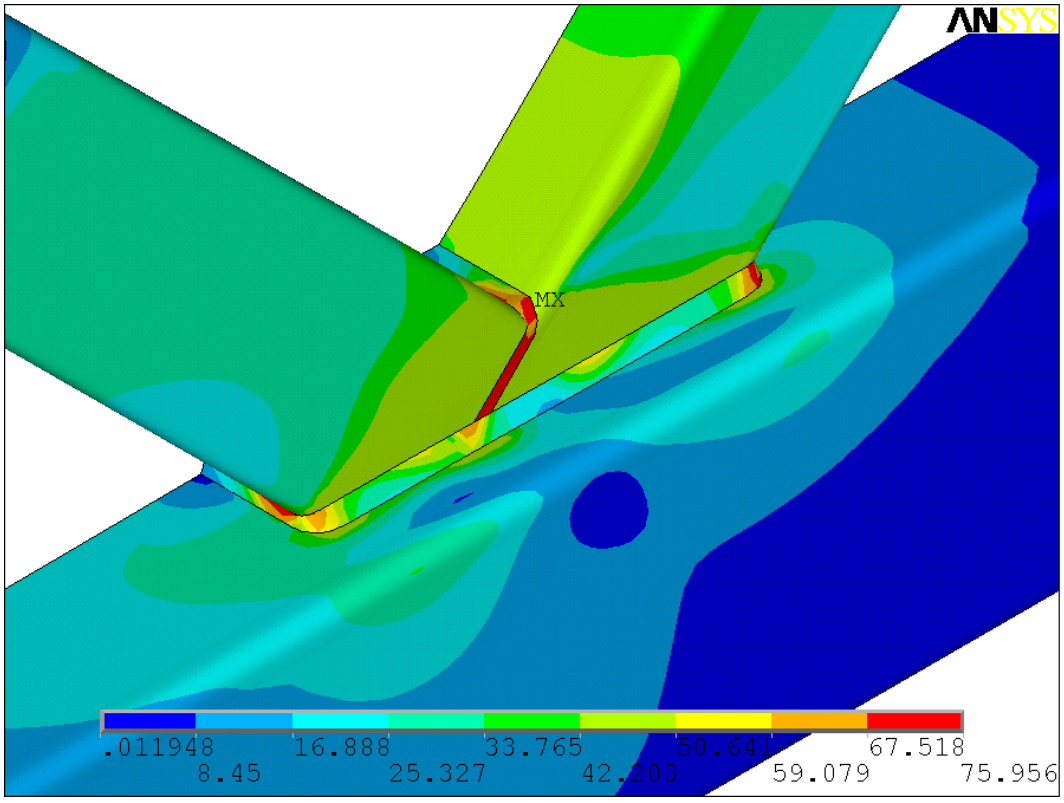

Figure A.C.9 – C1-B2-CP0-LS7 Load-Von Mises Stress Contour (ksi)

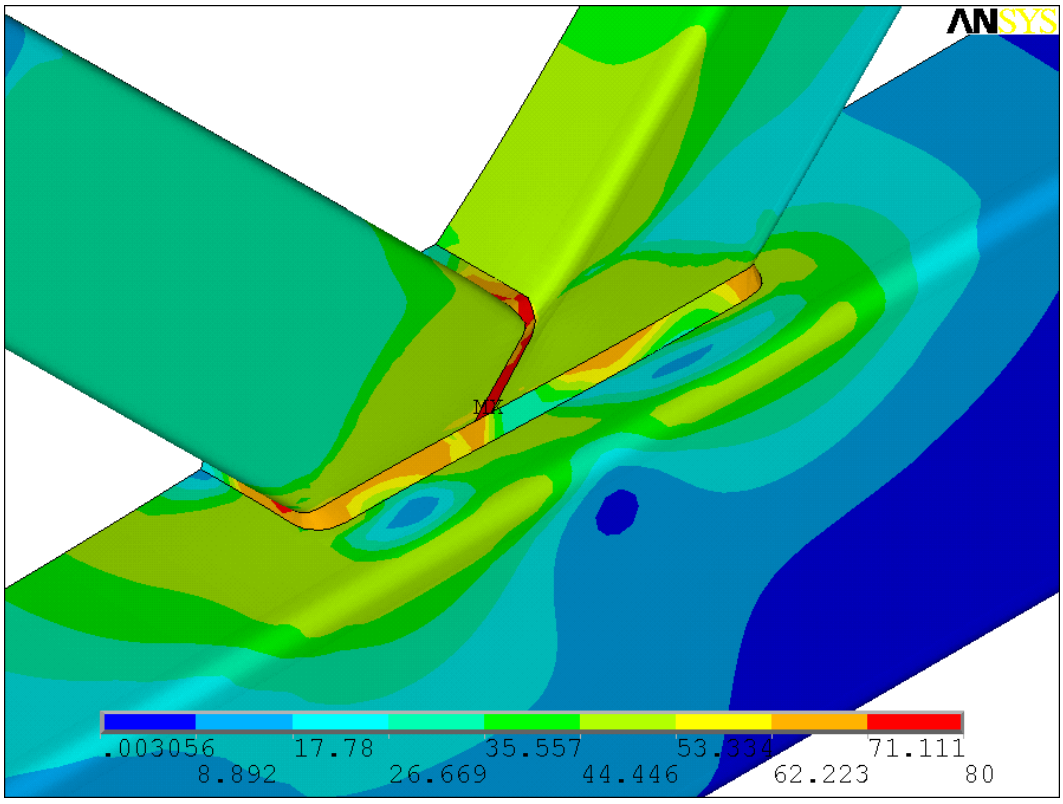

Figure A.C.10– C1-B2-CP0-LS8 Load-Von Mises Stress Contour (ksi)

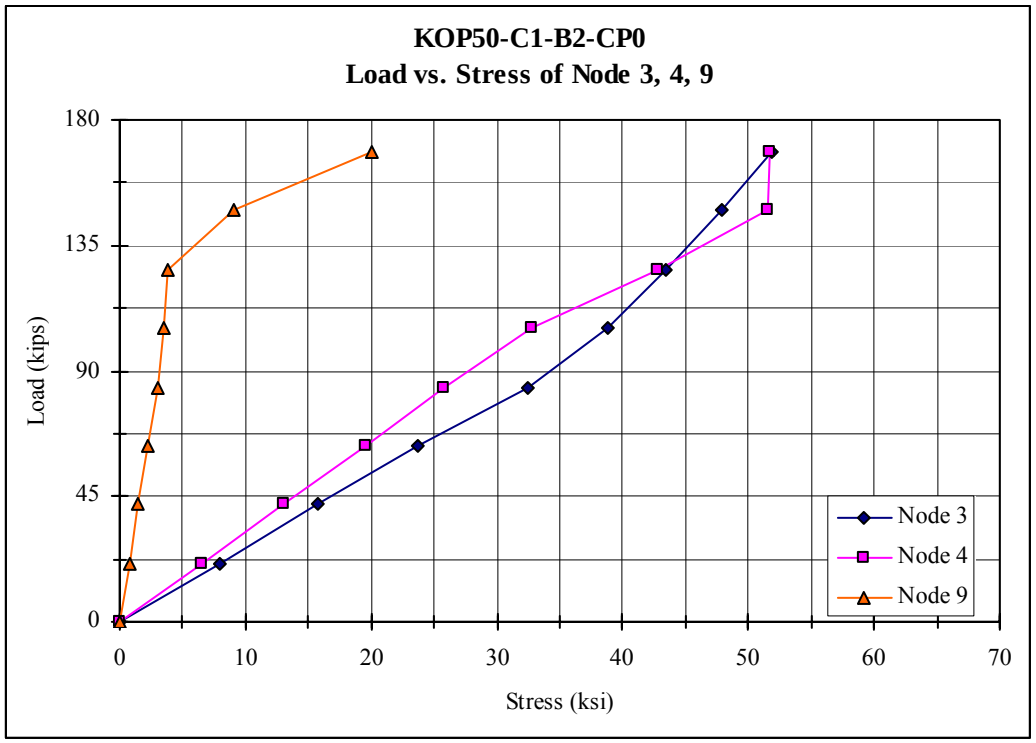

Figure A.C.11 – C1-B2-CP0 Node 3, 4, 9 Load-Stress

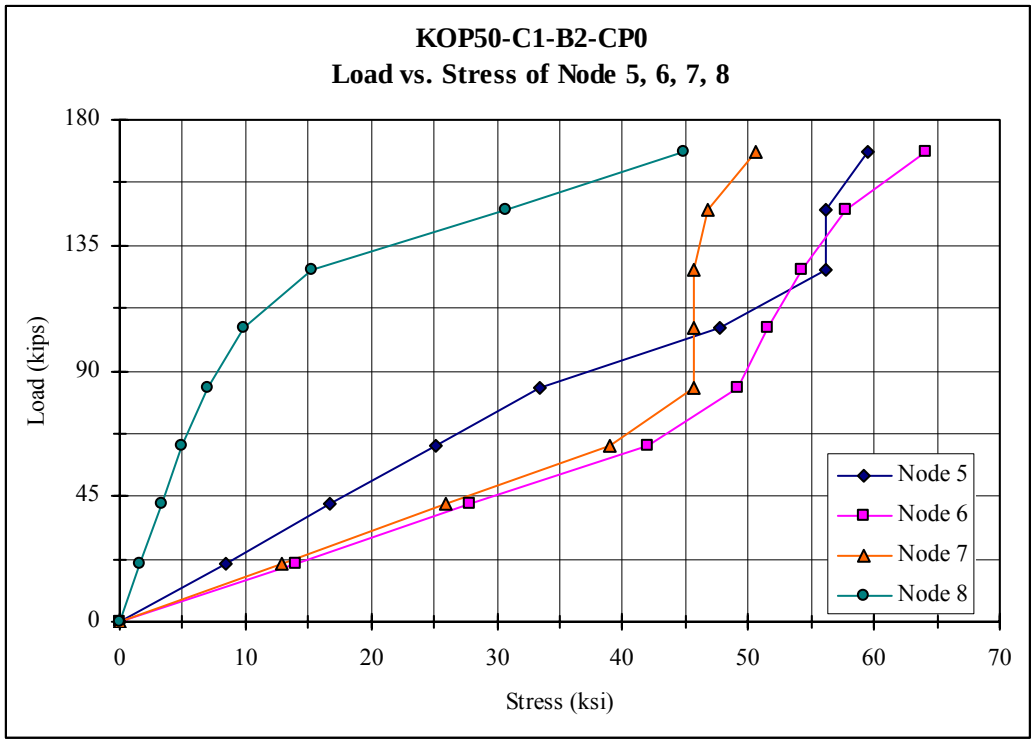

Figure A.C.12 – C1-B2-CP0 Node 5, 6, 7, 8 Load-Stress

Appendix D

ANSYS Result for KOP50-C2-B1-CP0

Table A.D.1 –Geometric & Load Configuration for KOP50-C2-B1-CP0

	Geometric & Load Configuration
Chord member	14 ×14 × 5/16
Branch Member	8 × 8 × 1/4
Branch ramp Load In 8 load steps	208.73 kips
Chord Step Load	0 kips
Chord ramp Load In 8 load steps	295.19 kips

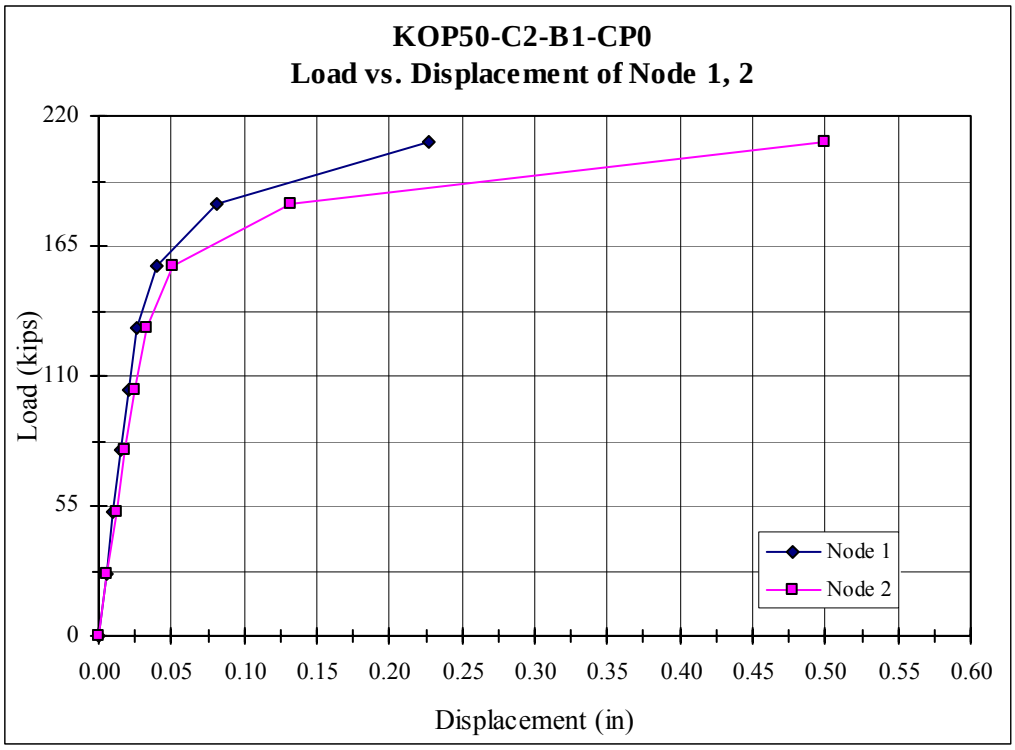

Figure A.D.1 – C2-B1-CP0 Node 1, 2 Load-Displacement

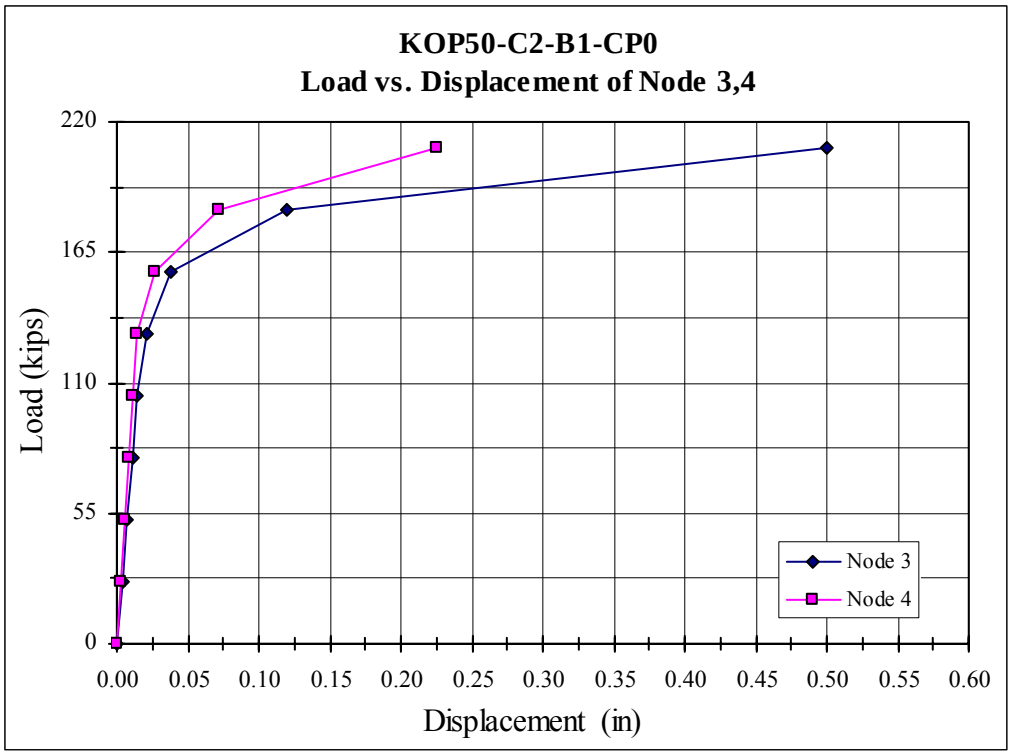

Figure A.D.2 – C2-B1-CP0 Node 3, 4 Load-Displacement

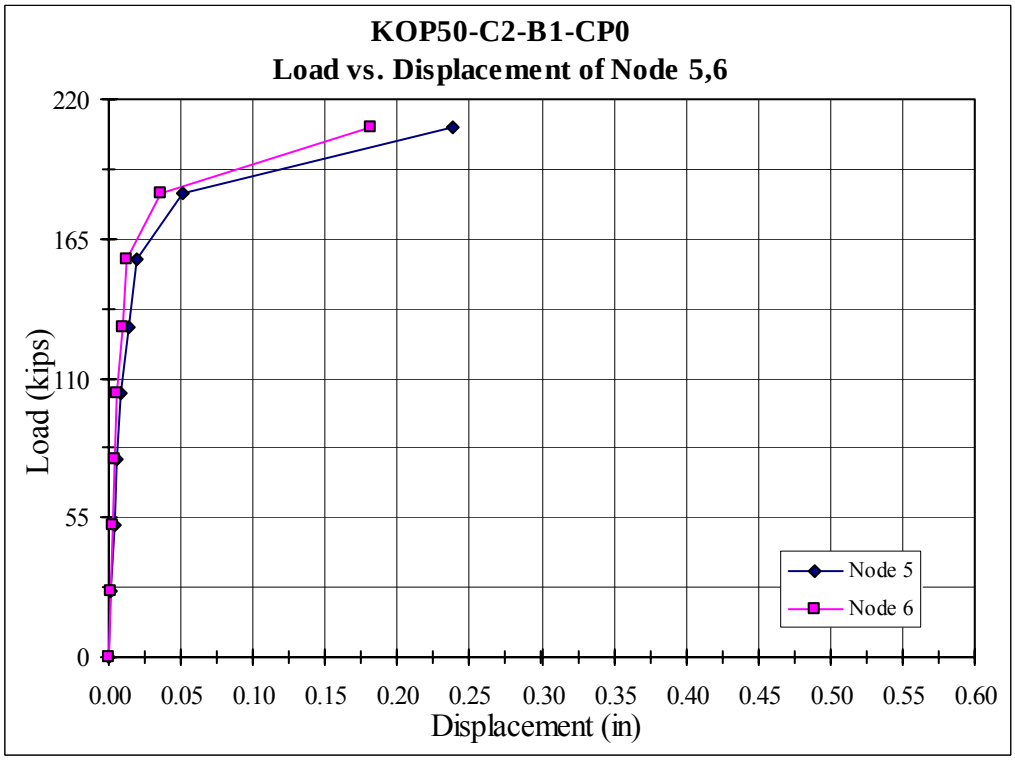

Figure A.D.3 – C2-B1-CP0 Node 5, 6 Load-Displacement

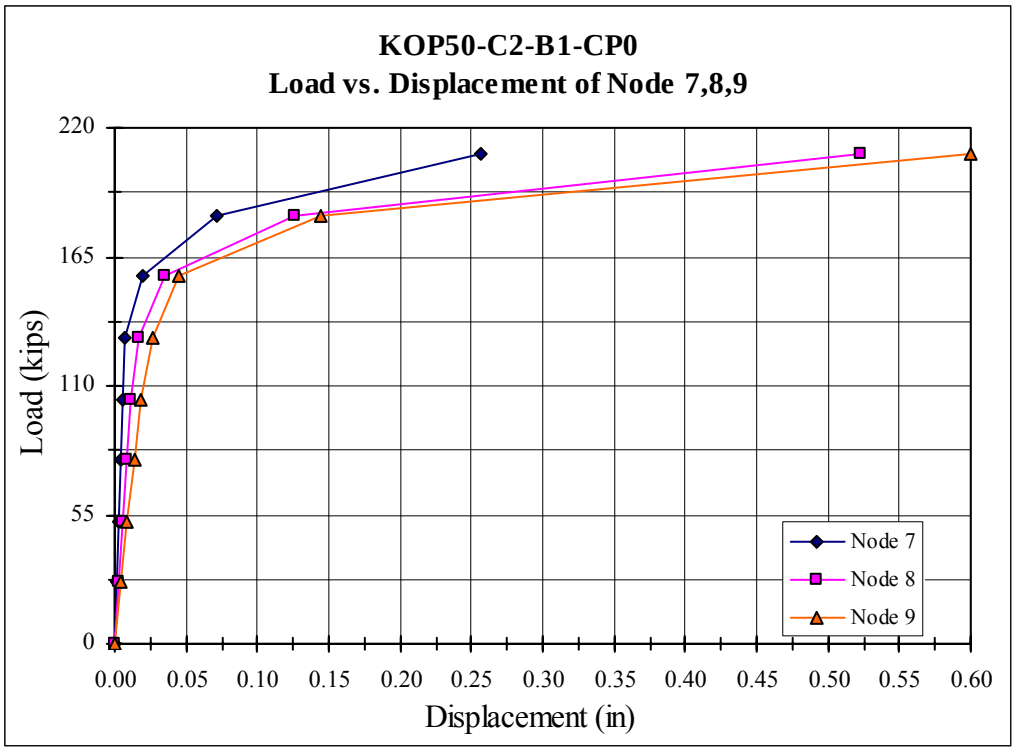

Figure A.D.4 – C2-B1-CP0 Node 7, 8, 9 Load-Displacement

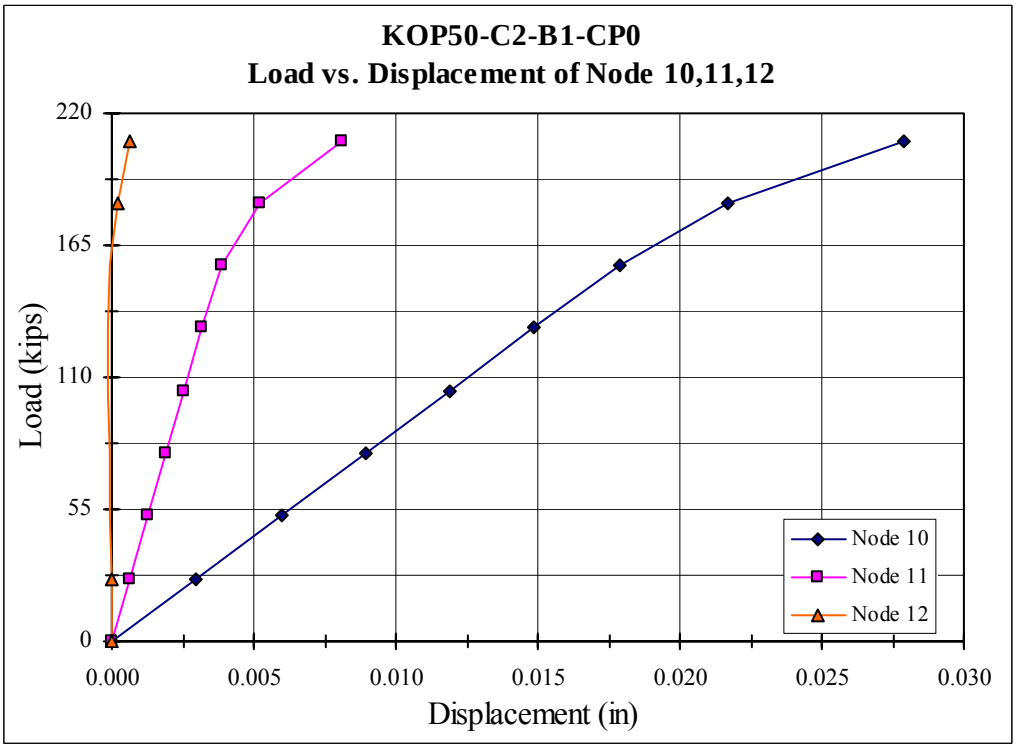

Figure A.D.5 – C2-B1-CP0 Node 10, 11, 12 Load-Displacement

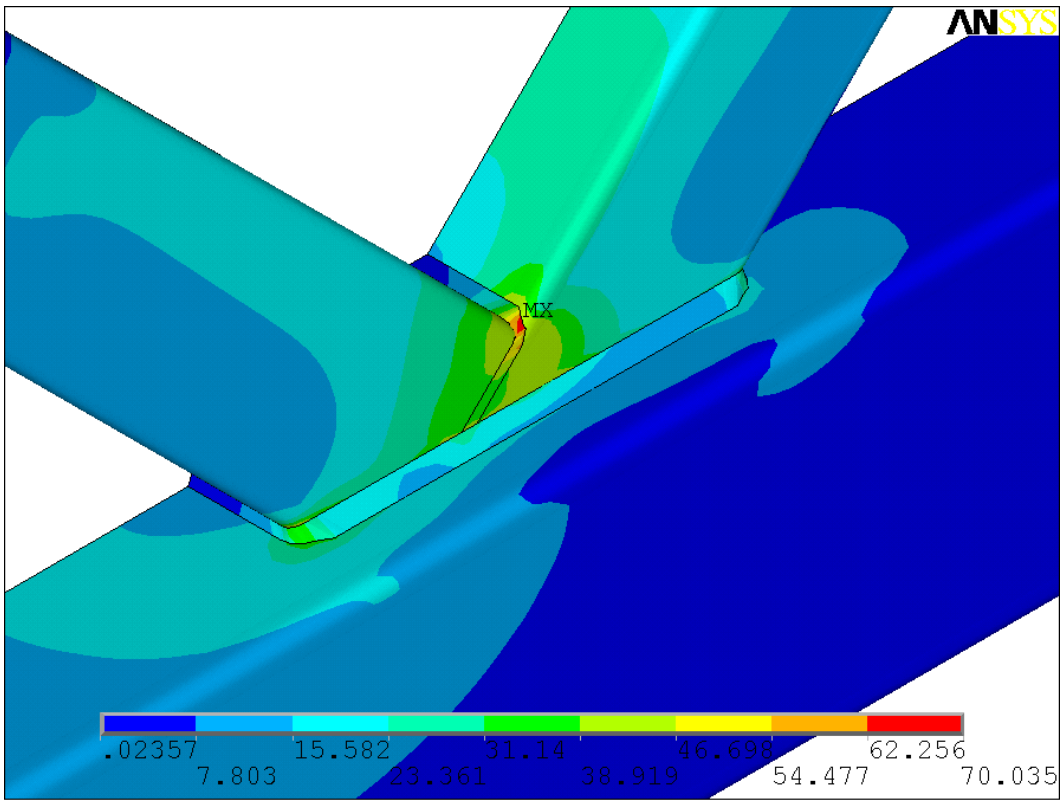

Figure A.D.6 – C2-B1-CP0-LS4 Load-Von Mises Stress Contour (ksi)

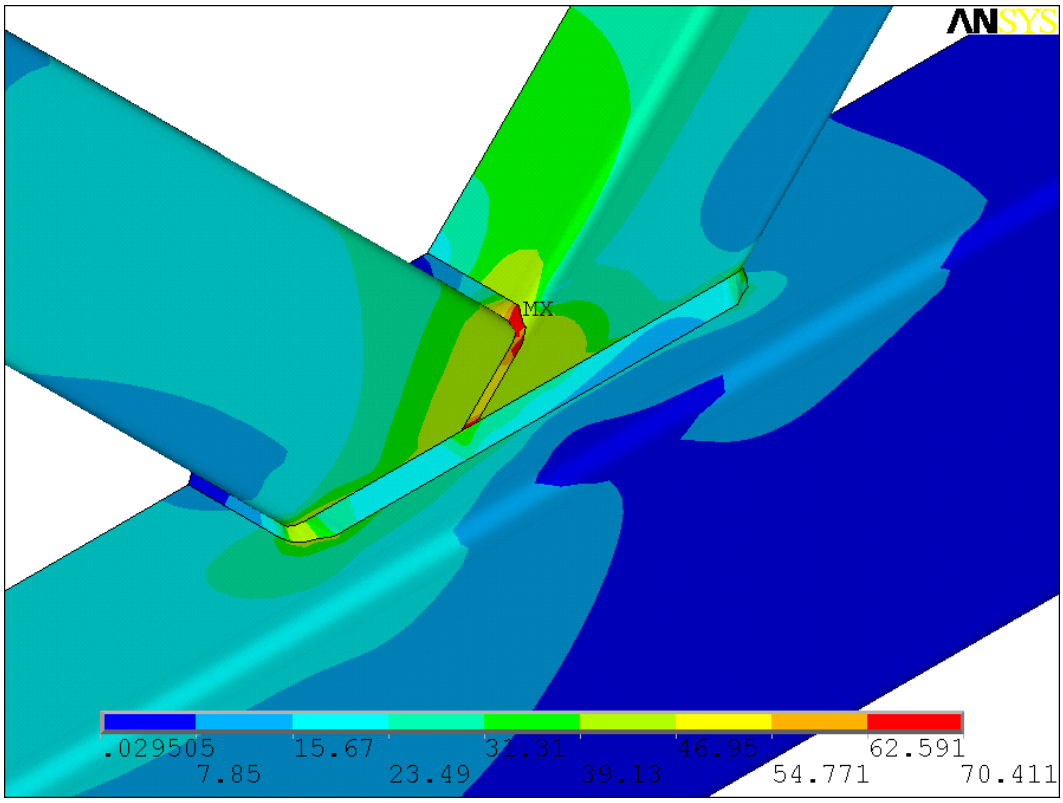

Figure A.D.7 – C2-B1-CP0-LS5 Load-Von Mises Stress Contour (ksi)

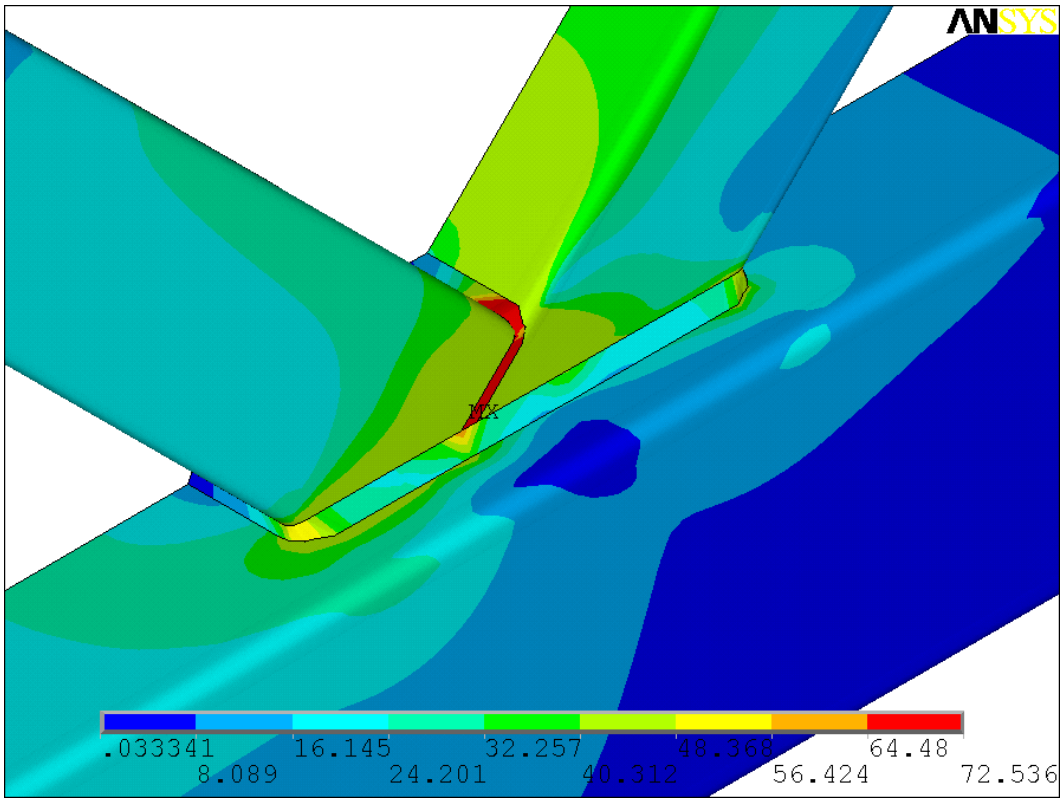

Figure A.D.8 – C2-B1-CP0-LS6 Load-Von Mises Stress Contour (ksi)

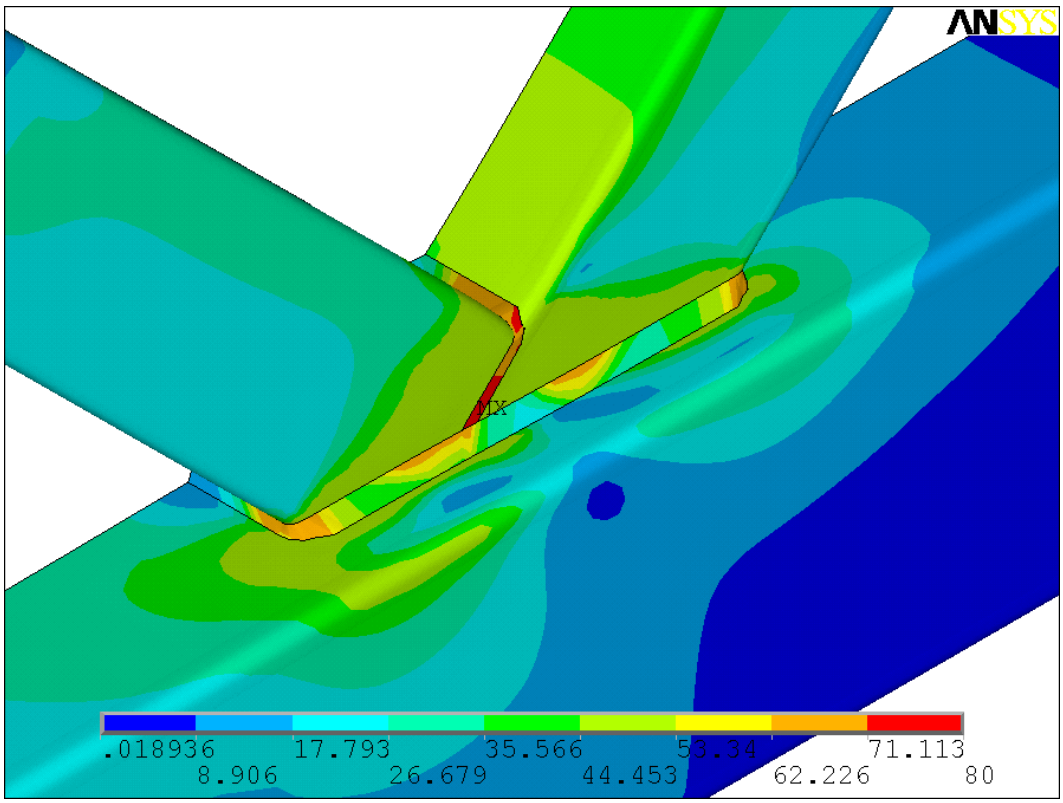

Figure A.D.9 – C2-B1-CP0-LS7 Load-Von Mises Stress Contour (ksi)

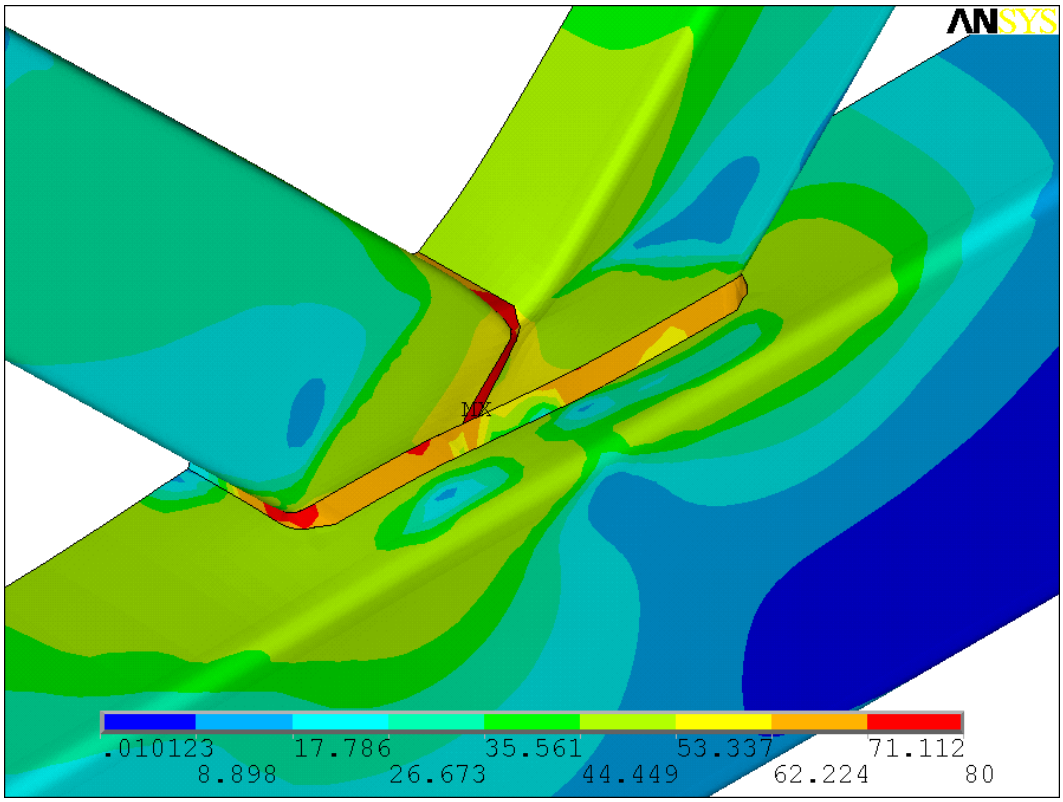

Figure A.D.10 – C2-B1-CP0-LS8 Load-Von Mises Stress Contour (ksi)

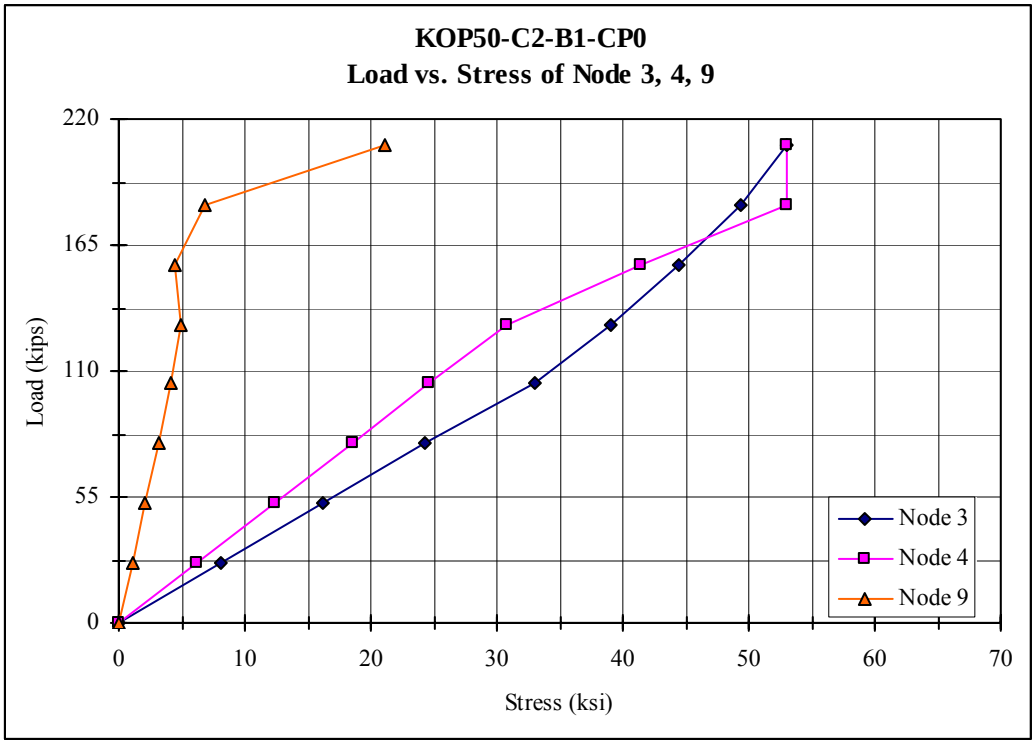

Figure A.D.11 – C2-B1-CP0 Node 3, 4, 9 Load-Stress

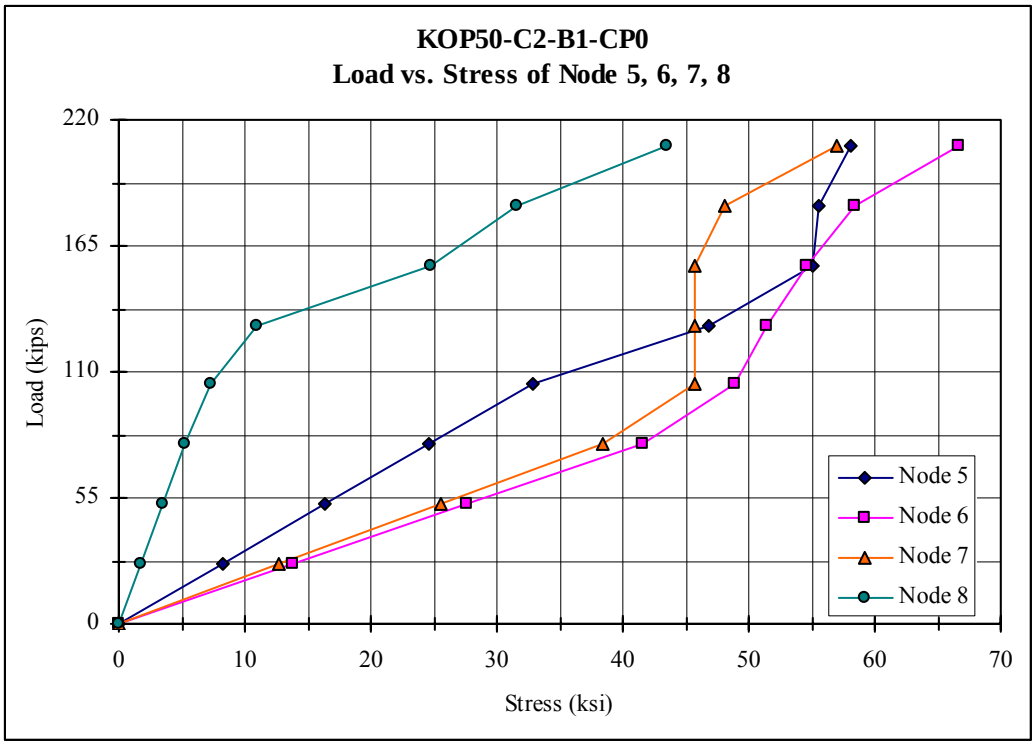

Figure A.D.12 – C2-B1-CP0 Node 5, 6, 7, 8 Load-Stress

Appendix E

ANSYS Result for KOP50-C2-B2-CP0

Table A.E.1 –Geometric & Load Configuration for KOP50-C2-B2-CP0

	Geometric & Load Configuration
Chord member	14 ×14 × 5/16
Branch Member	8 × 8 × 3/16
Branch ramp Load In 8 load steps	158.68 kips
Chord Step Load	0 kips
Chord ramp Load In 8 load steps	224.41 kips

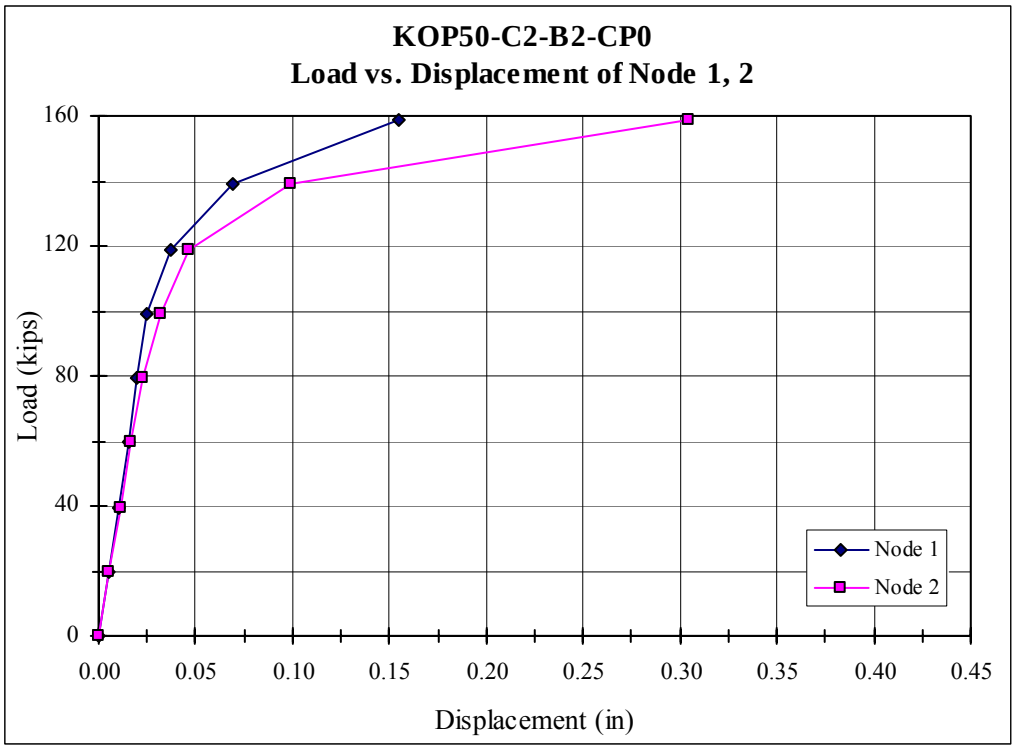

Figure A.E.1 – C2-B2-CP0 Node 1, 2 Load-Displacement

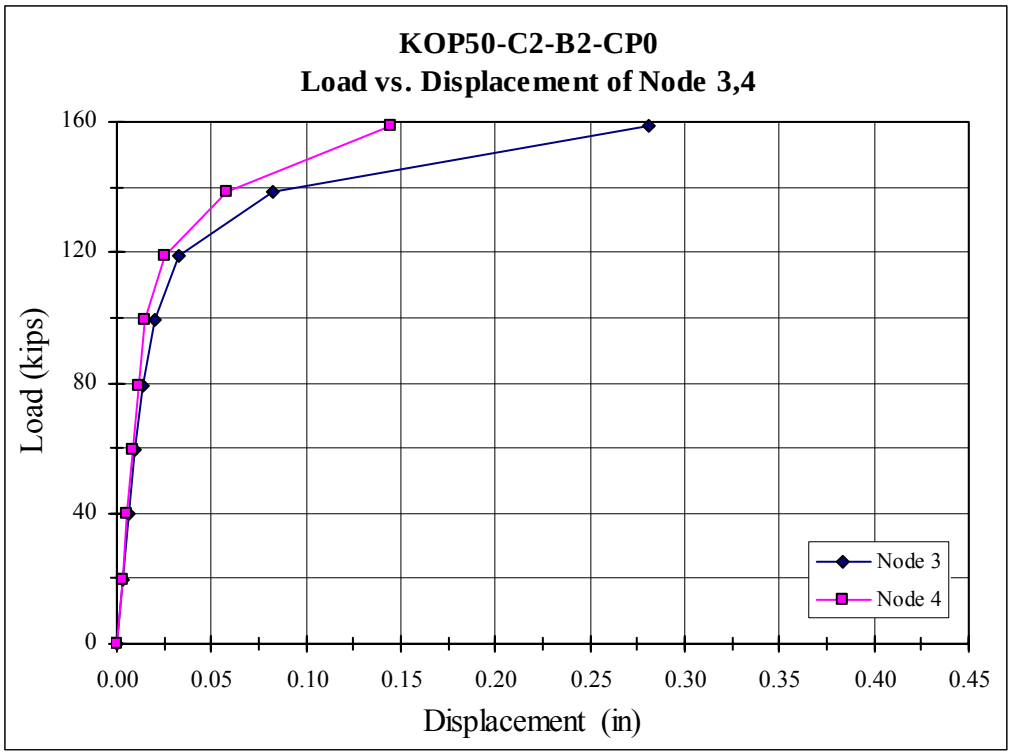

Figure A.E.2 – C2-B2-CP0 Node 3, 4 Load-Displacement

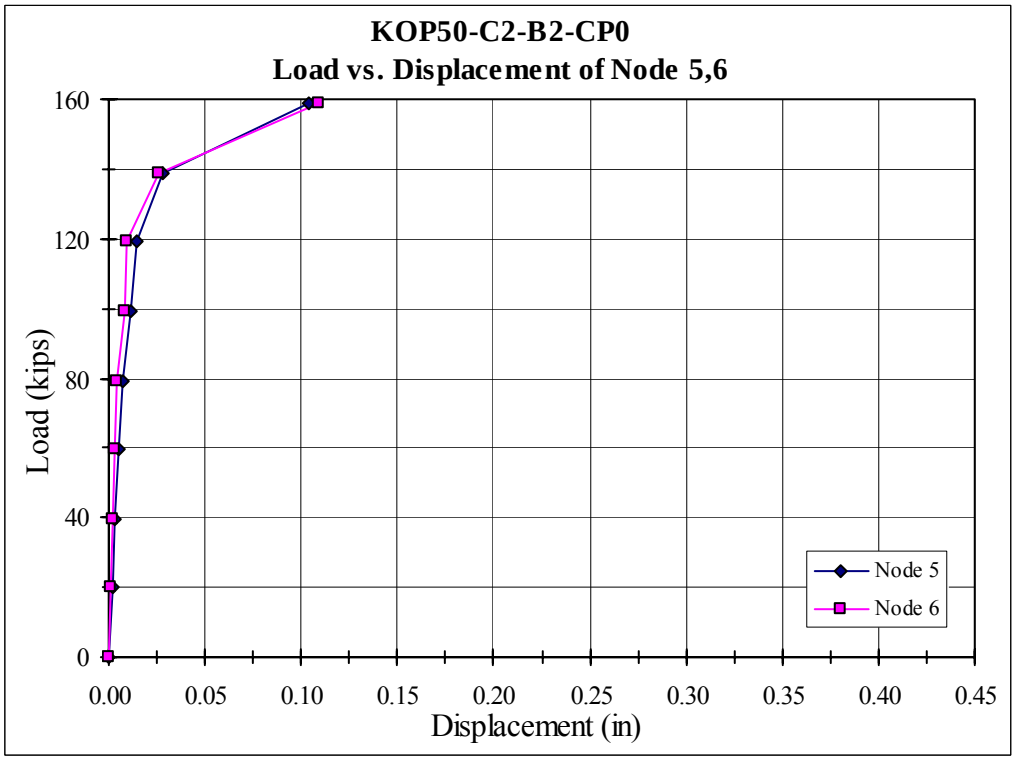

Figure A.E.3 – C2-B2-CP0 Node 5, 6 Load-Displacement

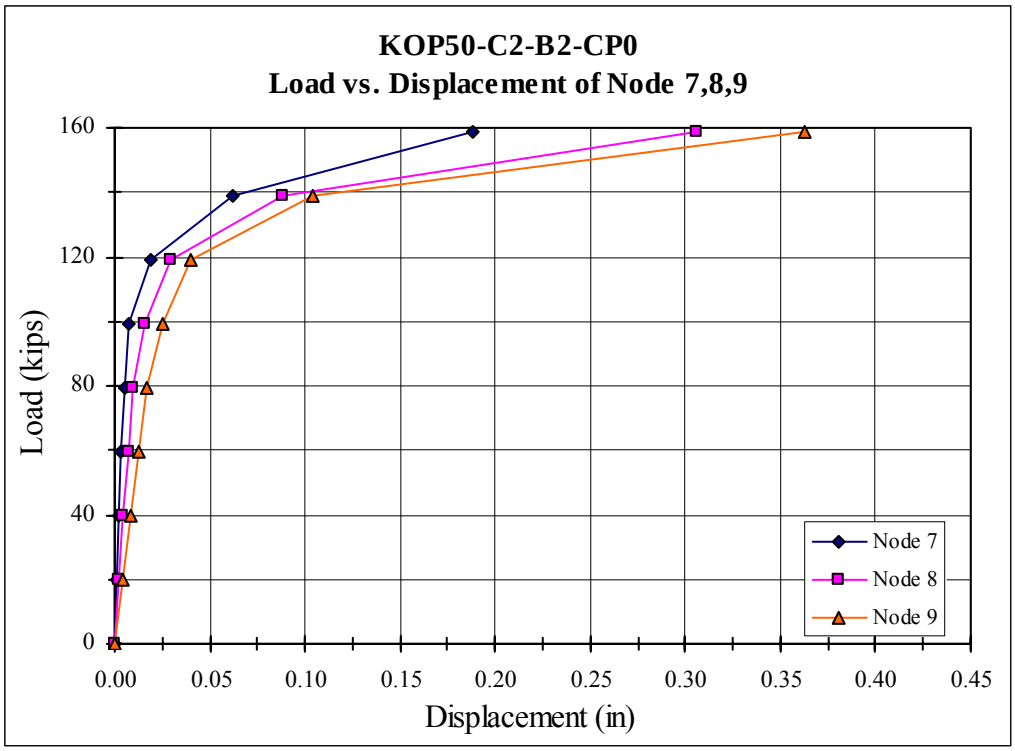

Figure A.E.4 – C2-B2-CP0 Node 7, 8, 9 Load-Displacement

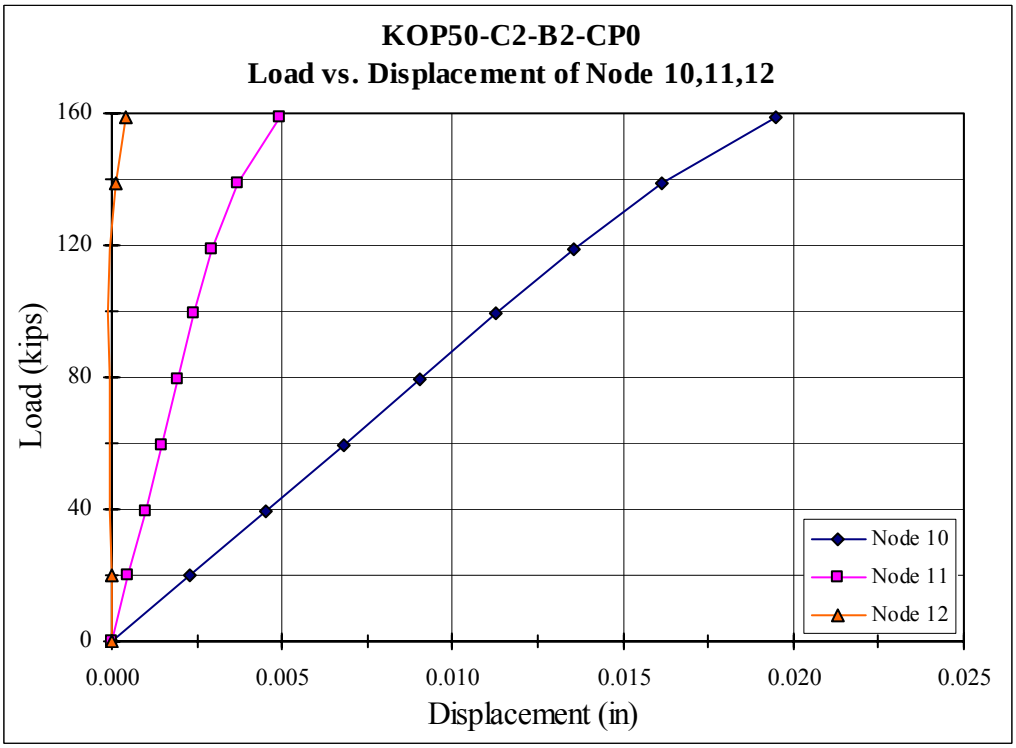

Figure A.E.5 – C2-B2-CP0 Node 10, 11, 12 Load-Displacement

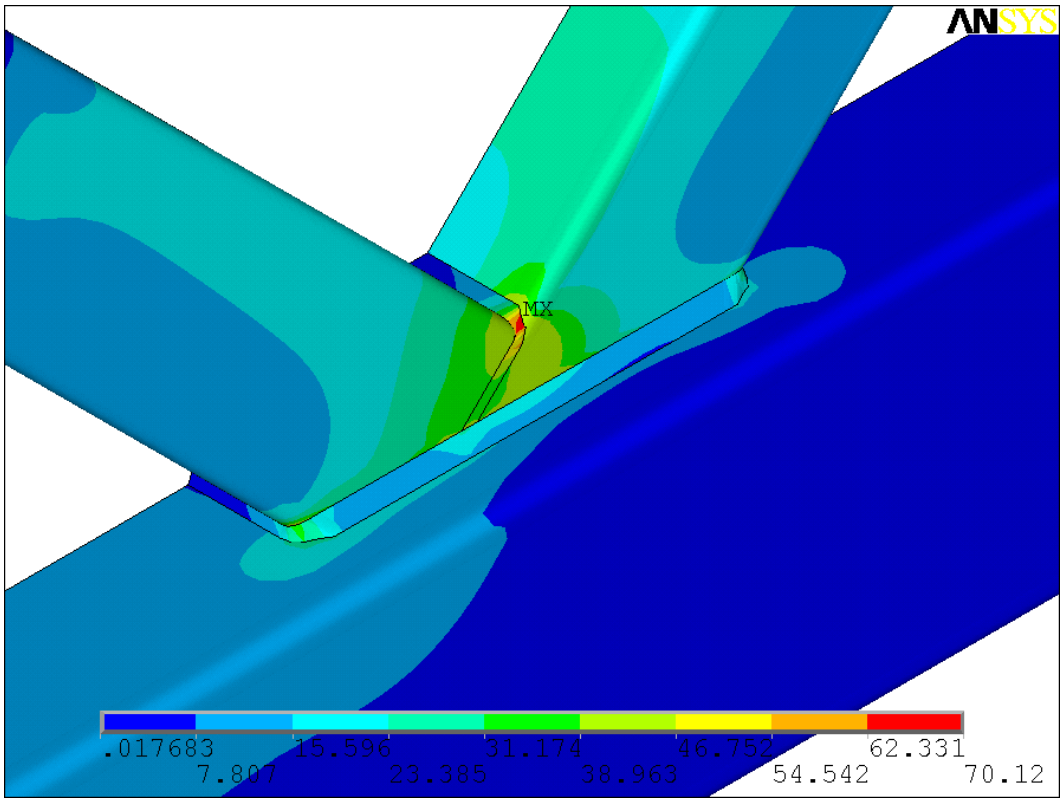

Figure A.E.6 – C2-B2-CP0-LS4 Load-Von Mises Stress Contour (ksi)

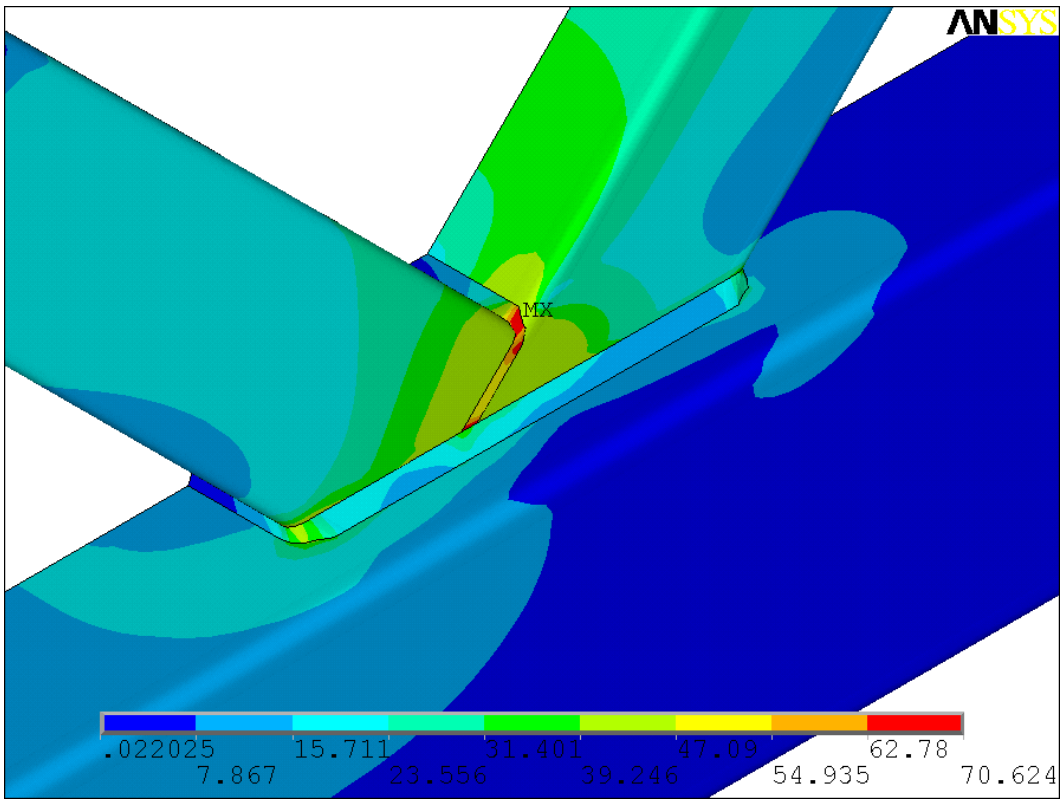

Figure A.E.7 – C2-B2-CP0-LS5 Load-Von Mises Stress Contour (ksi)

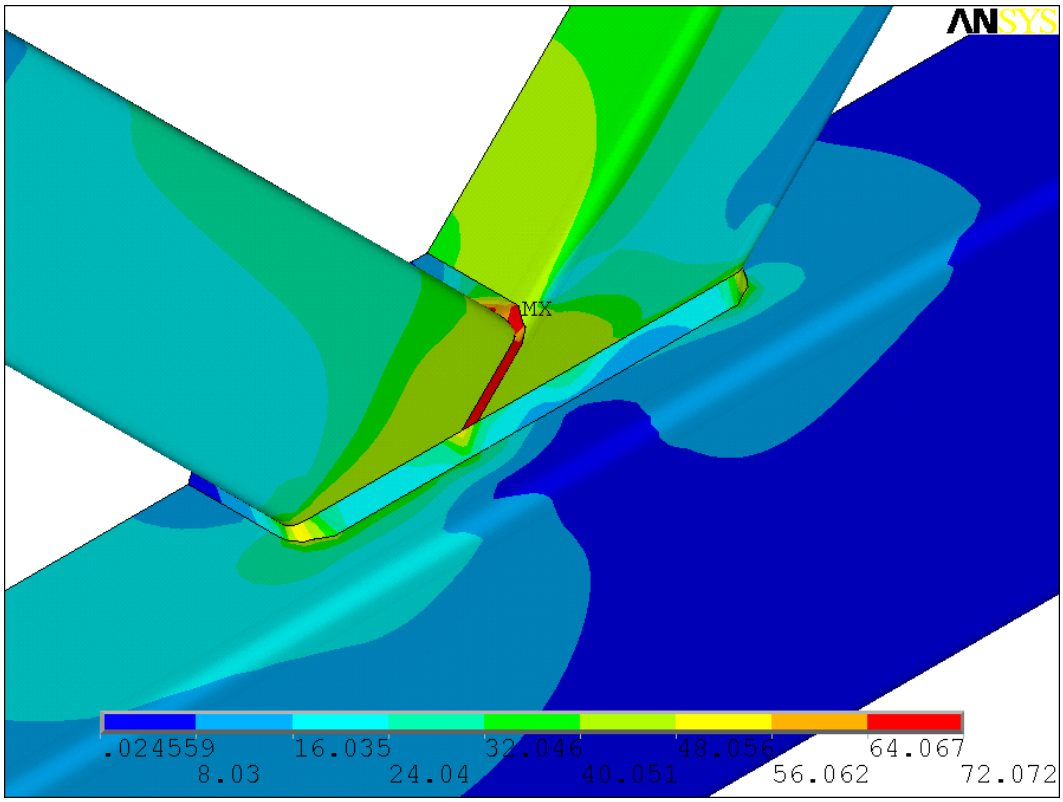

Figure A.E.8 – C2-B2-CP0-LS6 Load-Von Mises Stress Contour (ksi)

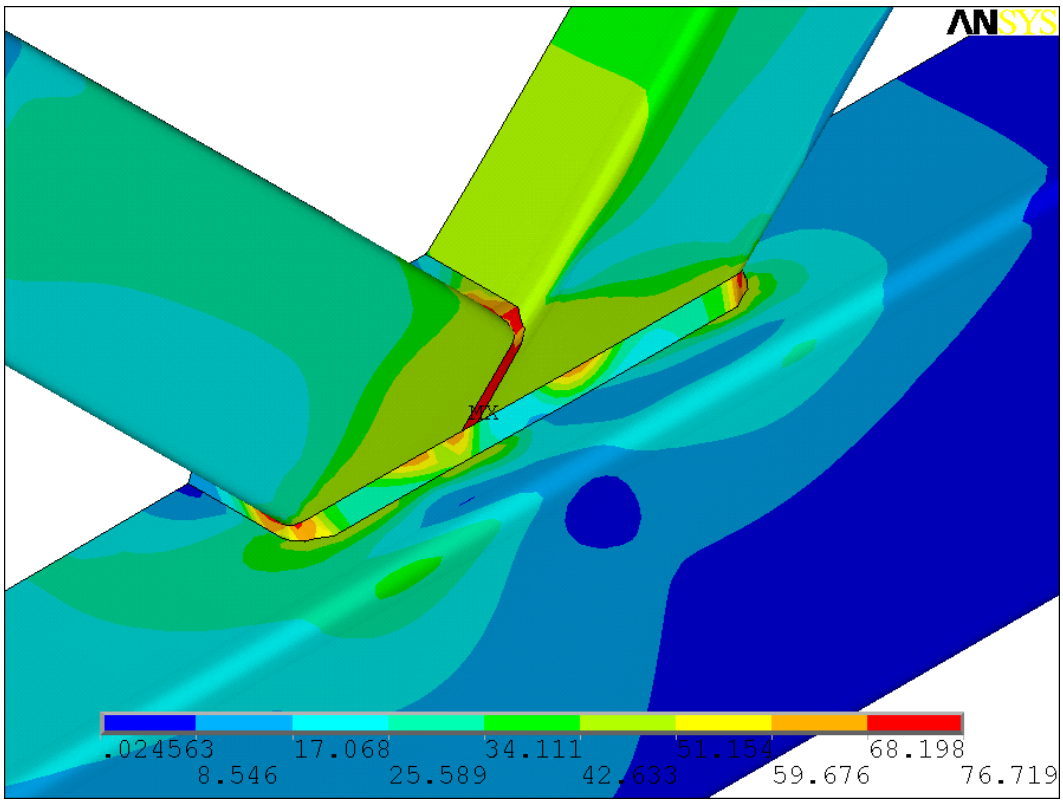

Figure A.E.9 – C2-B2-CP0-LS7 Load-Von Mises Stress Contour (ksi)

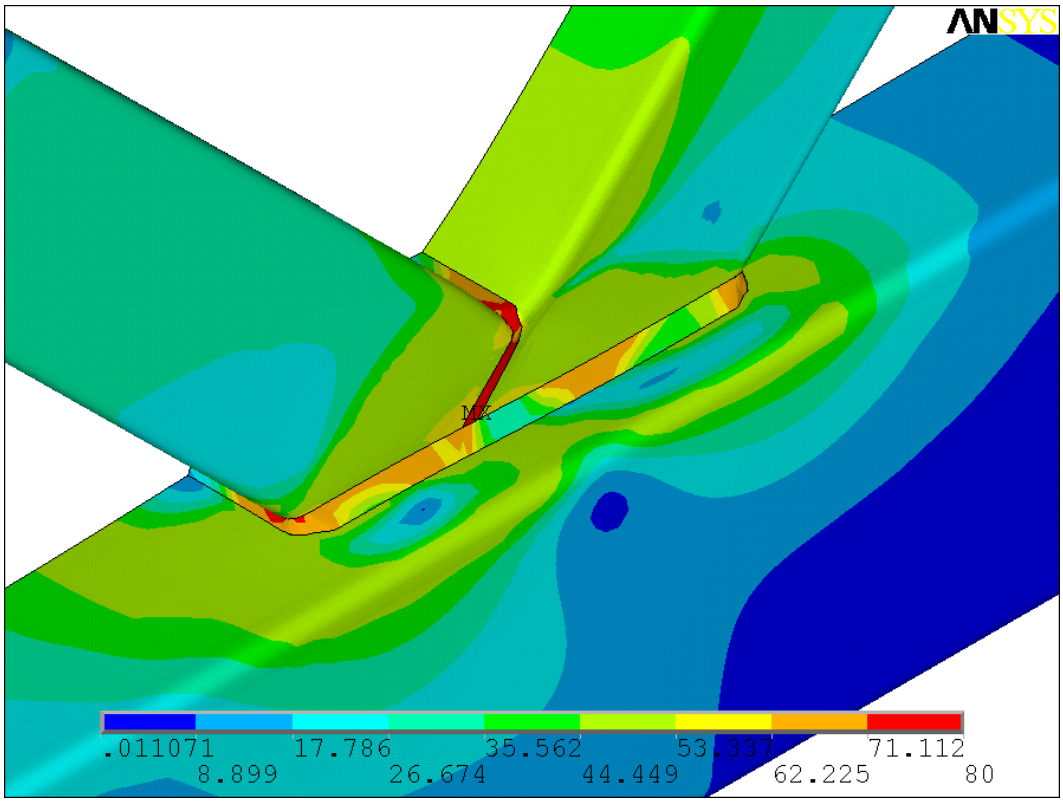

Figure A.E.10 – C2-B2-CP0-LS8 Load-Von Mises Stress Contour (ksi)

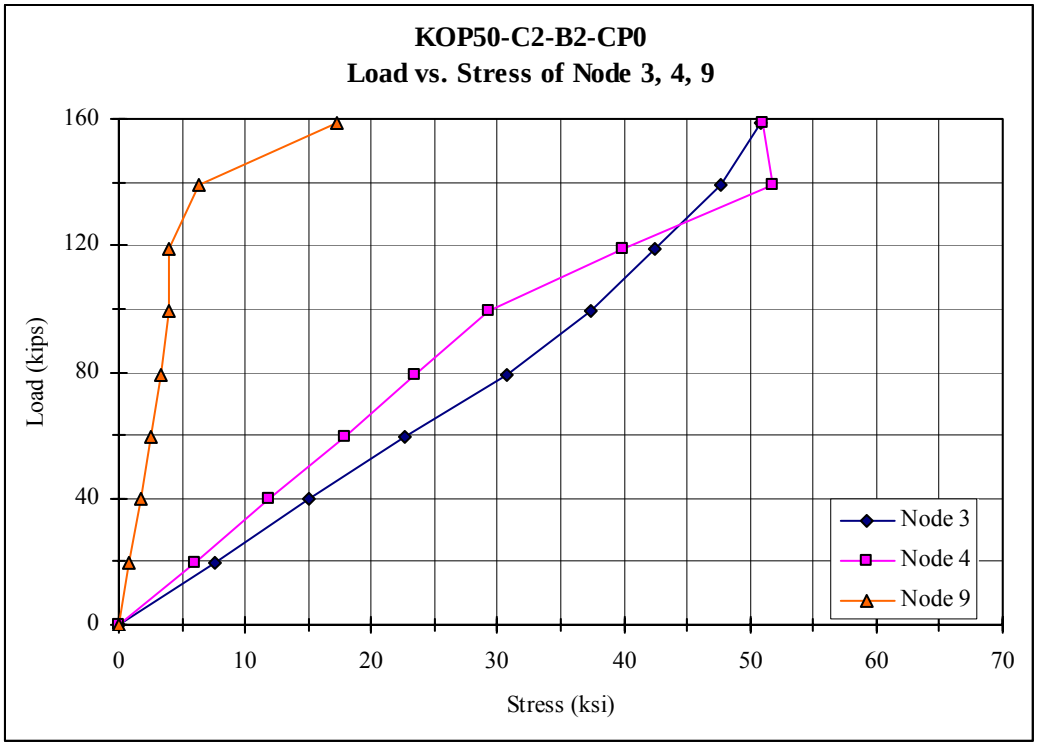

Figure A.E.11 – C2-B2-CP0 Node 3, 4, 9 Load-Stress

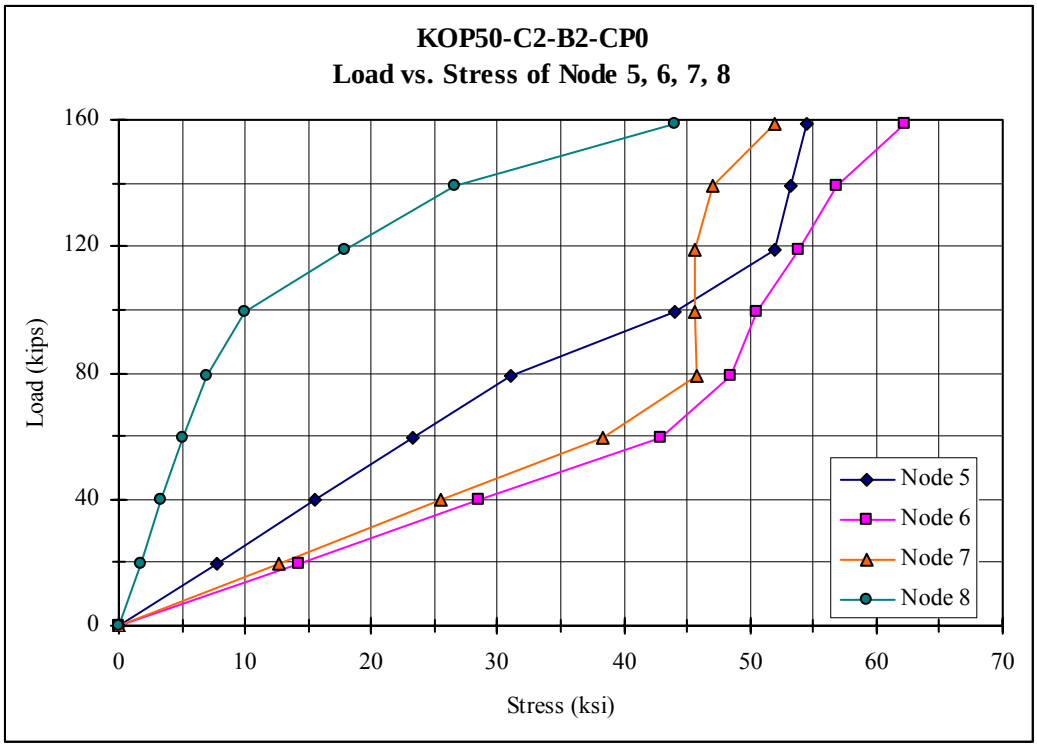

Figure A.E.12 – C2-B2-CP0 Node 5, 6, 7, 8 Load-Stress

Appendix F

ANSYS Result for KOP50-C1-B1-CP50

Table A.F.1 –Geometric & Load Configuration for KOP50-C1-B1-CP50

	Geometric & Load Configuration
Chord member	14 ×14 × 3/8
Branch Member	8 × 8 × 1/4
Branch ramp Load In 8 load steps	218.48 kips
Chord Step Load	188.845kips
Chord ramp Load In 8 load steps	308.98 kips

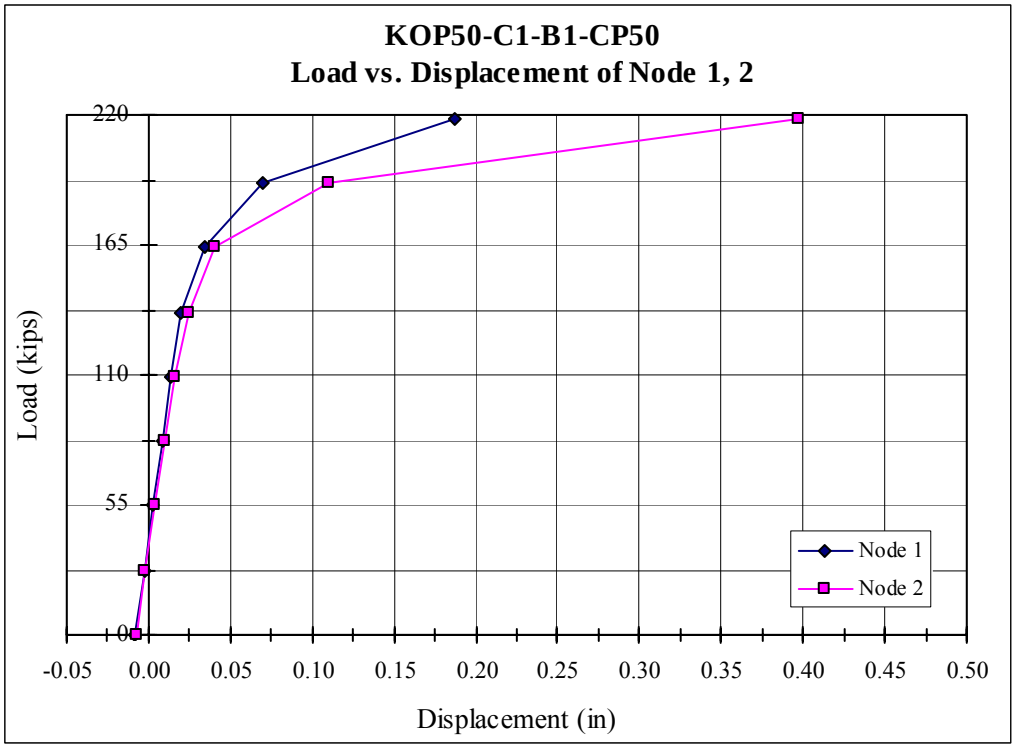

Figure A.F.1 – C1-B1-CP50 Node 1, 2 Load-Displacement

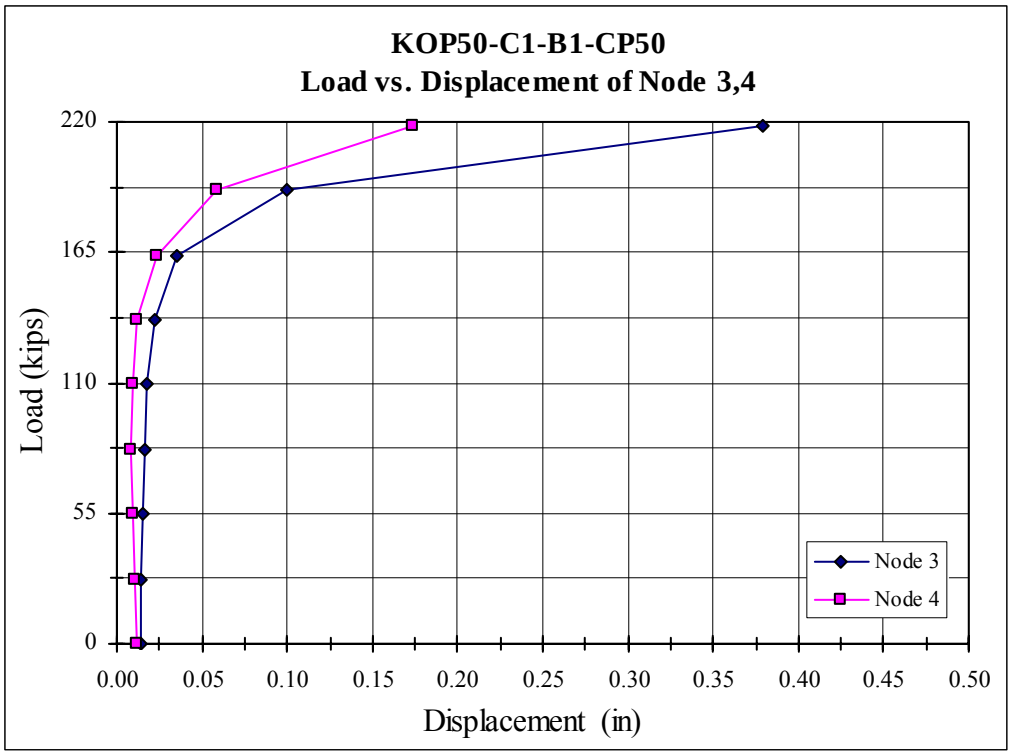

Figure A.F.2 – C1-B1-CP50 Node 3, 4 Load-Displacement

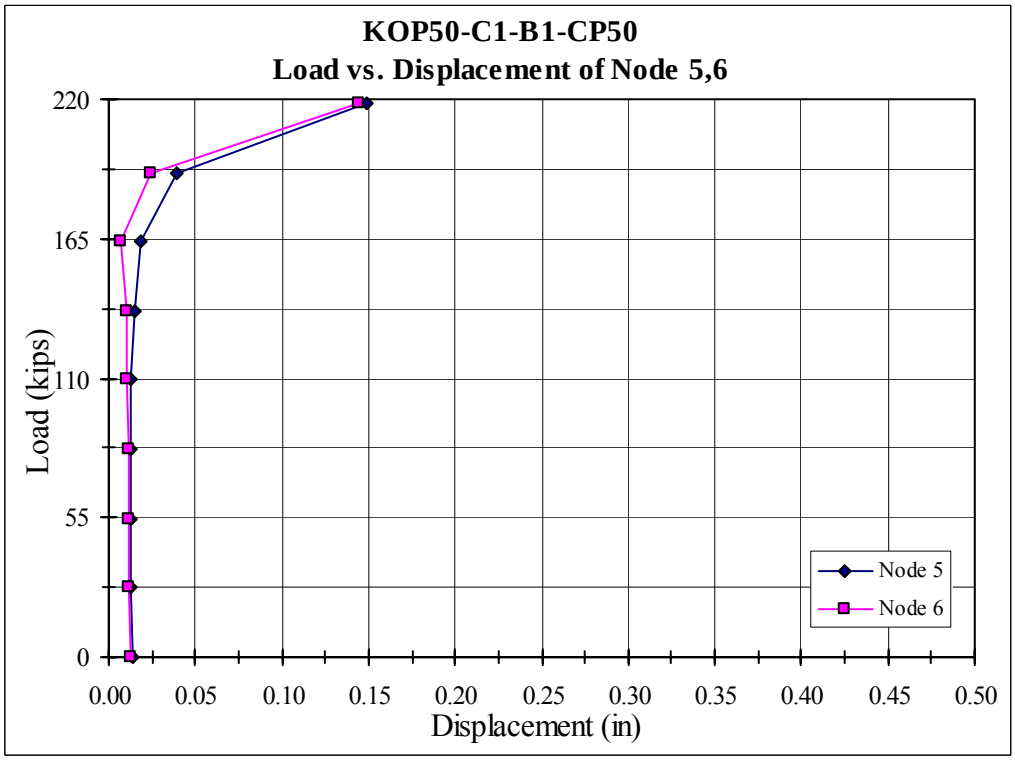

Figure A.F.3 – C1-B1-CP50 Node 5, 6 Load-Displacement

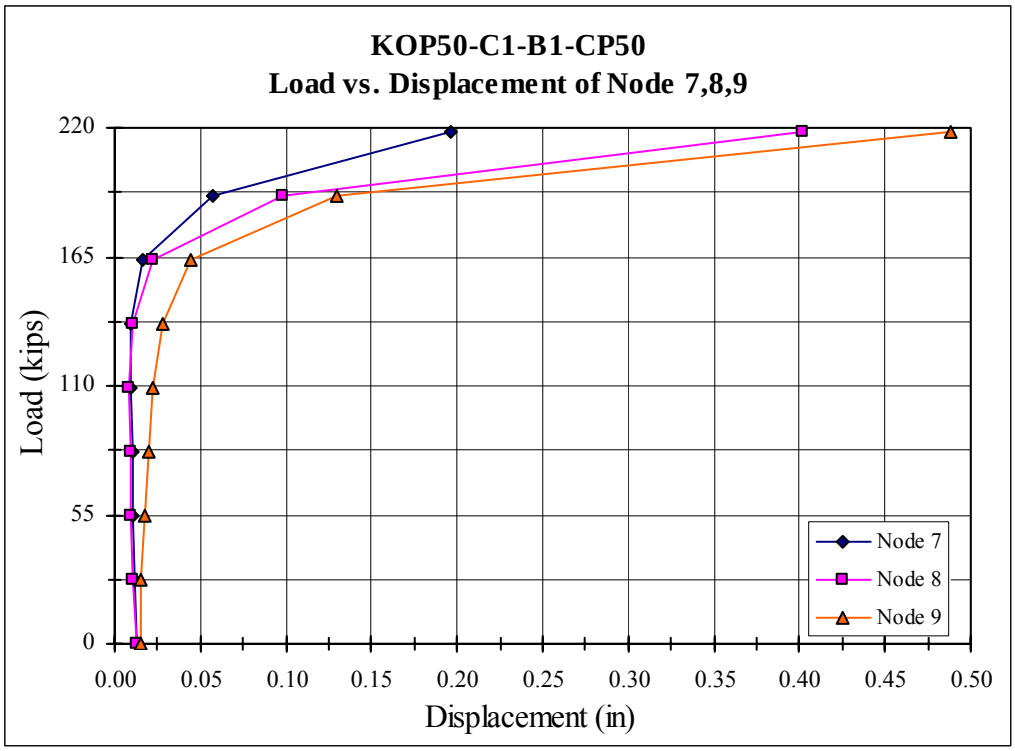

Figure A.F.4 – C1-B1-CP50 Node 7, 8, 9 Load-Displacement

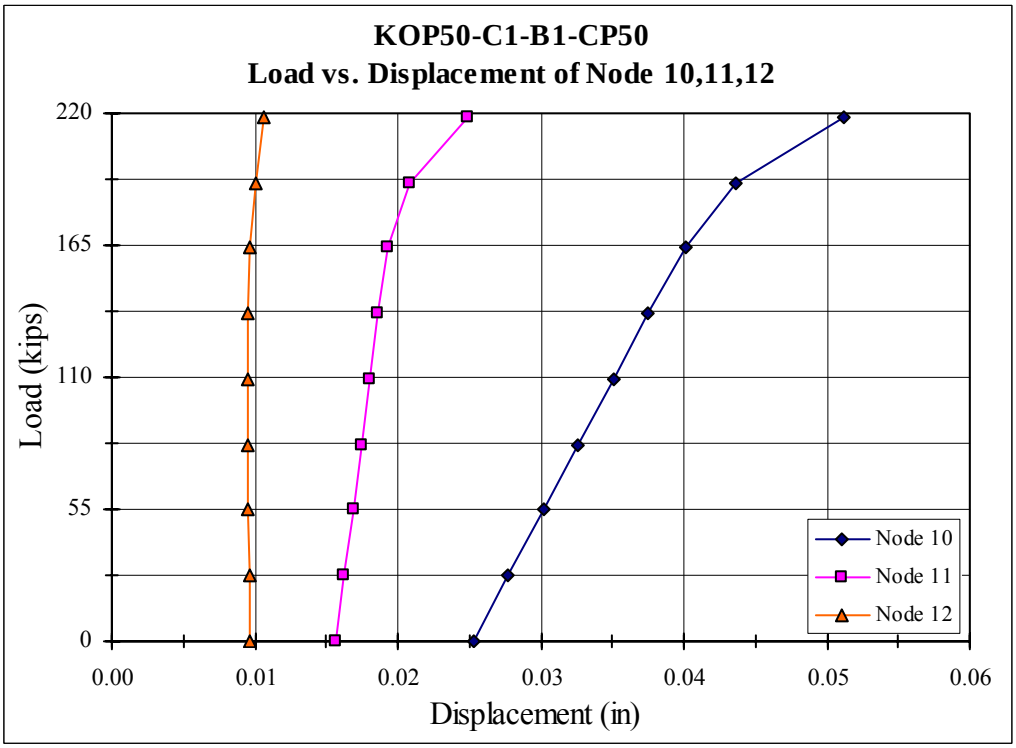

Figure A.F.5 – C1-B1-CP50 Node 10, 11, 12 Load-Displacement

Appendix G

ANSYS Result for KOP50-C1-B1-CP100

Table A.G.1 –Geometric & Load Configuration for KOP50-C1-B1-CP100

	Geometric & Load Configuration
Chord member	14 ×14 × 3/8
Branch Member	8 × 8 × 1/4
Branch ramp Load In 8 load steps	218.48 kips
Chord Step Load	377.69 kips
Chord ramp Load In 8 load steps	308.98 kips

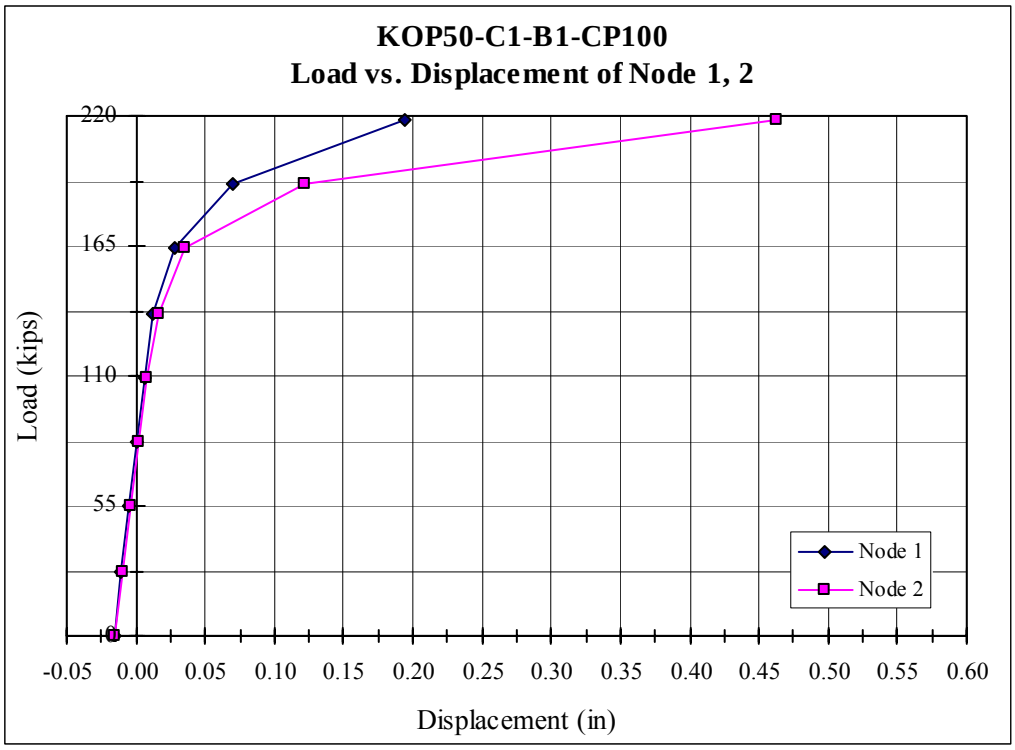

Figure A.G.1 – C1-B1-CP100 Node 1, 2 Load-Displacement

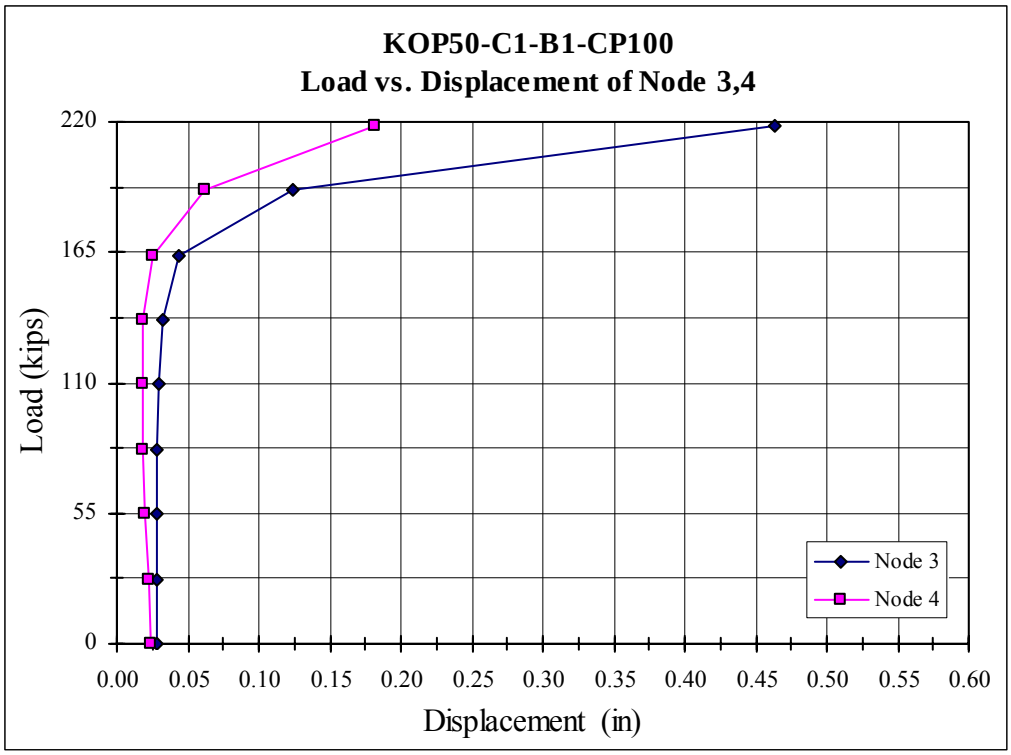

Figure A.G.2 – C1-B1-CP100 Node 3, 4 Load-Displacement

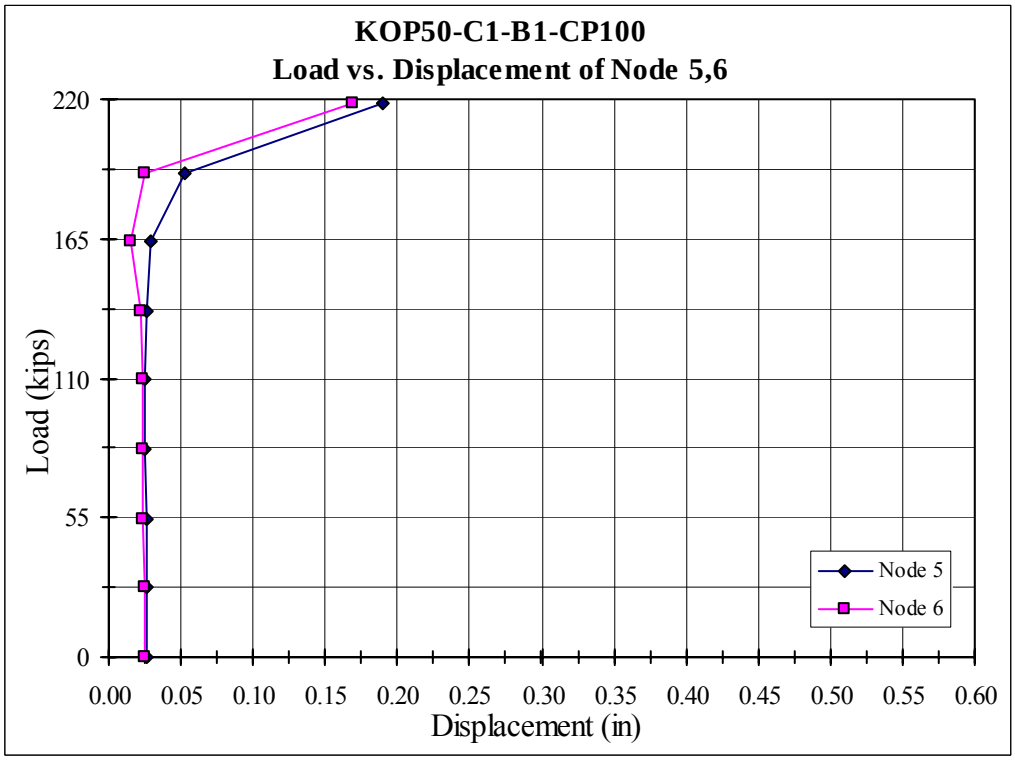

Figure A.G.3 – C1-B1-CP100 Node 5, 6 Load-Displacement

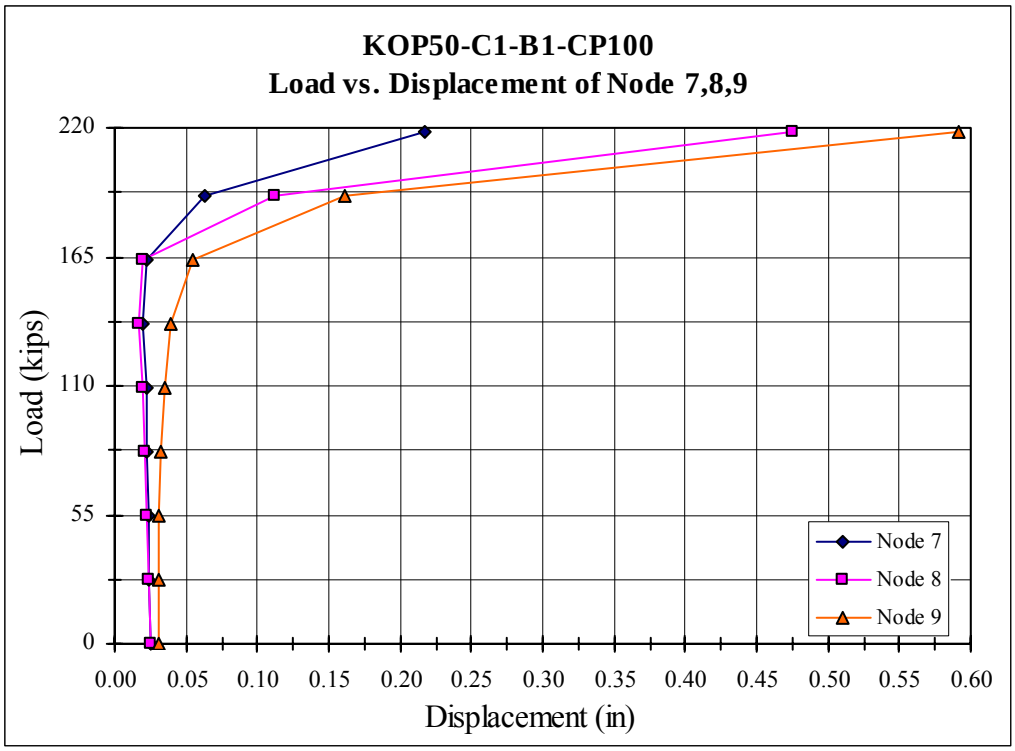

Figure A.G.4 – C1-B1-CP100 Node 7, 8, 9 Load-Displacement

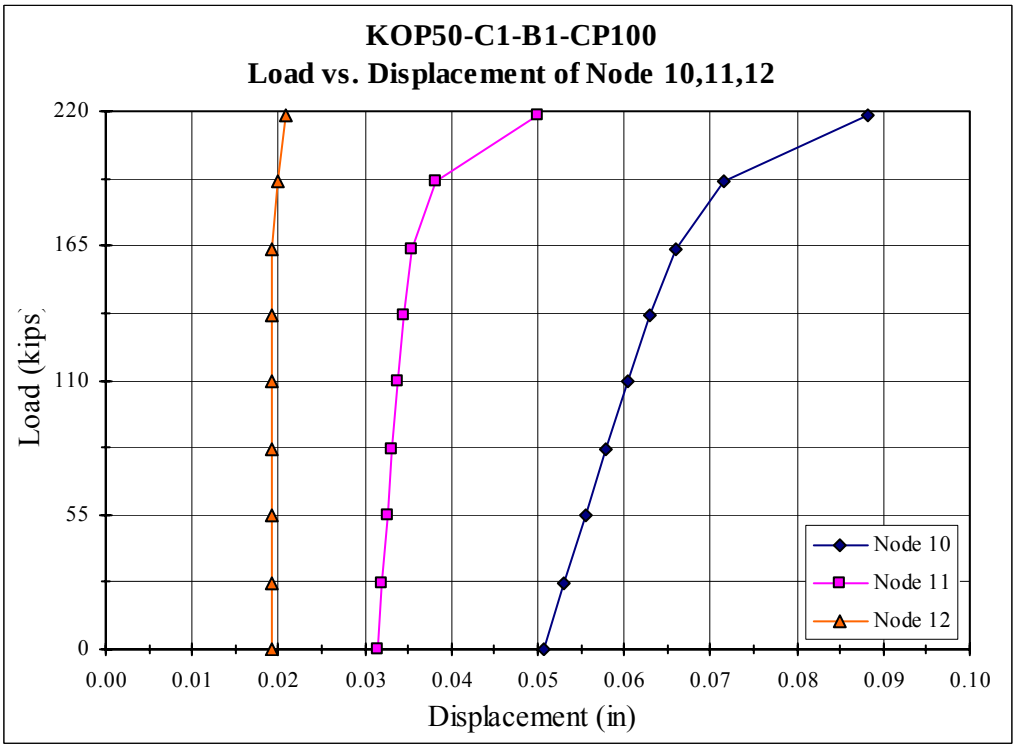

Figure A.G.5 – C1-B1-CP100 Node 10, 11, 12 Load-Displacement

Appendix H

ANSYS Result for KOP50-C2-B2-CP50

Table A.H.1 –Geometric & Load Configuration for KOP50-C2-B2-CP50

	Geometric & Load Configuration
Chord member	14 ×14 × 5/16
Branch Member	8 × 8 × 3/16
Branch ramp Load In 8 load steps	158.68 kips
Chord Step Load	142.76 kips
Chord ramp Load In 8 load steps	224.41 kips

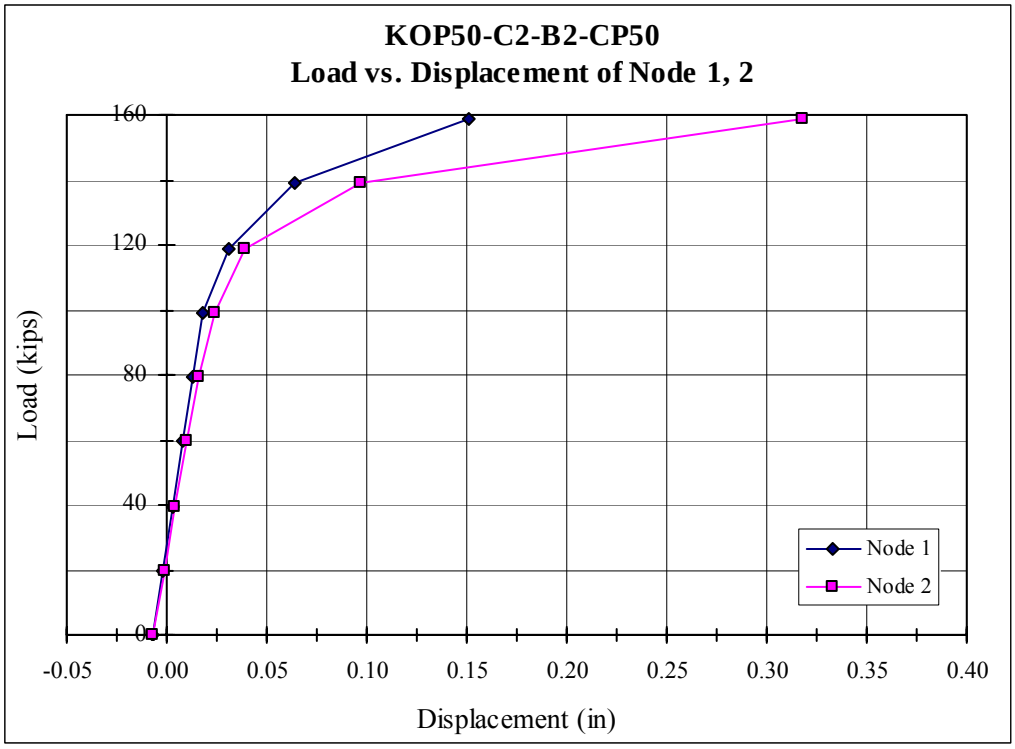

Figure A.H.1 – C2-B2-CP50 Node 1, 2 Load-Displacement

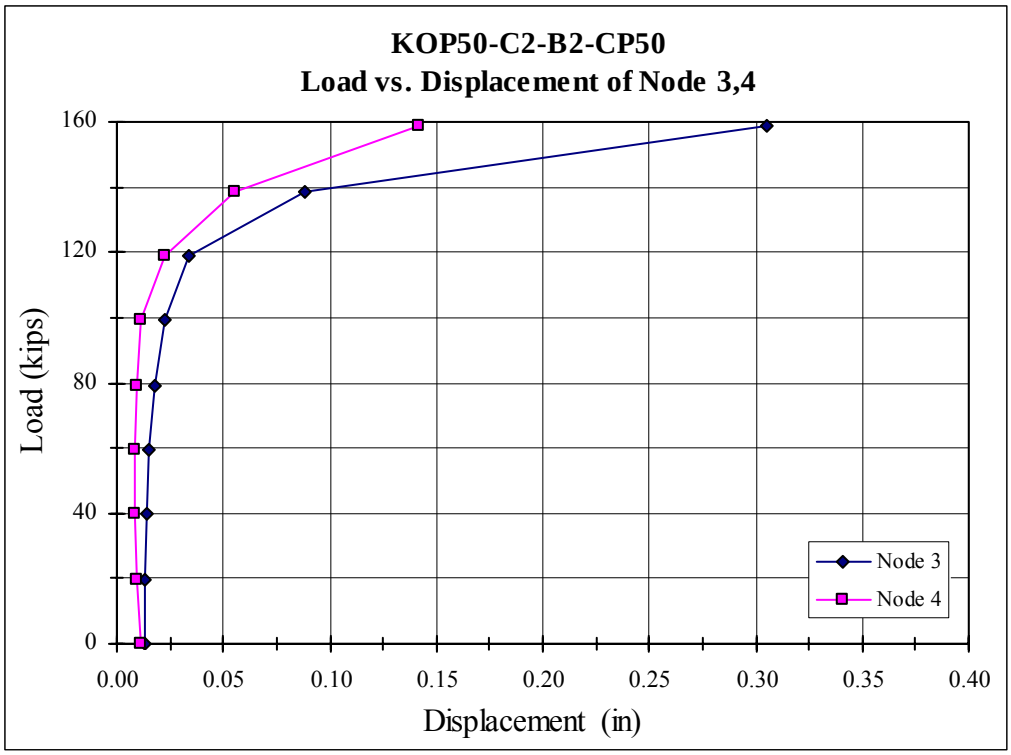

Figure A.H.2 – C2-B2-CP50 Node 3, 4 Load-Displacement

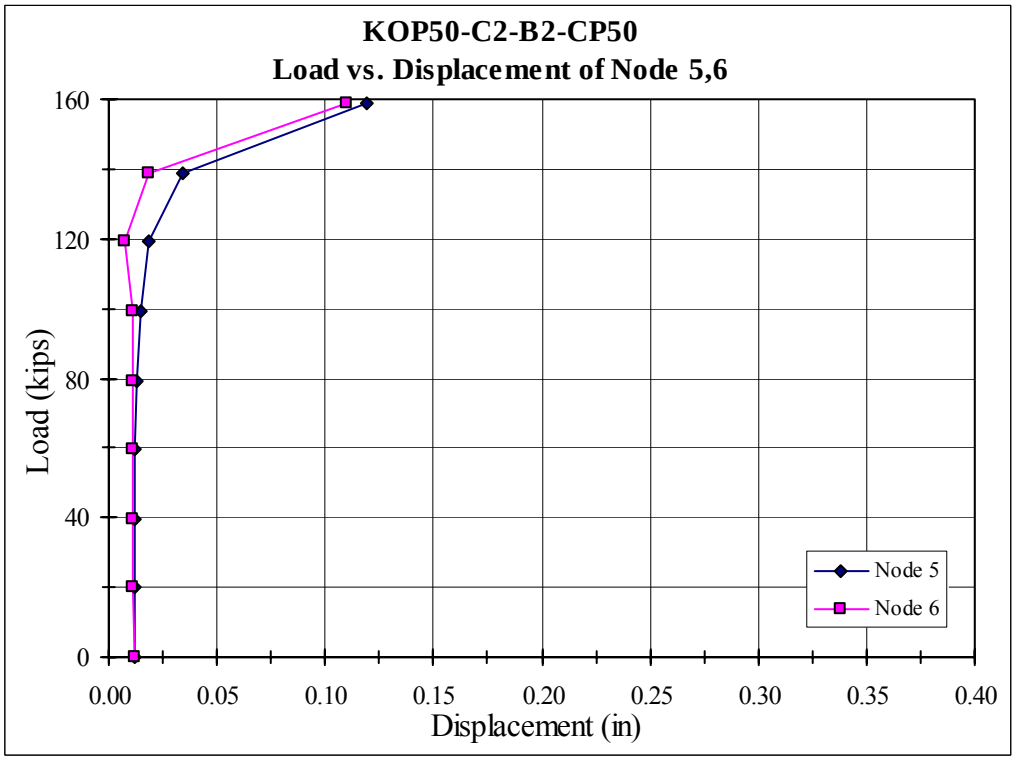

Figure A.H.3 – C2-B2-CP50 Node 5, 6 Load-Displacement

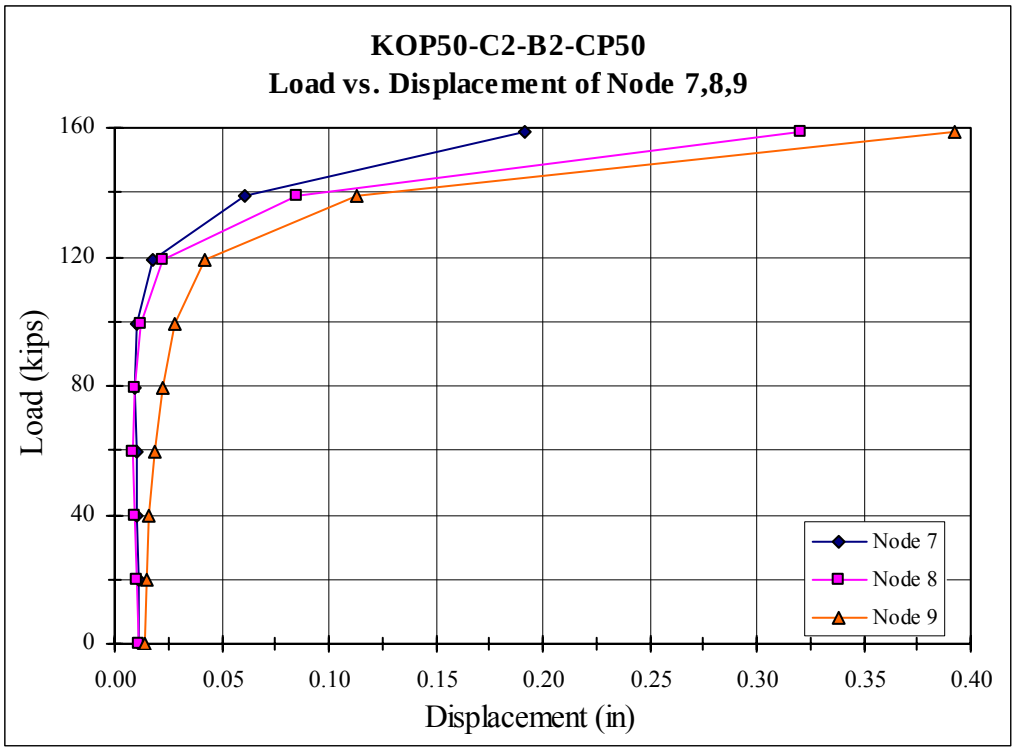

Figure A.H.4 – C2-B2-CP50 Node 7, 8, 9 Load-Displacement

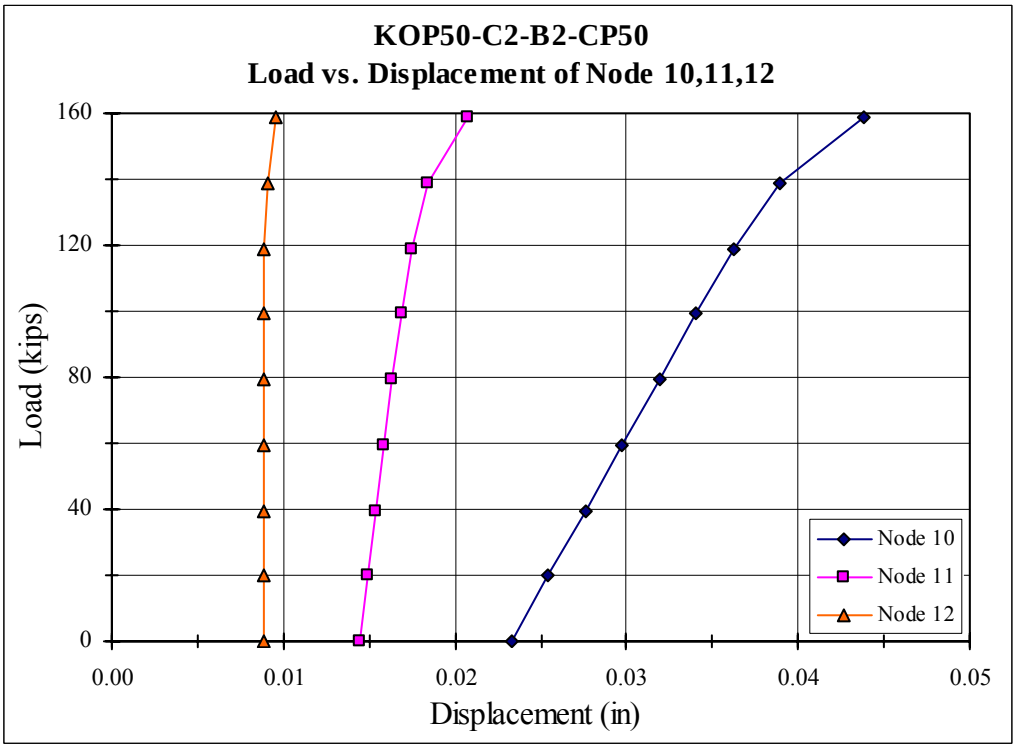

Figure A.H.5 – C2-B2-CP50 Node 10, 11, 12 Load-Displacement

Appendix I

ANSYS Result for KOP50-C2-B2-CP100

Table A.I.1 –Geometric & Load Configuration for KOP50-C2-B2-CP100

	Geometric & Load Configuration
Chord member	14 ×14 × 5/16
Branch Member	8 × 8 × 3/16
Branch ramp Load In 8 load steps	158.68 kips
Chord Step Load	285.53 kips
Chord ramp Load In 8 load steps	224.41 kips

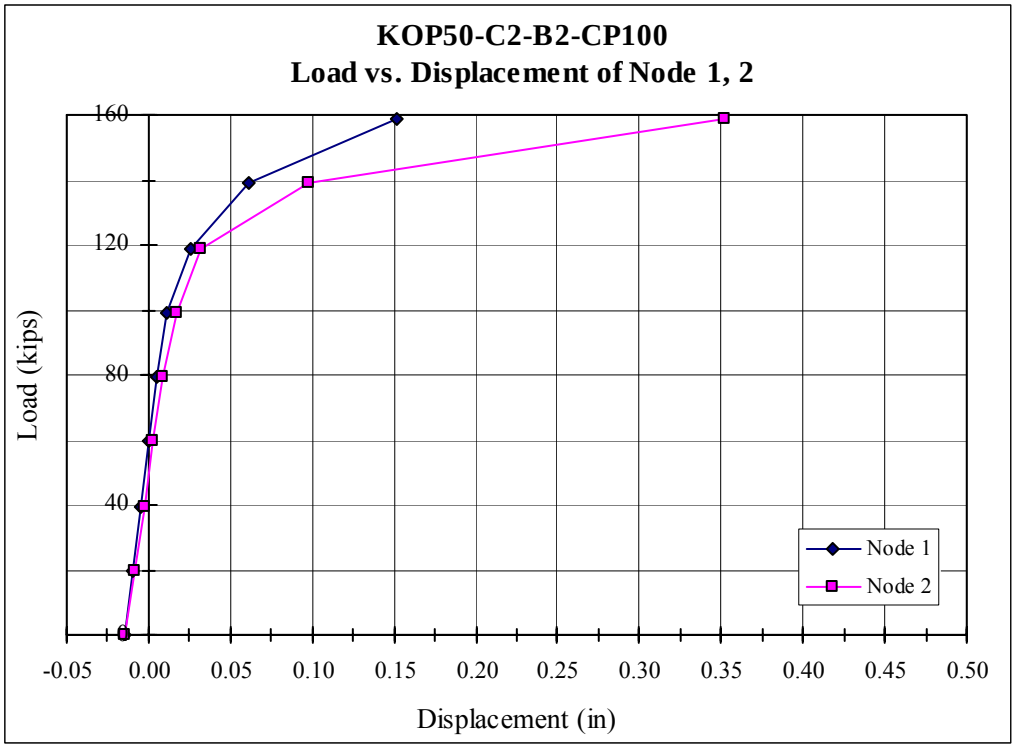

Figure A.I.1 – C2-B2-CP100 Node 1, 2 Load-Displacement

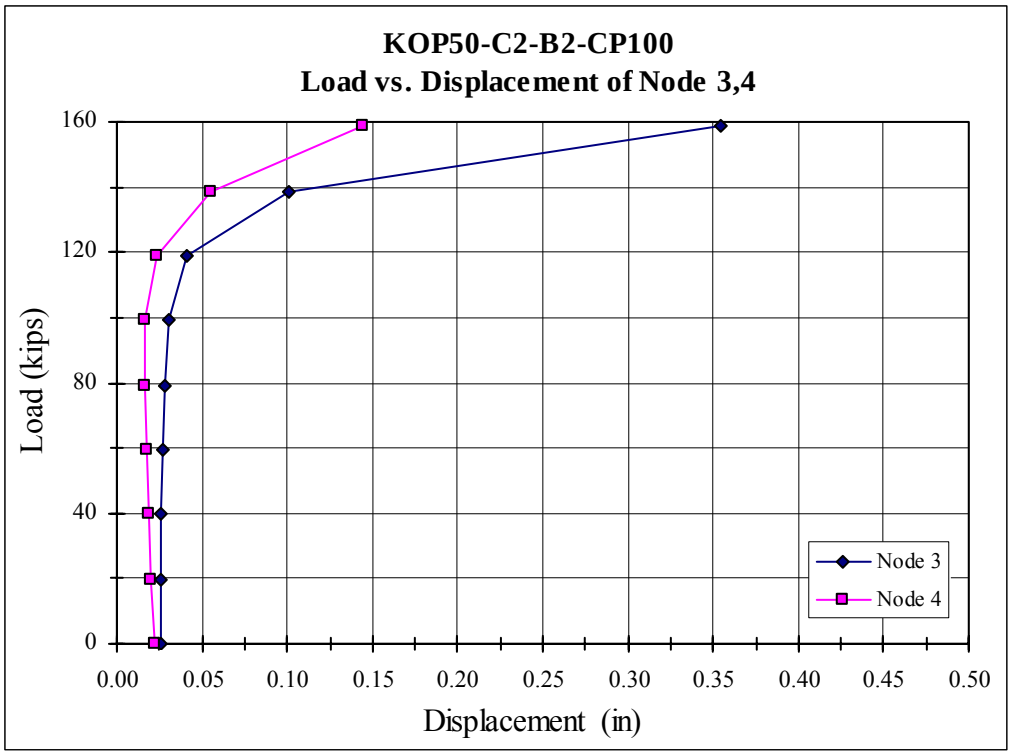

Figure A.I.2 – C2-B2-CP100 Node 3, 4 Load-Displacement

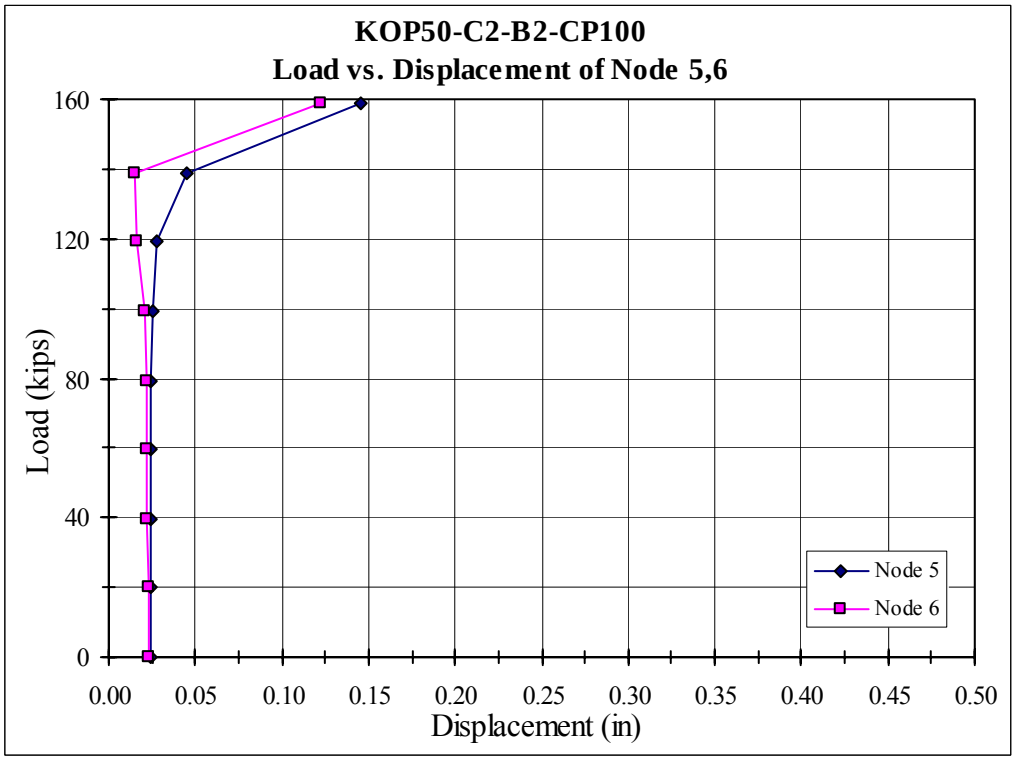

Figure A.I.3 – C2-B2-CP100 Node 5, 6 Load-Displacement

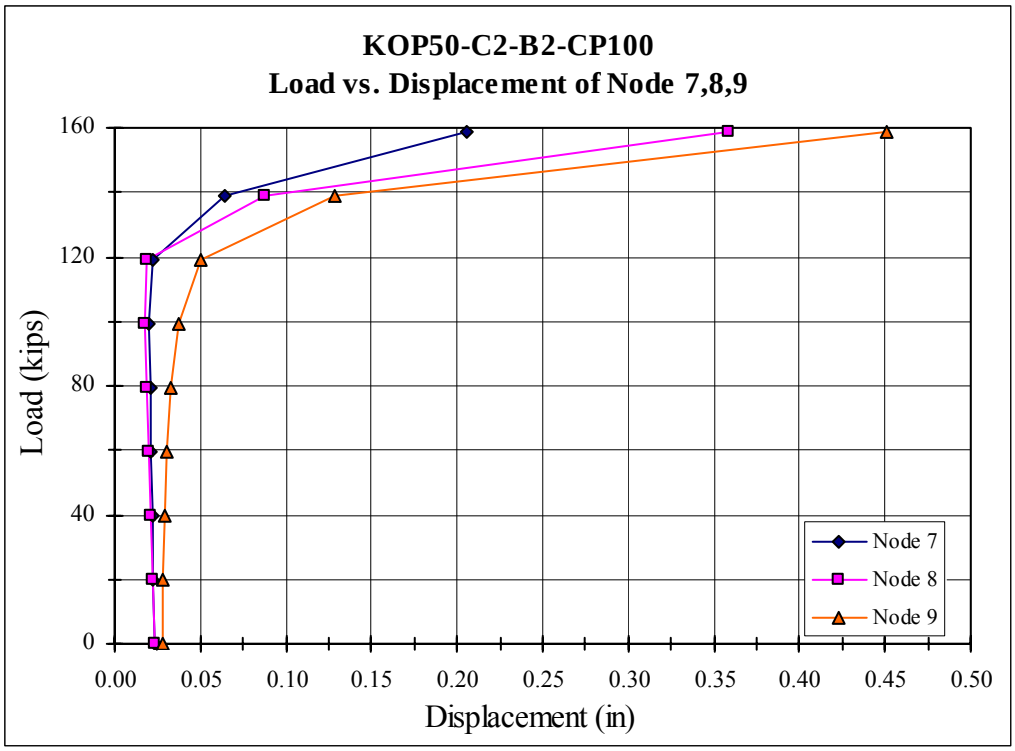

Figure A.I.4 – C2-B2-CP100 Node 7, 8, 9 Load-Displacement

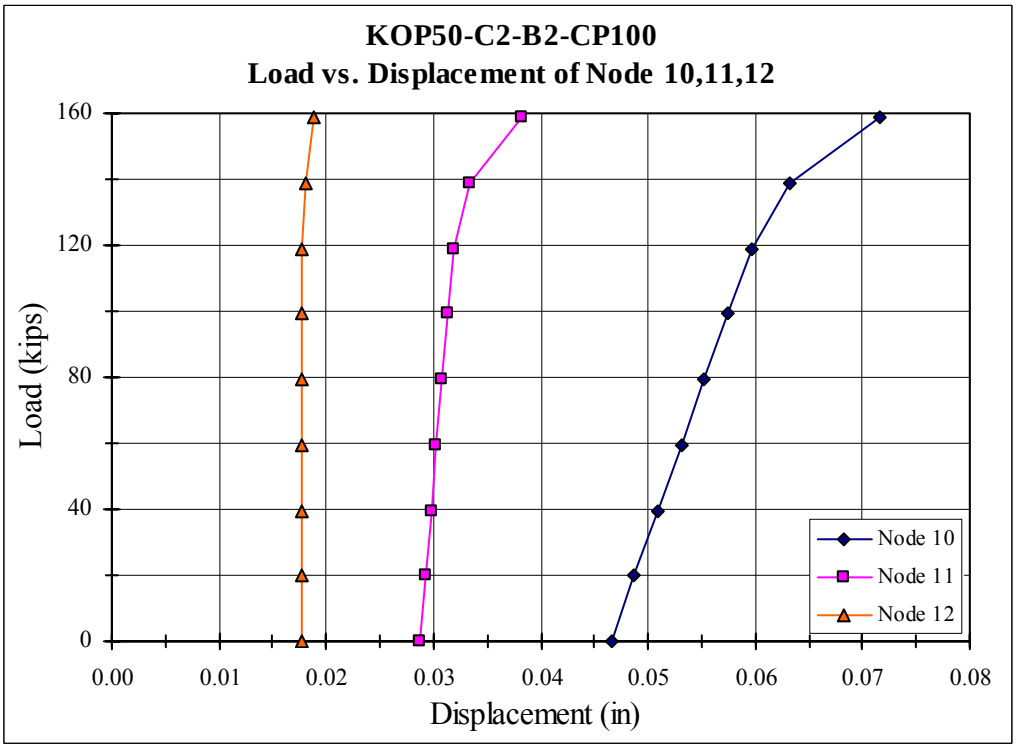

Figure A.I.5 – C2-B2-CP100 Node 10, 11, 12 Load-Displacement